

Single particle and single cell ICP- MS applications in nanomaterial safety assessment

Benjamin James Fryer

Submitted for the fulfilment of the degree of Doctor of
Philosophy (PhD), School of Earth and Environmental
Sciences, University of Birmingham

September 2019

UNIVERSITY OF
BIRMINGHAM

University of Birmingham Research Archive

e-theses repository

This unpublished thesis/dissertation is copyright of the author and/or third parties. The intellectual property rights of the author or third parties in respect of this work are as defined by The Copyright Designs and Patents Act 1988 or as modified by any successor legislation.

Any use made of information contained in this thesis/dissertation must be in accordance with that legislation and must be properly acknowledged. Further distribution or reproduction in any format is prohibited without the permission of the copyright holder.

Abstract

This thesis describes the development of single particle (spICP-MS) and single cell inductively coupled plasma mass spectrometry (SC-ICP-MS) analytical techniques for environmental and ecotoxicological analysis. Single particle and single cell ICP-MS protocols and application notes were developed within this thesis for a nanomaterials characterisation and interactions with living systems.

It was shown that the composition of complex multi-element nanoparticles could be determined by measuring each of the individual elements and converting particle volume to particle size, using a quadrupole based ICP-MS. The resulting particle sizes and density of multiple, multi-element nanoparticles results were comparable to other analytical techniques (DLS, DCS and TEM), but the measurement is faster and easier.

Using single particle ICP-MS, gold nanoparticles that had been ingested by isopods were analysed and quantified. A surprising result from this investigation was that irrespective of the form in which gold was presented to the isopods, i.e. as gold nanoparticles of 80 nm or ions, the gold measured in the Isopods was consistently characterised as being nanoparticle of around 60nm found within the main body and hepatopancreas of the isopods, indicating nanoparticle formation and transformation in situ.

Single cell ICP-MS was used to measure the intrinsic metal within multiple cell lines, but was found to be inconsistent or irreproducible between biological replicates, but it was possible to measure the metal concentration reliably within cells that had been spiked with a target metal.

Finally, single organism ICP-MS was developed, with the analysis of entire daphnids (*daphnia magna* and *daphnia pulex*), pushing the instrument capabilities further.

Acknowledgements

The work that encompasses this thesis couldn't be possible without the help and support of my supervisors at the University of Birmingham; Professor Eva Valsami-Jones and Professor Iseult Lynch. Their academic guidance throughout the four years has provided me with the opportunity to grow as a researcher and an academic. The many hours spent discussing and reviewing my work, debating the possible hypothesis of the results and directions that should be next taken were very much appreciated.

I would also like thank the superb help and technical support from PerkinElmer, specifically Dr Chady Stephan and Dr David Price for the four years of answers to any and all queries relating to the instrument. From fixing issues that arose to providing expert guidance on the feasibility of a study, I would also like to thank them for the opportunities to present and experience the non-academic world of science as well as including me on many projects and work related to the instrument and encouragement for my work.

In the University of Birmingham, I would like to thank Laura-Jayne Ellis for the titanium dioxide nanoparticles used in chapter four, and Katie Reilly for the supply of isopods that we analysed in chapter seven. The members of my office especially Danny Croghan and Alex Hurley for the random but deep conversations at lunch. Also my research group for the many pizzas and drinks at Bratby after work were also very much appreciated.

I want to thank my family and friends for the continuous support and encouragement throughout the four years of my PhD, especially my parents for

providing me with a relaxing environment away from the office to finish my final draft of the thesis. I am eternally grateful for their support while I was writing up.

Finally, I want to thank my fiancée Rebecca for all of her love and support throughout my PhD, from helping to proof read work and giving constant encouragements, I cannot thank her enough for being there at my most stressful.

This PhD studentship was funded by a NERC case grant (grant code NE/M009947/1), between the University of Birmingham and PerkinElmer. Work that was published as a result of the work outlined in this thesis was Core-Shell NaHoF₄@TiO₂ NPs: A Labeling Method to Trace Engineered Nanomaterials of Ubiquitous Elements in the Environment. ACS Appl. Mater. Interfaces 11, 19452–19461 (2019).

Table of Contents

Abstract.....	1
Acknowledgements.....	3
Tables of Contents.....	5
List of Tables.....	11
List of Figures	15
List of Equations	23
List of Abbreviations	25
List of Appendices	28
Chapter One - Introduction and Literature review	29
Preview of work.....	29
Aims of Work.....	31
Background to the work	32
What are nanoparticles	32
Single Particle ICP-MS	34
Single Cell ICP-MS	37
Chapter Two - Introduction of analytical methods	40

Inductively Coupled Plasma Mass Spectroscopy	40
Introduction to the system.....	40
The mathematics behind single particle ICP-MS (and by extension single cell ICP-MS)	45
Line Start differential centrifugation sedimentation (DCS).....	55
Dynamic Light Scattering (DLS).....	56
Transmission Electron Microscopy (TEM)	57
Cell Lines	58
Isopods.....	59
Daphnia (<i>pulex</i> and <i>magnia</i>)	60
Chapter Three - Development of a standard operating procedure for single particle ICP-MS	61
Aims and Overview	61
Materials and Methods	62
Chemicals and Materials	62
Sample preparation/Extraction procedure.....	62
Instrumental optimisation and analysis.....	66
QA/QC criteria	67

Statistical analysis	68
Results/Discussion	68
Silver nanoparticle standard analysis	68
Standard nanoparticle concentration	71
Comparison of storage techniques	76
Conclusions	83
Chapter Four - Developing single particle ICP-MS analysis for the detection and characterisation of complex bimetallic core-shell or mixed phase nanoparticles.....	86
Aims and Overview	86
Determining size of bimetallic NPs.....	91
Calculations to determine complex NP density	97
Materials and Methods	98
Chemicals and Materials	98
Sample preparation/Extraction procedure.....	100
Instrumental optimisation and analysis.....	102
QA/QC criteria	106
Statistical analysis	106

Results/Discussion	107
Au@Ag NPs Size	107
Hafnium doped TiO ₂ NPs Size	110
Au@Ag NPs Density.....	112
Hafnium doped TiO ₂ NPs Density.....	113
Conclusions	115
Chapter Five - Considerations on particle recovery from tissue to enable analysis of Gold nanoparticle uptake by Isopods (Porcellio scaber)	117
Aims and Overview	117
Materials and Methods	120
Chemicals and Materials	120
Sample preparation/Extraction procedure.....	120
Instrumental optimisation and analysis.....	122
QA/QC criteria	122
Statistical analysis	123
Results/Discussion	123
Batch two – Analysis of isopod bodies	126
Batch three – Analysis of isopod bodies and hepatopancreas	137

Comparison of batches and exposures.....	148
Conclusions	151
Chapter Six - The intrinsic metal content of individual biological cell lines as a baseline for cellular exposure to metal nanoparticles	154
Aims and Overview	154
Choice of Elements of Analysis	158
Materials and Methods	162
Chemicals and Materials	162
Sample preparation/Extraction procedure.....	162
Instrumental optimisation and analysis	163
QA/QC criteria	165
Statistical analysis	165
Results/Discussion	166
Conclusions	175
Chapter Seven - Application of single cell ICP-MS for quantification of interaction of <i>Daphnia pulex</i> with gold nanoparticles.....	177
Aims and Overview	177
Materials and Methods.....	179

Chemicals and Materials	179
Sample preparation/Extraction procedure.....	180
Instrumental optimisation and analysis	181
QA/QC criteria	183
Statistical analysis	183
Results/Discussion	184
Conclusions	195
Chapter Eight – Recommendations for Future Study.....	186
References	206
Appendices	225

List of Tables

Table 3.1: The dilutions used to reach desired concentrations for the ionic silver calibration standards	63
Table 3.2: The multiple dilutions of the original silver particles and the exact volumes that were used for those dilutions.	65
Table 3.3: The outline of the method of storage that each sample utilised and the timeframe to which the particles were left stored.....	66
Table 3.4: Instrumental parameters used during single particle analysis of silver nanoparticles.	67
Table 3.5: The average diameter and particle concentration of five replicates that were repeated three times for both 40nm and 80nm silver nanoparticles.	70
Table 3.6: Results for the mean diameter and response of various silver nanoparticle dilutions.	75
Table 3.7: The particle concentration, ionic concentration and particle size of various samples of 80nm silver nanoparticles that were stored in a variety of methods both diluted and undiluted concentrations are shown.....	78
Table 4.1: The dilutions used to reach desired concentrations for the ionic gold calibration standards.....	101
Table 4.2: Instrumental parameters used during single particle analysis for complex nanoparticles.	102

Table 4.3: DLS Instrumental parameters utilised for Au@Ag nanoparticles and TiO ₂ .Hf nanoparticles.	103
Table 4.4: Instrumental parameters used for DCS analysis of complex nanoparticles.	105
Table 4.5: Size of complex particles determined using spICP-MS, DCS, DLS and TEM.	108
Table 4.6: Particle concentrations of each component within Hafnium doped TiO ₂ particles, each component is measured separately before being used to calculate the total particle size and density.	112
Table 4.7: Collated results for NanoComposix 60nm Au@Ag NPs obtained from spICP-MS, DLS and DCS.	113
Table 4.8: Collated results for the hafnium doped TiO ₂ NPs obtained from spICP-MS, DLS and DCS.	114
Table 5.1: Instrumental parameters of the NexION 300D to analyse Isopods.	122
Table 5.2: Collected results for isopod samples of batch two. With the nanoparticle size, nanoparticle concentration, dissolved ion concentration and the dilution factor for the isopods.	126
Table 5.3: Collected results for isopod samples of batch three. With the nanoparticle size, nanoparticle concentration, dissolved ion concentration and the dilution factor for the isopods.	137

Table 6.1: Elemental ranking based on equation 6.1, used to prioritise those elements present in cells that could potentially be used for cell counting via scICP-MS.	161
Table 6.2: NexION 300D Operating Conditions for intrinsic metal concentration of cell lines.	165
Table 6.3: Cell concentration of A549 cells averaged over replicates, based on detection of the intrinsic metal contents, and compared to the haemocytometer concentration of the cells.	167
Table 6.4: The concentrations of cell like events detected in washes and final cell sample for each cell line.	169
Table 6.5: The concentrations of A549 cells dependent on the element analysed.	170
Table 6.6: The concentrations of HeLa and MDA cells dependent on the element analysed.	172
Table 6.7: The concentrations of spiked HeLa and spiked MDA cells dependent on the element analysed.	174
Table 7.1: NexION 300D Operating Conditions for D. pulex containing 100nm Au NPs.....	183
Table 7.2: Averaged mass and cell concentration for multiple Daphnia pulex samples - in all cases the number of organisms and sample volume was constant, indicating that there is a wide variation in the mass of gold and concentration of the daphnia that were analysed.	190

Table 7.3: shows the averaged mass of gold and cell concentrations of daphnia of the samples that had above average peaks where above average was larger than 100 counts.194

List of Figures

Figure 1.1: The number of publications per year from 1990 to 2018 that mention spICP-MS found on Web of Science.	37
Figure 2.1: Exploded diagram of the NexION ICP-MS instrument set up for single cell ICP-MS, the autosampler is an ESI prepFAST.	40
Figure 2.2: Live response of a sample of nanoparticles (or cells), with 800,000 individual data points analysed over a 40 second period. While it seems as there is an almost constant level of response, if this figure was zoomed in to show only few datapoints it would become clear that there are large gaps where no ions hit the detector. The larger peaks are the result of particles (or cells).....	53
Figure 3.1: The size distribution of 40 nm silver nanoparticle standards with a bin size of 3 nm. There is a maximum peak in the figure at 41 nanometres that corresponds closely to the stated size from BBI.	69
Figure 3.2: The size distribution of 80 nm silver nanoparticles with a bin size of 3 nm. The maximum peak is measured to be about 80 nm with some smaller peaks at around 40 nm.	71
Figure 3.3: The response of each concentration of silver nanoparticles tested with the particle concentration against the maximum frequency for that concentration.	73
Figure 3.4: The increase in size of silver nanoparticles as the nanoparticle concentration increases.	74

Figure 3.5: The varying sizes of 80nm silver nanoparticles after being stored with a variety of methods. There is a close size correlation between the freshly made sample and the two fridge samples (Fridge and 50% Methanol Fridge) while there is a decrease in nanoparticle size for all the other samples.	79
Figure 3.6: The varying particle concentrations in ppb of 80nm silver nanoparticles after being stored with a variety of methods.....	80
Figure 3.7: The silver ion concentrations in ppb of 80nm silver nanoparticles after being stored with a variety of methods.....	81
Figure 3.8: The size distribution of 80 nm silver nanoparticles against the true intensity of each sample. It can be clearly seen that the Fresh sample has a significantly higher response than any of the other samples.	82
Figure 3.9: The size distribution of 80 nm silver nanoparticles against the normalised intensity of each sample, this allows for easier comparison of any secondary peaks that are present within a sample. In this case there are multiple secondary peaks for In-Box, Out-Box, Liquid Nitrogen and 50% methanol fridge samples, with freezer having the hint of a secondary peak forming.	83
Figure 4.1: Flow diagram of the mathematical procedure to determine the diameter DT of a spherical complex NP; whether the NP is core-shell or chemically doped does not influence the result.	92
Figure 4.2: Core-shell single phase spICP-MS results for one of the elements within a core-shell nanoparticle.	94
Figure 4.3: Agglomeration of Core-shell single phase spICP-MS results for one of the core-shell components.	95

Figure 4.4: Polydispersity of core-shell single phase and other nanoparticles spICP-MS results for one of the core-shell components.	96
Figure 4.5: Flow diagram of the mathematical procedure to determine the density of a spherical complex NP, utilising the volume data from spICP-MS to finalise the density of the mixed phase rather than taking an average of the elemental densities present. Whether the NP is doped or core-shell does not influence the final result. Utilising the spICP-MS (inorganic) diameter versus the DLS (hydrodynamic) diameter in the volume calculations provides the inorganic and hydrodynamic densities, respectively, which are quite different.	98
Figure 4.6: TEM screenshots of steric acid coated TiO ₂ Hf (left) and no surface coating TiO ₂ Hf (right).	106
Figure 4.7: Representative spICP-MS analysis result for the 60nm nanoComposix Au@Ag NPs: the gray size distribution represents the silver shell whilst the yellow is the gold core. The mean NP size (the sum of the Au Core and 2X the Ag shell) is used in size calculations.	110
Figure 5.1: spICP-MS gold calibration standard for ionic gold with a R ² value of 0.9996 demonstrating the high level of precision that the analysis was captured at on the day of analysis.	125
Figure 5.2: The mean size of gold nanoparticles found within the bodies of the isopods of batch two's control samples. Sample identification can be found in Table 5.2.	130
Figure 5.3: The particle concentration of gold within the bodies of isopods analysed in batch two's control samples.	130

Figure 5.4: The dissolved concentration of gold ions within the bodies of the isopods analysed in batch two's control samples.	131
Figure 5.5: The mean size of gold nanoparticles within the isopods of batch two's positive control samples.	133
Figure 5.6: The particle concentration of gold within batch two's positive control samples. PC3 has a significantly larger particle concentration than the other samples.	133
Figure 5.7: The dissolved concentration of gold within the isopods of batch two's positive control samples. Shown is a wide variance in ionic concentration.....	134
Figure 5.8: The mean size of gold nanoparticles within the isopods of batch two's nanoparticle fed samples. There is a close correlation of nanoparticle size across the samples.	135
Figure 5.9: The particle concentration of gold within the isopod bodies of batch two's nanoparticle fed samples.	136
Figure 5.10: The dissolved concentration of gold within batch two's nanoparticle fed samples. Only one sample Au1 showed any significant levels of gold ions.....	136
Figure 5.11: The mean size of gold nanoparticles within batch three's control samples. These samples showed consistent gold nanoparticle sizes suggesting a gold ion contamination.	142
Figure 5.12: The particle concentration of gold within isopods and hepatopancreas of batch three's control samples. The hepatopancreas have consistently higher particle concentrations.....	143

Figure 5.13: The dissolved concentration of gold within the isopods and hepatopancreas of batch three's control samples. The hepatopancreas have consistently higher ionic concentrations.	143
Figure 5.14: The mean size of gold nanoparticles within batch three's positive control samples. PCHep8 did not have any particles detected. There is less variation between the isopod bodies and hepatopancreas in these samples.....	145
Figure 5.15: The particle concentration of gold within batch three's positive control samples. PCHep2, PCHep4 and PCHep6 showed an elevated particle concentration compared to the other samples.	145
Figure 5.16: The dissolved concentration of gold within batch three's positive control samples. PCHep2 and PCHep6 had large gold ion concentrations.	146
Figure 5.17: The mean size of gold nanoparticles within batch three's nanoparticle fed samples. The sizes of the hepatopancreas samples was consistently lower around 60nm in comparison to the isopod bodies.....	147
Figure 5.18: The particle concentration of gold within the bodies and hepatopancreas of the isopods analysed in batch three's nanoparticle fed samples.	147
Figure 5.19: The dissolved concentration of gold within batch three's nanoparticle fed samples. The ionic concentration of the hepatopancreas samples was consistently higher the isopod bodies.	148
Figure 5.20: Comparison of the particle size of gold nanoparticles within isopods between batch two and three.	149

Figure 5.21: Comparison of the particle concentration of gold nanoparticles within isopods between batch two and three.	150
Figure 5.22: Comparison of the particle size of gold nanoparticles between batch two and three. Note the large ionic concentration variance of the positive control hepatopancreas samples.	151
Figure 6.1: A schematic that shows the steps related to analysing the intrinsic metal content of a cell, from the wash steps to the final analysis of the cells.	159
Figure 6.2: Cell concentration of cell lines spiked and unspiked as well as the washes that were aliquoted and tested before the cells were analysed.	168
Figure 6.3: Intrinsic metal content within spiked cells. Note the similar distributions across the elements but differing masses. This is indicative of both the differing densities of the elements and differing uptake levels of the spiked metals by the cells.	171
Figure 7.1: A graphical presentation of the route that daphnia undertake from the autosampler well to the ICP-MS detector. Firstly, the daphnia enter the autosampler probe and are taken up in a “sample plug” which is a 100µL plug of sample separated from other fluids by two air bubbles. The daphnia are then nebulised in the nebuliser and ionised in the plasma before entering the ICP-MS for analysis.	179
Figure 7.2: Real-time data from the gold nanoparticle calibration standard when run in the single cell ICP-MS.	184

Figure 7.3: A zoom-in of a small section of the real-time results shown in figure 7.2, to demonstrate that there are large gaps between peaks that are not implicitly clear when viewing figure 7.2. Each peak corresponds to a gold nanoparticle. ...185

Figure 7.4: The first 40 seconds of a daphnia pulex analysis, with the daphnia arriving at the detector after 10,000 readings equivalent to 5 seconds.186

Figure 7.5: Zoom in of the first 150 seconds of the Daphnia pulex scan shown in figure 7.4. This scan continues for 360 seconds. Along the X axis is the length of time that the scan has been progressing, take note the increasing peak sizes as time increases.187

Figure 7.6: Average section of a scan, where most peaks are around 15 to 30 counts in height, corresponding to one 100 nm Au NP per daphnid event. There was a trend that the peak size increased over time but the majority of peaks were within the range of 15 to 30 counts, corresponding to 1 and 2 Au NPs, respectively.189

Figure 7.7: A representative scan indicating the large variance in size that can occur within a single the daphia pulex sample. The between sample variance further exaggerates these differences.190

Figure 7.8: Examples of the doublet peaks that are consistently present within the Daphnia pulex analysis, most likely a result of the expanded ion cloud leading to two detection events for many of the individual daphnids.192

Figure 7.9: Examples of the larger peaks that were detected in the various Daphnia pulex samples. This particular sample's real-time data showed multiple very large peaks above 100 counts, many times larger than the average peak size

of 15 – 30 counts, potentially indicative of ingestion of agglomerates of Au NPs.

.....193

Figure 7.10: The frequency against mass in ag for the large peaks show in figure

7.9s real time, the mass of the peaks was regularly around 33,000 ag.194

List of Equations

Equation 2.1: Nanoparticle standard mass calculation.....	47
Equation 2.2: Nanoparticle standard equation of the line.	48
Equation 2.3: Dissolved standard mass of a particle.....	48
Equation 2.4: Sample flow rate equation.....	49
Equation 2.5: Dissolved standard equation of the line.	50
Equation 2.6: Equivalence in equations 3 and 4.	50
Equation 2.7: Removal of background count levels.	50
Equation 2.8: Multiplication of transport efficiency to both sides.	51
Equation 2.9: Isolation of the transport efficiency.....	51
Equation 2.10: Final transport efficiency calculation.....	51
Equation 2.11: Corrected mass of dissolved standard.....	52
Equation 2.12: Nanoparticle mass calculation.....	53
Equation 2.13: Molar mass ratio equation.	54
Equation 2.14: Diameter of spherical nanoparticle.....	54
Equation 2.15: Modified Stokes equation utilised in DCS.....	56
Equation 3.1: Standard dilution equation using concentration and volumes.....	63

Equation 6.1: Equation to calculate the validity of an element for intrinsic metal analysis.	160
--	-----

List of Abbreviations

A549	Adenocarcinomic human alveolar basal epithelial cells
Ag	Silver
ag	Attogram
ArO	Argon Oxide
ASTM	American Society for Testing and Materials
Au	Gold
Au@Ag	Gold core Silver shell
AuCl₃	Gold Trichloride
BBI	BBI Solutions
CaO	Calcium Oxide
Cd	Cadmium
Co	Cobalt
CPI	Consumer Products Inventory
CPS	CPS Instruments, Inc.
Cu	Copper
DCS	Differential centrifugation sedimentation
DLS	Dynamic Light Scattering
DMEM	Dulbecco's Modified Eagle's medium

DRC	Dynamic Reaction Cell
Fe	Iron
FFF	Asymmetric Field Flow Fractionation
HEN	High Efficiency Nebuliser
HfCl₄	hafnium (IV) chloride
HeLa	Henrietta Lacks cervical cancer cells
Hf	Hafnium
HH COMBO	High Hardness COMBO
ICP-MS	Inductively Coupled Plasma Mass Spectrometry
ISO	International Organization for Standardization
KED	Kinetic Energy Discrimination
LA-ICP-MS	Laser Ablation
MDA	MDA-MB-231 Cell Line human breast adenocarcinoma
Mn	Manganese
Ni	Nickle
NIST	National Institute of Standards and Technology
NM	Nanomaterials
NP	Nanoparticle
PBS	Phosphate-buffered saline

PC	Positive Control
QID	Quadrupole Ion Deflector
SC-ICP-MS	Single Cell Inductively Coupled Plasma Mass Spectrometry
spICP-MS	single particle Inductively Coupled Plasma Mass Spectrometry
TEM	Transmission Electron Microscopy
Ti	Titanium
TiO₂	Titanium Dioxide
TMAOH	Tetramethylammonium hydroxide
TOF-ICP-MS	Time Of Flight Inductively Coupled Plasma Mass Spectrometry
Zn	Zinc

List of Appendices

Appendix 1: Worked example of nanoparticle calculations from chapter two...	225
Appendix 2: SOP for NexION 300 spICP-MS Analysis: Metal nanoparticle size and concentration.	233
Appendix 3: SOP for NexION 300 single cell ICP-MS Analysis.	272

Chapter One

Introduction and Literature review

Preview of work

Nanotechnology offers incredible opportunities, in the form of novel materials ¹⁻⁴ and processes capable of solving problems such as energy capture and storage, climate change mitigation, minimisation of the use of finite resources ^{3,5}, but also significant challenges due to the potential of these novel materials to present unknown and unforeseen behaviour ⁶⁻⁸ and toxicity ^{6,9-11}. Limitations in a full assessment of the environmental safety of nanomaterials (NMs) stem from analytical difficulties ¹²⁻¹⁴, in relation to identification, characterisation and tracking of engineered nanosized objects in aqueous media and particularly in complex environmental matrices (sediment & soil) containing naturally occurring particles of similar sizes ^{15,16}. A further level of complexity is introduced by the need to trace NMs within individual organisms, or even cells ^{4,17-26}. Single particle ICP-MS (spICP-MS) is an extremely novel method, which has emerged in the past ten years, and although robust, it is currently only tested with a small number of NMs and mostly in simple matrices ²⁷⁻³². Further developments expand and augment the capability of spICP-MS and transform it into a powerful analytical tool for assessing and potentially monitoring, NMs in real environmental matrices ³³⁻³⁸. The aims of the work that encompass this thesis were to develop the analytical technique of single particle and a very recent further development, single cell ICP-MS, towards novel applications that could be further utilised in environmental and ecotoxicological analysis.

In developing single particle and single cell ICP-MS analytical techniques for environmental and ecotoxicological analysis, the first part of the work was to establish a standard operating procedure for which all subsequent work could be built upon. In the goal to determine the optimal instrumental working conditions multiple short studies took place into various analytical parameters. These studies which make up chapter three helped identify the limits of particle concentration, the standard transport efficiency set-up, the dwell time for the detector and the method of storage of the particles to see a visible quantifiable difference in particle size and ionic concentration.

After establishing a standard operating procedure for single particle ICP-MS that could be expanded for single cell ICP-MS with minimal deviation. Analysis of single element nanoparticles was performed in chapter four on standard gold and silver nanoparticles; once analysis of single element nanoparticles could be consistently replicated with confidence for nanoparticle samples with unknown sizes, the technique was expanded to measure multiple elements within nanoparticles whether the particle was core shell or doped. As an additional component to this work determining nanoparticle density using the spICP-MS was also developed, this added an analytical capability to the instrument.

After analysing single and multielement nanoparticles within ultrapure water the next analytical challenge was to measure, using single particle ICP-MS, nanoparticles that had been ingested by organisms, specifically here isopods. The work that was done within chapter five was based around developing the method of extraction that would minimise the effect on the particles that digestive

chemicals would have, and analysis of the fate of gold nanoparticles within the isopods.

Expanding the remit again the next step was to analyse metals and nanoparticles within individual cells, this is discussed in chapter six. Firstly it was necessary to adapt the standard operating procedure for single particle ICP-MS to be compatible with single cell ICP-MS, this is due to the differing introduction systems that the techniques utilise; so to maintain consistency the only variable that was changed was the transport efficiency, while the dwell time and storage technique was maintained. The work that was performed for this section had the aim of measuring the intrinsic metal within multiple cell lines, both pushing the limits of the instrument and providing a key variable that is usually calculated as a total of the population not by a cell by cell analysis.

Finally, the last set of work which composes chapter seven was to further single cell ICP-MS into single organism ICP-MS, with the analysis of entire daphnids (*Daphnia Magna* and *Daphnia Pulex*) that had been fed gold nanoparticles. This pushed the boundaries of the limits of size of the nanoparticles, cells and complexity of samples analysed with both single particle and single cell ICP-MS.

Aims of Work

The main aims of the thesis are twofold; firstly to explore the expansion of size and complexity of samples that are analysed by either single particle ICP-MS or single cell ICP-MS, secondly to meet the needs of the increasing uptake of use of ICP-MS, and the continued development of analytical techniques within ICP-MS that push the boundaries of what is currently possible. The work that has been

done within this thesis is partially independent from one another but has threads of work based upon these aims that link and build upon previous chapters.

Background to the work

What are nanoparticles

Nanomaterials is a term that encompasses all materials that are defined by the European commission as:

"A natural, incidental or manufactured material containing particles, in an unbound state or as an aggregate or as an agglomerate and where, for 50 % or more of the particles in the number size distribution, one or more external dimensions is in the size range 1 nm - 100 nm.

In specific cases and where warranted by concerns for the environment, health, safety or competitiveness the number size distribution threshold of 50 % may be replaced by a threshold between 1 and 50%.

*By derogation from the above, fullerenes, graphene flakes and single wall carbon nanotubes with one or more external dimensions below 1 nm should be considered as nanomaterials."*⁵

This description of nanomaterials can be applied to the basic description of nanoparticles being particulate matter within the size range of 1 nm to 100 nm, that can be found in either anthropogenic or natural particulate matter. Anthropogenic nanoparticles include anything from engineered nanoparticles such as silver nanoparticles added to antibacterial sprays ^{6,10,35,39}, titanium dioxide particles added to sunscreens ⁴⁰⁻⁴², and nanodrugs like cisplatin ^{17,43}. Anthropogenic nanoparticles also include incidental nanoparticles which are

nanoparticles produced via by-products of human production, such nanoparticles include the particulates produced during sand blasting and metalworking ^{44,45}. Natural sources of nanoparticulate matter includes the dusts such as those expelled from deserts or volcanic ash clouds ⁴⁶⁻⁴⁹, there are many other forms of natural nano particulate that form important processes within the natural world including regulation of global temperatures (dusts in the atmosphere), fertilisation of soils and food sources for microorganisms in the oceans.

One of largest current environmental concerns with nanotechnology is the increasing release of nanoparticles into the environment without detailed toxicological data. A recent hot topic issue is the use of intentionally added nano-plastics, which were recently proposed to be restricted ^{50,51} by the European Union in cosmetics industry for the prolonged degradation times and the potential effects they may have on the ecosystems they are exposed in to ^{52,53}. Some current methods of analysis of nanoparticles include UV-VIS spectroscopy, Dynamic Light Scattering (DLS), X-ray diffraction, various microscopy techniques and conventional ICP-MS, which all provided the analyst with a snapshot of the physiochemical properties of the nanoparticle. These techniques have a wide array of challenges in analysing nanoparticles, with many having long sample analysis times or complex sample preparation. This is where single particle ICP-MS can provide some answers with relatively small sample analysis times at around a minute per sample to the capability to analyse samples with minimal sample preparation other than having an upper limit of concentration and interferences ^{27,54-56}.

Single Particle ICP-MS

Single particle ICP-MS (spICP-MS) is a relatively new technique that has been pushed in the field of environmental and ecotoxicological studies in the last decade, with numerous advances in the analytical capabilities and range of samples spICP-MS has been utilised for the analysis of river water systems, dissolution of nanoparticles and biological uptake rates within complex organisms, among many other projects; in total there are almost 550 published articles that utilise single particle ICP-MS in analysis of nanoparticles. Single particle ICP-MS allows for the analysis of the very low concentrations of metals with some elements having a limit of detection estimated to be in the femtograms.

In environmental studies spICP-MS has been used to analyse many relevant samples ranging from river water and sewage water to the uptake of metals within trophic chains. It is quickly building a reputation as a fast and effective analytical technique for preliminary and detailed analysis of environmental relevant samples.

The earliest published work on single particle ICP-MS was in 2003 with the analysis of colloids ³¹ by Degueldre and Favarger with subsequent publications mainly consisted in analysis of exotic nanoparticles such as thorium ⁵⁷ and zirconia colloids ³², for about five years the two had the only significant published work in single particle ICP-MS.

By 2010 there had been with 114 papers published in various journals that had seen significant developments and uptake in the use of ICP-MS with single particles, of significance is the burgeoning collaborations between research groups and manufacturers. The Colorado School of Mines was one of these early

collaborations working with the characterization of silver nanoparticles using field flow fractionation coupled with ICP-MS ^{58,59}. This work combined the two analytical techniques of ICP-MS and asymmetric field flow fractionation (FFF) to separate the particles by size with the FFF before analysis by ICP-MS. While this work did not utilise spICP-MS its measurement of nanoparticles provided the basis of the work that would later be adapted to become spICP-MS. The group followed this work up with detection of silver nanoparticles using a spICP-MS to analyse silver nanoparticles in wastewaters collected from local treatment plants ^{35,36,59,60}, this work which used a Perkin Elmer Elan 6100 is one of the first major examples of single particle ICP-MS published.

The use of silver nanoparticles in this work is characteristic as the element being at the forefront of nanoparticle work during this point of time ^{8,22,33,35,36,59-68}. Silver nanoparticles are described as the most commonly commercially used nanomaterial ¹⁰ with the Nanotechnology Consumer Products Inventory (CPI) estimating that silver nanoparticles are used in roughly a quarter of all nanoparticle containing products ⁶⁹. Silver nanoparticles provide many medical applications examples being disinfection of wounds ^{6,8,70}, drug delivery to cells ^{4,26,70} and organs where nanoparticles show a 250 times quicker cellular uptake than micro particles ^{4,71}, and the inhibition of the HIV-1 to bind to host cells in-vitro ⁷⁰. However, whilst silver nanoparticles are being used for medical applications there is evidence that silver nanoparticles have toxicological effects ^{70,71} to cells with silver nanoparticles being shown to cause oxidative stresses ^{6,11,20,22,71-73}, DNA fragmentation ⁷³, apoptosis ^{4,10,18,70} and decrease in the mitochondrial membranes potential ^{18,22,23}.

Since 2015 there has been a shift in focus to more complex and diverse nanoparticles with nanoparticles of all shapes, elements and sizes being analysed, from gold nanoparticles in tomatoes ²¹, to titanium, hafnium and zirconium nanoparticles in engineered nanoparticles for environmental labelling ^{38,40,74} and complex nanoparticles of various elements, predominantly gold silver core shell nanoparticles ^{38,40,41,75,76}.

The advantage of single particle ICP-MS is primarily the increased capability to measure the form in which the measured metal exists, and thus to quantify the proportion of ions and the number and size of any nanoparticles present. While standard ICP-MS can measure the entire metal content of a population of nanoparticles from which the rough concentration can be determined from additional size measurements by DLS for example, spICP-MS can accurately measure the mass and concentration of individual nanoparticles, as well as the non-particle background metal levels. Thus spICP-MS provides significant improvements on the characterisation of nanoparticles over ICP-MS. With a single measurement, and subject to prior calibration, the instrument can measure background ionic metal concentration, the particle concentrations, and the average particle mass/size and particle mass/size distribution. Achieving this level of information with conventional ICP-MS would require a separation process to isolate the ionic fraction, and measurement of this sample for background metal concentrations, along with an additional measurement of total metal concentration of the sample following digestion, in conjunction with a size-based measurement such as DLS (Dynamic Light Scattering) to obtain an average particle size. Therefore, spICP-MS is vastly superior for particle measurements in comparison to conventional ICP-MS.

Single particle ICP-MS has steadily grown a presence at analytical conferences with the technique gaining significant traction as an emerging technique in 2016 for the environmental laboratory within conference talks and posters. In the following year the uptake of spICP-MS was evident with the technique being mentioned in many talks and posters. Since then the technique has become one of the key techniques for an environmental laboratory and the rate of publications has greatly increased from 2010, this is graphically shown in figure 1.1.

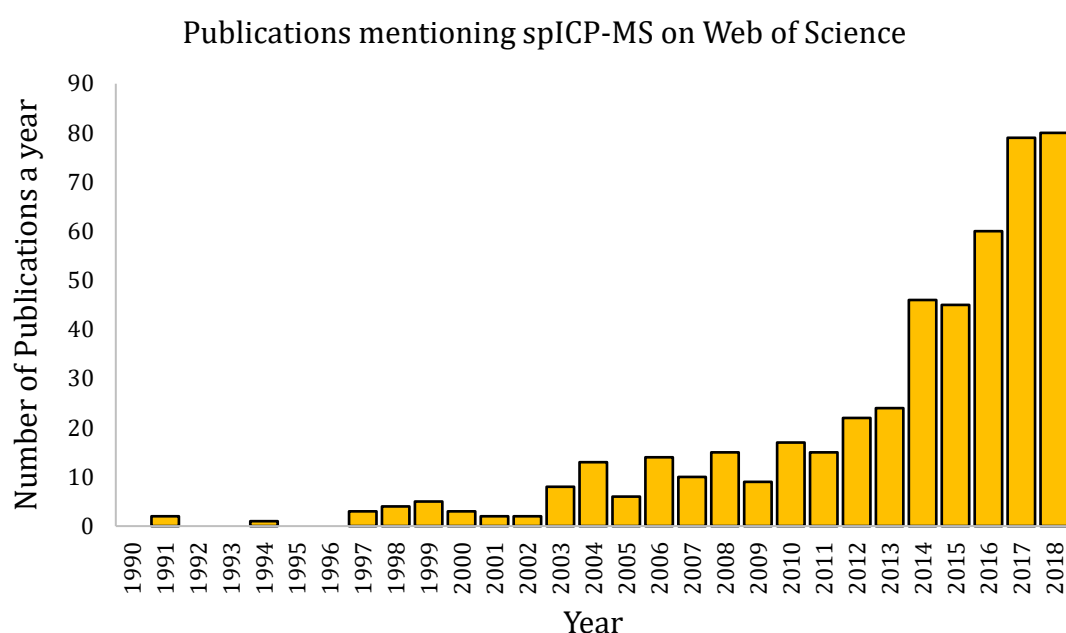


Figure 1.1: The number of publications per year from 1990 to 2018 that mention spICP-MS found on Web of Science.

Single Cell ICP-MS

Single Cell Inductively Coupled Plasma Mass Spectrometry (SC-ICP-MS) is an emerging analytical technique in the fields of environmental and biological sciences that enables the quantification of metals (ions or particles) on a single-cell basis coming about in the last five years. The method has been shown to work

in principle and we are now in the process of applying the method to problems that previously could not be addressed. The specific examples currently under development are the detection and quantification of metal or metal oxide nanoparticle uptake by algae ^{17,77} and cancer cell lines ^{17,43}.

Currently the most common form of single cell ICP-MS is time resolved ICP-MS ^{78,79}. The 'time resolved' part of time resolved ICP-MS is in reference to the data acquisition time per data point ⁷⁸. The method that time resolved ICP-MS uses is to introduce the cell suspension into the ICP-MS via nebulisation and when the rate of data acquisition per data point is faster than the rate cell introduction then individual cells can be identified.

In analysing single cells the size affects the rate of sample introduction and plasma generation, with an optimum cell introduction rate being around 500-2,000 cells per second when integration time is 100 μ s ⁷⁸. Each peak that is reported will have a unique count size; this will correspond to the concentration of the element of interest in the cell.

This is in a sense the exact method of analysis that single particle ICP-MS utilises with the difference being that time resolved ICP-MS commonly uses other forms of ICP-MS instrumentation like sector field ICP-MS and time of flight ICP-MS ^{78,79}. Recently this method has had significant development with multiple manufacturers releasing instrumentation that is able to analyse single cells.

In the field of single cell ICP-MS PerkinElmer has had the longest association with method, developing the technique through collaborations with research laboratories around the world (USA, UK, France, South Korea, Poland), this has resulted in the slow but increasing uptake of the technique. The method of using a

quadrupole ICP-MS to analyse single cells has enabled PerkinElmer to become the world leaders in quadruple based single cell analysis ^{17,80}. In response there has been a delayed development of similar instrumentation from competitor companies like Agilent ²⁵ who are now beginning to release instruments that can compete with PerkinElmer's NexION series of ICP-MS in terms of analytical capabilities.

One of the most common uses for single cell ICP-MS so far has been the analysis of the effects of metals and particles on *in vitro* cancer cells with significant work being done on cisplatin and similar compounds with regards the toxicity and uptake rates ^{17,43}. As the uptake of single cell ICP-MS increases there has been increasing developments of analysis of more complex cells and systems but most of this work is still ongoing and is yet to be published ^{17,43,76,77}.

Chapter Two

Introduction of analytical methods

Inductively Coupled Plasma Mass Spectroscopy

Introduction to the system

In this section it is discussed how a sample travels through the instrument (instrument shown schematically in figure 2.1), this does not address how the instrument interprets data but the mechanical aspects involved in the process of gathering data. It should be noted that the instrument used is a PerkinElmer NexION 300/350, a quadrupole ICP-MS system. How the instrument interprets the data will be discussed later in this chapter.

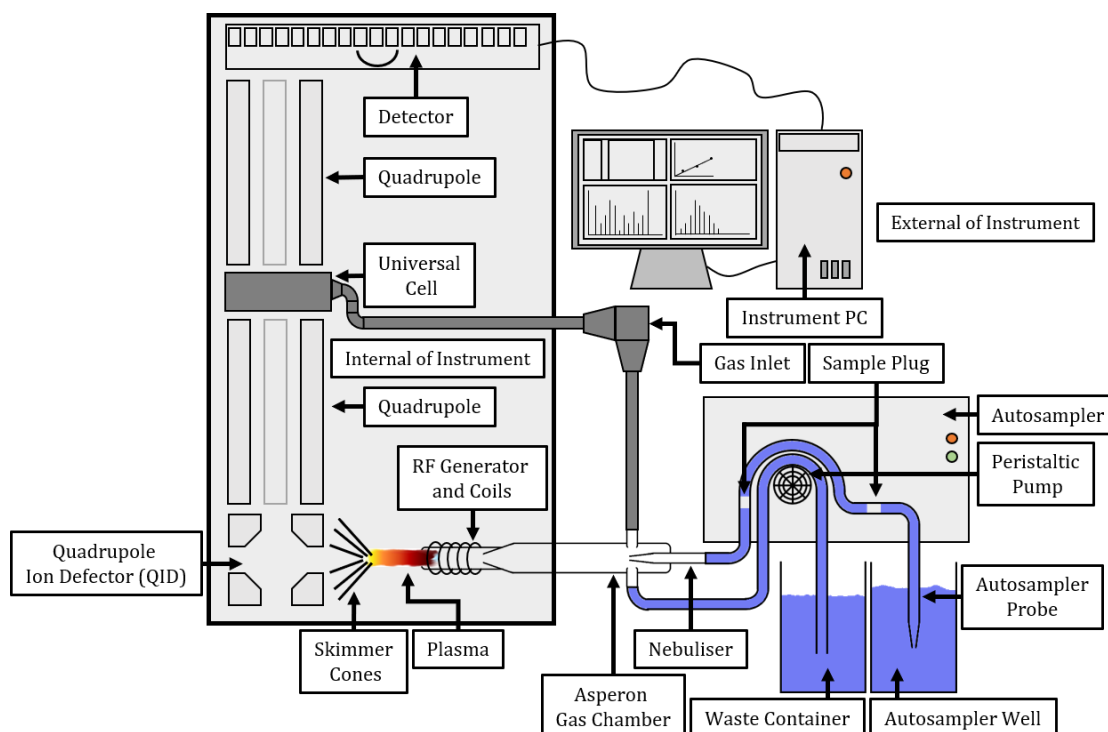


Figure 2.1: Schematic diagram of the NexION ICP-MS instrument set-up for single cell ICP-MS, the autosampler is an ESI prepFAST.

Commonly ICP-MS instruments are connected to an autosampler and in the case of the instrument used there were two variants: the S10 and ESI prepFAST. Both of these autosamplers had very specific purposes within the analysis of work presented in this thesis. The S10 is the standard autosampler for the NexION 300/350/1000/2000 instruments, with a variety of sample racks; it uses a peristaltic pump to transport a sample to the nebulisers. Due to the use of a peristaltic pump, the flow rate of samples varies based on a variety of factors from the atmospheric pressure to the condition of the tubing. This variability of sample uptake makes the S10 become unsuitable for low flow and controlled flow situations such as single cell ICP-MS (SC-ICP-MS), which will be discussed later. However, for regular ICP-MS and single particle ICP-MS (spICP-MS) this is not a problem, as long as a flow rate measurement is recorded before sample analysis. In contrast to this, the ESI prepFAST is a controlled flow system where using syringe injection the rate of sample introduction to the nebuliser is controlled. This allows for specific amounts of sample to be up-taken and dispensed at a rate that suits the needs of the analysis. In the case of SC-ICP-MS the autosampler allows for analysis of 100µL of sample over a 10-minute period at 10µL a minute, this very small sample requirement is perfect for cell analysis where commonly 200µL well plates are used. Comparing this 10µL/min to the S10's variable flow rate of around 200 – 400 µL/min, it is clear that the ESI prepFAST is ideally suited to very small samples. The one downside of the ESI prepFAST compared to the S10 is the analysis time, due to the syringe uptake the ESI prepFAST takes around 7 minutes to analyse a sample, which while still fast compared to other instrumentation (for example Differential centrifugation sedimentation or DLS) is a lot slower than its peristaltic pump counterpart with an average analysis time of

1 minute. As it is best to analyse all samples in one run so as to avoid any significant changes to the instrumental setup (that may occur due to the daily instrumental calibration), it is therefore crucial to determine which autosampler best suits the needs of the analysis, in terms of sample numbers, sample type/quality/matrix and sample quantity.

ICP-MS technology offers a range of introduction systems to the plasma chamber. The two that are used in the work that this thesis presents are a cyclonic spray chamber (used in chapters three, four and five) and a High Efficiency Nebuliser (HEN) coupled with an Asperon full consumption chamber (used in chapters six and seven). The main difference between the two is the method in which the sample is transported to the plasma. A cyclonic spray chamber creates a cyclone of the sample of which almost all is lost during uptake resulting in a transport efficiency of around 3 – 15% depending on the sample matrix and conditions both ambient and instrumental. This loss is due to the sample mist coming into contact with the side of the spray chamber and condensing onto the side. On the other hand, the Asperon full consumption chamber has a much higher transport efficiency of 50+% and typical transport efficiency for the chamber is around 70% but can be as high as near on 100%. The reason for this massive jump in efficiency is the way that the chamber works, instead of creating a cyclone the chamber has three entry points for the nebuliser gas, one with the nebuliser and two directly into the chamber itself; the two that are facing directly into the chamber are positioned 180° away from each other which allows the gas that is pumped in to wrap around the chamber to form a sheath of argon gas that prevents the sample that is being propelled by the nebuliser from any contact with the sides of the chamber. With this sheath of gas all of the sample reaches the plasma without any

loss from the nebuliser or spray chamber. Within this work the Asperon spray chamber was not yet developed until late 2017 and is primarily used for the small sample sizes introduced with the ESI prepFAST.

After the samples have passed through the nebuliser, they enter the torch and plasma, where the plasma dries, then atomises and finally ionises the samples, as they progress through a series of metal cones that dissipate the heat of the plasma to protect the sensitive inner parts of the instrument. These cones have small pinprick sized holes which allow the sample to pass through, and where some of the sample may be lost, if it fails to cross the centre of the cones. During the instrumental set up the torch is aligned to maximise the effective uptake of sample passing through the holes, however this does not mean that all the sample will pass through the hole in the cone, in fact the cones are designed to remove much of the unionised sample.

The samples then progress into the quadrupole ion deflector (QID), the first of three quadrupoles within the instrument. The QID deflects the ions around a 90° bend while the material which has not been ionised within the sample continues to travel in a straight line. This process removes a vast majority of the other ions in the sample leaving behind only the ions and any interferences of the same mass to charge ratio.

The problem of interferences is corrected at the next step within the instrument via kinetic energy discrimination (KED) or dynamic reaction cell (DRC), which are found near and within the second quadrupole of the instrument called the universal cell. Depending on the amount of an interference and the options available for use of a different isotope of the element of interest either the sample

is left to progress to the third quadrupole or interference removal is performed. KED creates a sheath of helium gas that the sample has to pass through with the aim to knock enough of the larger polyatomic interference ions off course via collisions with helium while leaving a significant amount of the smaller ions of interest untouched to reach the detector. The KED will reduce the number of ions of interest that reach the detector but this decrease should be far lower in relation to the interference ions. DRC on the other hand is a very powerful technique for analysis when it would be impractical to use KED. A classic example of where DRC is useful is in the analysis of iron 56, iron 56 has a significant interference with argon oxide. As argon is the primary nebuliser gas for ICP-MS and is oxidised in the high energy of the plasma it means that iron 56 cannot be measured effectively without taking specific precautions, namely using a different isotope of iron or changing the nebuliser gas to not argon. This is where DRC comes in: the dynamic reaction cell will utilise a gas (in our case ammonia) to react with and remove the interferences, by shifting the mass of the reacted ions away from that of the ions of interest.

When the interferences have been removed the sample passes into the final quadrupole which acts as a final mass filter to remove the last remnants of any ions in the range of mass to charge ratio that has been excluded, and finally the stream of ions that have made it this far reach the detector. The NexION has is a dual detector, with an analogue and digital component that work in tandem to ensure that the instrument has a very large range of detection. When the ions hit the detector, they create a pulse of charge that the detector measures. When the charge is small the instrument uses the digital detector, with a range of 0-2,000,000 counts at close to 2,000,000 counts the instrument will switch to the

analog detector which can increase the count limit to around 100,000,000. For reference an 80 nm gold nanoparticle will typically generate a response of about 250 counts. This allows the instrument to have a very wide range of detection from femtograms per litre to hundreds of milligrams per litre.

The mathematics behind single particle ICP-MS (and by extension single cell ICP-MS)

In the following pages mathematical formulas are described that can be used to calculate the diameter and mass of nanoparticle in samples run using an ICP-MS in single particle detection mode, this could be a dedicated application such as those found in a single particle ICP-MS instrument or a method that separates the particles into individual particles. These calculations allow for larger dwell time than those commonly found in Single Particle ICP-MS. The formulas were derived from a excel spreadsheet ²⁸ generated by RIKILT Wageningen UR as part of a service provided by Wageningen University and Research Centre, available as freeware from their website ²⁸. The institute provides a standard operation procedure for the spreadsheet ²⁸ and used two ICP-MS; a quadrupole based Thermo Scientific X-series 2, and a Thermo Finnigan Element 2, a sector field based ICP-MS ²⁸. It is important to note that the diameter of the nanoparticles assumes that the nanoparticles are spherical in nature and not of any other shape for example rod shaped although this is mathematically possible with complimentary techniques like Transmission Electron Microscopy (TEM) to provide the aspect ratio.

To calculate the nanoparticle diameter the NexION 300/350 uses Syngistix a programme that allows quick and easy analysis of nanoparticle size. The method

to which it follows has four main steps split into two phases, this begins with calibration of the instrument for the elements that would be analysed by firstly calculating the transport efficiency of particles, followed by calibration of a dissolved standard (and particulate standard but focus is on the dissolved standard). Then after the instrument has been calibrated the particles are analysed and calculations of each individual nanoparticles mass are used to calculate the diameter of the nanoparticle.

Calculation of transport efficiency (η_n)

In the NexION 300/350 there are primarily two methods that are used to calculate the transport efficiency; “Particle size” and “Particle concentration” method. Within the training notes provided by Perkin Elmer the particle size method is the method suggested to use for calculating the transport efficiency.

Using the particle size method requires both a particle and dissolved metal ion calibration with the results used to correct for the transport efficiency.

Nanoparticle standard calculation equations

A nanoparticle standard of known diameter and density is introduced into the ICP-MS and the mass of the nanoparticle is used to generate a number of values that are needed for calculation of the transport efficiency and later the sample nanoparticle. This analytical standard does not have to be necessarily of the same element of the nanoparticle that is to be analysed, and there are multiple reasons as to why this may be the case, for example the element may not have a standard particle. An example of this is in present in chapter four, which did not have a standard particle for the engineered particles but did have ionic standards for the

elements analysed which was enough in conjunction with a transport efficiency calculated with a known particle standard (gold), but it is preferable for the transport efficiency to be calibrated with the same element of the samples as this minimises the discrepancies between the instrumental response to the samples and calibrants.

The following values must be known for the particle standard; the size/diameter of the nanoparticle standard, the ionic and particle concentration of the nanoparticle standard, and the density of the nanoparticle. All these values should be either on the standard's data sheet or can be found online. The method of nanoparticle sizing that is employed by the instrumental programming and in the wider literature is to convert particle mass into spherical diameter, so to begin with the mass of the standard nanoparticle is calculated using equation 2.1.

Equation 2.1: Nanoparticle standard mass calculation.

$$M_p = \frac{\left(\frac{\pi \cdot d^3}{6} \cdot \rho\right)}{\omega_i}$$

Where M_p is the mass of the nanoparticle standard per event in grams, d is the diameter of the nanoparticle standard in cm, ρ is the density of the nanoparticle standard in g cm⁻³ and ω_i is the mass fraction of the element within the nanoparticle. Often M_p is presented in femtograms and the diameter of the nanoparticle is presented in nm, it is therefore important to convert to the correct units.

For example, if a BBI Solutions 40 nm gold nanoparticle standard was used for calibration, then to work out the mass of a single nanoparticle in the standard solution then first the diameter has to be converted from nm to cm, i.e. 40 nm to

0.000004 cm. The density of gold can be found online or in data books to be 19.3 g/cm³. In the case of BBI solutions the mass (g) per mL and the number of nanoparticles per mL are provided so it is a simple case of multiplying the calculated mass of the nanoparticle standard by the number of nanoparticles per mL to check if the mass is correct.

By using more than one nanoparticle standard during calibration then a calibration graph is constructed from the counts/response that are measured against the mass of the nanoparticle standard. From the calibration graph the equation of the line is determined and given the following terms as shown in equation 2.2.

Equation 2.2: Nanoparticle standard equation of the line.

$$Y = m_{rp} \cdot (M_p) + b$$

Where Y is the instrumental response (counts), m_{rp} is the linear slope of the calibration curve, M_p is the mass of the nanoparticle standard per event and b is the background noise response (counts).

For the transport efficiency m_{rp} is also needed after calibration of the dissolved standard.

Dissolved standard calibration for transport efficiency

A calibration series of elemental ionic standards of known concentration are introduced into the ICP-MS and the mass of each of the ionic standard are calculated using equation 2.3.

Equation 2.3: Dissolved standard mass of a particle,

$$M_D = q_{liq} \cdot t_{dt} \cdot C$$

Where M_D is the mass of the dissolved standard per event in grams, q_{liq} is the flow rate in $\text{cm}^3 \text{ ms}^{-1}$, t_{dt} is the dwell time in ms and C is the concentration of the dissolved standard in g cm^3 . As it was with the particle standards the units have to be equivalent to the nanoparticle standard calculations; this means that both the flow rate and concentration usually need to be converted; the flow rate is calculated in $\text{cm}^3/\text{minute}$ so needs to be divided by 60,000 (as there are 60,000 ms in a minute) to give a correct flow rate and the ionic concentration needs to be converted from $\mu\text{g}/\text{cm}^3$ to g/cm^3 by 1,000,000 (as a μg is 1 million times smaller than a g).

To work out the sample flow rate, a simple procedure is performed. A vial of fluid is filled to a known mass is allowed to run through the sample introduction tubes for a known amount of time before the change in mass is recorded. A rate equation is used constituting of three terms; m for the mass of fluid eluted, t for the time in minutes that the fluid was allowed to elute and ρ for the density of the fluid. This calculation is shown in equation 2.4.

Equation 2.4: Sample flow rate equation.

$$S_f = \frac{m}{t \times \rho}$$

Once the mass of the dissolved standard per event has been calculated for the ionic standards, then the standards can be analysed and the mass of the dissolved standard per event can be plotted against the counts in a calibration graph. From the calibration graph the equation of the line is determined and given the following terms as shown in equation 2.5.

Equation 2.5: Dissolved standard equation of the line.

$$Y = \frac{m_{diss}}{\eta_n} \cdot (M_D) + b$$

Where m_{diss} is the linear slope of the calibration curve, M_D is the mass of the dissolved standard per event, η_n is the transport efficiency and b is the background noise response (counts).

Final transport efficiency calculations

If it is assumed that the transport efficiency is equal for both the nanoparticle and ionic content in the solutions then the transport efficiency can be worked out using the two slopes of the curves by deriving equation 2.10 via equations 2.6-2.9.

At the point of intersection between the two calibration curves both the Y values are equal so it can be inferred that equation 2.2 is equal to equation 2.5 as shown in equation 2.6.

Equation 2.6: Equivalence in equations 3 and 4.

$$m_{rp} \cdot (M_P) + b = \frac{m_{diss}}{\eta_n} \cdot (M_D) + b$$

If the blank value (b) from the nanoparticle calibration curve is subtracted from both sides of equation 2.6 then the two blanks should negate each other and cancel out due to the background being assumed to be equal for both calibrations as shown in equation 2.7.

Equation 2.7: Removal of background count levels.

$$m_{rp} \cdot (M_P) = \frac{m_{diss}}{\eta_n} \cdot (M_D) + b - b$$

If both sides are multiplied by the transport efficiency (η_n) then the transport efficiency switches to the nanoparticle side as shown in equation 2.8 allowing the final step to occur in equation 2.9.

Equation 2.8: Multiplication of transport efficiency to both sides

$$\eta_n \cdot m_{rp} \cdot (M_p) = m_{diss} \cdot (M_D)$$

In equation 2.9 both sides have been divided by the mass of the nanoparticle standard (M_p) and gradient of the nanoparticle slope (m_{rp}); due to the point of intersection meaning that M_D is equal to M_p they will negate each other in the calculations.

Equation 2.9: Isolation of the transport efficiency.

$$\eta_n = \frac{m_{diss} \cdot (M_D)}{m_{rp} \cdot (M_p)}$$

As seen in the final equation (equation 2.10) the transport efficiency is calculated by dividing the two slopes to produce a ratio of dissolved ions to nanoparticles.

Equation 2.10: Final transport efficiency calculation.

$$\eta_n = \frac{m_{diss}}{m_{rp}}$$

Calibration of the dissolved standard

After the transport efficiency has been calculated the calibration of dissolved standard can be corrected to provide a correct M_D (mass of the dissolved standard per event) that incorporates the losses to mass of the dissolved standard per event from the transport efficiency.

To do this, equation 2.3 is modified to become equation 2.11 by including the term for the transport efficiency η_n .

Equation 2.11: Corrected mass of dissolved standard.

$$M_D = q_{liq} \cdot t_{dt} \cdot \eta_n \cdot C$$

Where M_D is the mass of the dissolved standard per event in grams, q_{liq} is the flow rate in $\text{cm}^3 \text{ms}^{-1}$, t_{dt} is the dwell time in ms, η_n is the transport efficiency and C is the concentration of the dissolved standard in g/cm^3 .

By using equation 2.11, a new calibration curve for the dissolved standard can be constructed and the linear gradient of the calibration curve is then used in the calculation of the nanoparticle mass. Depending on the element of interest within the nanoparticle, this calibration may be of a different element to that of the ionic standard used in the transport efficiency equations. The reason for this is simple, some elements do not have a suitable particle standard to which to calibrate the instrument for transport efficiency, examples of this are the analysis of hafnium doped titanium dioxide nanoparticles explored in chapter four ⁴⁰ and holmium doped sodium tetrafluoride titanium dioxide nanoparticles ³⁸; where there were no suitable standard particles for calibration. Instead of finding a particle standard, an ionic standard alone will provide all the relevant data required to analyse the nanoparticles.

Calculation of sample nanoparticle mass

After calibrating the instrument for analysing the element of interest within the particles, the samples are run and a series of pulse events occurs within the instrument as each particle hits the detector as can be seen in figure 2.2 where multiple large pulses can be seen.

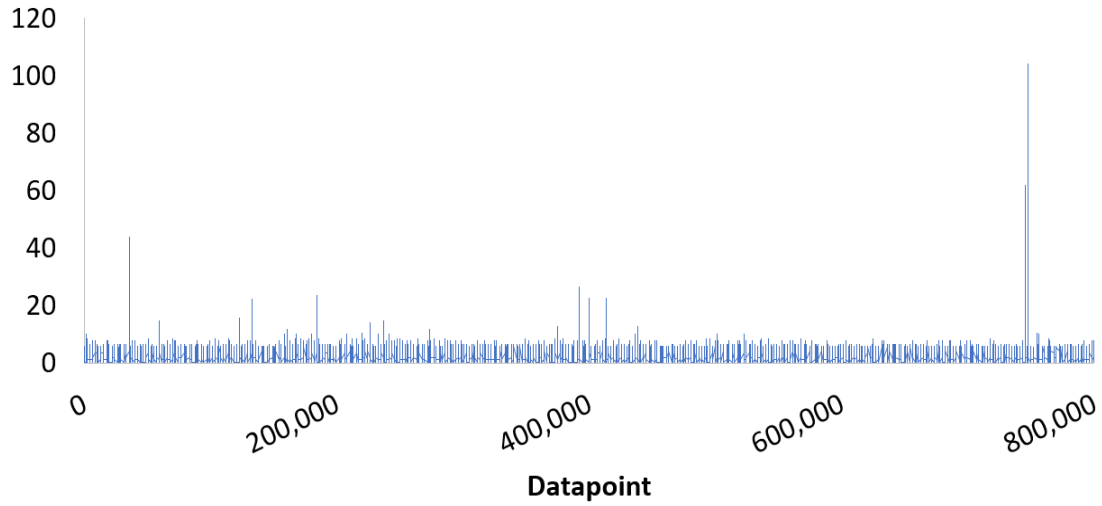


Figure 2.2: Live response of a sample of nanoparticles (or cells), with 800,000 individual data points analysed over a 40 second period. While it seems as there is an almost constant level of response, if this figure was zoomed in to show only few datapoints it would become clear that there are large gaps where no ions hit the detector. The larger peaks are the result of particles (or cells).

Each of the high intensity pulses relates to an individual nanoparticle and as such can be used to calculate the mass of the nanoparticles in a sample, by using equation 2.12 – note that the small intensity pulses represent the ionic background.

Equation 2.12: Nanoparticle mass calculation.

$$M_p = f_a^{-1} \cdot \left[\frac{\left(\frac{(I_p - I_{Bgd})}{\eta_i} \right)}{m} \right]$$

Where M_p is the mass of the nanoparticle in grams, f_a^{-1} is the mass fraction of the element in the nanoparticle, I_p is the counts for the pulse, I_{Bgd} is the background level of counts, η_i is the particle ionisation efficiency which is assumed to 100% and m is the linear gradient of the dissolved standard calibration curve. Due to the

previous step in which the ionic standard calibration was calculated, the mass of the particle is calculatable from the ionic standard calibration curve.

The molar mass ratio of the nanoparticle is a factor that takes into account the amount of mass the analyte has, compared to the total mass of the particle. For single element nanoparticles this ratio will be 1 but for multi-element nanoparticles primarily only one element will be quantified and thus the counts that this element exhibits will be a portion of the total mass of the particle and as such the counts need to be corrected for this. Equation 2.13 provides the calculation for the molar mass ratio.

Equation 2.13: Molar mass ratio equation.

$$f_a^{-1} = \frac{\text{Molar Mass Particle}}{\text{Molar Mass Analyte}}$$

Calculation of the sample nanoparticle diameter

Finally, after determining the mass of the nanoparticle the diameter of the nanoparticle can be calculated with a simple tweak to the equation of the diameter of a sphere to incorporate the effects of density on the nanoparticle, by including the density of the particle into the equation (equation 2.14).

Equation 2.14: Diameter of spherical nanoparticle.

$$d = \sqrt[3]{\frac{6 \cdot M_p}{\pi \cdot \rho}}$$

Where d is the diameter of the nanoparticle in cm, M_p is the mass of the nanoparticle in grams and ρ is the density of the nanoparticle standard in g cm⁻³. If calculated correctly (i.e. all the units throughout all the equations have been

equivalent) then the diameter will be calculated in cm; to convert to nm the diameter needs to be multiplied by 10,000,000.

For an example on how these calculations would work on a theoretical nanoparticle see appendix 1.

Line Start differential centrifugation sedimentation (DCS)

Line start differential centrifugation sedimentation (DCS) is an analytical technique that uses a density gradient to determine the size and density of a particle. A known density gradient of sucrose solutions of various concentrations is prepared within a spinning disk and samples are introduced to the centre of the disk. When the density of the particle is larger than that of the density gradient the particle will move to the outer edge of the disk whereby a photodiode is used to detect the particle. Stokes' law of sedimentation (or settling velocity) is used to calculate the drag force of spheres within viscous fluids by measuring the time required for the particles to settle a known distance through the fluid of known density or viscosity. DCS is able to measure the size of a particle by operating under the assumption that since all particles enter the centre of the disk, particles of the same size and density will have the same sedimentation time⁸¹⁻⁸³. DCS utilises a variation of Stokes' equation that takes into account the variation of g-force that arises with distance from the centre of rotation. Equation 2.15 shows the DCS variation of the Stokes law of sedimentation⁸¹⁻⁸³. Using DCS, all components of equation 2.15 are known apart from time, thus to determine the size of a nanoparticle the instrument is calibrated to a particle of known size and density which is sedimented over time. When calibrated, DCS becomes one of the most precise techniques for particle size determination with high differentiation

between nanoparticles with even small size differences, such as with a coating or protein corona, or between particle monomers and particle dimers or larger agglomerates ^{82,83}. DCS was used here as a confirmatory technique for nanoparticle size determination by spICP-MS.

Equation 2.15: Modified Stokes equation utilised in DCS.

$$D = 2 \cdot \sqrt{\frac{18\eta \cdot \ln\left(\frac{R_f}{R_i}\right)}{(\rho_p - \rho_l) \cdot \omega \cdot t}}$$

where D is the particle diameter in cm, η is the density gradient fluid viscosity in poise (equivalent to $1 \text{ g cm}^{-1} \text{ s}^{-1}$), R_f is the final radius that the particles will inhabit (end point) in cm, R_i is the initial radius that the particles will inhabit (the start point) in cm, ρ_p is the particle density in g cm^{-3} , ρ_l is the density of the density gradient fluid in g cm^{-3} , ω is the rotational velocity in radians sec^{-1} and t is the time required to sediment particles from R_0 to R_f in seconds ^{82,83}.

Dynamic Light Scattering (DLS)

Dynamic Light Scattering (DLS) measures the diffusion rate of particles due to Brownian motion; this is achieved by measuring the intensity of Raleigh scattering from a laser source.

From Raleigh scattering of light by the Brownian motion of particles the particle size can be calculated using the Stokes-Einstein equation. The size of a nanoparticle dictates the amount of light that is scattered, with larger nanoparticles having larger scattering, which scales with $1/D^6$. However, with the larger scattering there is the possibility that smaller particle signals will be lost within those of the larger nanoparticles. DLS is highly dependent on knowledge of

the temperature, viscosity, ionic strength of the medium and the shape of the particle as these all impact on the Brownian motion of a particle ^{84,85}. DLS is the most commonly used particle sizing technique due to its relative speed of preparation and analysis, and its ease of use. However, it does not provide elemental composition analysis or density analysis of particles. It also tends to overestimate the size of inorganic particles as it provides the hydrodynamic particle size, and has problems identifying small particles in solutions with larger particles as larger particle light scattering causes loss of differentiation between particles ^{84,85}. There are three main outputs for size analysis, the intensity of the light scattering, calculated mass of the particles and number of particles; within chapter four number-based distributions for size are presented as this was found to give the clearest and most repeatable results.

Transmission Electron Microscopy (TEM)

Transmission Electron Microscopy (TEM) has been a staple of cell biologist for over 80 years with the capability to view cells at nanoscale the technique has since branched out to a multitude of uses from cells to microplastic and nanoparticle analysis, with the ability to truly see the shape and size of a sample there are many analytical applications ⁸⁶. TEM utilises a beam of electrons transmitted through a sample to provide an image of very high resolution allowing for analysis of particle size, shape and morphology. The disadvantages are the time for preparation and analysis, cost and that only a small representation of the sample is analysed unlike spICP-MS, DCS, and DLS where the entire population of the particles is analysed. Furthermore, TEM is an *ex-situ* method, i.e. requires particles to be removed from

media and characterised in dry form, resulting in loss of information relating to suspension properties ⁸⁶.

Cell Lines

Metals and nanoparticles are regularly used in toxicity and uptake studies within cell lines as either a measure of the affect exposure to anthropogenically produced nanoparticles may have on cells or to measure the drug delivery capabilities of engineered nanoparticles. In many cases the mode of toxicity from the released ions needs to be able to distinguished between the fraction of ions and particles in the sample matrix initially, and those internalised in cells / organisms. In this regard SC-ICP-MS and spICP-MS can be a powerful tool due being able to detect and differentiate between ions, cells and particles within cells at an individual cell level as outlined in the studies in chapter five, six and seven.

A549 Type II pulmonary epithelial cell line

The A549 cell line was first cultivated in 1973 by Donald Giard, who was attempting to establish new cell lines for research by mincing cancer tissues to pieces of around 2mm, covering the tissue with bovine calf serum and incubating at 37°C for a week. One of the cell lines that was established from this work was the rapidly growing A549 ⁸⁷. A549 is used as a Type II pulmonary epithelial cell model due to its ability to mimic the biological responses of lung cells ⁸⁸. Modern practice to prepare A549 cells is to mount the cells on a plastic culture flask or Petri dish ⁸⁹ and the cells are maintained by addition of a growth medium containing bovine foetal serum ^{6,73,88,90}. A549 cells are often cultured for at least 24 hours ^{73,88} by incubating at 37°C under a 5% carbon dioxide atmosphere

6,73,88,90. When A549 cells are needed for analysis they are un-mounted using an appropriate chemical like EDTA ⁸⁸ or NAC ⁷³.

HeLa Cells

The HeLa breast carcinoma cell line is one of the oldest and most used cell lines in biological cell work. Extracted from Henrietta Lacks ⁹¹ in 1951 from a cervical biopsy, the cell line was immortalised and has been a key cell line within biological research ever since with growing evidence that the cell lines' survivability and prolificity to grow have resulted in it becoming a containment in cell culture work. Mentioned in over 50,000 published pieces of work, HeLa has been widely used for a variety of research projects from studies into polio ⁹² and Human papilloma virus (HPV) ⁹³ to genome mapping ^{94,95}.

MDA cells

MDA-MB-231 cells are an immortalised breast carcinoma cell line extracted from a 51-year-old female, and is used in studies of triple negative cancer cells. Triple negative means that the cell line does not have any of the three most common cancer cell receptors making them much harder to target via conventional cancer treatment methods ⁹⁶. MDA cells have been used as a model cell line for research into the effectiveness of cancer treatments against triple negative cell lines ⁹⁶.

Isopods

Isopods are an order of crustacean that can be found both terrestrially and aquatically ⁹⁷. The order is colloquially known as woodlice, but there are many species of isopod of which many are useful as model organisms for research. Because many isopods are detritivores, they can provide crucial environmental

ecotoxicological data of soil systems ⁹⁸ that leads isopods to being an ideal model organism for research.

Daphnia (pulex and magna)

Daphnia magna and *daphnia pulex* are two commonly used species of Daphnids for analytical research. Daphnids are planktonic crustaceans ⁹⁹, which feed on small suspended particles in a water system; the organism is widely used in research due to their transparent carapaces, being transparent allows for ease of study into the uptake and inter-bodily functions such as studies of the organs. Present in wide variety of water systems they can also function as a model organism for changes in the chemical structure of a body of water, such as in environmental and toxicological studies ^{100–103}. The University of Birmingham maintains a daphnia laboratory and is involved in numerous studies into nanoparticles, microplastics and environmental aspects measured using daphnia ^{104–106}. The daphnia that were used in this body of work were cultivated within the University of Birmingham daphnia laboratory.

Chapter Three

Development of a standard operating procedure for single particle ICP-MS

Aims and Overview

The aims of this chapter are to present a standard operating procedure (SOP), firstly for the single particle ICP-MS and then a working procedure for the operation of the single cell ICP-MS, which at the time of development either did not exist as in the case of single cell ICP-MS where the technique was still novel or for single particle ICP-MS was in a confusing uneasy to follow state. By developing and writing a standard method that could be utilised throughout the body of work that this thesis covers subsequent method development could build on a basic foundation.

The SOP was developed by optimising the working conditions of the ICP-MS to a level that is deemed acceptable within a research laboratory. To achieve this, a silver nanoparticle standard suspension was tested for size and concentration before being used to determine the standard working particle concentration, and optimum particle storage method. At the end, these results allowed for a greater understanding into the instrument's operation and the development of a standard operating procedure that has been published online ¹⁰⁷ to enable its use outside the University of Birmingham.

After the development of a standard operating procedure for the single particle ICP-MS, the process was repeated to produce a single cell ICP-MS standard

operating procedure. Both the single particle ICP-MS and single cell ICP-MS standard operating procedures were used as a basis of analysis for all subsequent chapters in which the changes from the standard method established in this chapter are listed and described in detail.

Materials and Methods

Chemicals and Material

Silver nanoparticle standard analysis: Silver nanoparticle standards of diameter 20 nm, 40 nm and 80 nm were obtained from BBI solutions. 1,000 mg dm⁻³ (1,000 ppm) ionic silver standards were obtained from Perkin Elmer. The 40 nm silver nanoparticle standard acquired from BBI solutions was also used as the sample for Standard nanoparticle concentration examination. An in-house synthesised silver nanoparticle was used as our sample for nanoparticle storage analysis its size and concentration were unknowns before analysis.

ICP-MS: A PerkinElmer ICP-MS Setup Solution was obtained for the setup and daily calibration of the instrument. Ultrapure water is used for flow rate calculations.

Sample preparation/Extraction procedure

Silver nanoparticle standard analysis: The ionic standard and nanoparticles were all diluted in triplicate with aliquots into either 1.5 or 5 dm³ falcon centrifuge tubes and filled up to the mark with deionised water that was pipetted with calibrated 5,000 and 1,000 µL pipettes. The dilution protocol used was as follows:

Ionic standard preparation: The ionic standards were prepared from the stock solution of ICP-MS Silver standard, with a starting concentration of 1,000 mg dm⁻³

³ (1,000 ppm) that was sonicated and diluted with ultra-pure water using the dilutions outlined in table 3.1.

Using the calculation shown in equation 3.1, the following dilutions were performed to provide the ionic standards for calibration.

Equation 3.1: Standard dilution equation using concentration and volumes.

$$Concentration_1 \times Volume_1 = Concentration_2 \times Volume_2$$

where both concentration terms have the units, and both volume terms have equivalent units.

Table 3.1: The dilutions used to reach desired concentrations for the ionic silver calibration standards.

Concentration ₁ (mg dm ⁻³)	Volume ₁ (dm ⁻³)	Concentration ₂ (mg dm ⁻³)	Volume ₂ (dm ⁻³)	Concentration ₂ in µg dm ⁻³
1,000	0.0005	10	0.05	1,000
10	0.0005	0.1	0.05	100
0.1	0.0005	0.001	0.05	1
0.1	0.0010	0.002	0.05	2
0.1	0.0015	0.003	0.05	3

Applying the above dilution sequence using calibrated pipettes provides an estimated maximum error of 2.3% from the desired concentrations as determined using the estimated errors described within the pipette manual.

Nanoparticle standard preparation: Nanoparticle standards are prepared in the following method using BBI Solutions ^{34,54,99} silver standards.

Each nanoparticle solution starts with a differing number of nanoparticles per mL, it is recommended that standards need to have around 50 nanoparticles dm⁻³; as

such each of the BBI solutions will need to be diluted in a different way. Pipette inaccuracy is of less importance here as the particle concentrations need to be just around 50 nanoparticles dm^{-3} .

The method of dilution is the same using the calculation found in equation 3.1.

Where the units are the same for both concentration terms and also the volume terms are of the same units.

Standard nanoparticle concentration: For the 40 nm nanoparticles the BBI nanoparticle Solution is provided at a nanoparticle concentration of 9.00×10^7 nanoparticles per dm^{-3} , after dilution of the standard by 1000, aliquots are taken to dilute the standard to the correct levels shown in table 3.2.

Table 3.2: The multiple dilutions of the original silver particles and the exact volumes that were used for those dilutions.

Concentration ₁ (nanoparticles per dm ⁻³)	Volume ₁ (dm ⁻³)	Concentration ₂ (nanoparticles per dm ⁻³)	Volume ₂ (dm ⁻³)
1,000,000	0.00005	1,000	0.05
1,000	0.00015	10	0.015
1,000	0.00038	25	0.015
1,000	0.00060	40	0.015
1,000	0.00075	50	0.015
1,000	0.00090	60	0.015
1,000	0.00113	75	0.015
1,000	0.00150	100	0.015
1,000	0.00188	125	0.015
1,000	0.00225	150	0.015
1,000	0.00263	175	0.015
1,000	0.00300	200	0.015
1,000	0.00338	225	0.015
1,000	0.00375	250	0.015
1,000	0.00413	275	0.015
1,000	0.00450	300	0.015
1,000	0.00750	500	0.015

Nanoparticle storage analysis: To test the standardisation, in-house synthesised silver nanoparticles were used as unknowns. The silver nanoparticles were diluted ten-fold in ultrapure water by taking 5,000 μL of the stock solution and diluting with 45,000 μL of ultrapure water to give an intermediate stock which was then separated into 27 sample flasks by taking 500 μL of the intermediate stock and dilution with either 9,500 μL of ultrapure water or 4,500 μL of ultrapure

water and 5,000 μL of HPLC grade methanol to give final samples volumes of 10,000 μL and 200x dilution.

The samples were in made triplicate with the guidelines outlined in table 3.3:

Table 3.3: The outline of the method of storage that each sample utilised and the timeframe to which the particles were left stored.

In-Box	<i>Left in the box and darkness for 48 hours before analysis</i>
Out-Box	<i>Left on top of box for 24 hours before being placed in box and darkness for 24 hours before analysis</i>
Fridge	<i>Left in fridge and darkness for 24 hours before being placed in box</i>
Freezer	<i>Left in freeze and darkness for 24 hours before being placed in box</i>
Liquid Nitrogen	<i>Left in Liquid nitrogen and darkness for 24 hours before being placed in box</i>
50% Methanol Fridge	<i>Left in fridge and darkness for 24 hours before being placed in box</i>
Blank	<i>Left in the box and darkness for 48 hours before analysis</i>
Methanol Blank	<i>Left in the box and darkness for 48 hours before analysis</i>
Fresh Sample	<i>Prepared one hour before analysis</i>

Instrumental optimisation and analysis

A Perkin Elmer NexION 300 ICP-MS was used for analysis. At the start of analysis, the instrument was calibrated using the PerkinElmer set up solution. After the instrument was shown to be calibrated for general use the flow rate was calculated using ultrapure water uptake over three minutes. Next the transport efficiency was calculated using the silver nanoparticle and ionic standards; unfortunately due to the original instrument PC suffering serious memory leaks that caused large amounts of data to be lost the transport efficiency and flow rate are not available

to be stated. Backups from this time were not retrievable due to the same memory leaks resulting in loss of the backups as well. Instrument parameters are listed in table 3.4.

Next after the instrument had been calibrated, flow rate and transport efficiency determined; standard calibrations of the silver nanoparticles and ions were performed. Finally, the samples were analysed in replicate using spICP-MS mode to determine the size and concentration of any silver nanoparticles present.

Table 3.4: Instrumental parameters used during single particle analysis of silver nanoparticles.

Nebulizer Gas Flow [NEB]	1.12
Auxiliary Gas Flow	1.2
Plasma Gas Flow	18
ICP RF Power	1600
Flow Rate	N/A*
Transport Efficiency	N/A*
Dwell Time	80 us

*Data was lost in 2018 due to memory leaks within the original instrument PC. Backups from this time were not retrievable.

QA/QC criteria

Quality assurance was obtained by the daily instrumental setup and by statistical analysis of multiple replicates for each sample. Due to the nature of the instrument being sequential it is not possible to use an internal standard as the internal standard would not be analysed with each sample. In lieu of the presence of an

internal standard the certified silver nanoparticle standards were routinely compared to the limits of size as stated in the certification.

Statistical analysis

The statistical analysis that was performed upon the results gathered within this chapter are R^2 correlation analysis of the standard ionic and particle calibration. A R^2 value of less than 0.996 was not utilised and the calibration was repeated either by reruns or remakes of the standards. Samples were all analysed at least three times in replicate and the average was calculated using the mean. From the mean the standard deviation was used to identify outliers that would be investigated on a sample by sample basis.

As described later in this chapter the analysis of nanoparticles using single particle ICP-MS is explained.

Results/Discussion

Silver nanoparticle standard analysis

Each of the silver nanoparticle standards was run on three different occasions with five replicates which was then averaged for each occasion (noted as samples 40 nm -1, 40 nm -2, etc.). This was to measure the reproducibility and the stability of the particles over multiple analyses, both as a measure quality control for the standards and the laboratory. This was also to ensure that there was a statistically significant level of replicates. The size of both 40 and 80 nm nanoparticles are very close to the sizes that stated by BBI, this can be visually seen in Figure 3.1 and Figure 3.2 with the disparity between the replicates being very low with all replicates being within less than 1 nm.

In Figure 3.1 is a near normal distribution with most of the peak curve being at around 40 nanometres, however there was some particle responses that trended towards a larger side of the size distribution at around 80nm but this is not significant and does not suggest any meaningful secondary particle present as the frequency for these peaks is often less than 1 count and does not show a distribution that would correspond to a nanoparticle.

The maximum peak in Figure 3.2 is measured to be about 80 nm with some smaller peaks at around 40 nm. The peaks at the lower end of the size range have a maximum frequency of two counts which is significantly smaller to the peak maximum of 138 counts found for the peak at 80nm and again should not be counted as any significant response.

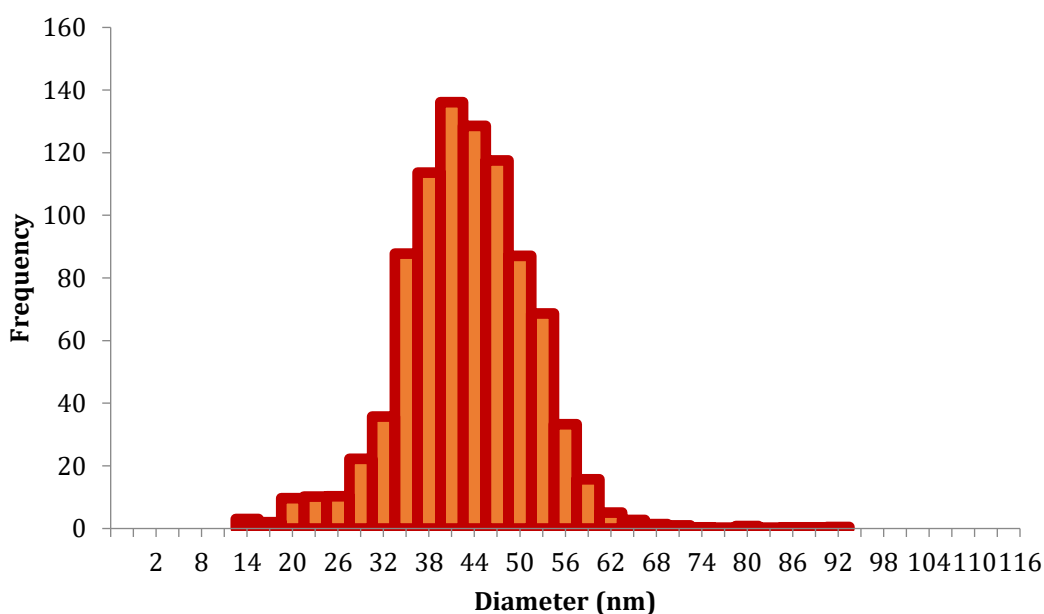


Figure 3.1: The size distribution of 40 nm silver nanoparticle standards with a bin size of 3 nm. There is a maximum peak in the figure at 41 nanometres that corresponds closely to the stated size from BBI.

From the analysis of the 40 nm silver nanoparticles the particle number concentration measured by the spICP-MS was over 7 million particles per dm^{-3} (see table 3.5) which is much higher than the concentration stated by BBI solutions at 1 million particles per dm^{-3} . The exact reason for such disparity between concentration stated by the manufacturer and experimentally obtained results is unknown but the concentration showed to be stable over multiple repeats with minimum variance of 1.98% between the three replicates of five repeats. The 80 nm particles in comparison are much closer to the stated concentrations from BBI solutions of 1.1 million particles per dm^{-3} , compared with 1.3 million particles per dm^{-3} measured using the spIC-MS. The replicates again had minimum variance 0.79%. The low variance between the replicates suggests a high repeatability and that the concentrations determined for the nanoparticles are of good validity, even if they differ from the ones stated by BBI solutions.

Table 3.5: The average diameter and particle concentration of five replicates that were repeated three times for both 40nm and 80nm silver nanoparticles.

Standard	Diameter (nm)	Concentration (particles/ dm^3)
40 nm – 1	41.77	7,119,599
40 nm – 2	41.87	7,349,546
40 nm – 3	41.73	7,384,923
Mean	41.79	7,284,689
Variance (RSD)	0.17%	1.98%
80 nm – 1	80.34	1,334,401
80 nm – 2	80.21	1,323,080
80 nm – 3	80.01	1,321,666
Mean	80.18	1,322,020
Variance (RSD)	0.21%	0.79%

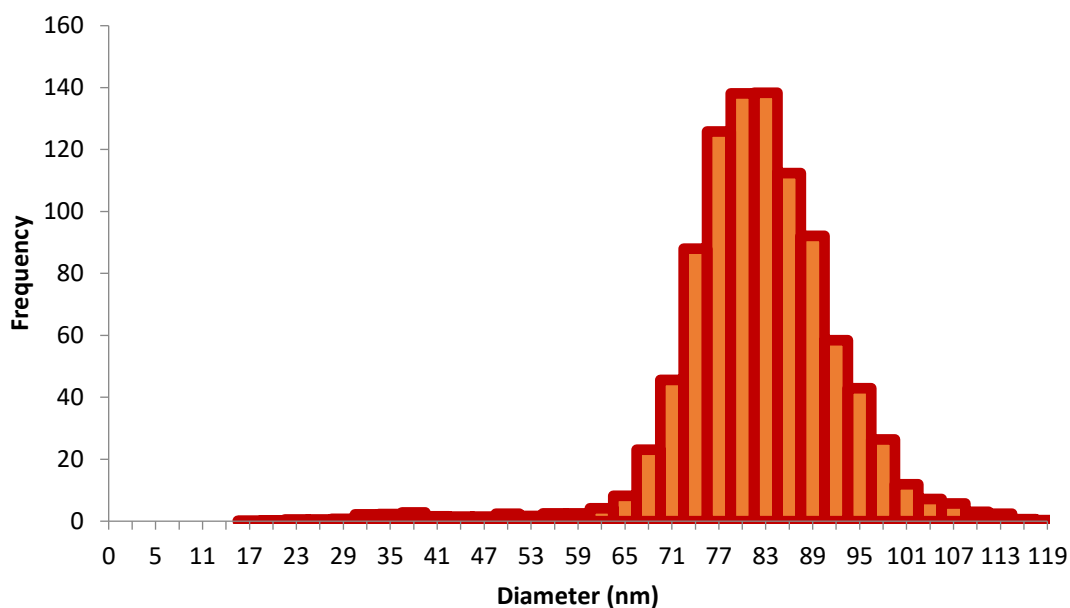


Figure 3.2: The size distribution of 80 nm silver nanoparticles with a bin size of 3 nm. The maximum peak is measured to be about 80 nm with some smaller peaks at around 40 nm.

Standard nanoparticle concentration

The results for the particle diameter against concentration show that as the concentration of the nanoparticles increases there is also increase in the size of nanoparticle diameter, the size of the nanoparticles should not increase due to the same nanoparticles being measured irrelevant of the concentration of the particle assuming that the nanoparticle have not agglomerated or dissolved.

The increase in the size of the particles as the concentration of the particle increases has a couple possible explanations; firstly, as an increasingly higher concentration of particles enter ICP-MS the detector becomes saturated. This results in the ionic background baseline measured by the detector increasing to

the level at which average sized particles are indistinguishable from one another; only larger particles are significantly distinguishable in this situation.

Alternatively, another possible reason for the increase in particles size is due to multiple nanoparticles hitting the detector within the dwell time. Possibly due to the high concentration of nanoparticles in the sample the rate to which an individual nanoparticle hits the detector is quicker than the dwell time, this will result in a larger signal measured during each dwell time artificially increasing the nanoparticle diameter. The nanoparticle silver standard increase in mass from 5.2×10^{-16} g at low concentrations (10,000 to 100,000) to 1.4×10^{-15} g and 2.4×10^{-15} g at 500,000 particles mL^{-1} and 1 million particles mL^{-1} represents four times increase of particle mass over 10,000 particles mL^{-1} .

Conversely when we look at the samples with low concentrations (i.e. 10,000, 25,000, and 40,000 nanoparticles mL^{-1}) it can be seen that the size of the particles is close to that stated by the manufacturer for the silver nanoparticle standard. This strongly suggests that at these lower concentrations there is strong confidence in the spICP-MS size measurements.

However, as these nanoparticles were analysed there is a clear trend to a lower instrumental response from the detector, with the average response for the lowest concentration (10,000 nanoparticles mL^{-1}) being 20 counts which when compared to the recommended concentration for nanoparticle analysis (around 50,000 particles mL^{-1}) is only about a quarter of the 83 counts that was measured at that concentration. Visually this is shown in Figure 3.3 with 10,000 particles mL^{-1} having a smaller response than concentrations of up to 250,000 particles mL^{-1} , Table 3.6 shows the exact responses for each concentration. While there is a lower

response for lower concentration there does not seem to be any effect on the measured size of the nanoparticles. There is a clear trend of rapidly increasing frequencies from the lowest particle concentration of 10,000 particles mL⁻¹ with a response of 20 counts to the maximum at 200,000 particles mL⁻¹ with 167 counts before rapidly decreasing at higher concentrations.

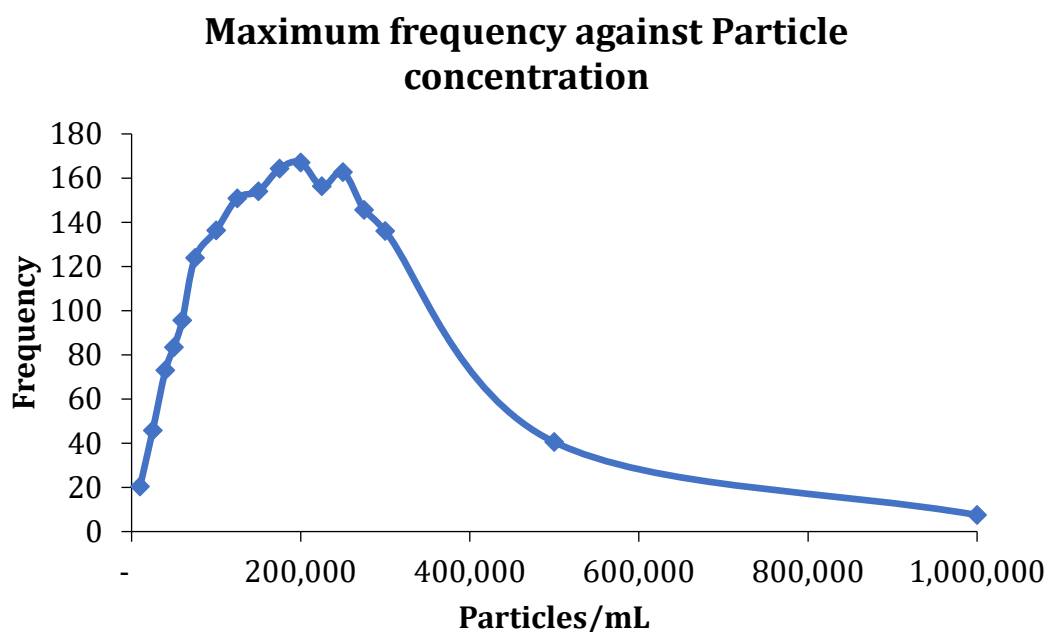


Figure 3.3: The response of each concentration of silver nanoparticles tested with the particle concentration against the maximum frequency for that concentration.

The mean diameter of the particles within the working concentration range of 10,000 to 150,000 particles mL⁻¹ are close to that stated by the manufacturer for increases; figure 3.5 shows this increase in nanoparticle diameter, with both the modal and mean the silver nanoparticle standard at 46 – 50 nm with the size increasing as the concentration average nanoparticle size, with the modal nanoparticle size consistently lower than the mean. As the concentration increases there is an increase in the particle size from 46 nm to 76 nm, with a slower increase in particle size in concentrations up to 150,000 mL⁻¹. Additionally,

the increase in nanoparticle concentration within the working range also sees an increase in the response from the detector with the lowest concentration sample (10,000 particles mL⁻¹) having a frequency of 20 counts and the highest concentration sample (150,000 particles mL⁻¹) having a frequency of 154. Note that this frequency increase reaches its maximum at 200,000 particles mL⁻¹ with a frequency of 167 and has a nanoparticle size that is 2 nm larger than the standard particle size range.

When the concentration gets above 300,000 particles mL⁻¹ we start to see significant amounts of increases in the diameter with the sample at 500,000 particles mL⁻¹ having a size of 64 nm and 1 million particles mL⁻¹ having a size of 76 nm. Conversely with the increase in diameter the frequency rapidly decreases with the 1 million particles mL⁻¹ sample having a frequency of 7 which is even lower than that of the 10,000 particles mL⁻¹ response of 20.

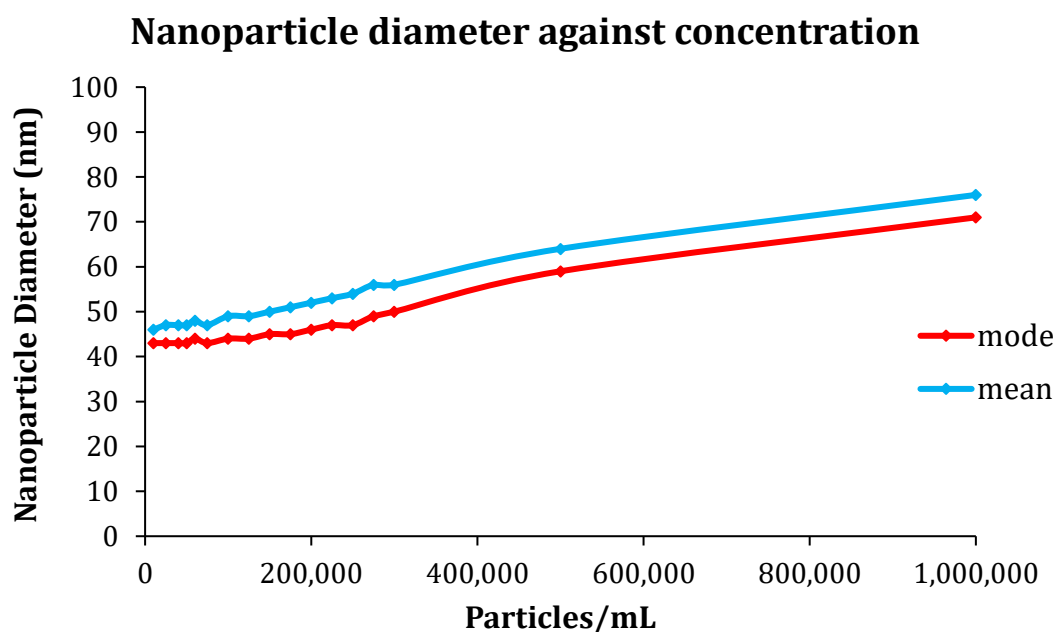


Figure 3.4: The increase in size of silver nanoparticles as the nanoparticle concentration increases.

As a result of the work that was done in determining the effect of particle number concentration on size, the working range for the instrument for subsequent chapters of the thesis has been kept in the concentration range of between 10,000 and 300,000 particles mL⁻¹ with confidence that lower concentrations of particles are detectable at a standard that is acceptable by the quality control criteria set in our laboratory. The reason that we will use a concentration range up to 300,000 particles mL⁻¹ is due the still identifiable differentiation between particles that is not seen in the higher concentrations where only large particles can be distinguishable from the background. Above 300,000 particles mL⁻¹ the particles begin to merge into the background.

Table 3.6: Results of the mean diameter and response of various silver nanoparticle dilutions.

Ag particle concentration (particles mL ⁻¹)	Mean diameter (nm)	Frequency (counts)
10,000	46	20
25,000	47	46
40,000	47	73
50,000	47	83
60,000	48	96
75,000	47	124
100,000	49	136
125,000	49	151
150,000	50	154
175,000	51	164
200,000	52	167
225,000	53	156
250,000	54	163
275,000	56	146
300,000	56	136
500,000	64	40
1,000,000	76	7

Comparison of storage techniques

There were eight different methods of nanoparticles storage tested on the 80 nm silver nanoparticle standard, in addition there are two blanks. Of these, seven required preparation of the nanoparticles by dilution at the start of the exposure and the final (8th) method involved fresh dilution of the particles just before analysis. The first methods of storage were labelled In-Box, wherein after the particles were diluted, they were placed into an opaque box that prevented exposure to ultraviolet light; this ensured that although the particles were exposed to the standard ambient temperature and atmospheric pressure within the lab, they were not affected by ultraviolet light. Building from the In-Box storage was Out-Box storage in which the silver nanoparticles were placed on top of the opaque box used for In-Box variants. By placing the Out-Box samples as close to the In-Box sample the aim was to ensure minimum variance of environmental conditions between the two samples while exposing the Out-Box samples to ultraviolet light. The two samples were placed on a secluded windowsill within the lab to minimise disturbance by other laboratory users and to ensure the Out-Box samples were exposed to sunlight.

The next three samples were Fridge and Freezer, after being diluted the samples were placed either in the fridge where the pure stock was being stored or into a freezer. The main aims for the Fridge sample was to observe the effects that dilution had on the particles when stored in the same conditions as the stock solution, and for the Freezer samples it was expected that due to the freezing of the water in the samples the particles become denatured and physicochemical

changes in size could take place. To compare whether it was the formation of ice crystals in the particle that causes the particle size to change or just the freezing processes itself the next sample was Liquid Nitrogen where the diluted silver nanoparticles were frozen rapidly with liquid nitrogen preventing the formation of ice crystals in the sample.

The last two of the diluted storage techniques attempted to prevent the freezing of the sample matrix by mixing water with methanol in a 50:50 ratio. At this ratio of methanol (alcohol) to water the freezing temperature of the sample matrix is reduced to below freezing, stopping the samples from freezing in the freeze.

The final sample (Fresh) was made fresh up on the day from undiluted stocks, used as a baseline for storage of the nanoparticles. With the sample being freshly made on the day, the nanoparticles in this sample were exposed to the minimum amount of outside conditions, a viable storage technique was deemed to be any that maintained a nanoparticle size and concentration equivalent to the Fresh sample.

Additionally, there were two blanks; a ultrapure water blank and a 50% methanol blank, the tabulated results are shown in table 3.7.

The analysis of the 80 nm silver nanoparticles through the various storage techniques can be broken down into effects observed for three main variables: nanoparticle size, nanoparticle concentration, and ionic concentration of silver in each sample.

Regarding the size that was determined for each sample it is observed that all but two (50% methanol fridge and fridge) have decreased in size by about 20 nanometres. There is no significant difference between the In-Box, Out-Box,

Liquid Nitrogen samples, and while the Freezer sample is slightly smaller at 54nm to 59 nm for the In-Box sample this is not significantly smaller than the other samples that have decreased in size (see figure 3.5). The two samples that have not changed in size are the two that were stored in the fridge; this is in agreement to previous work that suggests that nanoparticles should be stored at low temperatures ^{68,108-112}

Table 3.7: The particle concentration, ionic concentration and particle size of various samples of 80nm silver nanoparticles that were stored in a variety of methods both diluted and undiluted concentrations are shown.

Sample	Particle Concentration (ppb)		Ionic Concentration (ppb)		Particle size (nm)
	Diluted	Undiluted	Diluted	Undiluted	
In-Box	15,808	1,580,874,778	0.87	87,383	59
Out-Box	14,444	1,444,463,598	0.88	87,782	63
Fridge	22,339	2,233,966,664	0.22	2,234	80
Freezer	8,198	819,868,568.76	0.71	70,729	54
Liquid Nitrogen	13,940	1,394,010,147	0.93	92,889	62
50% Methanol Fridge	29,973	2,997,308,682	1.82	181,543	81
Blank	92	92	0.33	33,477	22
Methanol Blank	49	49	0.06	5,877	47
Fresh Sample	221,983	2,219,838,596	0.17	1,666	82

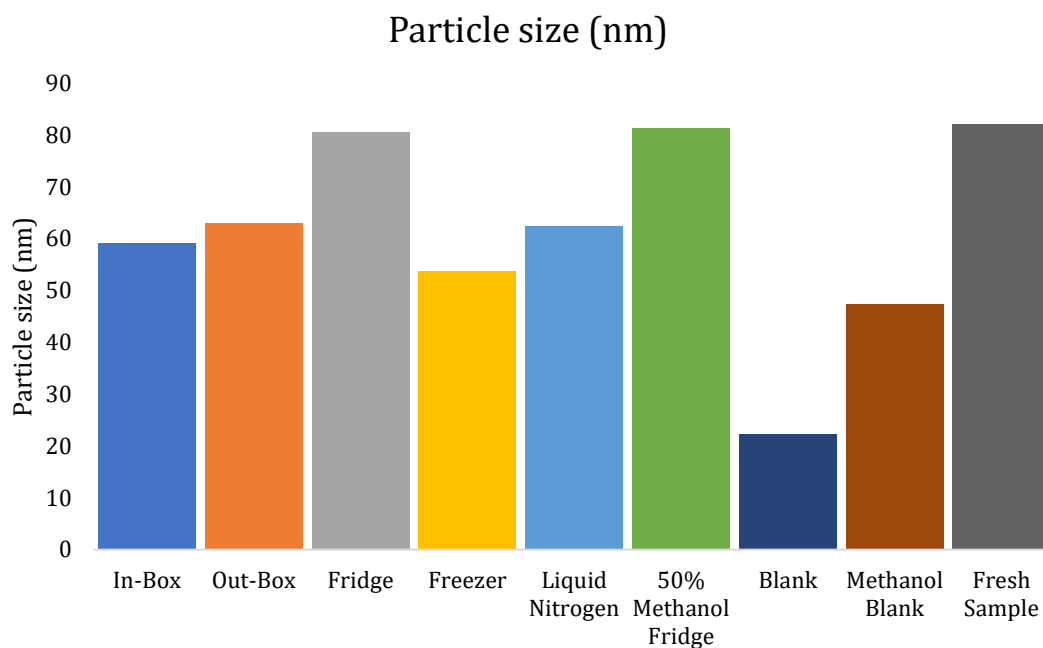


Figure 3.5: The varying sizes of 80nm silver nanoparticles after being stored with a variety of methods. There is a close size correlation between the freshly made sample and the two fridge samples (Fridge and 50% Methanol Fridge) while there is a decrease in nanoparticle size for all the other samples.

Considering the effects on particle concentrations (see Figure 3.6) within the samples, it can be seen that there is a decrease in the particle concentrations for most of the samples with only the Fridge sample having an undiluted particle concentrations that is statistically close to the Fresh sample with a concentration difference of only 0.6%, both having a undiluted particle concentration of 2.2 million particles per dm^{-3} . The 50% methanol fridge sample had significantly (25%) larger particle concentration and all the other samples have significantly less particle concentrations than the fresh sample. This loss in particle concentration is offset by the dramatic increase in ionic silver concentration with concentrations around 80,000 parts per billion compared to the fresh sample with ionic concentration of 1600 parts per billion.

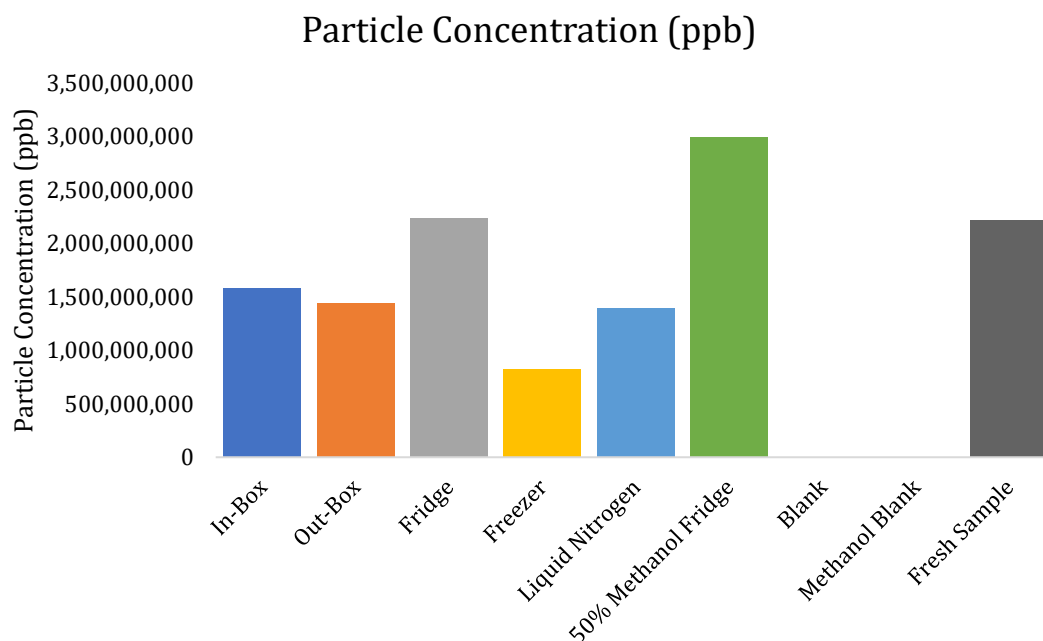


Figure 3.6: The varying particle concentrations in ppb of 80nm silver nanoparticles after being stored with a variety of methods.

The ionic concentration of the samples showed a trend where all but the Fridge sample has significantly higher concentrations with the 50% methanol fridge sample having an ionic concentration over 100 times larger, this can be seen in Figure 3.7. There was a close ionic correlation between the freshly made (1,666 ppb) sample and the fridge (2,234 ppb) samples while the 50% Methanol Fridge has a much larger ionic concentration and all other samples have an increased ionic concentration on average (84,711 ppb) over fifty times larger.

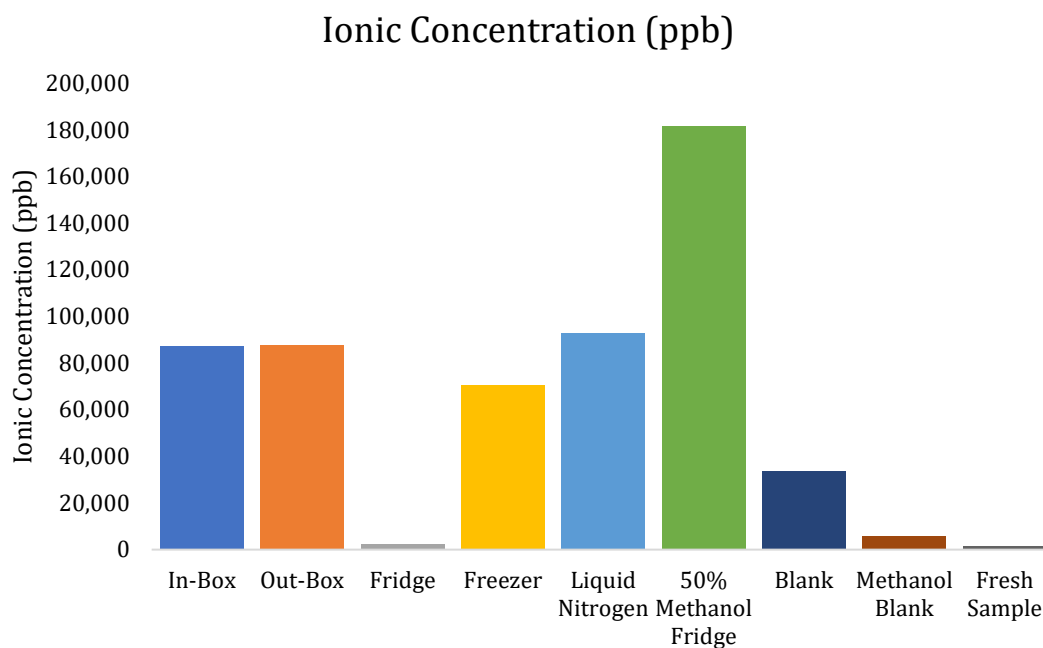


Figure 3.7: The silver ion concentrations in ppb of 80nm silver nanoparticles after being stored with a variety of methods.

In Figure 3.8 and 3.9 the size distributions of the various storage techniques is shown with Figure 3.8 showing the numbers of counts as a function of size and Figure 3.9 showing the frequency normalised as a percentage to the maximum frequency of each storage technique so as to better see the differences in the size distributions. From the size distributions of the storage techniques there are a couple key points to make, firstly the response from the storage techniques is far lower than the Fresh sample and secondly there is some additional particle peaks present in a couple of the samples. The size of the 50% methanol sample was similar to the fresh sample with the most prominent peak almost overlapping the fresh samples distribution curve but there are additional peaks at 120nm and 150nm that are not present within the fresh sample.

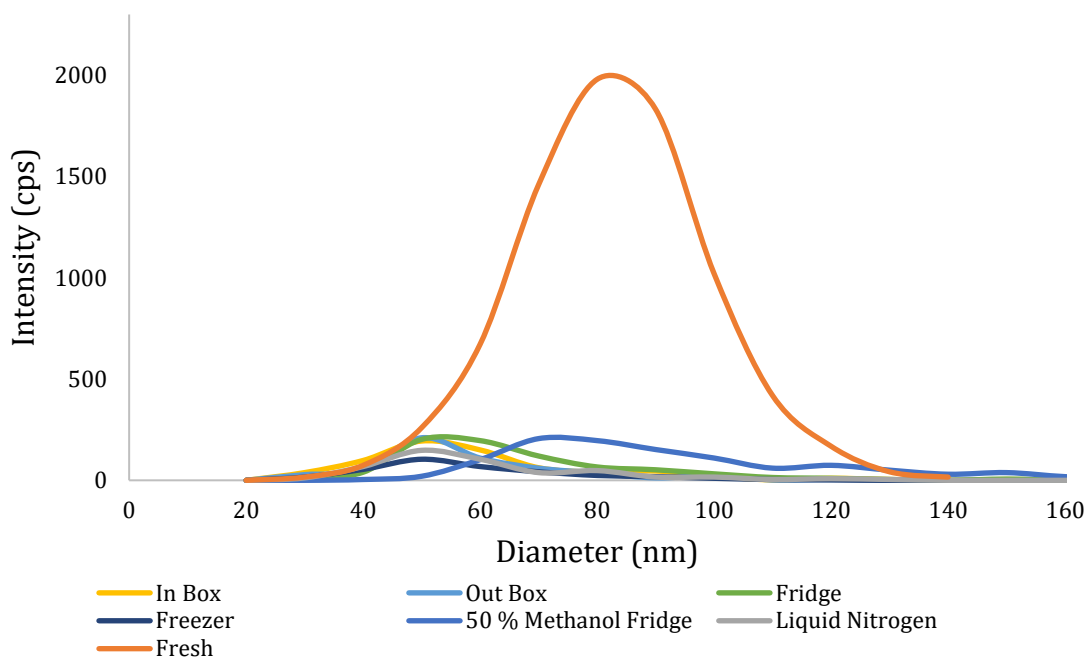


Figure 3.8: The size distribution of 80 nm silver nanoparticles against the true intensity of each sample. It can be clearly seen that the Fresh sample has a significantly higher response than any of the other samples.

The fridge sample has a clean curve that falls entirely within the Fresh sample with a shift that pushes the curve to be smaller, suggesting minimal difference in the particle events between the Fridge and Fresh sample. There are irregular peaks present multiple times throughout the different storage techniques being most prominent in 50% methanol, but also significantly in the liquid nitrogen and both box samples, with the liquid nitrogen and Out-Box having a peak at around 100nm. Liquid nitrogen also had a small peak at 80nm suggesting that the rapid freezing had maintained some of the nanoparticles at their original size, In-Box had a similar peak at 90 nm that was had an equivalent response to the liquid nitrogen 80nm peak at 46 counts to the 48 counts from liquid nitrogen. These responses are tiny in comparison to the response of the fridge sample with all other samples having a response that was at least five times smaller at their maximum than the

maximum for the Fridge sample. The Fridge sample had a response that was about half that of the Fresh sample at 846 counts to the 1980 counts of the Fresh sample, this difference in response can be explained by the concentration of the silver nanoparticles in the Fresh sample being higher and therefore the result is subsequently higher, as was demonstrated in the first section of this chapter.

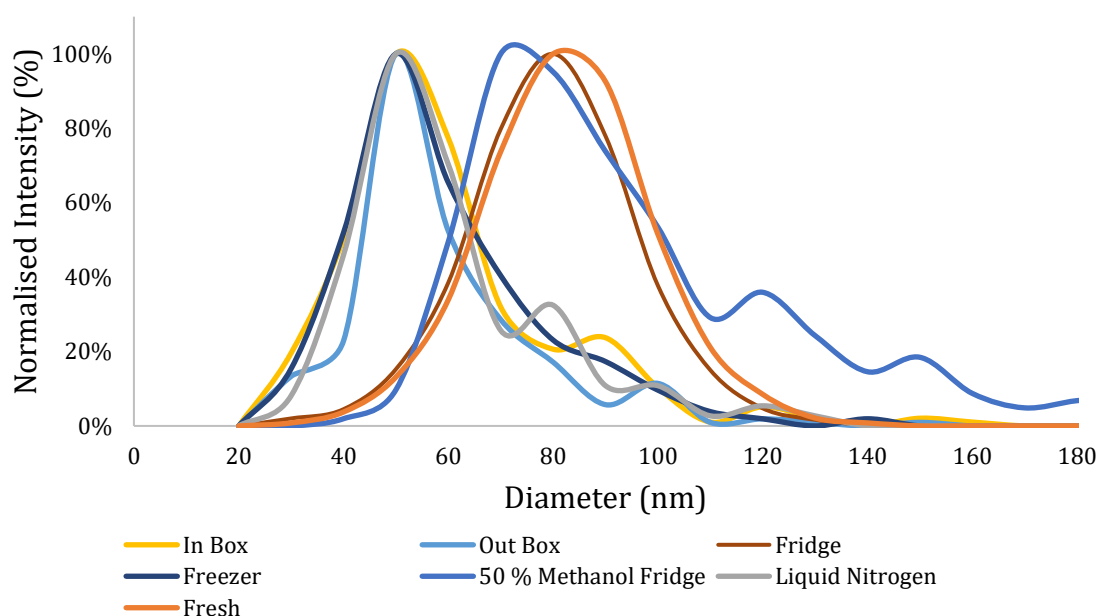


Figure 3.9: The size distribution of 80 nm silver nanoparticles against the normalised intensity of each sample, this allows for easier comparison of any secondary peaks that are present within a sample. In this case there are multiple secondary peaks for In-Box, Out-Box, Liquid Nitrogen and 50% methanol fridge samples, with freezer having the hint of a secondary peak forming.

Conclusions

The low variance in nanoparticle concentrations described in this chapter, provided confidence in the results being an accurate representation of the nanoparticle standard concentration and size for 40 nm and 80 nm BBI silver

nanoparticle suspensions. With this confidence, further method development and use of Single Particle ICP-MS could begin, with the knowledge that the instrument was measuring accurately and with a high level of replicability and subsequent methods that were developed could not be completed with confidence in the accuracy of the results. Subsequent work from this chapter led to the development of a standard operating procedure ¹⁰⁷ which can be found in appendix 2.

The analysis of the effect of nanoparticle concentration on the response that was measured by the instrument demonstrated that there was a preferential working range for nanoparticles, while this range will vary based on a number of factors, specifically: size of the particles, density of the particles and the sample matrix. By using a wider range of particle concentration from 50,000 – 300,000 nanoparticles mL⁻¹ to ensure a steady but not over/underwhelming stream of particles, all samples could easily be diluted to within this concentration range. In practice the standard dilution was to dilute a sample by 100,000 or 1,000,000 times depending on the available information about the rough concentration of the sample (for example if the sample was expected to have a very high concentration [over 100 mg L⁻¹] then a 1,000,000 times dilution would be measured) then analyse the sample, often this would put the sample within 50,000-300,000 nanoparticles mL⁻¹, if the concentration of the particles is too low then a higher dilution concentration is used next. This practice has the benefit of simplifying the preparation of samples and protecting the instrument from saturation from samples with unknown concentrations which can damage the detector and sensitivity of the instrument over time.

From the data on storage of nanoparticles it was concluded that the preparation of ionic/nanoparticle standards would be carried out on the day of analysis. The analysis of samples was also optimised so that the preparation of samples was performed immediately before analysis, so that the samples had minimum exposure to the environment once collected for analysis. By minimising the exposure to the environment of the lab particle samples were analysed with greater confidence that the results represented the true size and concentration of the sample. In cases where the route to analysis was unknown, for example in analysis of samples from a collaborator, it was assumed in good faith that the samples were prepared and stored in optimum conditions before being stored in the fridge in Birmingham prior to analysis. All samples were stored in the fridge in a cool box so as to minimise the exposure of ultra-violet light upon the incidental times the fridge was opened by another laboratory user. It was hoped that by taking such precautions there was minimal physiochemical changes to the structure and dispersity of the nanoparticles.

Chapter Four

Developing single particle ICP-MS analysis for the detection and characterisation of complex bimetallic core-shell or mixed phase nanoparticles

Aims and Overview

Bimetallic core-shell or mixed phase nanoparticles present a challenge in determination of accurate size, composition and concentration, which are needed for their characterisation and assessment of their potential risks to humans and the environment if incorporated into products. The development of a method for determination of complex (multi-component) nanoparticle size and composition using single particle inductively coupled plasma mass spectroscopy (spICP-MS) is presented. Analytical approaches and mathematical manipulation of the data for the determination of core-shell nanoparticles and composite or mixed-phase nanoparticles are discussed in detail. To date, spICP-MS has mainly been applied to Au core Ag shell (Au@Ag) nanoparticles to determine shell thickness and overall particle size. Here, the same principle is extended to characterisation of a series of hafnium doped titanium dioxide nanoparticles, of unknown Ti/Hf ratio with unknown distribution of the dopant. We demonstrate that spICP-MS can be used to determine the nanoparticle diameters and elemental content, from which their structure and the distribution of the dopant in the particles can be determined. The calculated data are benchmarked against other methods that can provide part of the total information gained from spICP-MS, i.e. differential

centrifugal sedimentation (DCS) for size and density, dynamic light scattering (DLS) for size and transmission electron microscopy (TEM) for size and structure/morphology, adding robustness and confidence to the method. The data presented show that spICP-MS is a versatile and powerful technique, which allows for accurate characterisation of multi-element nanoparticles with complex structures and morphologies.

Core shell nanoparticles have been developed for a variety of applications, mostly as a means of further enhancing nanoparticle properties by the dual composition, or shielding/isolating the core from the surrounding environment, or conferring specific surface functionality by the shell. An example of one such core shell system was aimed to enable study of dissolution rates and the chemical effects of the shell; this was achieved by having a core which does not readily change or react with analytes of interest and as such will not be affected by the matrix or environmental conditions; the advantage of this method is that the core may be coated with any desired shell, and used to measure the rate of dissolution of the shell and its potential environmental effects whilst maintaining an accurate knowledge of nanoparticle concentration from measuring the abundance of the core. Labelling methods capitalising on a dopant or a core shell structure provide a technique to measure more complex particles, compensating for the lack of traceable materials by using reliable elements (whether dispersed within the particle or concentrated in the core) for calibration.

Nanoparticles (NPs) have become a common component of many consumer ^{3,7,41,42,54,69,113,114} and industrial ^{3,6-8,41,42,54,69,70,113,114} products, where their presence enables specific effects, such as silver NPs in socks to provide

antibacterial properties ^{3,8,34,37,41,63,113,115}, titanium dioxide to protect against environmental damage from air or water ⁶⁹ and in sun creams ⁴², gold and silver in cosmetics such as skin creams ^{69,116}, healthcare (dietary supplements ^{69,116}) and dental care, e.g. toothpastes ^{69,116}. However, with greater use there is a need to understand their effects on organisms following release from products into the environment, as well as on humans e.g. through occupational or product exposure. This has led to the development of a suite of techniques to characterise NPs, as a fundamental underpinning for assessment of their safety and/or toxicity.

Single particle inductively coupled plasma mass spectrometry (spICP-MS) is a relatively new method of analysing NPs ^{21,55}, which allows for accurate and repeatable measurement of both NP size and concentration ^{21,27,55}. Since the majority of other analytical techniques can measure either one or the other variable, spICP-MS has great potential. Although the technique has been increasingly used in routine analysis, with ISO and ASTM standard methods either recently published (e.g. ISO/TS 19590:2017) or in development, it has yet to be streamlined to provide routine analysis of complex environmental samples containing NPs of unknown composition ⁵⁵. To date, the majority of development work has focused on NPs of a single composition ^{31,32,41}, using a handful of NIST and other reference and benchmark NPs (gold ^{14,56,75,117–120}, silver ^{7,21,27,41}, or titanium ^{13,28,121}).

spICP-MS has recently begun to be applied for the determination of multi-element NPs ^{75,117,121,122}, mainly Au@Ag NPs to date ^{75,117}. Previous work on multi-element particle analysis has been performed primarily using time of flight (TOF)-ICP-MS ¹²¹. TOF-ICP-MS and quadrupole ICP-MS (including spICP-MS), each of which have

advantages and disadvantages: TOF-ICP-MS separates elements based on their mass to charge ratio but unlike quadrupole instruments does not discriminate between elements and thus measures all available ions by mass, allowing TOF-ICP-MS to simultaneously measure many elements, which is useful for multi-component particles^{75,117,121,122}. However, quadrupole ICP-MS, and specifically spICP-MS is able to determine particle concentrations by calibration and via detection of individual NPs¹²²⁻¹²⁴; it does this by sacrificing simultaneous elemental determination, although, more recently, this shortcoming is being addressed with the development of dual analyte quadrupole systems^{75,117}. Additionally, spICP-MS has been used with core shell particles developed to enable study of dissolution rates and the chemical effects of the shell; this is done by having a core which does not readily change or react with analytes of interest and as such will not be affected by the matrix or environmental conditions; the advantage of this method is that the core may be coated with any desired shell, and used to measure the rate of dissolution of the shell and its potential environmental effects whilst maintaining an accurate knowledge of NP concentration⁷⁵. spICP-MS provides a higher quantitative representation of the sample population, a greater level of detail in the characterisation of complex NPs is achievable using spICP-MS than could be achieved from a combination of other methods such as electron microscopy and DLS.

The work presented here explores the detection and characterization of less well studied and compositionally more complex NPs, specifically bimetallic core-shell or metal-doped NPs, and NPs containing uncommon dopants, such as hafnium (Hf). The need to understand the fate and transformations of nanomaterials in the environment has led to the development of advanced NP labelling strategies to

enable tracking of their fate in complex environments. Chemical doping of a common element with a high natural background using a rare-earth element in order to track both within the environment is one such approach. Thus, rarer elements like hafnium, when incorporated into compositionally more common nanoparticles, become a unique tracer as chemical labels for biological and environmental studies allowing quantification of the overall engineered NP against a background of particles compositionally similar to the common element engineered NP core. However, an important consideration is that the dopant should be well distributed throughout the particle without changing its crystal structure or surface characteristics, so that the doped NP's behaviour is equivalent to the undoped particle it should mimic.

By demonstrating an advance of spICP-MS towards multi-element particle analysis, this work which incorporates determination of particle density, size and composition from a single measurement, demonstrated for both core-shell and chemically doped mixed-phase NPs. The approach involved first working out the mathematical and physical requirements underpinning detection by spICP-MS and then studying model systems in more detail, in order to develop a robust model that users can feed their spICP-MS data directly into to determine size, concentration and composition and morphology of bimetallic NPs. Systems included in this study were: 1) Au@Ag NPs to compare with the existing work in the field ^{75,117}, and 2) hafnium doped TiO₂ NPs chosen to allow discrimination between naturally occurring TiO₂ particles and the hafnium doped TiO₂ NPs to be traced, for example following incubation in sewage sludge.

Determining size of bimetallic NPs

spICP-MS: Single Particle ICP-MS (spICP-MS) is based on two principles: that each pulse of ions detected represents an individual NP and that the intensity of each pulse is proportional to the mass of the element detected^{31,32,55,124}. The challenge posed by complex NPs for size determination using spICP-MS is that this technique does not have extensive simultaneous element detection capabilities. Thus, in order to calculate the diameter of a complex (e.g. bimetallic) NP, irrespective of whether it is a core-shell or a chemically doped (atom substituted) particle, three main steps are applied (see Figure 4.1): the particle is ionised within the spICP-MS and the instrument is calibrated to measure the abundance at a specific mass of the known elements within the particle. The elements are treated by the instrument as being distinct individual particles and are each given distinct particle masses; in doped or core-shell particles, however, it is assumed that all measured elements are not distinct particles but are the constituent elemental parts of one multi-element particle. Thus, to calculate the multi-element particle size the data is processed as follows: (i) the elemental masses are used to calculate elemental spherical diameters; (ii) elemental volumes are calculated from the elemental diameters and summed to form the total particle volume; (iii) the total particle diameter is then found from the total particle volume. This process is demonstrated in Figure 4.1 for a core-shell arrangement complex NP, where V_T is the total NP volume; V_a and V_b are element a and b's volumes, D_a and D_b are element a and b's diameters. After the total volume has been calculated for the complex NP the diameter is determined using the final equation given in the red box in Figure 4.1, where D_T is the calculated total diameter of the complex NP. Note that these equations assume that the NP is spherical.

Here, this limitation is overcome by sequential elemental detection of a small number of elements. In such case, and if the elements within the particle are assumed to be all that is measured by spICP-MS, then the nanoparticle size can be determined accurately.

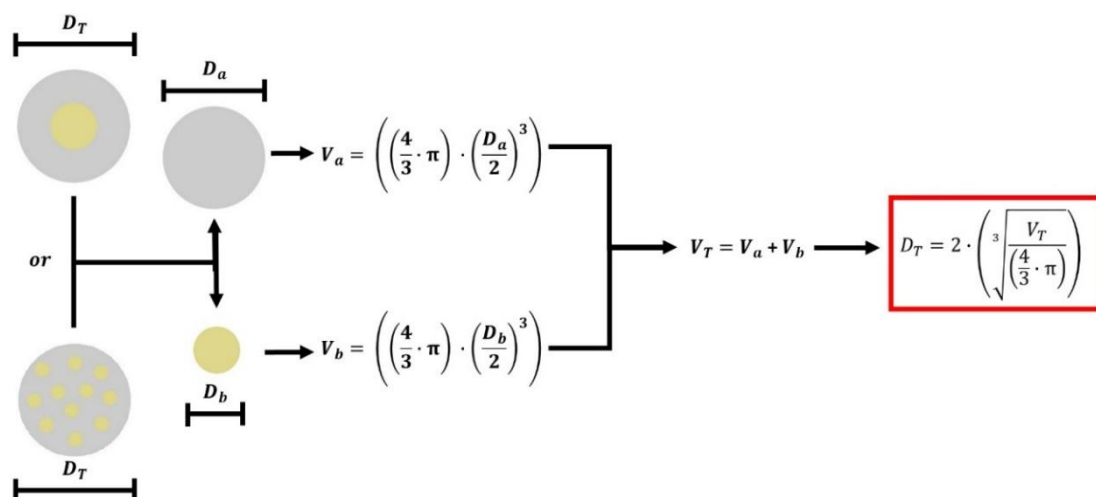


Figure 4.1: Flow diagram of the mathematical procedure to determine the diameter D_T of a spherical complex NP; whether the NP is core-shell or chemically doped does not influence the result.

If the particle concentrations for the elements differ, then it cannot be determined that the solution consists of only one phase; this is because the calculations used to determine the particle size assume that all particles detected belong to the complex NP and nothing else. If it was known that other particles of the same elements were present, then these particles would have to be accounted for by subtracting the concentration of the element with lower concentration from the element of higher concentration; this will give two NP populations, one of the multi-element particles and the other of the single element particle. This process can be further enhanced if there is particle polydispersity as it is possible to select individual peaks using the spICP-MS software (in our case PerkinElmer's

Syngistix) where the peak with the concentration corresponding to the concentration of another element within the multi-element particle will be the peak of the multi-element particle. This suggests there is an important role for spICP-MS in quality control of NPs and analysis of batch-to-batch variability, for example. The ability to determine if a particle is polydisperse, or whether degradation of the shell (for example) has occurred, allows spICP-MS to become a powerful method of particle analysis, with which dissolution rates and quality of NPs can be accurately determined.

Demonstrated in figures 4.2, 4.3 and 4.4 the approach utilized to distinguish between different particle populations (e.g. single and agglomerated) versus samples that are compositionally inhomogeneous whereby there are some core-shell particles and some single element particles. In each case, a single element of a multielement particle is analysed by spICP-MS.

In figure 4.2 a single peak is seen, as would be the case when there is just one particle population, in this case the core shell nanoparticles, this is the optimal scenario for analysis as there is a clear single peak that can only relate to a single nanoparticle, if all elements of the complex nanoparticle also show a singular peak with similar particle concentrations then it can be assumed with high confidence that all that is being detected is the complex nanoparticle.

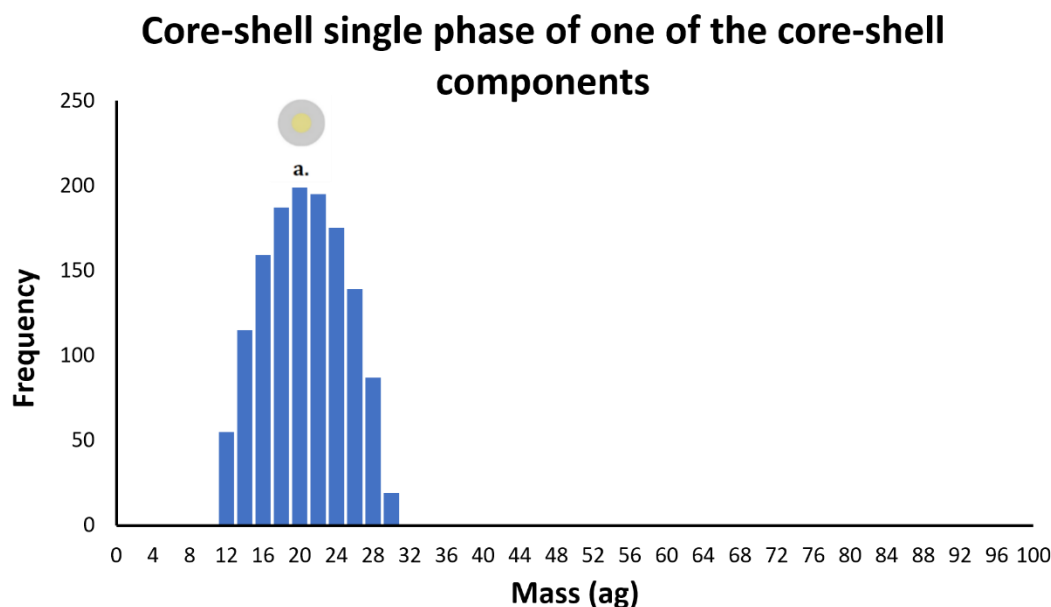


Figure 4.2: Core-shell single phase spICP-MS results for one of the elements within a core-shell nanoparticle.

Figure 4.3 shows multiple peaks, but these still represent one single nanoparticle in this case the particle has undergone some agglomeration and there are corresponding peaks showing evidence of double, triple and quadruple particle agglomeration, again as before if the other elements that constitute the nanoparticle show this pattern of agglomeration and have a similar particle concentration it can still be assumed that there is only a single particle being detected although now agglomerated.

In figure 4.4 the nanoparticle population is now polydispersed, in the case of the particle that is present in figure 4.2 the particle population is dispersed enough to clearly see the core shell nanoparticle as a separate entity (peak a), but when it comes to the agglomerated core shell particle it is harder to differentiate the agglomerate (peak c) from other nanoparticles in the sample. The method to determine which peak is from the multi-element particle is to determine which

peak has the same particle concentration as the other elements within the multi element particle. If a gold core silver shell nanoparticle is considered and the silver is found to be monodispersed with a particle concentration of 10,000 particles/mL; then to find the size of the gold core in a sample which has polydispersed gold, the peak that contains 10,000 particles/mL should correspond to the multi-element particle whilst the remaining peaks are either other particles in solution or agglomerated multi-element particles, it is however difficult to have high confidence in the concentration of peaks like peak C in figure 4.4 however the size may be determinable with some degree of confidence.

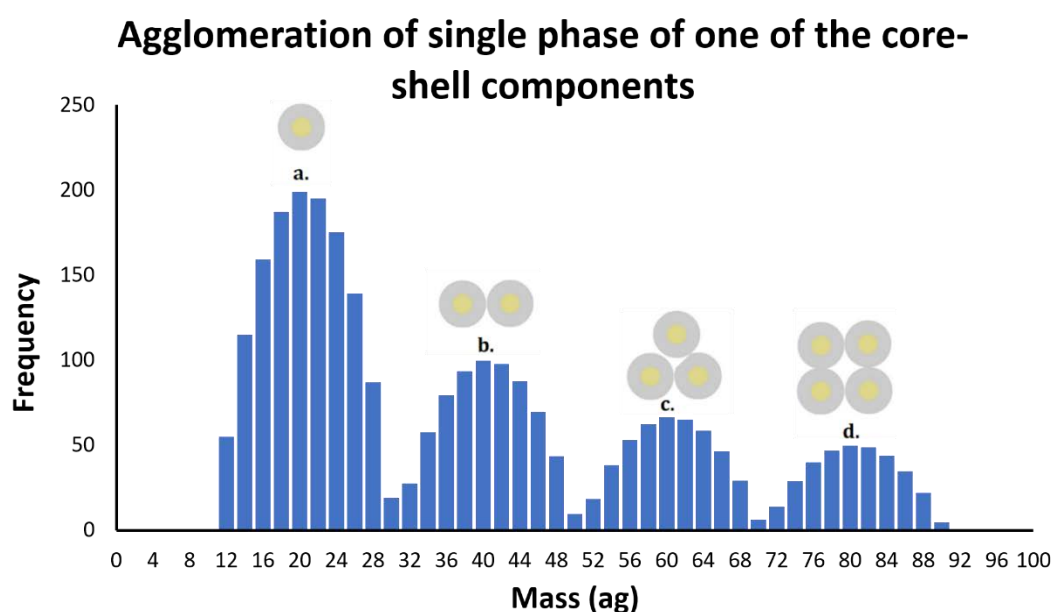


Figure 4.3: Agglomeration of Core-shell single phase spICP-MS results for one of the core-shell components.

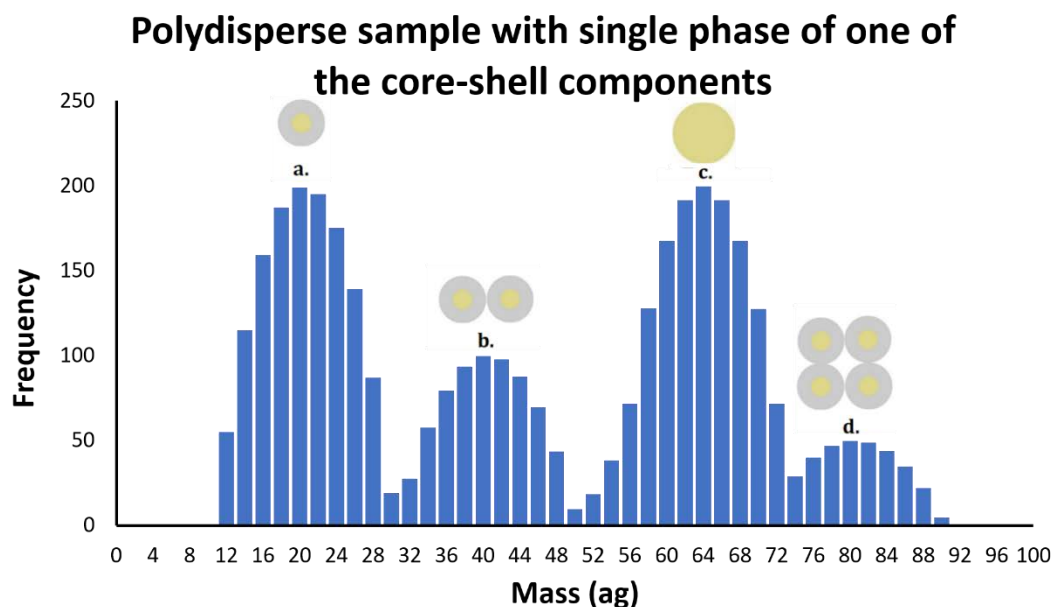


Figure 4.4: Polydispersity of core-shell single phase and other nanoparticles spICP-MS results for one of the core-shell components.

The basic idea behind determining the size of a (complex) nanoparticle is that the nanoparticle will have a specific volume that is proportional to the diameter of the nanoparticle, so by determining the volume of the nanoparticle the diameter can be calculated. In spICP-MS it is possible to determine the diameter of a spherical nanoparticle based on the mass of atoms detected within each ‘pulse’.

The reason that the nanoparticle does not have a diameter equal to the two elemental nanoparticle diameters added together is because sphere volumes do not increase linearly but cubically; i.e. when the diameter of a sphere is doubled the volume increases eightfold. This relationship also applies to the mass with the mass increasing cubically in relation to the diameter of a sphere.

DCS: Differential centrifugation sedimentation (DCS) uses the density of a particle to determine its size, using a density gradient whereby the larger a particle is the faster it flows through the gradient. DCS uses Stokes’ law of sedimentation (or

settling velocity) which calculates the drag force of spheres within viscous fluids by measuring the time required for particles to settle a known distance through a fluid of known density or viscosity ^{82,83}.

All components of the Stokes equation are known apart from time, thus to determine the size of a NP the instrument is calibrated to a particle of known size and density. When calibrated, DCS becomes one of the most precise techniques for particle size determination with high differentiation between NPs of even small size or density differences ^{82,83}. DCS was used here as a confirmatory technique for NP size determination by spICP-MS. The disadvantage of DCS is that the density of the particle being determined needs to be known in order to calculate the size accurately. This can be achieved by calibrating DCS with a reference particle of known size and changing the input density value until the DCS determines the correct particle size (when size is known). An alternative is using the NP density calculated otherwise, e.g. from spICP-MS, in the DCS measurements to correctly determine the size of the NPs ^{82,83}, as presented next.

Calculations to determine complex NP density

spICP-MS: To determine the density of a complex NP using spICP-MS a series of calculations need to be undertaken. Figure 4.5 shows the steps to determine the density of a complex NP: (i) The volumes of the elements within the NP are calculated (V_a and V_b respectively are volumes of elements a and b derived from the diameter of the particle in the same method as determining the total particle size.); (ii) the total volume of the particle (V_T) is calculated from the sum of the volumes of the elements; (iii) the mass of each element within the particle (M_a and M_b respectively for mass of elements a and b) is calculated from the volume of the

element and the elemental density (ρ_a and ρ_b for elements a and b). The density of an element or component of a multielement nanoparticle should be derived from literature; (iv) The total mass of the particle (M_T) is calculated from the sum of the masses of the elements. (v) The NP density (ρ_T) is calculated from the total particle mass (M_T) divided by the total particle volume (V_T).

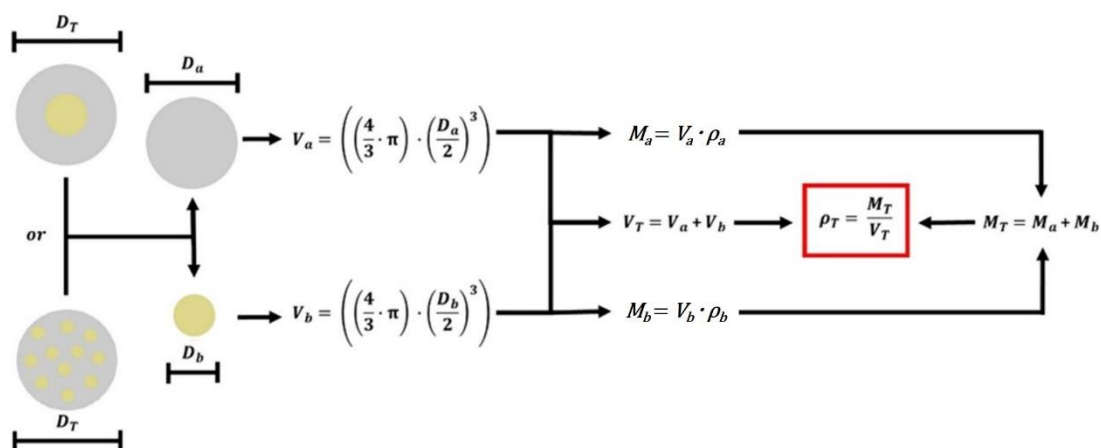


Figure 4.5: Flow diagram of the mathematical procedure to determine the density of a spherical complex NP, utilising the volume data from spICP-MS to finalise the density of the mixed phase rather than taking an average of the elemental densities present. Whether the NP is doped or core-shell does not influence the final result. Utilising the spICP-MS (inorganic) diameter versus the DLS (hydrodynamic) diameter in the volume calculations provides the inorganic and hydrodynamic densities, respectively, which are quite different.

Materials and Methods

Chemicals and Materials

Au@Ag particles: 60nm silver shelled gold core NPs were purchased from nanoComposix.

Hafnium doped TiO₂: The synthesis of the labelled particles has been described elsewhere ¹¹⁷. Briefly, a 4 mL solution of Ti (IV) isopropoxide was added to a solution containing 17 mL benzyl alcohol, 3 mL of stearic acid and 0.01M hafnium (IV) chloride (HfCl₄) (Note: for uncoated particles there was no stearic acid added). The solution was mixed for 30 minutes before loading into a teflon lined autoclave vessel (Parr Instruments) and maintained at 200°C for 24 hours for hydrothermal synthesis. After 24 hours the precipitate was removed, washed with ultra-pure water (UPW) and centrifuged at 5000 rpm for 30 minutes. The remaining precipitate was dried at 60°C to obtain a white powder containing the hafnium doped TiO₂ NPs.

spICP-MS: Transport efficiency of the instrument was determined using 20 nm, 40 nm, and 80 nm gold NPs obtained from BBi solutions. NIST 1,000 mg dm⁻³ (1,000 ppm) gold ion standards, and 40 nm and 80 nm silver NPs obtained from BBi solutions were used to calibrate the NexION 300D for analysis of each element in the Au@Ag particles. Individual NIST hafnium, and titanium 1,000 mg dm⁻³ (1,000 ppm) ion standards obtained from Aristar were used to calibrate the NexION 300D for analysis of each element in the hafnium doped TiO₂ particles.

DCS: A size and density standard were used to calibrate the DC24000 instrument, sucrose was obtained from in house stocks for the creation of a density gradient. Dodecane was obtained to help reduce evaporation losses, which could have affected the results. A polystyrene size and density standard between 0.1 micron and 1 micron in size was obtained from CPS instruments this was used to calibrate the DC24000 instrument.

DLS: There were no additional chemicals required for analysis using DLS other than the samples.

Sample preparation/Extraction procedure

The hafnium doped TiO₂ NPs were diluted by weighing 0.1g of powder and diluting in 10 mL of ultrapure water, this was then sonicated for 1 hour to ensure full suspension of the particles; these became the hafnium doped TiO₂ NP stock solutions.

Au@Ag and hafnium doped TiO₂ NPs were prepared for analysis via spICP-MS using a NexION 300D. The Au@Ag NPs were diluted 250,000 times. Hafnium doped TiO₂ NPs were prepared for analysis by taking the prepared stock solutions and diluting 1 million times to give particle concentrations within the range of detection of the NexION 300D. All solutions were diluted in UPW.

Gold nanoparticle standards: The ionic standard and nanoparticles were all diluted in triplicate with aliquots into either 0.015 or 0.05 dm³ falcon centrifuge tubes and filled up to the mark with deionised water that was pipetted with calibrated 5,000 and 1,000 µL pipettes. The dilution protocol used was as follows:

Ionic standard: The ionic standards were prepared from a stock solution of ICP-MS Gold standard, with a starting concentration of 1,000 mg dm⁻³ (1,000 ppm) that was sonicated and diluted with ultra-pure water using the dilutions outlined in table 4.1.

Using the calculation shown in equation 3.1, the following dilutions were performed to provide the ionic standards for calibration.

Table 4.1: The dilutions used to reach desired concentrations for the ionic gold calibration standards.

Concentration ₁ (mg dm ⁻³)	Volume ₁ (dm ⁻³)	Concentration ₂ (mg dm ⁻³)	Volume ₂ (dm ⁻³)	Concentration ₂ in μg dm ⁻³
1,000	0.0005	10	0.05	1,000
10	0.0005	0.1	0.05	100
0.1	0.0005	0.001	0.05	1
0.1	0.0010	0.002	0.05	2
0.1	0.0015	0.003	0.05	3

Applying the above dilution sequence using calibrated pipettes provides an estimated maximum error of 2.3% from the desired concentrations as determined using the estimated errors described within the pipette manual.

DCS Two sucrose solutions were prepared by introducing combinations of sucrose and ultra pure water to create an 8 % and 24 % sucrose solutions.

TEM Samples were prepared by suspending 0.01g of the hafnium doped TiO₂ solids into 5 mL UPW. TEM grids were prepared by drop casting, depositing a 20 μL drop of hafnium doped TiO₂ suspension onto a 300-mesh carbon-coated copper TEM grid (Agar Scientific, UK) and leaving for 30 minutes to allow the NPs to adhere to the carbon membrane. Grids were rinsed with UPW and blotted to remove excess water to avoid aggregation.

Instrumental optimisation and analysis

spICP-MS Transport efficiency of the instrument was determined using 20 nm, 40 nm, and 80 nm gold NPs diluted to 50 particles per dm^{-3} by serial dilution in UPW (see table 4.2 for instrumental parameters). NIST gold 1 ppb, 2 ppb and 3 ppb ion standards, and 40 nm and 80 nm silver NPs from BBi solutions were used to calibrate the NexION 300D for analysis of each element in the Au@Ag particles. Individual NIST hafnium, and titanium, 1 ppb, 2 ppb and 3 ppb ion standards from Aristar were used to calibrate the NexION 300D for analysis of each element in the hafnium doped TiO_2 particles.

The sample particles were analysed for each element and the size was calculated from the spICP-MS results using the standard method described in Appendix 2 and Chapter three.

Table 4.2: Instrumental parameters used during single particle analysis for complex nanoparticles.

Nebulizer Gas Flow [NEB]	1.12
Auxiliary Gas Flow	1.2
Plasma Gas Flow	18
ICP RF Power	1600
Flow Rate	0.346 g min^{-1}
Transport Efficiency	5.11 %
Dwell Time	80 μs

DLS DLS analysis of the particles was performed using a Malvern Nanosizer 5000, setting the instrument to analyse for the reflection index of the outermost element of the particle (silver for the Au@Ag particles and assumed to be TiO_2 for the

hafnium doped TiO₂ particles) (see table 4.3 for instrumental parameters). Undiluted samples were transferred into cuvettes to two thirds full and particles were analysed for hydrodynamic size. The results of the spICP-MS size determination were used in conjunction with the DLS hydrodynamic size determination to calculate the hydrodynamic nanoparticle density using spICP-MS and DLS.

Table 4.3: DLS Instrumental parameters utilised for Au@Ag nanoparticles and TiO₂.Hf nanoparticles.

Variable	Au@Ag	TiO ₂ .Hf
Material	Silver	TiO ₂
RI	0.540	2.700
Absorption	0.100	0.010
Dispersant	Water	Water
Temperature	22.0 °C	25 °C
Viscosity	0.9540 cP	0.8872
RI	1.330	1.330
Cuvette type	ZEN0040	ZEN0040
Angle of detection	173° Backscatter	173° Backscatter
Measurement duration	Automatic	15 runs of 10 seconds
Number of measurements	5	5

DCS The instrument was set up with a disc speed of 14,000 revolutions per minute. A density gradient was created by introducing combinations of the 8 % and 24 % sucrose solutions, 0.5 mL of dodecane was then added to this density gradient. 0.1 mL of undiluted particle samples (with a concentration of 1.5×10^{10} particles mL⁻¹ for

the Au@Ag and around 50,000 for the hafnium doped TiO₂ NPs) were introduced with a syringe whilst the disc was spinning at the set disc speed.

Appropriate parameters (see table 4.4) were entered into the software to allow for accurate size determination. The parameter for particle density was adjusted by 1 g cm⁻³ between each measurement across a range of densities (1-18 g cm⁻³ for the Au@Ag particles and 1-10 g cm⁻³ for the hafnium doped TiO₂ particles) to form a single digit density series from which the size closest to the size obtained from spICP-MS was determined. The corresponding cross over point where the spICP-MS and DCS results for the complex nanoparticle size leads to accurate determination of NP density based on particle size calculated using spICP-MS. Undiluted 0.1 mL particle samples (with a concentration of 1.5e¹⁰ particles mL⁻¹ for the Au@Ag and around 50,000 for the hafnium doped TiO₂ NPs) were introduced with a syringe whilst the disc was spinning at the set disc speed.

Table 4.4: Instrumental parameters used for DCS analysis of complex nanoparticles.

Maximum read diameter	0.3 microns
Minimum read diameter	0.01 microns
Particle density	Variable
Particle refractive index	0.54 (Au@Ag) 2.49 (TiO ₂ .Hf)
Particle absorption	0.1 K (Au@Ag) 0.075 (TiO ₂ .Hf)
Non-Sphericity factor	1
Peak diameter	1.27 microns
Half height peak width	0.4 microns
Particle density (standard)	1.385 g/ml
Fluid density	1.045 g/ml
Fluid refractive index	1.344
Fluid viscosity	1.2 cps
Disk speed	14000 RPM

TEM Particle diameter measurements were conducted using Gatan Digital Micrograph software by measuring at least 100 particles (41), TEM images shown in figure 4.6. TEM analysis was provided with the nanoComposix Au@Ag NPs on a data sheet.

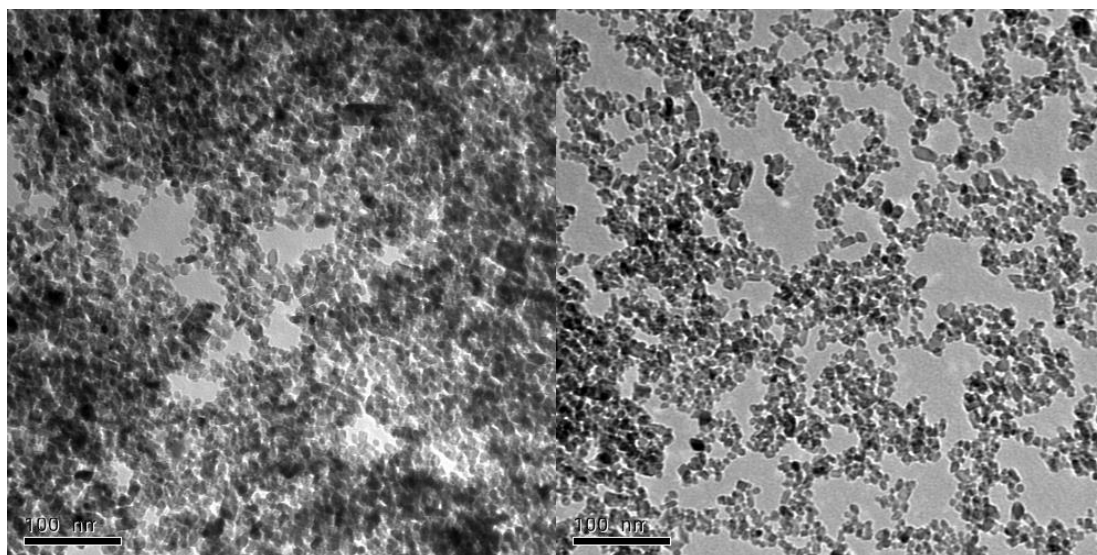


Figure 4.6: TEM images of steric acid coated TiO_2 Hf (left) and no surface coating TiO_2 Hf (right).

QA/QC criteria

Quality assurance was obtained by the daily instrumental setup and by statistical analysis of multiple replicates for each sample. Due to the nature of the instruments used being sequential in analysis it is not possible to use an internal standard as the internal standard would not be analysed with each sample. In lieu of the presence of an internal standard the certified gold nanoparticle standards were routinely compared to the limits of size as stated in the certification.

Statistical analysis

The statistical analysis that was performed upon the results gathered within this chapter are R^2 correlation analysis of the standard ionic and particle calibration. A R^2 value of less than 0.996 was not utilised and the calibration was repeated either by reruns or remakes of the standards. Samples were all analysed at least three times in replicate and the average was calculated using the mean. From the

mean the standard deviation was used to identify outliers that would be investigated on a sample by sample basis.

Results/Discussion

The NPs were analysed by four methods, namely DLS, spICP-MS, TEM and DCS (Table 4.5). DLS was used to determine the hydrodynamic diameter of the particles, which includes the layer of surface-associated water that travels with the particles during Brownian motion where water is the fluid matrix for the samples. spICP-MS was to determine the inorganic NP diameter, to verify the elemental composition, and particle concentration. TEM was used to measure the dry particle diameter and to optically characterise them. The spICP-MS inorganic diameter was used in conjunction with the hydrodynamic diameter determined by DLS to calculate the density of the particle by using the elemental composition and literature density values for each element. DCS was used to as an alternative size and density of the particle determination method; this was compared to the density based on the particle size determined by spICP-MS and TEM analyses by fitting the particle size to the particle density. Three replicates of NPs were analysed to obtain accurate reproducible results.

Au@Ag NPs Size

The analysis of nanoComposix Au@Ag NPs by spICP-MS showed that the mean particle size was 62 ± 1 nm with a mean size variance between replicates of 2.07 %. The mean particle size stated by the manufacturers was 61 ± 5 nm so the spICP-MS results are within the stated size limits. The gold core size was 28 nm and the silver shell was calculated to be 17 nm thick (but note that the total size includes

2× shell thickness since the core is surrounded on both sides in the 2D representation of the 3D volume); both of these sizes are within the stated size limits for the particle as described by nanoComposix. The hydrodynamic diameter derived from DLS was 68 ± 1 nm, close to the hydrodynamic size stated by nanoComposix of 69 nm. The close match of the experimental size determinations to the manufacturer's stated values and limits suggests that the NPs are a good reference material for complex NPs for use in size determination via multi-element spICP-MS.

Table 4.5: Size of complex particles determined using spICP-MS, DCS, DLS and TEM.

Material	spICP-MS Particle size (nm)	DCS Particle size (nm)	TEM Particle size (nm) ¹²⁵	DLS Particle size (nm)
Au@Ag	62 ± 1	61 ± 1	61 ± 6	68 ± 1
Hafnium doped TiO ₂ (no coating)	45 ± 3	47 ± 10	42 ± 10	49 ± 9
Hafnium doped TiO ₂ (stearic acid)	41 ± 1	41 ± 10	42 ± 10	43 ± 10
20 nm gold NPs	26 ± 2	18 ± 1	N/A	23 ± 1
40 nm gold NPs	39 ± 4	35 ± 1	N/A	36 ± 1
80 nm gold NPs	79 ± 1	79 ± 1	N/A	78 ± 2
22 10 15 Steric Acid Coated TiO ₂	149 ± 10	N/A	N/A	199 ± 3
16 10 15 TiO ₂ Hydrothermal 200C 24 hours	176 ± 1	N/A	N/A	206 ± 5
12 11 15 TiO ₂ Hf doped No Surface Coating 8-hour	161 ± 2	N/A	N/A	181 ± 4
10 06 16 TiO ₂ Hf Stearic 1.7.15 +	155 ± 3	N/A	N/A	160 ± 8
10 11 16 TiO ₂ Hf Stearic Acid	126 ± 1	N/A	N/A	127 ± 7
26 10 15 TiO ₂ Stearic Acid	94 ± 3	N/A	N/A	166 ± 4
2 11 15 8-hour TiO ₂ only Acetic acid Coating	159 ± 5	N/A	N/A	204 ± 9
10 11 15 TiO ₂ Hf doped stearic acid 24-hour	142 ± 1	N/A	N/A	162 ± 15

The size found using the density calculated from DLS and spICP-MS (9.01 g cm^{-3}) in DCS was 61 nm, which is slightly smaller than the size calculated using spICP-

MS. However, the agreement overall between the approaches is excellent, and shows that spICP-MS provides accurate inorganic mixed particle densities whilst DCS or spICP-MS with DLS provides accurate total particle densities.

Single particle analysis is performed on both elements, with the size distributions of each constituent of the core-shell particles shown in Figure 4.6. The average NP size for each element was derived from the replicates and used to determine the total NP size (as per Figure 4.1); this was then used to calculate the multielement NP density based off the composition and element density (as per Figure 4.5). In spICP-MS smaller particles produce more compact peaks whilst larger particles have peaks that spread due to the cubic correlation between mass and size of the particles; in both cases the mean point of the peak defines the particle size as calculated by the instrument.

From Figure 4.7 both elements have large peak areas, with the silver having a larger spread, however, this does not represent a larger polydispersity or variation in the shell size, rather, this spread is to be expected with larger particles (given the above-mentioned cubic correlation between mass and size) and is common in results from spICP-MS. Indeed, the particles present very little polydispersity, as the particle concentrations for both elements are closely aligned with around 10% RSD between replicates (calculated concentration was around 73 ± 7 particles per dm^{-3}), meaning that all NPs in the population were the requisite core-shell structure with no single-element NPs present. This is essential for determining that the solution has only one phase, i.e. that all NPs are core-shell rather than some being only gold or only silver. The single particle phase was further confirmed by TEM imaging ¹²⁵.

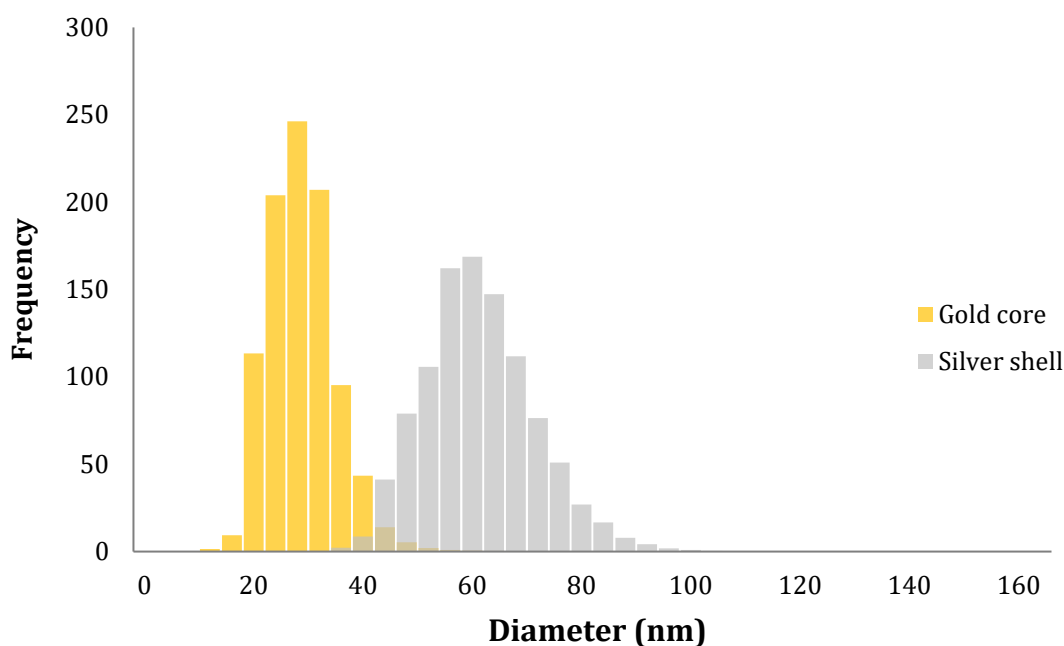


Figure 4.7: Representative spICP-MS analysis result for the 60nm nanoComposix Au@Ag NPs: the gray size distribution represents the silver shell whilst the yellow is the gold core. The mean NP size (the sum of the Au Core and 2X the Ag shell) is used in size calculations.

Hafnium doped TiO₂ NPs Size

In total ten nanoparticles with TiO₂ as a core component within the particle were analysed. Two samples were freshly synthesised, while eight were prepared for analysis three years after synthesis; of which five were Hf-doped TiO₂ particles and three were coated TiO₂ particles. TEM analysis of the original two sample showed that the samples were around 43 ± 8 nm¹²⁵ which matched closely with spICP-MS, DLS and DCS. The spICP-MS mean size of the uncoated hafnium doped TiO₂ particles was 45 ± 3 nm with a mean size variance between replicates of 4.97 % and the mean size of the stearic acid coated hafnium doped TiO₂ particles was 41 ± 1 nm with a mean size variance between replicates of 3.81 %. DLS analysis showed a marginally increased mean size of 49 nm including the hydration layer (a summary of this data is shown in Table 4.5).

There was a significant difference between the freshly synthesised particles and the particles after three years of synthesis. The freshly synthesised particles that were analysed had sizes that were around 40 nm (with the uncoated particles measured at 45 nm and the coated particles measured at 41 nm).

The hafnium doped TiO₂ NPs showed that the size detected by DCS was the same as the particle size detected by spICP-MS and TEM, while the density determined with DCS was close to the density derived from the size and composition calculated using spICP-MS and DLS. This was especially apparent for the stearic acid coated hafnium doped TiO₂ NPs where the mean size found is 41 nm found with DCS, TEM and spICP-MS.

The hafnium doped TiO₂ NPs showed variations in concentrations for each element as shown in Table 4.6, suggesting that there were two distinct phases present in solution, i.e. Hf NPs and hafnium doped TiO₂ NPs, which may not have been apparent from the TEM images ⁴⁰. This is likely due to using Hf in excess during synthesis, with the result that not all of the Hf was incorporated into the hafnium doped TiO₂ NPs resulting in the formation of Hf-only NPs. The ability of spICP-MS to determine this is an important new characteristic obtainable from a single spICP-MS measurement.

Table 4.6: Particle concentrations of each component within Hafnium doped TiO₂ particles, each component is measured separately before being used to calculate the total particle size and density.

Sample	Hafnium particle concentration	TiO ₂ particle concentration
Hafnium doped TiO ₂ no coating	486,243 ± 31,450	276,245 ± 5,679
Hafnium doped TiO ₂ stearic acid coating	102,916 ± 15,836	15,855 ± 1,657

Au@Ag NPs Density

Using the particle sizes found via spICP-MS (inorganic core), the density of the nanoComposix 60 nm Au@Ag NPs was calculated using the set of equations shown in Figure 4.5 to be 11.25 g cm⁻³ (a summary of the data is shown in Table 4.7). This shows the extent to which the elements have on the particle density (Au@Ag), increasing the overall NP density from silver's density of 10.49 g cm⁻³ to 11.25 g cm⁻³ in the core-shell NP, but lower than the density of purely gold NPs (19.32 g cm⁻³).

The density determined for the Au@Ag NPs using the spICP-MS calculated size (62 nm) in DCS was 9.04 g cm⁻³, a negligible difference higher than the calculated density using the combination of DLS and spICP-MS of 9.01 g cm⁻³. The NP size found using the density calculated from DLS and spICP-MS (9.01 g cm⁻³) as the input parameter in DCS was 61 nm, the same as TEM and spICP-MS.

Table 4.7: Collated results for NanoComposix 60nm Au@Ag NPs obtained from spICP-MS, DLS and DCS.

Sample	Diameter (nm)	Density of NP (g cm^{-3})
Au@Ag spICP-MS	62 ± 1	11.25 ± 0.06
Au@Ag DLS	68 ± 1	9.02 ± 0.06 (spICP-MS & DLS)
Au@Ag DCS	61 ± 1	9.04 ± 0.08

Hafnium doped TiO_2 NPs Density

The correlation between spICP-MS with DLS and DCS results is very close with the density calculated from spICP-MS with DLS (via the volumes) to be 3.68 g cm^{-3} for the uncoated hafnium doped TiO_2 , and 4.65 g cm^{-3} for the stearic acid coated hafnium doped TiO_2 and the density calculated via DCS at 3.61 g cm^{-3} and 4.69 g cm^{-3} respectively suggesting that the use of spICP-MS (volume) and DLS to calculate the density and spICP-MS to calculate size is highly comparable to that of DCS a summary of these results is shown in table 4.8.

Whilst the Au@Ag NPs were analysed for use as an spICP-MS size-standard materials and indeed the spICP-MS size and composition conformed to the size distribution stated by the manufacturer, the hafnium doped TiO_2 NPs were analysed as a means to assess the ability of spICP-MS to simultaneously provide data on NP size, composition, sample homogeneity or quality and density from a single measurement. Based on the data presented above, it is clear that it is possible to accurately determine the size of complex NPs using spICP-MS, and the homogeneity of the sample, i.e. to confirm whether or not all particles in a sample are multi-element or whether two NP populations co-exist, or that all have some

form of chemical doping, in addition to assessing changes in quality of the NPs over time, especially related to their multi-element composition.

Table 4.8: Collated results for the hafnium doped TiO₂ NPs obtained from spICP-MS, DLS and DCS.

	Sample	Particle Size (nm)	Density of NP (g cm ⁻³)
1	Hafnium doped TiO ₂ no coating spICP-MS (Core)	45±3	4.57 ±0.16
	Hafnium doped TiO ₂ no coating DLS (Hydrodynamic)	49 ±9	3.68 ±0.05
	Hafnium doped TiO ₂ no coating DCS (Core assumed but actually assumed but actually hydrodynamic)	47 ±10	3.61 ±0.43
2	Hafnium doped TiO ₂ stearic acid coating spICP-MS (Core)	41 ±1	5.16 ±0.20
	Hafnium doped TiO ₂ stearic acid coating DLS (Hydrodynamic)	43 ±10	4.65 ±0.18
	Hafnium doped TiO ₂ stearic acid coating DCS (Core assumed but actually hydrodynamic)	41±10	4.69 ±0.12

From the results it is suggested that an additional component was affecting the nanoparticle density, namely the matrix in which the nanoparticles were suspended. As all nanoparticles used were suspended in ultra-pure water, the additional density attributed to the matrix was easy to determine. The hydrodynamic shell (matrix layer) on the particles generally had the effect of lowering the overall “apparent” density. In ultra-pure water this change in density resulted in densities commonly very close to the density results derived from DCS analysis. Further testing of particles suspended in other matrices, such as aquatic media for standardised toxicity testing as well as “real” freshwaters, are needed to determine if the method of determining the particle density using a combination of spICP-MS and DLS is applicable in more complex matrices. The close agreement

on densities between the two methods (DCS versus spICP-MS paired with DLS) suggests that spICP-MS paired with DLS is an appropriate alternative method of particle density determination and sizing. Additionally spICP-MS provides the concentration and elemental distributions which DCS cannot, in all this allows the combination of spICP-MS paired with DLS to be an improvement to straight analysis with just the DCS.

Conclusion

The reliable measurement of particle size and composition by spICP-MS was demonstrated on two sets of complex NPs. Firstly, the Au@Ag NPs had a size of 62-67 nm by all four methods utilised (DLS, DCS, TEM and spICP-MS), while the hafnium doped TiO₂ NPs had sizes of 41 and 45 nm respectively for the uncoated and stearic acid coated variants as determined by spICP-MS. The sizes calculated by the three techniques show a close correlation suggesting that the spICP-MS method presented is appropriate for characterization of complex NPs. Triplicate NP dispersions were analysed to obtain accurate reproducible results with little variance in both size and concentration of the nanoparticles. The size variance between the NPs during spICP-MS replications was minimal (at most ± 3 nm). For the Au@Ag NPs the mean size variance between replicates was found to be 2.07 % and the mean size was 62 ± 1 nm. For the Hf doped TiO₂ NPs the mean size variance was found to be 1.11 %, and the size variance was 3.81 % for stearic acid coated and 4.97 % for uncoated particles.

Importantly, the spICP-MS method could also provide information on the composition of the samples, confirming the expected ratio of Au:Ag in the Au@Ag NPs, and was able to identify the presence of Hf within hafnium doped TiO₂ NPs,

which was not identifiable from DCS, DLS or from the TEM images. The use of spICP-MS as a technique for analysis of complex nanoparticles was previously almost exclusively a time resolved ⁷⁶ or laser ablation ICP-MS ^{54,68,113,122}, with only a few examples of this method of complex nanoparticle analysis ^{38,40,75}.

Chapter Five

Considerations on particle recovery from tissue to enable analysis of Gold nanoparticle uptake by Isopods (*Porcellio scaber*)

Aims and Overview

Contained within the work outlined in this chapter is the analysis of gold uptake within isopods using spICP-MS. The aim of this work was to develop and measure the exact levels of gold ions and particles that isopods consumed over a fourteen-day exposure. The results would elucidate the fate of gold nanoparticles within the isopod body, in terms of potential accumulation within specific organs, but also possible physiochemical changes that they may undergo within the organism body medium.

In environmental studies spICP-MS has been used to analyse many types of samples ranging from river water and sewage water to the uptake of metals within trophic ladders. It is quickly building a reputation as a fast and effective analytical technique for preliminary and detailed analysis of environmental relevant samples. In the work that is presented here, the spICP-MS technique is used to analyse isopods that have been fed various forms of gold.

Isopods of genus *Porcellio* are widely studied for ecotoxicological data of soil systems ^{126–129}. Within this genus are a number of isopods that are known as woodlice, including *Porcellio scaber* colloquially known as common rough woodlouse within the UK, the work that is presented within this chapter is of the

study of the uptake and physiochemical changes that gold ions and nanoparticles undergo after contact by *Porcellio scaber*.

Isopods are known to possess the ability to store metal in a process called metallo-sequestration; there have been numerous sources of work that have studied Isopod ability to store and remove metals. Primarily this work has been performed on the first-row transition metals of nickel, zinc, copper and iron. Within Isopods there is an organ called the hepatopancreas, this organ has two specific specialised cells 'B' and 'S' that allow for metallo-sequestration ¹³⁰, the removal or storage of metals within the organism. Often metallo-sequestration has been studied for the long term and epigenetic effects on the hepatopancreas from most commonly nickel ¹³¹, but other elements such as copper, iron and cadmium ¹²⁶ have also been studied.

In essence terrestrial isopods are able to utilise these specialised 'B' and 'S' cells to assimilate high concentrations of metals within the hepatopancreas ^{130,131}. The isopods then either store the metals for biological functions in the form of metal granules or expel the metal from their bodies in a similar function to the digestive system expelling toxic waste from within humans. It has been repeatedly observed that isopods will consume metals from organic matter and process the metals within the hepatopancreas, in the work that has been presented in this chapter the uptake of gold nanoparticles and gold ions by isopods is observed and evidence of the isopods metallo-sequestration of both the gold nanoparticles and ions within the hepatopancreas is shown ^{126,130,131}.

Gold as an element is a very good preliminary metal for uptake and exposure tests due to its physiochemical properties. Gold is highly resistant to corrosion, is not

photosensitive like silver, and is not found in significant quantities in the background of blank environmental samples ^{132,133}. This makes gold a metal that is unlikely to show significant changes in its properties due to environmental effects. Whereas silver will dissolve in water and exposure to photons, gold will likely remain stable over the course of an experiment ^{3,22,42,63,134}.

Due to this stability and sensitivity in analysis by ICP-MS, gold is an ideal metal for preliminary method development for analysis of metals, with the knowledge that the gold should stay relatively intact throughout the analysis. It is, thus, easy to determine the fate of gold within complex biological and environmental samples. In the method development of the analysis that follows gold nanoparticles were chosen so as to better observe the effects that any matrix may impose on the nanoparticles. In this case the complex matrix was that of biological matter that was digested by tetramethylammonium hydroxide (TMAOH), and samples in tetramethylammonium hydroxide alone. The physicochemical changes in the gold nanoparticles as a result of TMAOH were measured as a metric for the corrosive effect that matrix exposure had on the metal. The results from this preliminary experiment provided clearly that the TMAOH would not have a significant effect on the gold nanoparticles at the length of time that the samples were exposed for digestion. The caustic effect of the TMAOH when exposed to the isopods would be diluted due to the increased amount of buffering that the chitin shell of the isopods provided.

Tetramethylammonium hydroxide (TMAOH) is a basic chemical that has had a history for use in digestion of biological matter ^{28,135–137}. As a digester it is very effective as it breaks down all the proteins and biological matter within a sample,

a very caustic chemical it requires specific safety precautions to protect the user including protection of the lungs though a gas mask as well as other personal protective equipment such as multiple layers of gloves, clean lab coats and eye protection ^{136,137}. For all its hazards the chemical is perfect for the extraction of metal particles as it does not significantly interact with the metal during digestion, unlike many acids which would dissolve the particles resulting in incorrect results.

Materials and Methods

Chemicals and Materials

Isopods were provided by Ljubljana University having been pre-exposed to gold nanoparticles and AuCl_3 , TMAOH was procured from Alfa Aesar, gold nanoparticle and ionic standards were applied inhouse by Ljubljana University.

Transport efficiency of the instrument was determined using 20 nm, 40 nm, and 80 nm gold NPs obtained from BBI solutions. NIST ionic 1000 ppm gold was obtained for ionic standards.

Sample preparation/Extraction procedure

In Ljubljana University, isopods were prepared using a method published recently ²⁴. In brief three batches of isopods were grown simultaneously for 14 days, each batch of isopods was exposed to a different form of gold to give: (i) a control; (ii) a batch of isopods exposed to gold ions (AuCl_3) referred to as the positive control samples (PC); and (iii) a batch exposed to 80nm gold nanoparticles. After 14 days the stomach and hepatopancreas was removed and the isopods were lyophilised and transported to the university of Birmingham.

A method for TMAOH digestion as described ⁶³ was tested for isopods and the gold nanoparticles that were analysed. A range of TMAOH concentrations were analysed to determine the effects on the nanoparticles. It was found that digestion with 20% TMAOH was the most effective for a fast extraction but this needed to be diluted as prolonged exposure to TMAOH of 8% or higher was found to dissolve gold nanoparticles after 24 hours of exposure. At 1% TMAOH it was found that the nanoparticles were stable from the effects of TMAOH and as such after 24 hours all samples were diluted from 20% to 1% TMAOH. This also decreases the safety risk that TMAOH poses to those exposed to it in a Laboratory.

After arriving at the University of Birmingham the isopod samples were exposed to 2mL of 25% TMAOH (99.9999% purity) and 0.5mL of ultrapure water to give a digestive solution of 20% TMAOH. The isopods were left for 24 hours to digest, some red and orange colouration of the solution was observed with the solution tending towards orange as digestive time progressed. After 24 hours 47.5 mL of ultrapure water was added to the samples to give a final dilution of 1% TMAOH.

Concurrently three ionic gold standards (end concentrations after 24-hour dilution of 1ppb, 2ppb, 3ppb) were prepared and exposed to 20% TMAOH for 24 hours before also being diluted to 1% TMAOH. Three gold nanoparticle standards (20nm, 40nm 80nm) were also prepared and exposed to 20% TMAOH for 24 hours before also being diluted to 1% TMAOH. A blank was also prepared by taking 2mL of 25% TMAOH (99.9999% purity) and 0.5mL of ultrapure water and leaving for 24 hours before filling to 50ml with ultrapure water.

Instrumental optimisation and analysis

Transport efficiency of the instrument was determined using the 20 nm, 40 nm, and 80 nm gold NPs prepared in TMAOH (see table 5.1 for instrumental parameters). NIST gold 1 ppb, 2 ppb and 3 ppb ion standards were also used to calibrate the NexION 300D.

The sample particles were analysed for gold particles size and concentration as well as for the gold ionic background, both were calculated from the spICP-MS results using the standard method described in Appendix 2 and Chapter three.

During spICP-MS analysis all peaks with a mean area of 5 counts or below were treated as ionic, this was because the blank would show no particles at this threshold (suggesting the influence of the TMAOH matrix).

Table 5.1: Instrumental parameters of the NexION 300D to analyse Isopods.

Nebulizer Gas Flow [NEB]	1.12
Auxiliary Gas Flow	1.2
Plasma Gas Flow	18
ICP RF Power	1600
Flow Rate	0.346 g min ⁻¹
Transport Efficiency	5.11 %
Dwell Time	80 us

QA/QC criteria

Quality assurance was obtained by the daily instrumental setup and by statistical analysis of multiple replicates for each sample. Due to the nature of the instrument being sequential it is not possible to use an internal standard as the internal standard would not be analysed with each sample. In lieu of the presence of an

internal standard the certified gold nanoparticle standards were routinely compared to the limits of size as stated in the certification.

Statistical analysis

The statistical analysis that was performed upon the results gathered within this chapter are R^2 correlation analysis of the standard ionic and particle calibration. A R^2 value of less than 0.996 was not utilised and the calibration was repeated either by reruns or remakes of the standards. Samples were all analysed at least three times in replicate and the average was calculated using the mean. From the mean the standard deviation was used to identify outliers that would be investigated on a sample by sample basis.

Results/Discussion

During the analysis, it was observed over the 24 hours that the isopods were exposed to 20% TMAOH their exoskeleton was drained of colour, going from a dark brown / black (dependent on isopod) to become translucent white and some of the solutions became orange in colour. This outer exoskeleton of the isopods also became hollow suggesting that the chitin shell was the only biological component of the isopods to be unaffected by the TMAOH. The solutions that had become orange in colour became colourless after final dilution of the sample.

Three batches of *Porcellio scaber* isopods that had been exposed for fourteen days to gold in the form of ions and 80 nm gold nanoparticles were sent by Ljubljana University to the University of Birmingham for analysis via spICP-MS. The first batch of isopods were prepared at Ljubljana University in TMAOH that when analysed at the University of Birmingham were shown to have an impurity or

contamination of gold rendering the detection of low concentrations of gold unattainable. A second batch of isopods was shipped to the University of Birmingham where they were digested inhouse with ultrapure TMAOH (99.9999% purity). The third batch of the isopods that were shipped were also digested within the University of Birmingham but had, had their hepatopancreas gland removed for separate analysis in conjunction with the rest of the isopod body.

In the analysis of the first batch of isopods that were treated with the impure TMAOH the extent of gold contamination was such, that the isopod uptake of gold could not be analysed at all; there was a high background that swamped the signals and peaks of the gold nanoparticles within the isopods. It was subsequently found, after receiving and analysing a sample of TMAOH from Ljubljana, that their stock of TMAOH was heavily contaminated with gold, the origin of the contamination was never established with it possibly being due to the production methodology that of TMAOH in lower purities. It was therefore decided that the digestion of the samples would occur inhouse at Birmingham and that the acquisition of purer TMAOH would be necessary.

Analysis of the purer TMAOH at Birmingham showed no ionic or particulate gold, leading to the conclusion that any gold found within samples would originate from the isopods. The calibration of the gold (shown in figure 5.1) that occurred on the day of analysis provided an R^2 value that is above the minimum acceptable R^2 value (our inhouse R^2 value for ICP-MS calibrations being 0.995) for any standard ionic or elemental calibration with ICP-MS for the purposes of method development presented in this thesis. This level of accuracy with the calibration

provides confidence in the later analysis of the gold uptake within the isopods. The high R^2 value also provided confidence that the TMAOH had not chemically altered the particles and ions in a detrimental way for analysis.

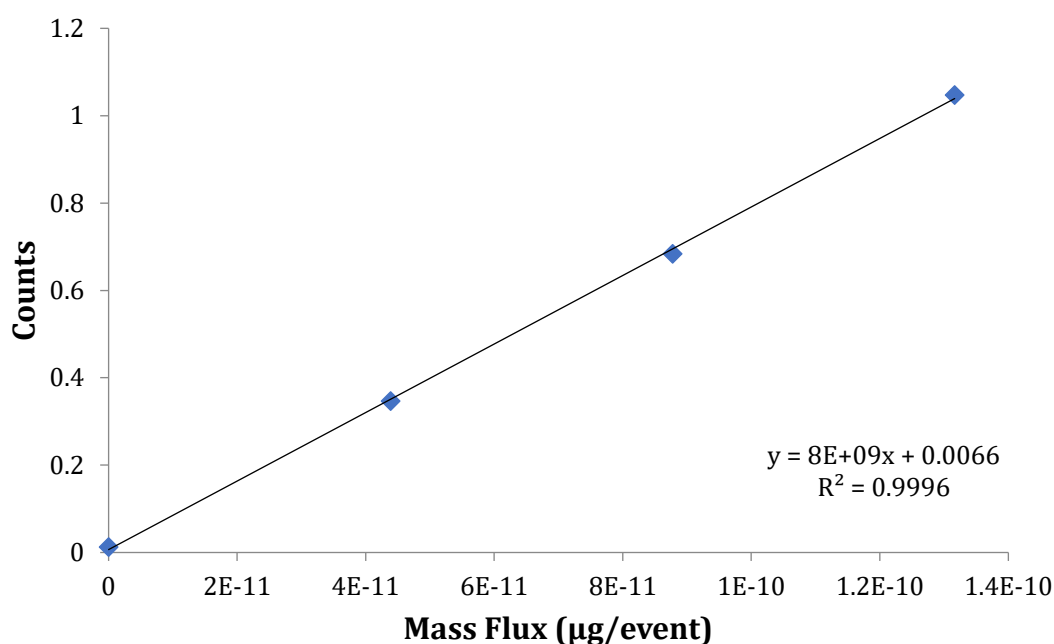


Figure 5.1: spICP-MS gold calibration standard for ionic gold with a R^2 value of 0.9996 demonstrating the high level of fitting that the analysis captured on the day of analysis.

Analysis of the second batch of isopods showed presence of gold nanoparticles in all isopods exposed to both gold particles and ions; this discovery led to the decision to produce a third batch of exposures, after which the hepatopancreas glands were to be removed from the isopods to determine if the gold was being stored within the gland. In all batches of isopods, the stomach was removed, this was to ensure that only the ions and particles that had been up taken within the body were analysed and not those that had been consumed.

Analysis of the batch two (exposures followed by digestion in “clean” TMAOH) and three (as before, but with hepatopancreas removed and digested separately) revealed the presence of gold within all batches of gold exposed isopods, with control samples having low gold ions and/or particle concentrations in comparison to the gold fed samples and levels comparable to background gold in isopods (150 ug L^{-1})¹³⁸ of 81.16 ug L^{-1} . In all the samples where the isopods had been exposed to gold whether in the form of ions or nanoparticles, gold was detected in significant concentrations. The comparatively low levels of gold background leads validity to the gold presence originating from exposure of the isopods.

Batch two – Analysis of isopod bodies

The data collected from the 2nd batch of exposures described above are presented in table 5.2.

Table 5.2: Collected results for isopod samples of batch two. With the nanoparticle size, nanoparticle concentration, dissolved ion concentration and the dilution factor for the isopods.

Sample	Mean Size (nm)	Particle Conc. (parts/mL)	Dissolved Conc. ($\mu\text{g/L}$)	Dilution Factor
C1	0	0	235.37	4,634
C2	0	0	27.98	4,704
C4	0	0	41.57	6,658
C5	84	869,411	19.73	7,153
C6	0	181,680	0	4,484

C7	52	918,003	0	7,553
C8	92	451,667	0	5,574
C9	0	0	0	7,974
C10	0	417,676	0	10,309
C11	0	0	0	5,020
C12	0	0	0	6,017
C13	0	0	0	3,441
C14	0	198,018	0	4,888
C15	0	0	0	7,310
PC1	63	186,014,559	4,092.84	8,696
PC2	66	15,842,222	1,824.43	6,410
PC3	59	468,798,755	6,191.32	5,308
PC4	59	58,474,586	3,513.33	8,591
PC5	58	10,661,720	4,333.13	8,224
PC6	59	4,083,212	2,348.58	5,599
PC7	73	4,351,722	2,225.12	5,371
PC8	63	9,636,554	1,872.27	5,061
PC9	53	8,691,237	4,725.10	8,251
PC10	68	20,034,660	2,706.16	5,495
PC11	70	2,464,388	1,757.33	6,083
PC12	72	3,880,703	4,190.46	6,386

PC13	71	3,646,673	2,748.62	4,500
PC14	55	1,741,312	2,263.24	7,163
PC15	62	5,249,233	3,766.72	5,889
Au1	79	7,447,525	308.85	9,191
Au2	82	5,194,171	0	8,013
Au3	85	21,026,531	0	6,329
Au4	84	42,141,031	0	9,124
Au5	88	5,772,796	0	12,953
Au6	81	12,896,707	0	7,764
Au7	84	25,683,321	0	8,929
Au8	85	24,448,426	0	9,579
Au9	85	9,306,555	0	7,657
Au10	78	13,651,637	0	10,870
Au11	82	11,506,770	0	6,605
Au12	86	21,070,515	0	9,124
Au13	85	22,191,060	0	7,825
Au14	87	19,233,546	0	7,657
Au15	79	6,784,731	0	7,974

Firstly, the observed Au particle count in the control samples is considered acceptable given it is much lower than any of the samples that had gold introduced (216,890 particles mL⁻¹ for the control samples compared to 37,139,032 particles

mL⁻¹ of the average of the positive control and gold nanoparticle samples) and agrees with other literature values ¹³⁸. The levels of gold present in the control samples C5, C7 and C8 (show in figure 5.1 and figure 5.2) did not correspond to any significant particle populations in comparison to the exposed samples. It is possible that, where control values appear to give a signal matching to that of a particle, this is likely to have derived from residual particles present in the tubing. This specifically applies to the first control sample in Table 5.2, which has an elevated ionic concentration.

Otherwise, the controls did not show significant signs of gold particles with samples lacking any distinct particle events in analysis with little to no ionic gold detected.

As can be seen in figure 5.4 above there is a quickly decreasing level of gold ions detected within the blank isopod samples, this is likely because any leftover gold within the tubing is being washed out, although it is important to point out that when the concentrations are reverted to their diluted numbers for both nanoparticles and ions the concentrations are minimal compared to actual exposed samples and close to 0 especially when in comparison to the levels that are present for ions and nanoparticles.

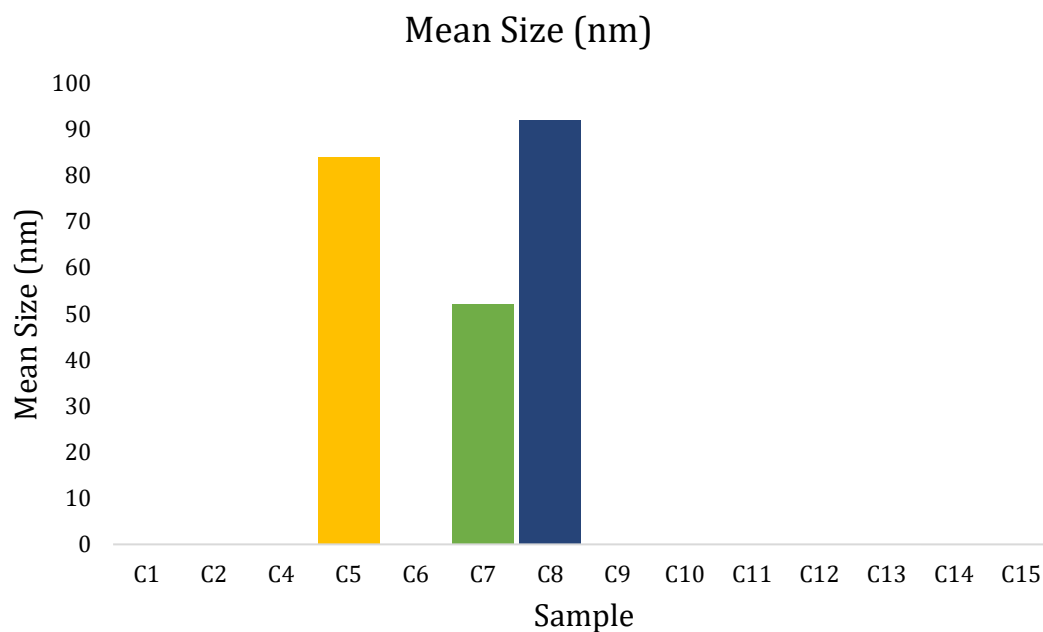


Figure 5.2: The mean size of gold nanoparticles found within the bodies of the isopods of batch two's control samples. Sample identification can be found in Table 5.2.

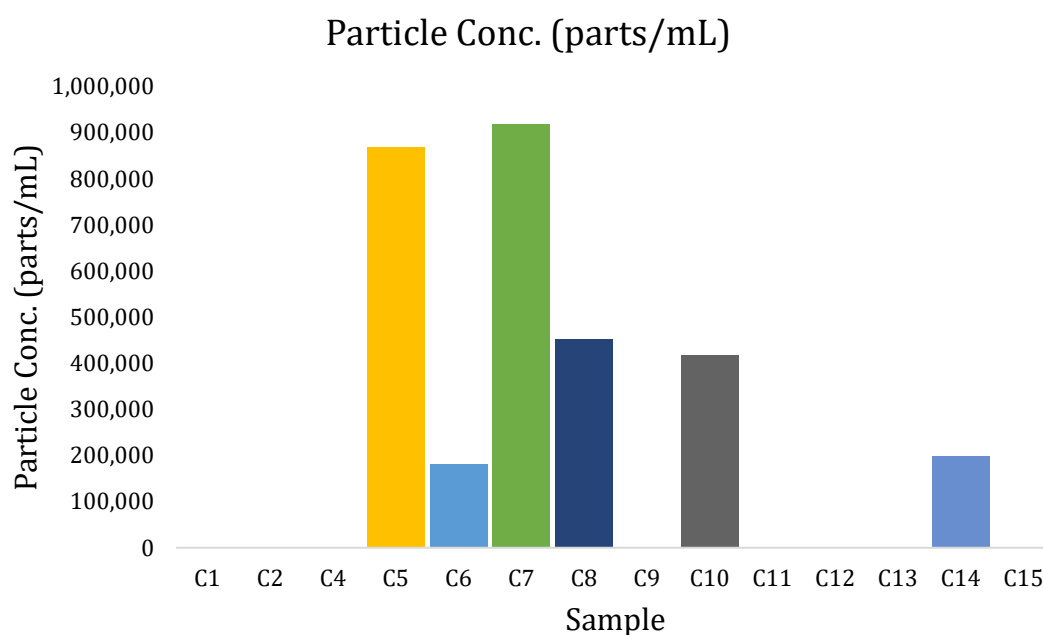


Figure 5.3: The particle concentration of gold within the bodies of isopods analysed in batch two's control samples.

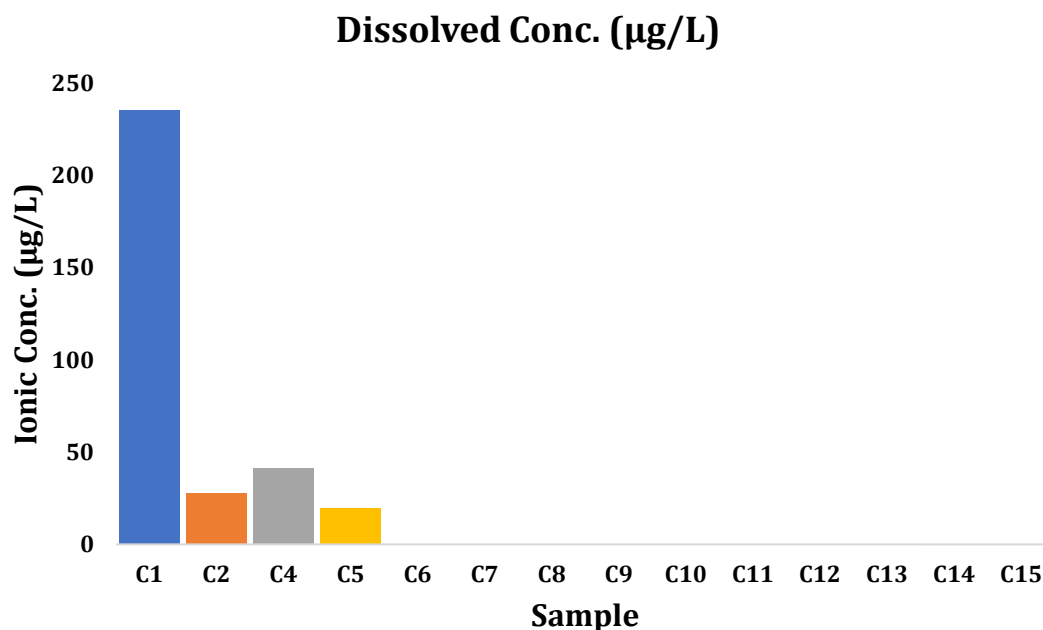


Figure 5.4: The dissolved concentration of gold ions within the bodies of the isopods analysed in batch two's control samples.

All the positive control (PC) samples for batch two have particles present with a wide range of particle populations all around 60-80 nm (see figure 5.5). The PC samples also show high levels of ionic gold (see figure 5.6), which is not a surprise seeing that the PC samples were fed AuCl_3 . However, the presence of particles was not expected (see figure 5.7). It is hypothesised (see discussion) that the ionic gold has likely nucleated and formed gold nanoparticles, which, in comparison to the particles found in the 80 nm gold samples exposures, appear a lot less uniform in size.

There is definitive presence of gold in the positive control samples, which when contrasted against the control samples show both particle uniformity and ionic concentration confirming that the controls are mostly devoid of gold. The positive control of ions that were fed to the isopods shows concentrations of particles and ions that were larger than that of the controls at $3,199 \mu\text{g L}^{-1}$ to $23 \mu\text{g L}^{-1}$ from the

control samples for the ions and 216,890 particles mL⁻¹ for the control samples compared to 57,023,022 particles mL⁻¹. With a wide variance in particle concentrations (standard deviation of 128,085,826 particles mL⁻¹) and some variance in ionic concentration it is clear that something has occurred within the isopods that has caused that ionic control to form particle like entities, and this is discussed later in depth as likely a key mechanism that isopods use to store metals. The wide variance in concentration of particles suggests that some of the isopods either consumed significantly larger amounts of gold ions. This could be either due to being in a position of the exposure environment that had higher concentrations of gold ions or by specifically consuming larger amounts of gold. It is interesting to note that while these isopods have higher than average concentration of nanoparticles and ions present within, they did not possess body masses (represented by the dilution factor) that were abnormal, this suggests that these isopods were not unnaturally large in comparison to the rest of the population.

The 80nm gold nanoparticle fed isopods all showed presence of 80nm gold particles, there was little to no particle dissolution in the isopods as the particles were all relatively uniform and the mean and most frequent sizes are very similar (see figure 5.8). These samples also have no ionic gold in the digested body mass (apart from Au1) meaning that the particles have not dissolved during exposure or sample preparation (see figure 5.9 and figure 5.10). Specifically, this suggests that the isopods are not causing dissolution of the particles once uptake has occurred.

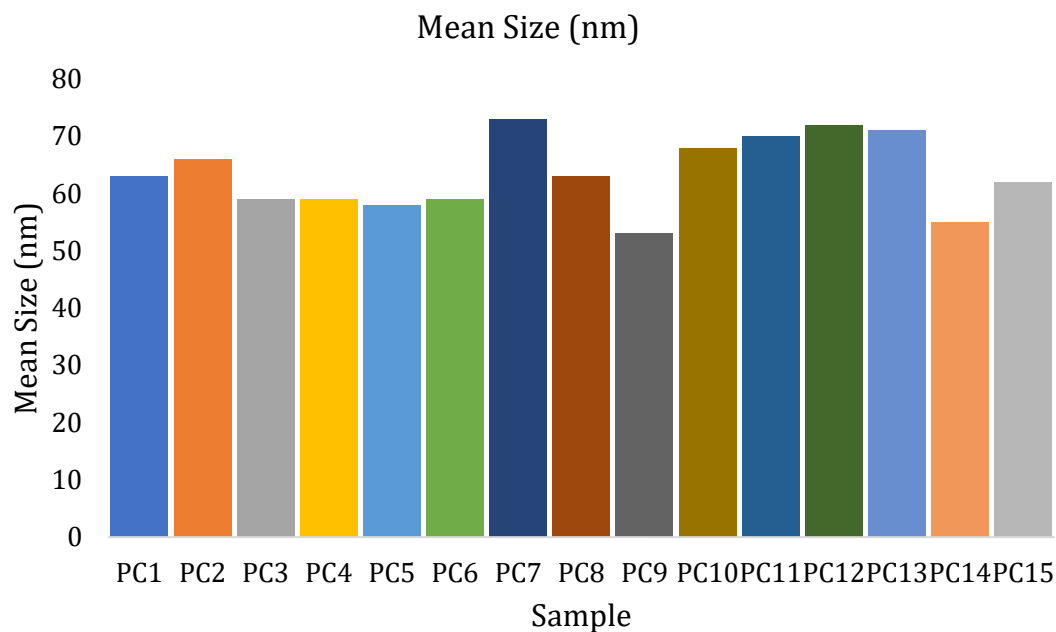


Figure 5.5: The mean size of gold nanoparticles within the isopods of batch two's positive control samples.

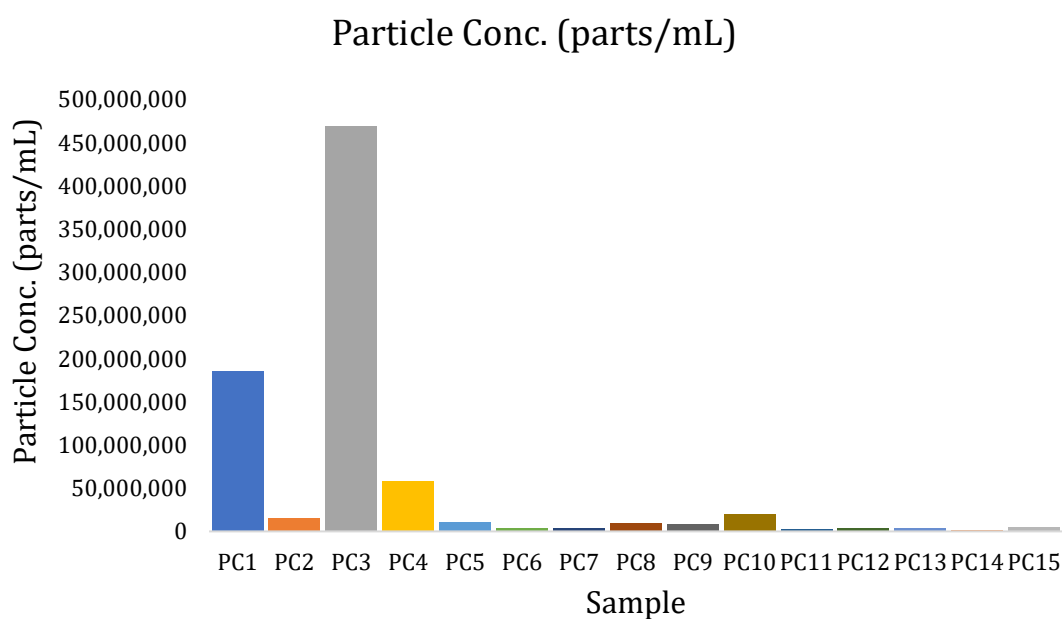


Figure 5.6: The particle concentration of gold within batch two's positive control samples. PC3 has a significantly larger particle concentration than the other samples.

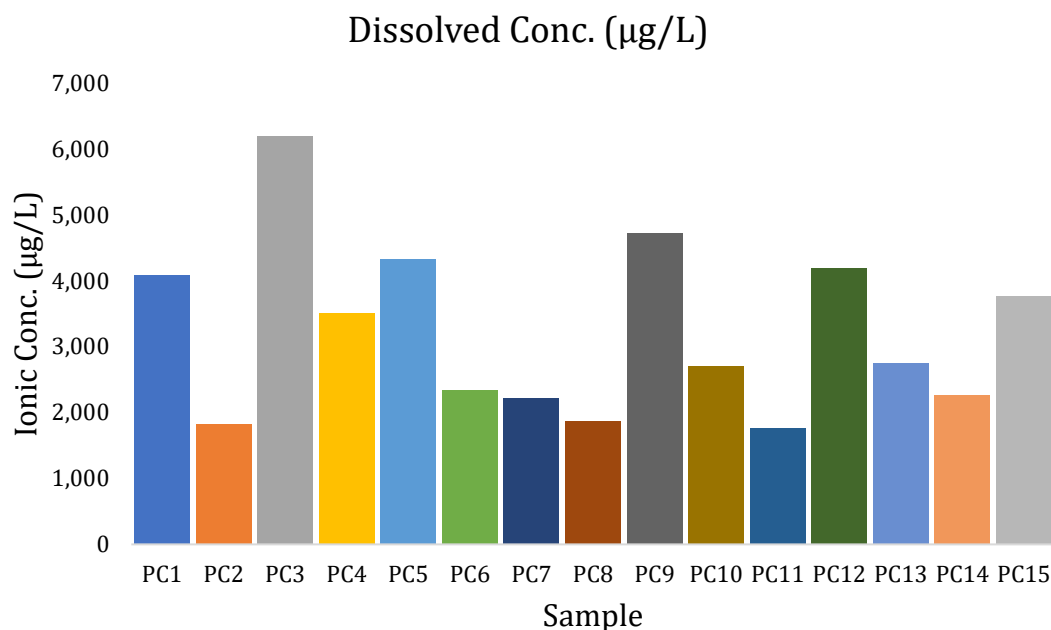


Figure 5.7: The dissolved concentration of gold within the isopods of batch two's positive control samples. Shown is a wide variance in ionic concentration.

When comparing the isopods that were exposed to gold nanoparticles and those that were exposed to gold ions there are some clear differences, namely the ion concentration that is found within the isopods. Where it is clear that the ion exposed isopods had a significant amount of gold within their bodies in both particles and ions form, the isopods that were exposed to nanoparticles have predominantly no ions found within their bodies. Where it was likely the case that the ions were being absorbed within the isopods body and agglomerated into particles here it is likely that the isopods are absorbing the particles and storing them for use later use or for expulsion as waste.

When the concentrations of nanoparticles between the particle and ion fed isopods are compared there is higher levels of gold particles within the ion fed samples of isopods at 57,023,022 particles mL⁻¹ compared to 17,255,042 particles mL⁻¹ for particle fed isopods, this difference in concentration is most likely due to

the difference in size of the measured nanoparticles that formed in the positive control vs particle fed isopods, where the decreased mass of particle allows for a higher concentration of particles to the larger particles found in the particle fed isopods. Again, while there is some variance in concentration of the particles within the isopods at 10,003,263 particles mL⁻¹, there is no significantly large isopods that have statistically large concentrations of nanoparticles within their bodies.

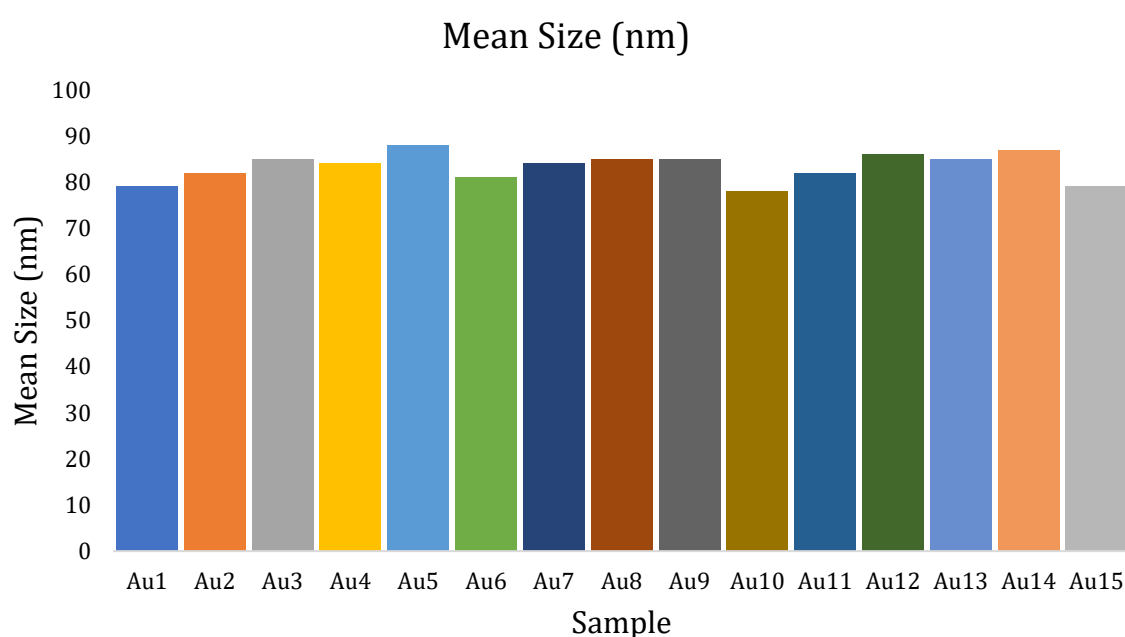


Figure 5.8: The mean size of gold nanoparticles within the isopods of batch two's nanoparticle fed samples. There is a close correlation of nanoparticle size across the samples.

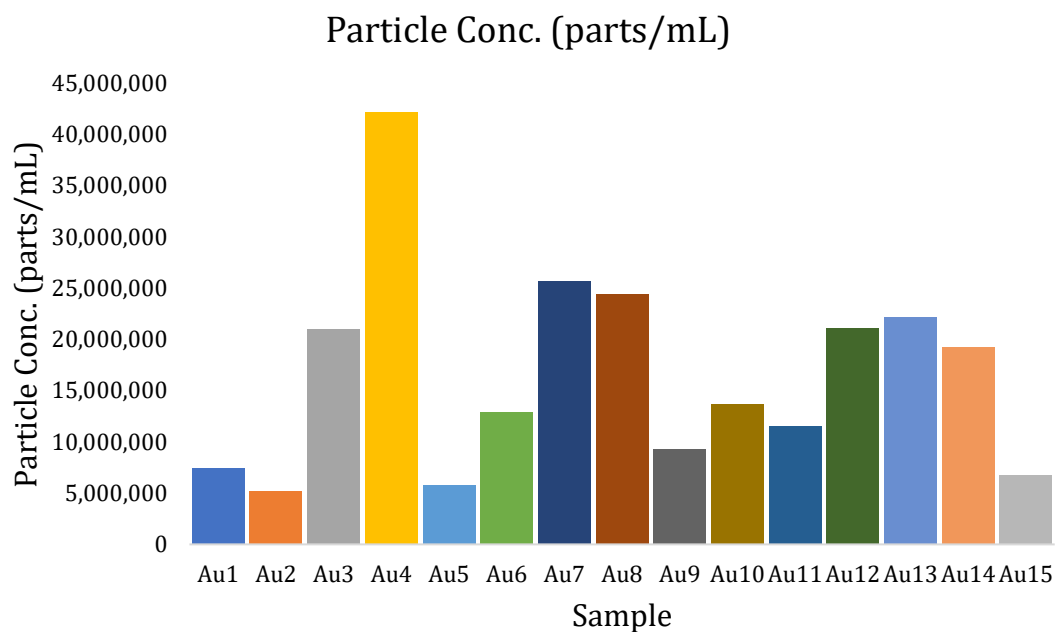


Figure 5.9: The particle concentration of gold within the isopod bodies of batch two's nanoparticle fed samples.

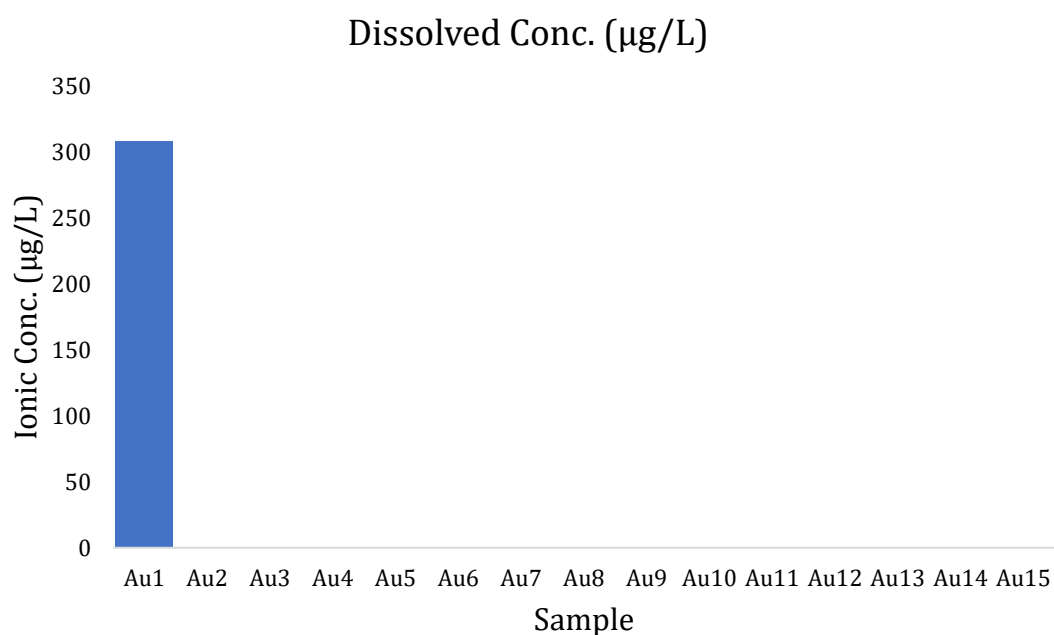


Figure 5.10: The dissolved concentration of gold within batch two's nanoparticle fed samples. Only one sample Au1 showed any significant levels of gold ions.

Batch three – Analysis of isopod bodies and hepatopancreas

The data collected from the 3rd batch of exposures described above are presented in Table 5.3.

Table 5.3: Collected results for isopod samples of batch three. With the nanoparticle size, nanoparticle concentration, dissolved ion concentration and the dilution factor for the isopods.

Sample	Mean Size (nm)	Particle Conc. (parts/mL)	Dissolved Conc. (µg/L)	Dilution Factor
C1	58	4,108,216	1,052	3,340
CHep1	58	70,528,609	9,880	87,719
C2	60	9,459,131	2,053	6,061
C3	63	3,431,200	693	2,902
CHep3	59	87,584,547	13,526	185,185
C4	58	2,954,132	801	3,123
CHep4	59	66,213,918	13,743	200,000
C5	62	2,040,805	748	5,394
CHep5	54	1,507,549,021	20,347	312,500
C6	57	13,601,365	1,681	6,536
CHep6	53	101,347,833	16,981	357,143
C7	58	35,455,913	4,109	6,693
CHep7	53	109,793,486	10,962	178,571
C8	55	3,410,744	861	4,006

CHep8	59	63,913,048	9,710	135,135
C9	58	12,320,142	1,137	7,236
CHep9	54	59,119,569	11,368	250,000
C10	65	13,664,876	2,021	8,026
CHep10	60	189,182,622	11,161	200,000
C11	58	36,167,266	1,956	8,403
CHep11	66	118,239,139	13,274	277,778
C12	57	9,440,251	1,823	4,990
CHep12	48	45,769,989	6,754	161,290
C13	59	4,855,230	1,484	6,039
CHep13	57	32,617,693	10,427	172,414
C14	57	9,048,914	1,410	6,378
CHep14	67	23,647,828	11,392	250,000
C15	65	3,513,141	900	4,643
CHep15	49	19,706,523	7,963	138,889
PC1	58	25,483,754	3,934	5,794
PCHep1	71	24,892,450	19,025	263,158
PC2	57	86,634,067	5,426	3,642
PCHep2	55	591,195,694	339,594	2,500,000
PC3	55	141,580,167	12,290	4,634
PCHep3	54	118,239,139	83,679	1,250,000

PC4	51	516,546,610	10,026	5,297
PCHep4	48	39,413,046	25,831	208,333
PC5	60	74,086,266	4,807	5,675
PCHep5	60	23,647,828	27,194	500,000
PC6	56	98,719,852	15,770	9,276
PCHep6	54	1,182,391,389	152,574	2,500,000
PC7	58	141,280,878	4,872	4,575
PCHep7	49	24,130,437	49,856	102,041
PC8	67	107,772,126	4,196	5,086
PCHep8	0	0	5,352	111,111
PC9	59	93,685,714	6,105	9,524
PCHep9	59	157,652,185	51,783	833,333
PC10	55	71,295,681	3,729	4,153
PCHep10	69	126,890,783	19,810	121,951
PC11	65	30,597,588	1,804	5,482
PCHep11	47	78,826,093	12,423	111,111
PC12	57	100,102,249	5,261	5,112
PCHep12	41	34,776,217	12,115	147,059
PC13	60	57,216,783	4,028	6,993
PCHep13	56	17,516,909	37,257	185,185
PC14	58	16,010,979	1,802	4,575

PCHep14	60	25,336,958	14,280	178,571
PC15	57	45,994,194	4,013	7,257
PCHep15	53	33,782,611	32,354	238,095
Au1	89	13,930,858	1,773	6,402
AuHep1	50	24,892,450	5,411	131,579
Au2	86	23,537,074	845	3,340
Au3	86	37,571,996	1,400	4,965
Au4	85	29,283,054	1,457	4,655
AuHep4	54	39,413,046	13,233	277,778
Au5	84	35,344,009	1,940	5,931
AuHep5	57	78,826,093	22,389	555,556
Au6	75	12,856,160	1,063	3,441
AuHep6	83	30,513,326	9,270	161,290
Au7	86	27,278,008	1,116	4,149
AuHep7	60	9,554,678	4,314	50,505
Au8	80	21,743,295	2,503	6,386
AuHep8	57	13,137,682	9,766	138,889
Au9	72	20,199,115	2,207	5,531
AuHep9	60	141,886,967	10,865	125,000
Au10	85	9,312,779	788	3,715
AuHep10	54	61,934,787	4,196	59,524

Au11	81	20,469,239	1,814	5,214
AuHep11	55	113,509,573	14,782	200,000
Au12	71	32,297,454	1,615	5,787
AuHep12	54	29,559,785	10,724	156,250
Au13	84	7,874,703	1,642	3,965
AuHep13	73	14,779,892	4,901	78,125
Au14	86	17,771,136	709	4,270
AuHep14	67	22,884,995	9,018	161,290
Au15	74	13,264,840	629	3,262
AuHep15	63	8,758,455	2,713	46,296

Batch three of the analysis of isopods was completed after it was found that the presence of so much gold within the bodies of the isopods warranted further investigation and it was decided that the hepatopancreas should be removed from the isopods and analysed separately. It was believed that the hepatopancreas would be the main sight of metal accumulation within the isopods, with there being little to no gold found in the rest of the body.

The control samples for the isopods which had their hepatopancreas removed showed a consistently higher concentrations of gold within the hepatopancreas in all samples with the exceptions of C10 and C12 which have smaller hepatopancreas particle size, with an average nanoparticle sizes of the gold to be around 60 nm (see figure 5.11), this size of gold is later shown to be consistent with the results that occur within the spiked samples. There were highly increased

number of particles (see figure 5.12) and ions (see figure 5.13) in comparison to the analysis of the second batches levels of gold. There has been clear indication that there was some sort of gold contamination that had occurred to the control. Looking at the diluted levels of gold ions that were detected it becomes clear that there is again little to no gold ions in solution but there is a significant and measurable amount of gold nanoparticles in the digestions. It is unclear where this gold has come from, as there should not be any gold present in the TMAOH matrix, it is possible that the isopods have become contaminated at some point in the exposure, but this cannot be confirmed.

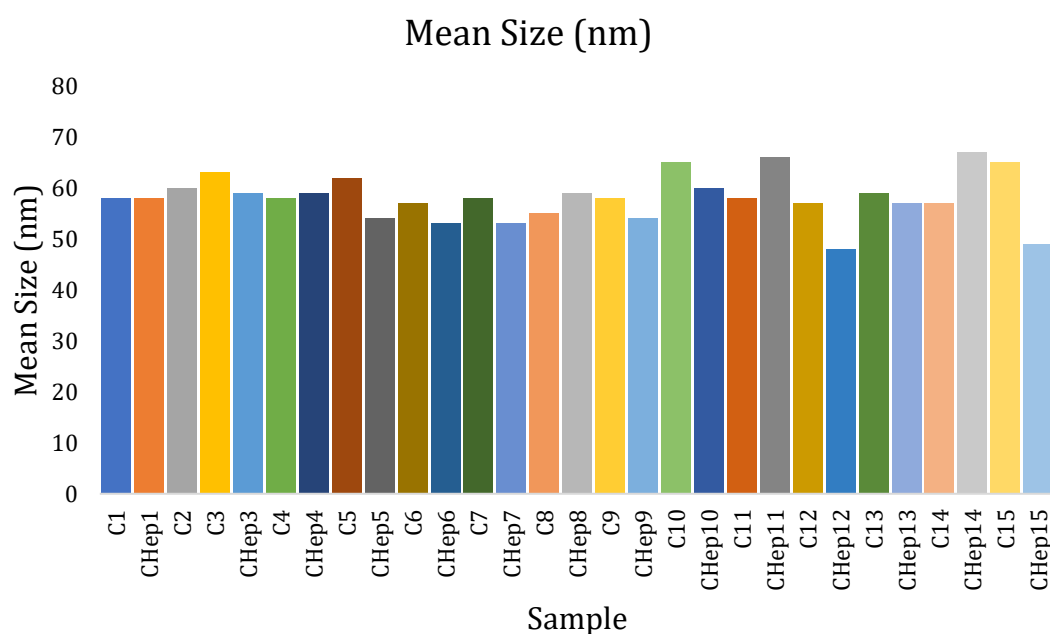


Figure 5.11: The mean size of gold nanoparticles within batch three's control samples. These samples showed consistent gold nanoparticle sizes suggesting a gold ion contamination.

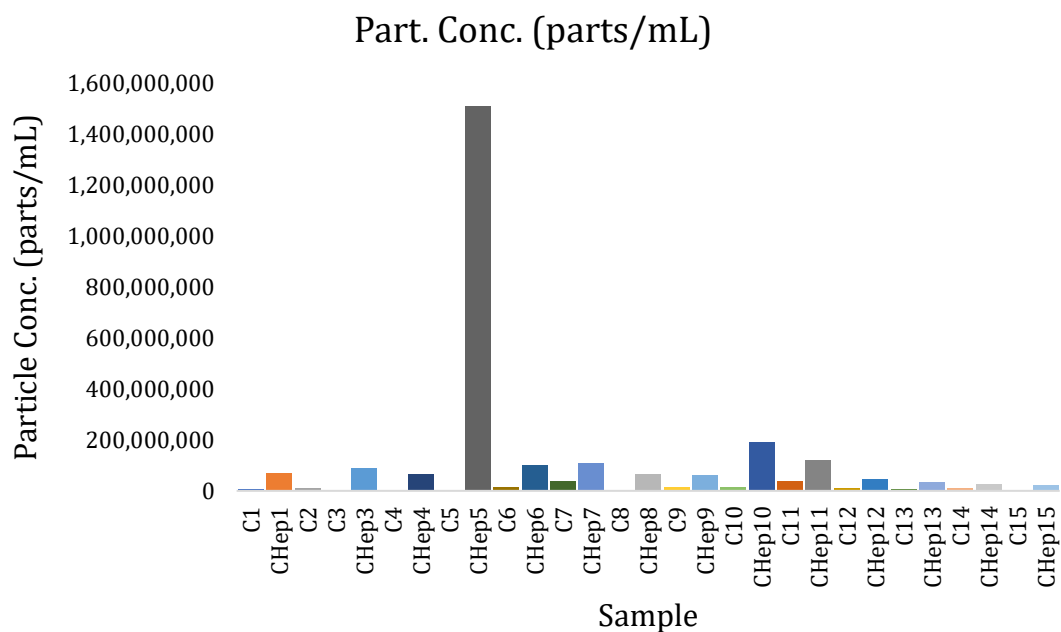


Figure 5.12: The particle concentration of gold within isopods and hepatopancreas of batch three's control samples. The hepatopancreas have consistently higher particle concentrations.

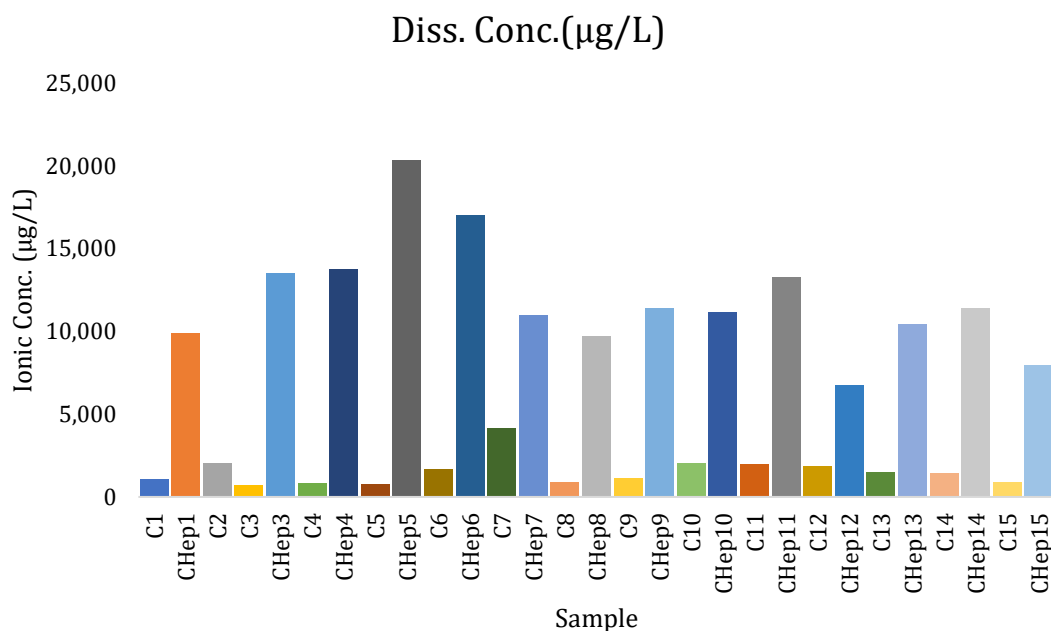


Figure 5.13: The dissolved concentration of gold within the isopods and hepatopancreas of batch three's control samples. The hepatopancreas have consistently higher ionic concentrations.

In order to overcome the limitations from the background contamination, and given that it was not possible to repeat the experiments again, we ignored the hep samples from the control, this removed the influence from any gold contamination and left just the particles that were present from the isopods of spiked samples. Looking at the results for the positive control there is some variation in the size (see figure 5.14) of the nanoparticles with the hepatopancreas samples particles commonly slightly smaller than the particles found within the rest of the isopod bodies, there are two outliers PCHep1 and PCHep10 (and potentially PCHep 14 but the size difference between the PC14 and PCHep14 are not statistically different in size), where the size of particles within the Hep samples are much larger than that found within the rest of the body with sizes closer to that of the particle fed isopods. While these large particle hepatopancreas samples contain some of the higher concentrations for both particles ($136,189,955 \text{ particles mL}^{-1}$) and ions (see figure 5.15 and figure 5.16), they are by no means the largest among the batch and are dwarfed in particle concentration by PChep2 ($591,195,694 \text{ particles mL}^{-1}$), PC4 ($516,546,610 \text{ particles mL}^{-1}$) and PChep6 ($1,182,391,389 \text{ particles mL}^{-1}$). There is a wide range of concentration of both the particles formed and ions in solution, with the hepatopancreas samples typically having significantly larger concentrations in comparison to the body at $88,063 \mu\text{g L}^{-1}$ and $1,607,006,908 \text{ particles mL}^{-1}$, in comparison to $883,127 \mu\text{g L}^{-1}$ and $2,478,691,739 \text{ particles mL}^{-1}$ for the hepatopancreas samples this is consistent with the results show within the control ($163,471,326 \text{ particles mL}^{-1}$ and $22,729 \mu\text{g L}^{-1}$ compared to $2,495,213,825 \text{ particles mL}^{-1}$ and $167,488 \mu\text{g L}^{-1}$) and particles ($322,733,720 \text{ particles mL}^{-1}$ and $21,501 \mu\text{g L}^{-1}$ compared to $589,651,729 \text{ particles mL}^{-1}$ and $121,582 \mu\text{g L}^{-1}$) results that are described.

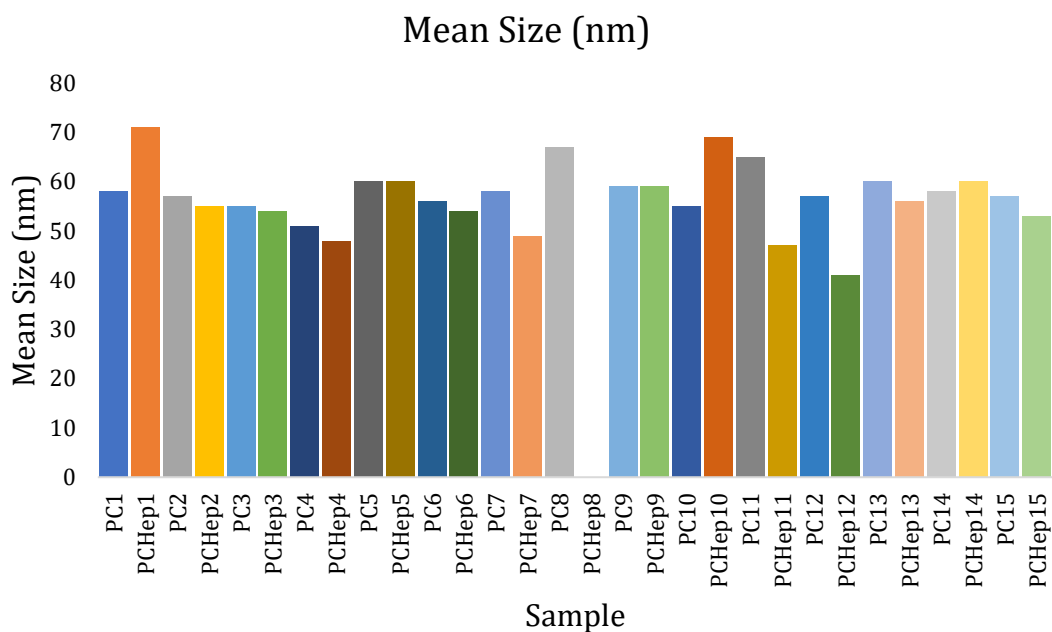


Figure 5.14: The mean size of gold nanoparticles within batch three's positive control samples. PCHep8 did not have any particles detected. There is less variation between the isopod bodies and hepatopancreas in these samples.

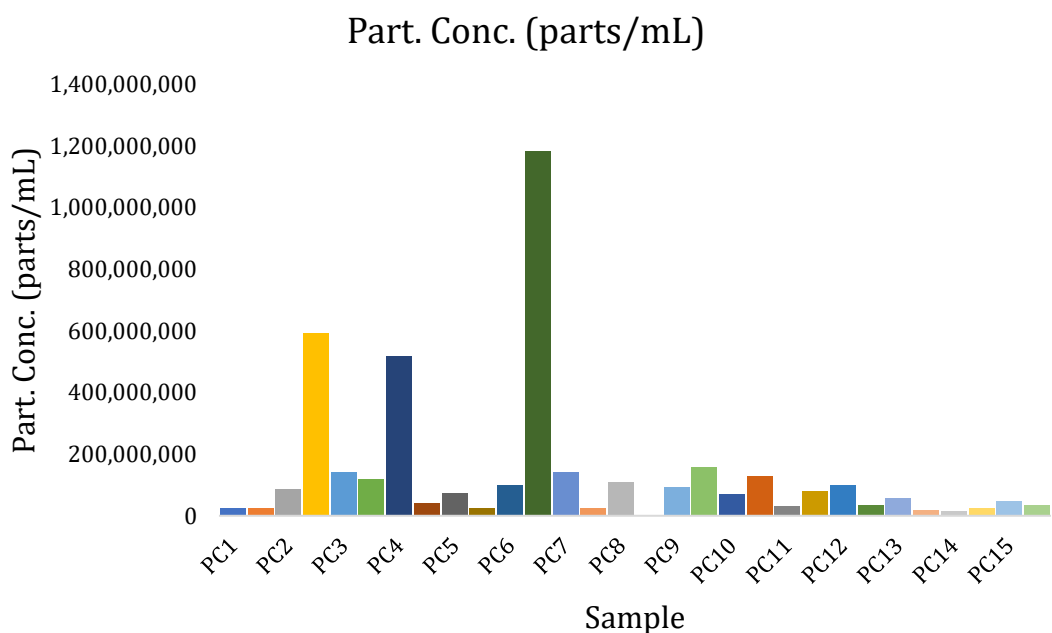


Figure 5.15: The particle concentration of gold within batch three's positive control samples. PCHep2, PCHep4 and PCHep6 showed an elevated particle concentration compared to the other samples.

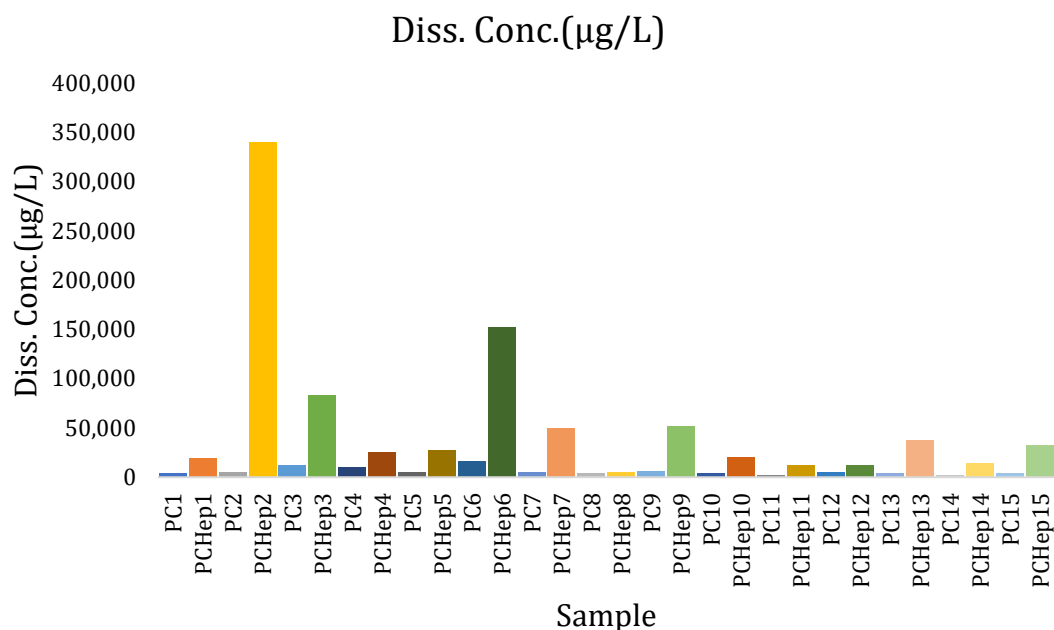


Figure 5.16: The dissolved concentration of gold within batch three's positive control samples. PC2Hep2 and PC6Hep6 had large gold ion concentrations.

When the results from the gold particle fed isopods are analysed there is a clear and repeating trend that the size of the particles within the hepatopancreas samples are lower with many being much lower in size (see figure 5.17). The size of the hepatopancreas samples is close to that of the isopods that were fed gold ions at around 60 nm. While the hepatopancreas particles are smaller than that of the rest of the body the concentration of both the ions (see figure 5.18) and particles (see figure 5.19) is consistently larger with the nanoparticles being many times more concentrated within the hepatopancreas than the body, with some outliers where the particle concentrations of Au7, Au8, and Au15 are have larger concentrations of than the hepatopancreas of the isopods. The nanoparticles that are present within the bodies of the isopods have particles that appear to have been unaltered remaining 80 nm.

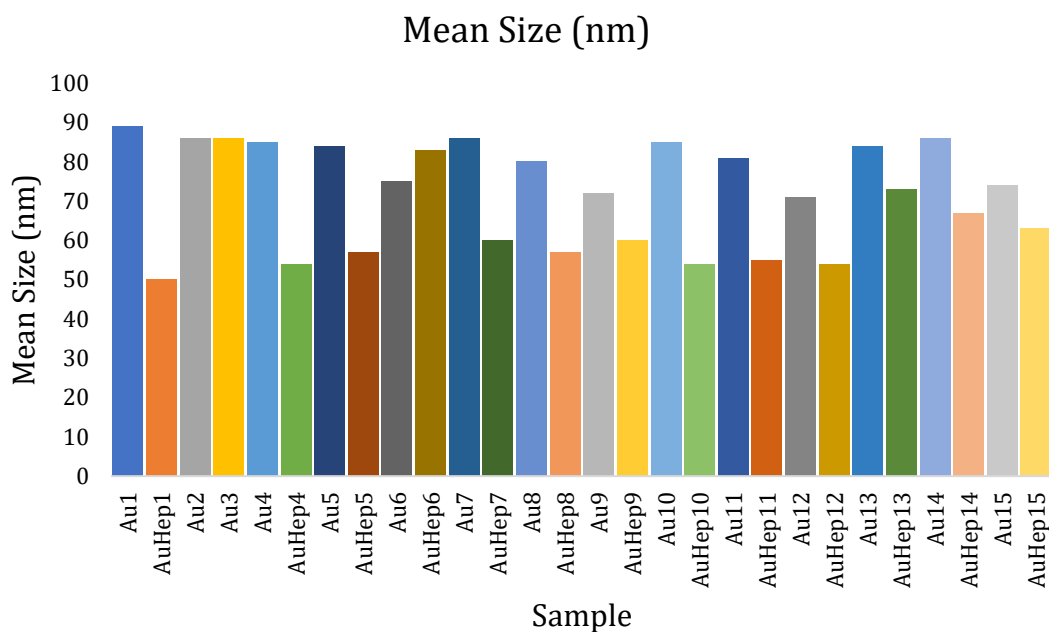


Figure 5.17: The mean size of gold nanoparticles within batch three's nanoparticle fed samples. The sizes of the hepatopancreas samples was consistently lower around 60nm in comparison to the isopod bodies.

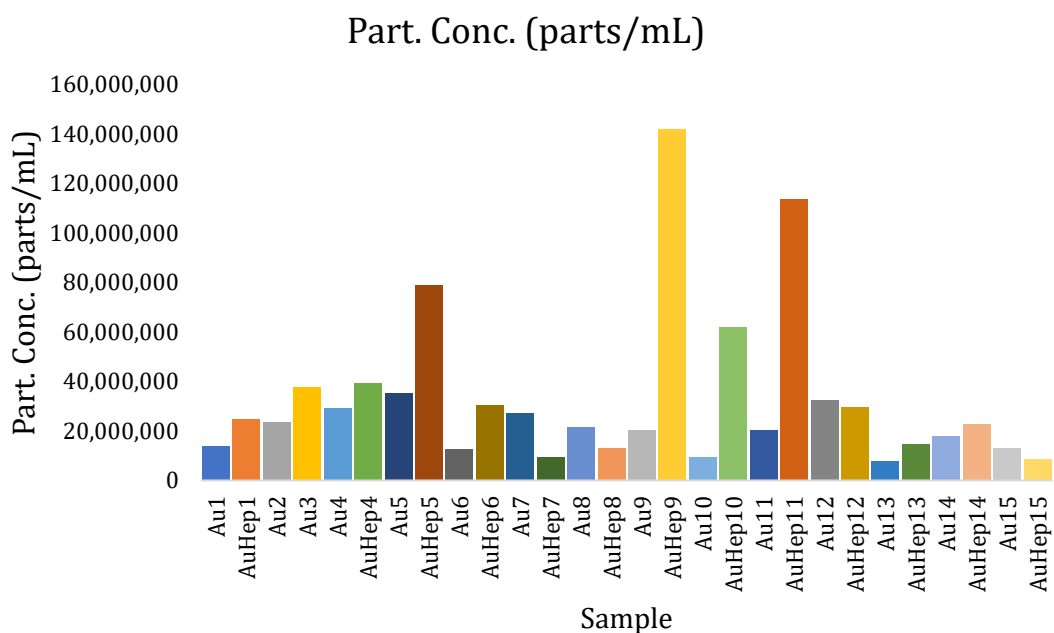


Figure 5.18: The particle concentration of gold within the bodies and hepatopancreas of the isopods analysed in batch three's nanoparticle fed samples.

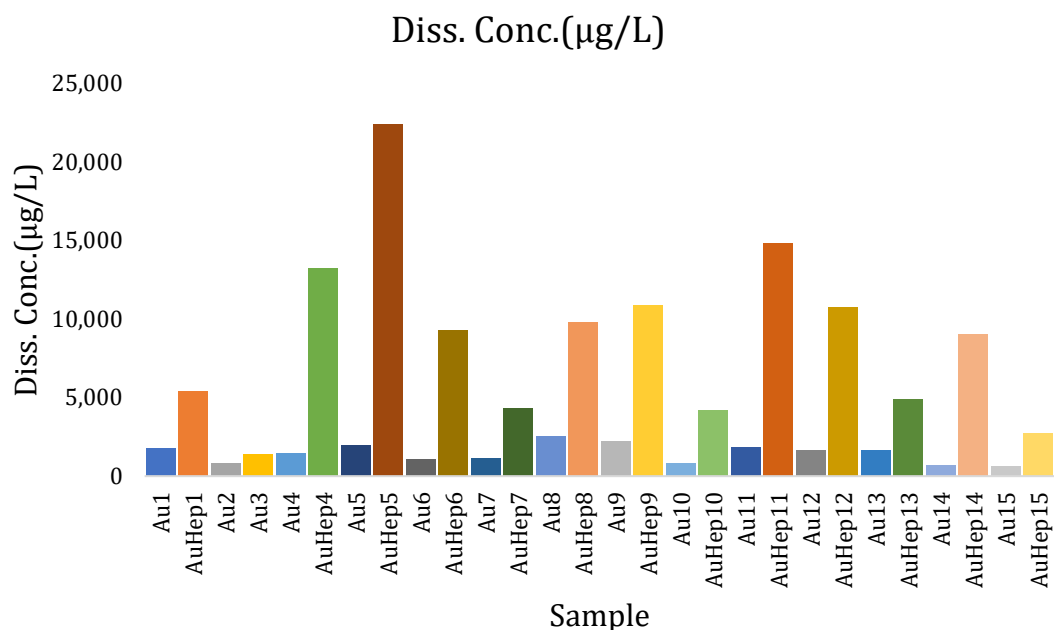


Figure 5.19: The dissolved concentration of gold within batch three’s nanoparticle fed samples. The ionic concentration of the hepatopancreas samples was consistently higher than the isopod bodies.

Comparison of batches and exposures.

When comparing the results of the particle size between the batches two and three of isopods and between the isopods and hepatopancreas of the isopods, there is a clear amount of similarity between all samples (shown in figure 5.20). In the control there was a larger amount of variance in the particle size with the second batch having a wide size range of nanoparticles detected (0 – 92 nm). This large amount of variance in the particle size is likely related to the concentration of the particles within the control samples which was low. In analysis of the nanoparticles for the third batch both hepatopancreas and the isopod bodies have similar size to the results for the ions for both batches. This is extended into the smaller average particle size for the hepatopancreas than the full body of the PC samples. The similar results suggest that there was some sort of contamination of

the isopods in the control samples. From the results that can be seen in figure 5.20 it becomes clear that the hepatopancreas is causing a limiting size of nanoparticles within the isopods, where all three samples have similar particle sizes. This is especially apparent within the gold nanoparticle samples where the particles have remained 80 nm. Within the hepatopancreas of the isopods the nanoparticles have lost 58% of their mass to ions. The loss of particle mass is contrasted with the concentrations of ions within the hepatopancreas, increasing in comparison to the rest of their bodies.

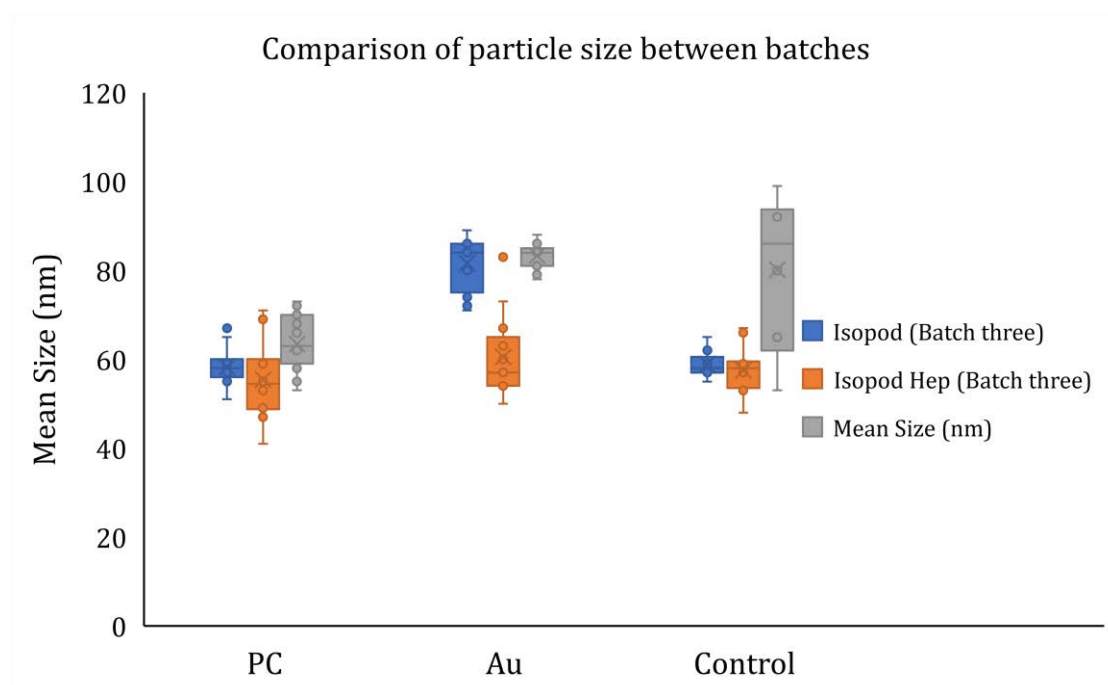


Figure 5.20: Comparison of the particle size of gold nanoparticles within isopods between batch two and three.

The particle concentration of gold within the three batches of isopods shows (see figure 5.21) that there is a lot of variation of nanoparticles within the PC and hepatopancreas samples. The change of gold from ions to particles suggests that the isopods are metallo-sequestering the gold at varying rates. The large amount of gold nanoparticles that are within the PC samples shows that there is a

significant amount of gold being stored within the isopods, as part of an active or passive biological process.

When the particle concentrations within particle fed isopods are analysed, it is clear that there is a large variance of the concentrations within hepatopancreas when compared to the bodies of isopods. Coupled with the smaller size of the nanoparticles within the hepatopancreas it is suggested that during metallo-sequestering the isopods are digesting the large 80 nm gold nanoparticles into ionic gold which is further metallo-sequestered into 60 nm gold nanoparticles/granules.

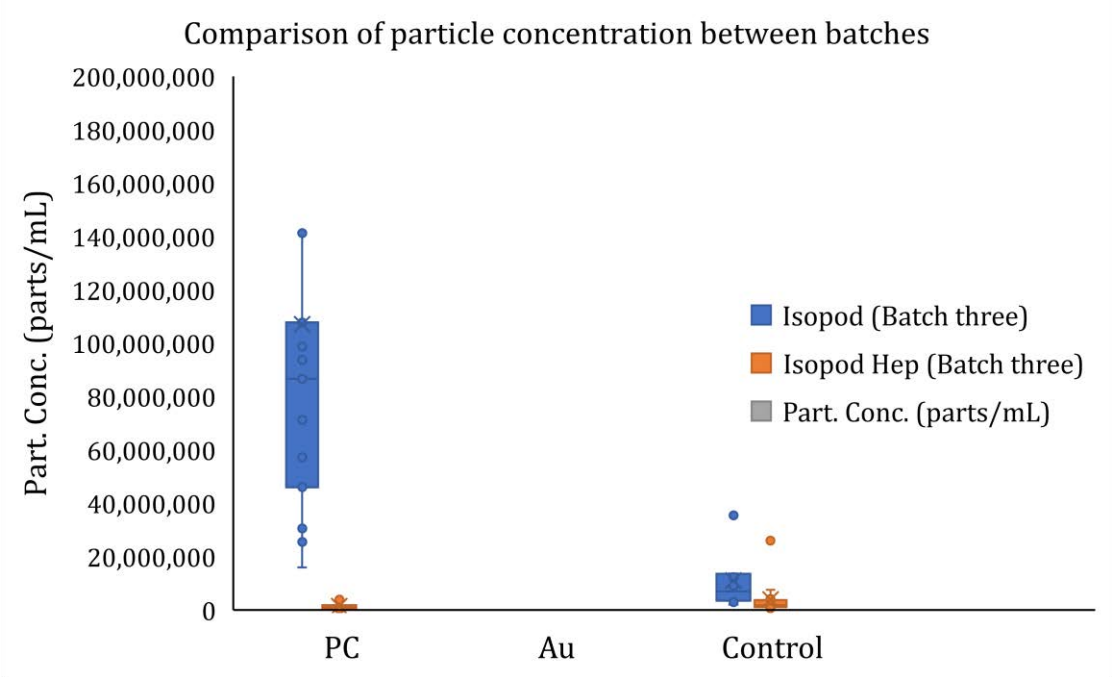


Figure 5.21: Comparison of the particle concentration of gold nanoparticles within isopods between batch two and three.

The concentration of ions within hepatopancreas is consistently larger and more variable than that found within the rest of the isopods, this follows that the isopods are expelling gold after processing the gold with metallo-sequestration within the hepatopancreas. The amount of the ions that are found within the rest of the

bodies of the isopods are consistently low and close to that found within the control samples suggesting that the isopods are not storing gold ions in significant levels within the rest of their bodies and only within the hepatopancreas. These variances are shown graphically in figure 5.22.

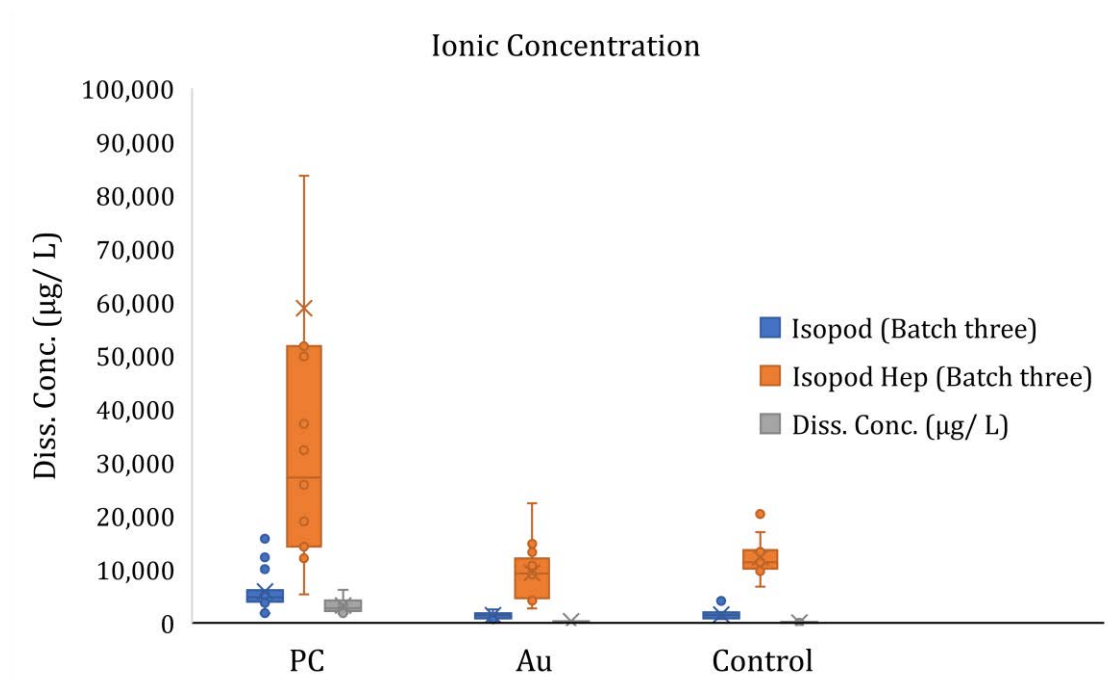


Figure 5.22: Comparison of the particle size of gold nanoparticles between batch two and three. Note the large ionic concentration variance of the positive control hepatopancreas samples.

Conclusions

In the results described above it is observed that the gold concentration (both particle and ionic) of hepatopancreas samples was almost always higher than that of the isopod body samples. There seems to be some background gold within the control samples as the isopods have comparable ionic and particle concentrations to the gold nanoparticle (Au and AuHep) samples. There is also dissolution and precipitation of gold in the hepatopancreas as both batches of isopod analysis

show the ionic samples (PC) have formed 60 nm gold particles. These ion formed nanoparticles are also seen within the Control and all hepatopancreas samples. When analysing the isopods that were fed gold nanoparticles it is seen that whilst 80 nm gold nanoparticles are present within the body, the particle size in the hepatopancreas is reduced to an average of 60 nm. The precise biological process that generates such complexity has yet to be described.

Nevertheless, some conclusions can be reached from the results that have been gathered over the two successive batches of isopods that have been analysed. There is evidence of metallo-sequestration of gold within isopods, in both the degradation and agglomeration of gold within the hepatopancreas. The isopods are ingesting gold from the environment and transforming it into metallic granules for a purpose not experimentally determined within this study. It is believed that the isopods are either storing the gold granules or expelling them as waste back into the environment. It should be expected that if the isopods were exposed to a controlled environment after the 14-day exposure there would either be presence of gold granules on the detritus that the isopods were living in or gold would only be found within the isopods after removing them from the new environment. Within the analysis the uptake of full 80 nm gold nanoparticles by the isopods demonstrates that they are not processing the gold until after it has entered into the cells of the body. This could mean that the 60nm gold granules that are detected within all the samples is the isopods hepatopancreas, regardless of whether gold was presented to them in ionic or particulate form, were formed locally within the organ.

Due to the fact that the TMAOH was tested on the particles on their own and no background or loss of particle size was observed in those results, it can be safely assumed that the difference in size is not related to the matrix of the sample solution but was a process that occurred within the isopods. This finding relates back to the known process of metal storage that isopods are able to undertake metallo-sequestration.

Chapter Six

Exploring the potential for use of the intrinsic metal content of individual biological cell lines as an internal standard for quantification of cell number

Aims and Overview

Single Cell Inductively Coupled Plasma Mass Spectrometry (SC-ICP-MS) is an emerging analytical technique in the fields of environmental and biological sciences that enables the quantification of metals (ions, particles, colloids) on a single-cell basis. The method has been shown to work in principle with simple unicellular organisms and algae ^{17,25,43,77,80}, and is now undergoing a period of development of specific applications of the method to address problems that previously could not be addressed except using fluorescent probes which have their own challenges ^{139,140}. The specific examples currently under development as part of this thesis are the detection and quantification of metal or metal oxide nanoparticle uptake by algae and cancer cell lines. The work outlined in this chapter focuses on assessing the potential for intrinsic metal content within cancer cell lines, specifically A549 ^{87,88}, MDA ⁹⁶, and HeLa ^{94,95}. cells, to act as an internal reference for cell counting and as a means to distinguish individual cell types, coupled to quantification of nanoparticle association with the cells on a cell-by-cell basis. Additionally, studied was the ratios between elements in the cell lines, with the theory being that individual cell lines would have a signature set of ratios of elements that could be used to fingerprint the cells. The ability to measure

cells on a cell-by-cell basis allows the quantification of the individual cell as opposed to the population, opening new avenues in the study of uptake rates of metals and nanoparticle, greater understanding of cell metal concentration variation, and the analysis of larger populations while maintaining individuality. The introduction of biologically relevant metals (i.e. ones that are needed in some concentration for cell function, and which are non-toxic at the concentrations utilized within this work) to the cell lines allowed accurate cell number determination. This can then be utilized as an internal control in cells exposed to nanoparticles to allow the number of nanoparticles per cell to be calculated and compared on a cell-by-cell basis. The data presents evidence of specific elements being preferentially present within different types of cancer cells, allowing rudimentary “fingerprinting” of the individual cell lines. Ongoing work will assess whether this is sufficiently robust to allow confirmation of whether one cell type preferentially takes up nanoparticles in a co-exposure. The analysis was also expanded to include results of non-spiked cells utilizing the intrinsic concentrations of these biologically relevant metals, although these appear to vary considerably on a cell to cell basis.

Metal uptake by cells is an important process that may contribute to metal bioaccumulation and toxicity ¹⁴¹⁻¹⁴³. Current methods of particle uptake such as microscopy, ICP-MS and flow cytometry provide various levels of information on the uptake of metals, but are limited to the either basic elemental detection and counting (microscopy, laser ablation ICP-MS and flow cytometry) or the analysis of the population (ICP-MS), as such single cell ICP-MS presents a technique that combines the counting capabilities of flow cytometry and the elemental detection of conventional ICP-MS. Metals such as copper (Cu) at 0.0001 g / kg ^{132,133,144,145}

within the human body, iron (Fe) at 0.006 g / kg ^{132,133,144,145} within the human body, manganese (Mn) at 0.00002 g / kg ^{132,133,144,145} within the human body, and zinc (Zn) at 0.003g / kg ^{132,133,144,145} within the human body (described as essential nutrients) are already present in the cellular environment as ions, albeit in quantities that are not well studied, especially at the individual cell level, due to the lack of appropriate instrumentation that would enable measurements of low levels cellular metal content easily and reproducibly. Other metals (e.g. cadmium (Cd)) have no known biological function and, when identified within cells, are assumed to have entered the cell inadvertently, confused, perhaps, by the cellular machinery for an essential metal, or better able to utilise the cellular machinery.

The use of ICP-MS in cell analysis to date has mainly utilised Laser Ablation ICP-MS (LA-ICP-MS), where a laser samples a portion of a cell for the metal content. This method has some limiting issues in that the size and intensity of the laser directly determine the resolution and depth into the cell that can be analysed. The main advantage that this technique has is that with sufficient resolution a cell can in effect be imaged elementally to very low levels of metal concentrations. The speed of per cell analysis of a LA-ICP-MS is somewhat slower than other methods of cellular analysis, take flow cytometry for instance a widespread and fast method of cell analysis. Primarily used for counting cells and performing analysis of cell phenotype flow cytometry is a fast and efficient method that is the staple of a cellular biologist's laboratory but does not have the same levels of elemental analysis as LA-ICP-MS. Single Cell ICP-MS attempts to bridge the gap between the two techniques by offering the fast and precise cell counting of flow cytometry with the very low levels of detection that ICP-MS can offer.

Single Cell ICP-MS (SC-ICP-MS) is a technique that has developed from a similar technique single particle ICP-MS (spICP-MS), but has a few major differences, primarily the focus is on measuring single cell-like objects instead of individual typically solid particles. Single Cell ICP-MS works by utilising a set of optimised instrumentation, with a micro flow autosampler that automatically agitates the cells in suspension (to discourage adherence to the flask walls, which is important given that many cell types are inherently adherent as this is how they exist in tissue, being in close contact with one another), a small sample (120 μ L) of which is transported via a syringe pump under a low flow rate to a high efficiency nebuliser (HEN). The low flow rate from the autosampler and the use of the HEN is instrumental in providing an environment in which the cells should not burst. An especially designed, full consumption, spray chamber provides a laminar flow to the cells that carries them to the plasma, and the use of a full consumption spray chamber which limits the chance of contact between the cells and the spray chamber, again providing an environment in which the cells should not burst. Though the combination of the introduction system and a lower than normal pressure (compared to the particle mode) the cells are kept safe from bursting and arrive at the plasma intact whereupon they are ionised like any other sample within an ICP-MS.

Wherein spICP-MS the particle forms a cloud of ions that go on to be detected as a peak upon contact with the detector, in Single Cell ICP-MS the cell is fully ionised and forms a cloud of ions from the contents of the cell. As a cell ion cloud hits the detector the metal ions within the cell cause a peak to form in the output reading, the instrumentation counts this peak as a cell, this allows Single Cell ICP-MS to count cells concentrations at a much faster rate than LA-ICP-MS or counting by

hemocytometer. The contents of a cell may contain particles (whether through doping or natural means like environmental exposure) but they are not separated from the cell ion cloud and will hit the detector at the same time as any other background metal that was within the contents of the cell. Through good calibration it is possible to determine the concentration of specific metal ions within an individual cell and by extension it is possible to calculate the distribution of particles within the cell population. A limiting factor to this is the number of elements that are analysed by the instrument in a single sample analysis, where set up time of the instrument becomes a factor, as each element requires a separate calibration the time from instrument switch on to analysis increases greatly. As such for the work outlined in this chapter in a method development capacity only a set few elements were chosen so to reduce the analysis time and increase the number of replicates.

Choice of Elements of Analysis

To determine the appropriate elements for analysis for use in this work, a detailed review of the literature into the relative elemental composition of human cells was performed ^{45,132,133,140,142-148}. The elements that are known to be present within the human body were investigated for the ease with which they could be analysed with ICP-MS, for example oxygen which is present at 640 g / kg of human tissue cannot be analysed with ICP-MS as it is far too abundant in the air, leading to a huge background during ICP-MS analysis. Elements that could not be easily measured with ICP-MS, either due to high background levels, or due to interference from other elements, etc. were removed from consideration see figure 6.1.

Next was to look at the isotopic interferences of the remaining elements and if there was an appropriate isotope with minimal interference that could be used for detection. For example, Fe^{56} has an interference with ArO while Fe^{58} does not have as much of an interference with the isotopic variants of ArO . The next step was to look at the relative background abundance of an element; would there be a chance that the environment could artificially increase the exposure of the element to cells (even though the cells are prepared in a laminar flow environment they are partially exposed to the surrounding environment during uptake into the scICP-MS unit for analysis). For example, there are many exposure routes for aluminium into the cells primarily in the form of various dusts in the air. Finally, the last consideration was the concentration of the element in the cell culture (growth) medium as this would have to be removed through the washes.

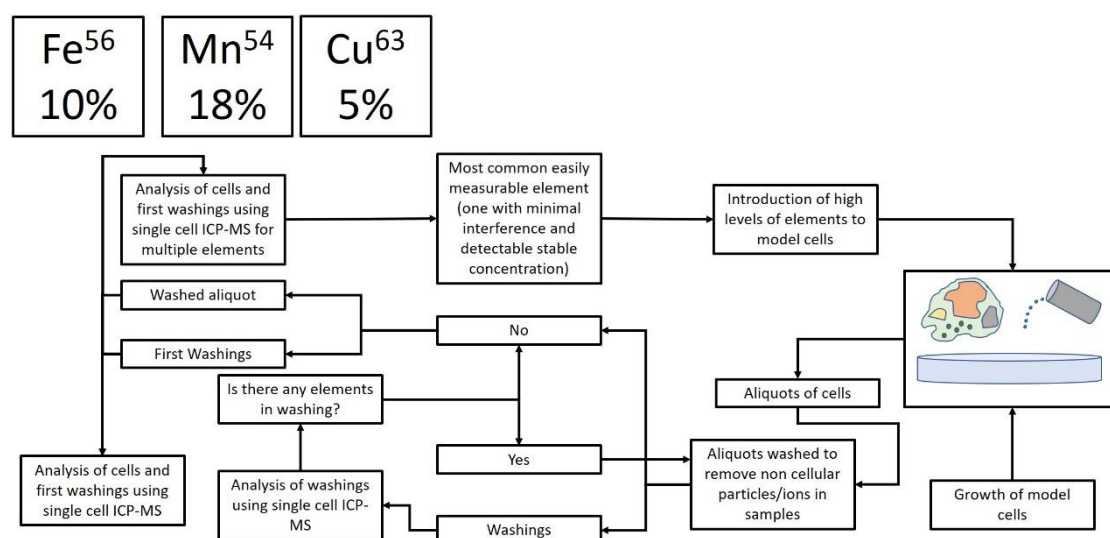


Figure 6.1: A schematic that shows the steps related to analysing the intrinsic metal content of a cell, from the wash steps to the final analysis of the cells.

These factors were formulated into equation 6.1 as a means to optimise the elements for analysis as a basis for cell counting, developed specifically for the purpose of identifying key elements that should be considered for analysis:

Equation 6.1: Equation to calculate the validity of an element for intrinsic metal analysis.

$$E_r = \frac{Ra_h \times I_{a\%}}{I_n + Ra_e + C}$$

where E_r is the ranking coefficient of the element, Ra_h is equal to the relative abundance of the element in humans, $I_{a\%}$ is the % abundance of an isotope, I_n is the number of isobaric interferences of the isotope, Ra_e is the relative abundance of the element within the earth's crust (used as a measure of background abundance), and C is the presence of the element within the cell culture media (if present $C = 1$).

Using equation 6.1, the following ranking of elements determined to be present in cells was reached, with elements that were tested but did not analysed in later sampling due to time constraints labelled in green, elements that were used in final analysis are labelled in yellow, and elements whose score was too low to merit evaluation shown in white in table 6.1.

Table 6.1: elemental ranking based on equation 6.1, used to prioritise those elements present in cells that could potentially be used for cell counting via scICP-MS.

Element	Rating
Tin	1945
Molybdenum	1918
Copper	99
Vanadium	70
Zinc	66
Nickel	61
Iodine	1.00
Sulfur	0.91
Manganese	0.91
Boron	0.78
Selenium	0.50
Magnesium	0.34
Potassium	0.29
Sodium	0.29
Chlorine	0.25
Bromine	0.17
Cobalt	0.17
Calcium	0.16
Iron	0.15
Cadmium	0.14
Phosphorus	0.14
Arsenic	0.12
Carbon	0.11
Chromium	0.09
Aluminium	0.08
Hydrogen	0.05
Silicon	0.03
Nitrogen	0.01
Oxygen	0.01
Fluorine	0.00

Materials and Methods

Chemicals and Materials

A549 lung epithelial, HeLa and MDA cells were obtained from in-house stocks that the Biosciences department maintains in a supercooled environment. Dulbecco's Modified Eagle's medium from BioWhittaker, Phosphate-buffered saline from Sigma and Trypsin from a university stock were used.

Co and Cu from Aristar ionic solutions, and Mn, Zn, Ni ionic solutions from Sigma were used as the spiking elements and in calibration of single cell ICP-MS for analysis.

Transport efficiency of the instrument was determined using 20 nm, 40 nm, and 80 nm gold nanoparticles from BBI solutions. NIST ionic 1000 ppm gold was also used to calibrate the NexION 300D for Transport efficiency.

Sample preparation/Extraction procedure

Cell preparation: A549 lung epithelial, HeLa breast cancer and MDA kidney cells were cultured in Dulbecco's Modified Eagle's medium (DMEM) stored at 37°C and 5% CO₂. The HeLa and MDA cells analysed had a passage number of six while the A549 lung epithelial cells had a passage number of seventy-three. Regular splitting, every three days, was performed using Phosphate-buffered saline (PBS) to wash the cells and trypsin to detach the cells from the container. This schedule of washing and splitting was used to maintain a low cell confluence. This procedure was repeated until the cells were used in analysis, which always occurred on a day that the cells were due to be split so as to minimise repeated daily exposure of the cells to Trypsin that may cause apoptosis within the cell. In

one set of experiments the DMEM used to grow the cells was spiked with $4,000 \mu\text{g L}^{-1}$ of Mn, Co, Zn and $40 \mu\text{g L}^{-1}$ of Ni, these dosages were chosen as being below the fatal metal concentrations but still sufficiently high that the metals would be elevated within the cells and thus were detectable. When the cells were to be analysed, they were washed in FBS (this became wash 1) and detached with 2cm^3 of Trypsin; after detachment the cells were transferred into a 15cm^3 Falcon tube and diluted with 2cm^3 of PBS before being centrifuged for 10 minutes at 1,500 rpm and 10°C . The cells clumped at the bottom and the fluids were decanted into a new Falcon tube to become wash 2, 4cm^3 of PBS was added to the cells and the cells were resuspended before being centrifuged again for 10 minutes. This was repeated once more to give wash 3, the cells were resuspended in 4cm^3 of PBS and both the cells and washes were processed for analysis.

The cells were exposed to a combined dose of $4,000 \mu\text{g L}^{-1}$ each of Co, Cu, Mn, Zn and $40 \mu\text{g L}^{-1}$ of Ni ionic solutions; these ions were also diluted to 1, 2, 3 ppb Mn, Ni, Co, and Zn ionic standards for use in ionic calibrations.

Transport efficiency of the instrument was determined using 20 nm, 40 nm, and 80 nm gold nanoparticles diluted to 50 particles per dm^{-3} by serial dilution in UPW. Gold 1 ppb, 2 ppb and 3 ppb ion standards, also diluted in UPW were used to calibrate the NexION 300D for transport efficiency.

Instrumental optimisation and analysis

A PerkinElmer NexION 300D was used for single cell ICP-MS analysis, a 0.0025 mm^2 Neubauer haemocytometer, and a Leica DMIRB microscope were used to give a rough analysis of cell health and cell count as well as a comparative measurement of cell concentrations.

SC-ICP-MS: All SC-ICP-MS measurements were made on a NexION 300D ICP-MS operating in Single Cell mode, using the conditions shown in Table 6.2. Sample introduction was accomplished with the Single Cell Micro DX Autosampler, HEN nebulizer, and Asperon spray chamber. Each of these components is crucial to obtaining meaningful results: the autosampler agitates the samples to prevent cell precipitation and uses a syringe pump for accurate, low-flow delivery of the cells to the HEN, which aspirates the cell solutions. This combination of autosampler and HEN is critical to ensuring that the cells do not burst when they are nebulized, thus maintaining the integrity of results. The Asperon spray chamber provides a laminar flow for maximum delivery of the cells to the plasma.

The transport efficiency of the Asperon was measured as 30.55% for the gold (Au) 20nm and 40 nm nanoparticles. The intrinsic metal content of the cells was determined against calibration curves made from 1, 2, 3 ppb Mn, Ni, Co, and Zn ionic standards. All data acquisition was accomplished with the Syngistix Single-Cell Application Module. A trypsin and PBS blank were run to provide a baseline for elemental backgrounds. When the cells and washes were run all analysis for each sample occurred within 5 minutes, with the elements measured sequentially, on a 0.1cm³ plug of sample that the autosampler dispensed over 10 minutes.

Multiple replicates of the A549 samples were tested throughout a year to determine the replicability of the technique, while for the HeLa and MDA cells the technique was repeated over multiple consecutive cell passages.

Table 6.2: NexION 300D Operating Conditions for intrinsic metal concentration of cell lines.

Parameter/Component	Value/Description
Sample Uptake Rate	0.02 mL/min
Nebulizer	MEINHARD HEN
Spray Chamber	Asperon
Injector	2.0 mm id Quartz
RF Power	1600 W
Analytes	Mn 55, Ni, Co 59, Zn 66, Cu63
Dwell Time	50 μ s

QA/QC criteria

Quality assurance was obtained by the daily instrumental setup and by statistical analysis of multiple replicates for each sample. Due to the nature of the instrument being sequential it is not possible to use an internal standard as the internal standard would not be analysed with each sample. In lieu of the presence of an internal standard the certified four element LC-MS polystyrene bead standard were routinely compared to the limits of size as stated in the certification.

Statistical analysis

The statistical analysis that was performed upon the results gathered within this chapter are R^2 correlation analysis of the standard ionic and particle calibration. A R^2 value of less than 0.996 was not utilised and the calibration was repeated either by reruns or remakes of the standards. Samples were all analysed at least three times in replicate and the average was calculated using the mean. From the

mean the standard deviation was used to identify outliers that would be investigated on a sample by sample basis.

Results/Discussion

In analysing the A549 cells the three wash waters of the A549 cells showed a rapid decrease in metal content, this is shown in figure 6.2 where it is clearly evident that the cells measured after the first wash had a much higher average number of cell-like events detected and the cells measured after the subsequent washes had an ever decreasing cell concentration, with the final cells sample having the lowest cell concentration detected. SC-ICP-MS analyses did not indicate significant concentrations of intrinsic ionic metal background concentrations for any of the target elements, with cobalt being present at a concentration of $0.4 \mu\text{g L}^{-1}$, a manganese concentration of $0.2 \mu\text{g L}^{-1}$, zinc having a concentration of $0.65 \mu\text{g L}^{-1}$ and copper having a concentration of $3.5 \mu\text{g L}^{-1}$ within an average A549 cell. However, the increased occurrence of cell-like events (i.e. more cell peaks) with a low ionic background allow strong inferring the actual presence of cells is being measured compared to the washes which showed little to no cell like events.

In A549 cancer cells grown in the DMEM spiked with the 5 metals, this distinction between cells and background was even more evident as a result of the increased levels of these intrinsic metals within the cells. The cell count averages of each of the five elements analysed from the two separate exposures were $47,993 \pm 7,450$ (21/11/18) versus $89,306 \pm 9,283$ cells per cm^3 (26/06/19). This relatively narrow standard deviations in both cases illustrate the close agreement in terms of cell number irrespective of which of the metals measured shown in Table 6.3. All the elements analysed were detectable within the spiked cells, but little to no

presence (apart from zinc with a blank cell concentration of 98,080 cells per cm³) was detected in trypsin or ultrapure water, which had average counts of 6,381 entities per cm³ strongly suggesting that the metal detected was intrinsic to the cells.

Table 6.3: Cell concentration of A549 cells averaged over replicates, based on detection of the intrinsic metal contents, and compared to the haemocytometer concentration of the cells.

Element	A549 Cell Sample 21/11/18		A549 Cell Sample 26/06/19	
	Cell Concentration (cells per cm ³)	Mean Mass (ag)	Cell Concentration (cells per cm ³)	Mean Mass (ag)
Zn 65.926	49,404	345	82,683	724
Cu 64.9278	57,973	331		
Mn 54.9381	42,298	119	85,318	241
Co 58.9332	42,295	79	99,917	118
Average	47,993		89,306	
Standard Deviation	7,450		9,283	
Haemocytometer Count	42,917		92,500	

Within Figure 6.2 the average cells per cm³ determined based on the metals analysed for the three cell lines is presented, where the concentrations for each replicate of nickel, zinc, manganese, copper, and cobalt for each cell line analysis have been averaged to give the average cells per cm³ from each of the intrinsic metal concentrations, which allows for ease of comparison of the cells following each washing step.

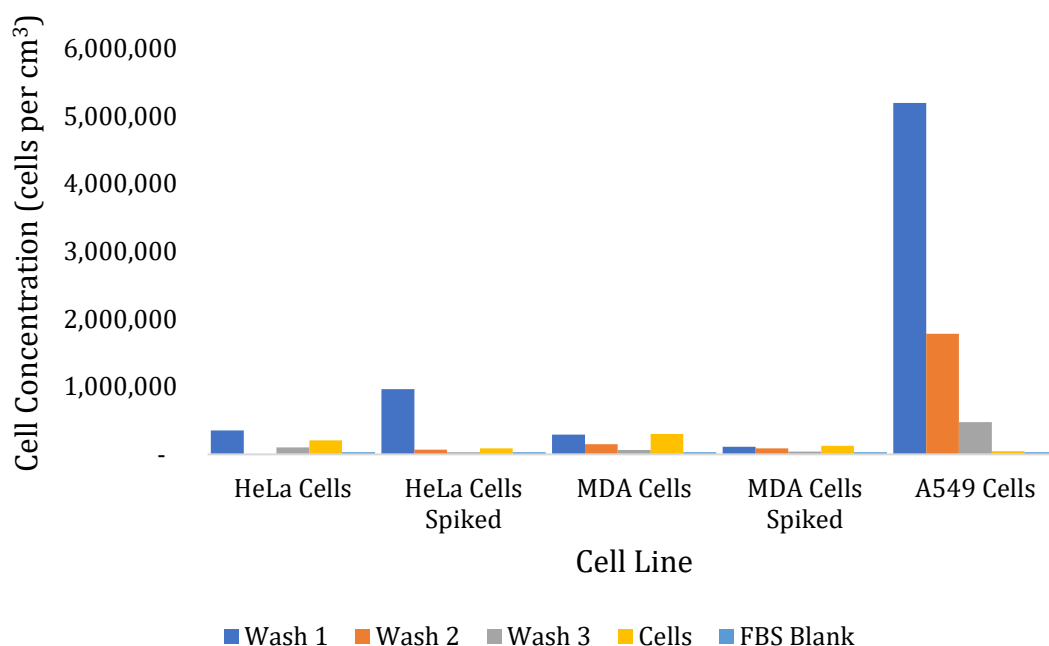


Figure 6.2: Cell concentration of cell lines spiked and unspiked as well as the washes that were aliquoted and tested before the cells were analysed.

Consistently, the concentration of cells following the first wash has the highest cells per cm^3 , with a decrease in cell numbers per cm^3 with subsequent washes, indicating loss of metal to the washwater at each wash. The first wash has both the highest concentration of spiking solution and the highest concentration of the media which contains some of the elements that were analysed (Zn, and Mn), therefore it was expected that this would have the highest concentration of metals of the analysed cells and washes. The quick decrease in metal (cell) detection frequency between the washes shows that the method of washing the cells is effective at removing any background that has not been up taken by the cells during growth in the spiked medium.

Table 6.4: The concentrations of cell like events detected in washes and final cell sample for each cell line.

	Cell concentration (cells per cm ³)				
	HeLa Cells	HeLa Cells Spiked	MDA Cells	MDA Cells Spiked	A549 Cells Spiked
Wash 1	353,341	965,578	290,382	113,134	5,191,924
Wash 2	-	69,561	150,612	85,997	1,782,357
Wash 3	101,248	33,179	65,064	39,672	477,045
Cells	204,996	86,716	300,021	125,382	47,993

In repeat analyses of the spiked A549 cells, it was seen that the cell concentration detected was consistent between all four metals. The amounts of the spiked metals taken up also varied, with A549 cells consistently taking up more zinc than the other metals, based on the Zn concentration detected in spiked cells being consistently higher than the other three elements analysed (table 6.4). This was the case with only spiked samples; for the un-spiked cells it was found that the concentration of each of the 4 metals within the cells was almost undetectable, with the amount of metal that was in the raw cells being at the limit of detection for the instrument. While it was possible to calculate the concentrations of metals on average within the unspiked cells (see Table 6.5) it was not possible to get a consistent cell population calculation, with the cell concentration for un-spiked cells being $57,676 \pm 38,784$ cells per cm³. The very low metal concentrations were shown to be repeated over multiple analyses of un-spiked A549 cells with several analysis of un-spiked cells detecting no metal present in the A549 cells, as shown in Table 6.5.

Table 6.5: The concentrations of A549 cells dependent on the element analysed.

Element	Cell Concentration (cells per cm ³)	Mean Mass (ag)
Zn 65.926	7,379	576
Mn 54.9381	69,535	81
Ni 59.9332	104,083	259
Cu 64.9278	77,787	199
Co 58.9332	29,596	29
Average	57,676	
Standard Deviation	38,784	

Figure 6.3 illustrates the responses of the four main elements zinc, manganese, nickel and cobalt that were analysed in spiked A549 cells. The four graphs in Figure 6.3 show some clear differences in masses for the four elements and this is to be expected as the cells will maintain different levels of metals naturally depending on their cellular functions. Elements that are more widely utilised by the cells like zinc and nickel are present at higher concentrations than elements like cobalt. Nickel has an isobaric interference with calcium; and as such the nickel response includes some calcium ions. Calcium is one of the most important elements within a cell ^{132,133,144}so by measuring nickel it is possible to measure both the nickel concentration and the calcium concentration. Whilst this may seem to compromise the results in that you can't determine between nickel and calcium it does ensure that there is a consistent result of cells being detected with the single cell ICP-MS.

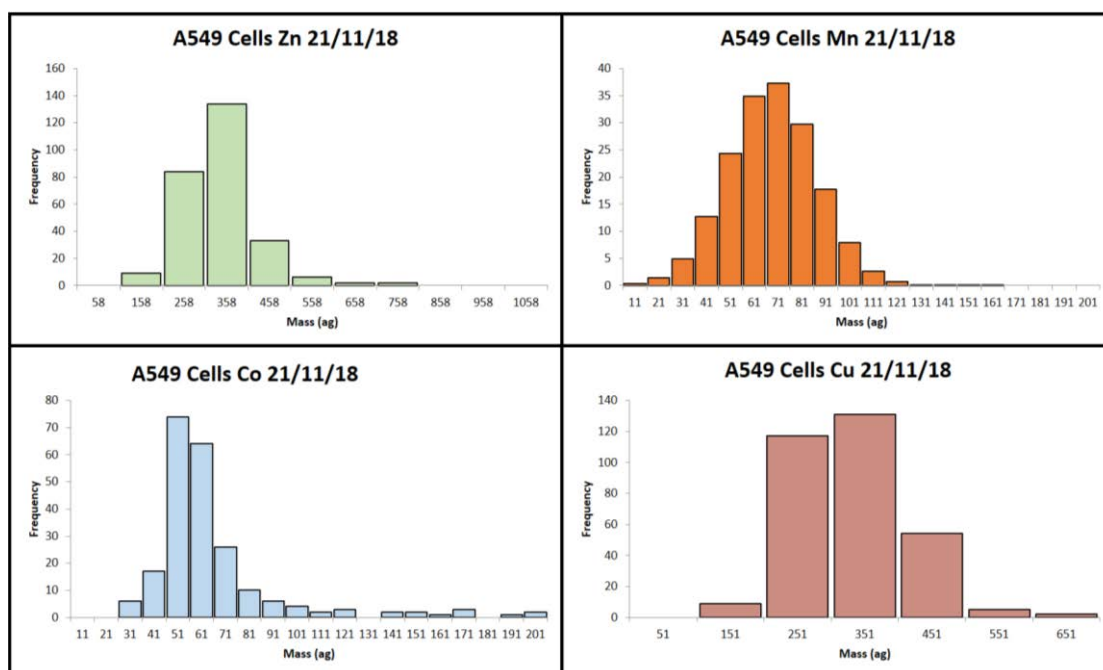


Figure 6.3: Intrinsic metal content within spiked cells. Note the similar distributions across the elements but differing masses. This is indicative of both the differing densities of the elements and differing uptake levels of the spiked metals by the cells.

Unlike the A549 cells, when HeLa and MDA cells were analysed it was found that they did not produce the same consistent cell concentrations between metals with no trend in concentration determined throughout the elements analysed apart from close cellular concentrations of Mn and Co for HeLa cells and Mn and Cu for MDA cells (see Table 6.6); this may be due to the large variance in metal concentrations within the cells. HeLa and MDA cells did still show evidence of cells even after the 3 washing steps, as metals were detected above the background although the amount (number of cells) detected decreased with each wash as shown in Figure 6.2.

Table 6.6: The concentrations of HeLa and MDA cells dependent on the element analysed.

Element	HeLa Cell Sample 21/11/18		MDA Cell Sample 21/11/18	
	Cell Concentration (cells per cm ³)	Mean Mass (ag)	Cell Concentration (cells per cm ³)	Mean Mass (ag)
Mn 54.9381	35,889	550	51,475	466
Ni 59.9332	294,415	686	278,751	762
Cu 64.9278	1,445	2,632	42,200	800
Co 58.9332	48,588	294	110,329	257
Zn 65.926	1,369	11,544	76	41,338
Average	76,341		96,566	
Standard Deviation	123,686		109,179	
Haemocytometer Count	70,000		15,000	

Even after the multiple washes to eliminate the ionic background from the cell culture medium, there was still visible evidence of metals within the cells with the plasma of the ICP-MS changing colour from white to orange, which is a clear indicator of calcium within the cells. When nickel was analysed in HeLa and MDA, repeats of the cells showed a consistent nickel concentration (294,415 and 278,751 cells per cm³) and it is likely that the signal for nickel that was detected was a combination of nickel within the cells and Ca that is present in culture media, as CaO is a polyatomic interference of nickel ¹⁴⁹.

When analysing the HeLa and MDA cells because the cells were prepared at a higher cell concentration the un-spiked cells were detectable to a greater level than the A549 via single cell ICP-MS. The metals that were analysed within the cells were more readily detectable with consistent levels of metal detected within both HeLa and MDA cells. This is likely due to the combination of a higher incidence of cells with higher metal concentrations and thus more cell like events detected within the ICP-MS instrumentation (see table 6.7). There was a wide range of metal concentrations between replicates of the cells, which based on the

doubling time of 24 hours could suggest that the cells were in various states of metal distribution between mother and daughter cells.

As noted previously there is some correlation between pairs of the elements that have been analysed. Within HeLa cells there was a close correlation of Zn and Co cell concentrations. Interestingly the ratio of concentrations of Co to Zn within both spiked HeLa cell and un-spiked HeLa cells was 1.9 times the ratio of Zn to Co per cell. In MDA cells there is not a consistent close concentration of two elements, while the spiked MDA cells having a close Zn and Cu cell concentration and the un-spiked MDA cells having a close Zn and Co cell concentration. While there is the hint that there may be complementary elements to which specific cell lines exhibit this conclusion cannot be thoroughly determined with the limited number of elements that were analysed for each cell line. Further work into measuring the extent of these relationships between elements was to be the next step in this line of analysis.

For both the spiked or un-spiked cell concentration of both HeLa and MDA the haemocytometer cell count was much lower than the average concentration determined by ICP-MS, with the spICP-MS giving an average concentration of un-spiked HeLa of $204,996 \pm 317,628$ cells per cm^3 which is a standard deviation larger than the average concentration of 70,000 cells per cm^3 counted by the haemocytometer. Similarly, the cell concentration of the MDA cells calculated by single cell ICP-MS is much larger at 125,382 cells per cm^3 compared to the haemocytometer count of 15,000 cells per cm^3 . In both HeLa and MDA and for both spiked and un-spiked cells none of the elements analysed resulted in cell counts close to the haemocytometer cell concentration; spiked HeLa cells have an average

concentration at 76,341 cells per cm³ but this is a result of the wide concentration range, with the standard deviation being 123,686 cells per cm³. At this early stage of the development of analysis intrinsic metal concentrations with cancer cell lines using single cell ICP-MS there is not a clear conclusive argument that can be made for its viability as an alternative method of cell counting; while there is clear evidence of the uptake and detection of metals within the cells the uncertainty of the cell concentration when compared to haemocytometry means that until concentrations between the two techniques are comparable the technique is not suitable as the primary technique for cell counting when using single cell ICP-MS.

Table 6.7: The concentrations of spiked HeLa and spiked MDA cells dependent on the element analysed.

Element	HeLa Un-spiked Cell Sample 21/11/18		MDA Un-spiked Cell Sample 21/11/18	
	Cell Concentration (cells per cm ³)	Mean Mass (ag)	Cell Concentration (cells per cm ³)	Mean Mass (ag)
Mn 54.9381	35,877	305	1,259	1,022
Ni 59.9332	175,880	890	198,987	910
Cu 64.9278	19,962	761	421,177	545
Co 58.9332	31,651	155	1,079	672
Zn 65.926	761,608	1,475	4,406	1,764
Average	204,996		125,382	
Standard Deviation	317,628		186,014	
Haemocytometer Count	70,000		15,000	

Conclusions

In conclusion the original aim of the experiment, which was to measure the intrinsic metal within the cells as a method of cell counting, to provide a basis for determining nanoparticle uptake on a cell by cell basis, was not entirely successful. When the inherent metal concentrations of interest (Zn, Mn, etc.) were found to be too low and too variable to produce consistent cell counting, an approach of spiking the cell culture medium with the target metals driving internalisation of these metal markers, resulted in a heightened ionic concentration and while promising results were obtained it is still does not fully meet those aims. However, there is clear evidence that the cells do take up (internalise) the spiked metals, that the cells are detected by single cell ICP-MS and that the cell metal concentrations detected are equal to those determined by other techniques, and are consistent with their natural ratios / abundances following uptake.

At the current state of development, what cannot be proven is the stage of the cells in their lifecycle, as the cells were not synchronised prior to the metal spiking. With synchronisation of the cells there may be new insights into the uptake rates and elemental distributions within the multiple cell lines. Also, currently it does not seem possible to “fingerprint” a cell based of the elemental distribution within different cell lines, however as shown with HeLa cells this may be possible upon investigation of an expanded suite of metals being analysed for each cell line.

Finally the accurate cell counting of cells using single cell ICP-MS requires levels of metal that are not at the limit of detection; with spiked A549 cells showing that with significant concentrations it is possible to get comparable cell concentrations as the haemocytometer provides, however this was not shown to be true with

other cell lines where there was a large variation in cell concentrations between elements that were also not comparable to the haemocytometer cell concentrations.

There were multiple difficulties in the development of this technique that limited the amount of valid results and while over time the measurement of intrinsic metal content within cells has been developed it is not at the degree of accuracy that was desired, with the results only scratching the surface of the metrics of metal determination that was originally aimed for in the development of cell fingerprinting and consistent cell concentration determination.

Chapter Seven

Application of single cell ICP-MS for quantification of interaction of *Daphnia pulex* with gold nanoparticles

Aims and Overview

This chapter explores the potential utilisation of single cell ICP-MS for analysis of uptake of nanoparticles by the water flea daphnia. Currently most single cell analysis focuses on the analysis of single cells mainly from cell cancer cell lines ^{43,77,80} (as described in chapter six) and algae ^{77,80}, while the work presented here aims to push the limits of the size that is measurable using single cell ICP-MS.

To analysed cells and organisms of increasing sizes there are a couple limitations, of which two are discussed cellular integrity and instrumental limitations. With the instrumental limitations there is currently a hard limit to the size of a sample that the single cell ICP-MS can analyses which is 400 μm , this is the width of the tubing that is used by the instrument. If a sample is any larger than 400 μm , they simple will not be able to traverse the tubing and more importantly could potentially block the exit of the nebuliser which may lead to back pressure breaking the delicate glassware. For most analysis this will never be a problem due to the fact that cells of over 100 μm generally become very fragile, as the cell gets larger the cell membrane is more susceptible to breaking from higher pressures, plant cells are especially susceptible to this as the process of cell preparation requires the removal of the cell wall.

These two problems are a real concern for multicellular organisms, as the organism as a whole is often much sturdier and can quickly grow larger than the hard size limit of 400 μm . To this end a model organism was required that would be smaller than the tubing, and was relatively easy to maintain and dose with nanoparticles for analysis.

Daphnia magna and *Daphnia pulex* are two commonly used species of Daphnids for analytical research. Daphnids are planktonic crustaceans ⁹⁹, which feed on small suspended particles in a water system; the organism is widely used in research due to their transparent carapaces, being transparent allows for ease of study into the uptake and inter-bodily functions such as studies of the organs. Present in wide variety of water systems they can also function as a model organism for changes in the chemical structure of a body of water, such as in environmental and toxicological studies ¹⁰⁰⁻¹⁰³.

Originally *Daphnia magna* were grown for analysis but these organisms grow to a maximum size of 1,500 μm which is far too large for analysis by single cell ICP-MS, however it was believed that the neonates less than a day-old which would grow are around 200 – 700 μm would be analysable. The first tests showed promise with there being some evidence of analysis of detection of *Daphnia magna* and of gold association by the organisms, however, unfortunately the species would regularly grow too large for repeated reliable analysis so it was decided that the smaller *Daphnia pulex* would be tested instead. *Daphnia pulex* grows to a maximum size of around 400 μm , which is right on the size limit of the tubing. Again, we analysed neonates less than a day-old, this time to greater repeated success with association of gold nanoparticles observed and the observation of

daphnia within the autosampler sample plug (see figure 7.1 for a graphical representation).

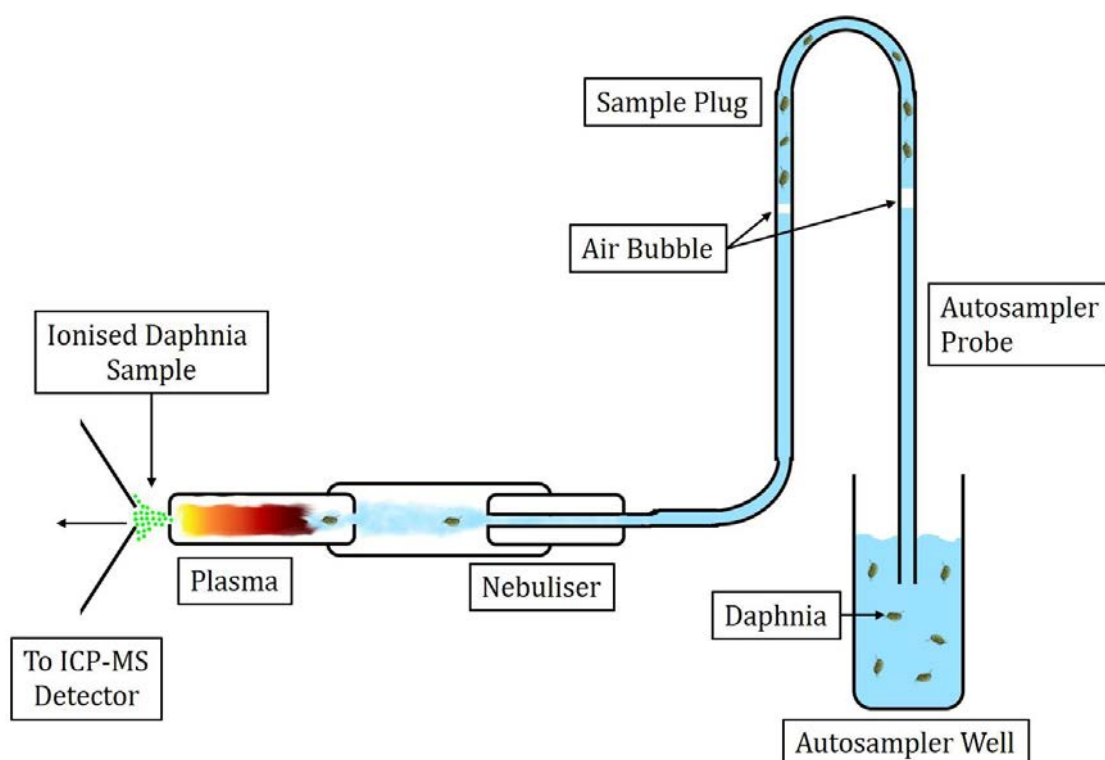


Figure 7.1: A graphical presentation of the route that daphnia undertake from the autosampler well to the ICP-MS detector. Firstly, the daphnia enter the autosampler probe and are taken up in a “sample plug” which is a 100 μ L plug of sample separated from other fluids by two air bubbles. The daphnia are then nebulised in the nebuliser and ionised in the plasma before entering the ICP-MS for analysis.

Materials and Methods

Chemicals and Materials

A 100 nm gold nanoparticle standard obtained from nanoComposix was used for exposure to the daphnia, this nanoparticle standard was also tested separately for

its stability, mass response and particle profile when analysed by single cell ICP-MS as a comparison to the responses measured from the daphnia.

The transport efficiency of the Asperon was measured at 84% for this work with gold (Au) 20nm and 40 nm nanoparticles and NIST gold 1 ppb, 2 ppb and 3 ppb ion standards.

Sample preparation/Extraction procedure

Daphnia pulex were cultured in High Hardness COMBO (HH COMBO) medium, pH range 7.3-7.6, on a 16:8 light: dark cycle. Daphnia were maintained in a 20°C controlled laboratory and fed a daily ration of algae of 1ml per day. Media was refreshed 3 times a week and neonates <24hours were used for exposures. Using a Pasteur pipette daphnids were transferred into 50ml glass vessels for exposure to 1mL the undiluted gold nanoparticles with an acclimation period of 12-16 hours prior to detection in the ICP. After 24 hours the daphnia were filtered and washed in ultrapure water (to try to remove any surface adherent nanoparticles) and then placed into a 2 mL sampling tube with 1 mL of ultrapure water, the final washed water was tested for presence of gold nanoparticles and the daphnia would be washed again if a presence of gold nanoparticles were found. Daphnia that had died or were deemed to be too large by visual comparison to the opening of a spare set of tubing were not placed into the sampling tube for analysis as they would likely clog the autosampler probe and tubing, in this early stage of method development which constituted a proof of concept that daphnia could be analysed the semantics on whether the daphnia had died due to the particle was not applicable. As a proof of concept we were only concerned with measuring daphnia that had reached the detector and proving that this was possible, future work that

explored the effects of the nanoparticles on the daphnia and that would take a much more detailed approach to analysis exploring various analytical aspects had been planned pending the success of this pilot study.

Instrumental optimisation and analysis

The base method for analysis of the daphnia using single cell ICP-MS was a modified from the method used for analysis of metals within the single cells described in chapter six above. Due to the large difference in sizes between cells and daphnia the concentration of the daphnia reaching the detector was much lower than the average number of cells or particles during analysis, so the length of the analysis was increased from 40 seconds to 360 seconds. The transport efficiency of the Asperon was measured at 84% for this work with gold (Au) 20nm and 40 nm nanoparticles and NIST gold 1 ppb, 2 ppb and 3 ppb ion standards.

In testing it was originally found that when using the standard 40 second analysis time there was likely most if not all of the daphnia signals were getting missed. It was decided that to ensure that there was maximum amount of responses all of the sample plug would be analysed (see figure 7.1); the sample plug being a 100 μL plug of sample that is taken up by the autosampler probe from the autosampler well. It is separated from other fluids within the sample tubing by two air bubbles, analysis of a sample is typically synchronised to start recording during the delivery of the plug from the sample tubing to the plasma and detector. This process takes around 140 seconds from autosampler well to detector, the sample plug is dispensed at a rate of 20 μL a minute giving a 5-minute analysis window. To ensure all the maximum amount of responses all of the sample plug was be analysed and the sample was analysed from before reaching the detector at 100

seconds from uptake from the autosampler well. Each sample was analysed for 360 seconds to give sample run time encompassing all of the sample plug.

As discussed later, the concentration of daphnia that was used in each sample well was around 30 individuals, this was due to both limited numbers of daphnia available for analysis (less than 1,000 individuals) and to avoid overcrowding in the sample well which resulted in clogging of the autosampler probe. Each autosampler with daphnia would be analysed until either all of the daphnia had been up taken by the probe or until the volume of fluid in the well decreased to a level where no uptake was possible without the risk of clogging the probe entrance.

Part of the optimisation revolved around the movement of the daphnia within the autosampler well, were due to being alive they had the ability to swim away from the probe, this was mitigated by decreasing the volume of water in the well. At a low volume the daphnia had nowhere else to swim and would go up the probe, but it was important to provide the daphnia some water so as to remain active decreasing the stress and rate of death of the daphnia.

The instrumental parameters for the analysis of gold NPs in *D. pulex* are listed in table 7.1.

Table 7.1: NexION 300D Operating Conditions for *D. pulex* containing 100nm Au NPs

Parameter/Component	Value/Description
Sample Uptake Rate	0.02 mL/min
Nebulizer	MEINHARD HEN
Spray Chamber	Asperon
Injector	2.0 mm id Quartz
RF Power	1600 W
Analytes	Au
Dwell Time/Reading	50 μ s

QA/QC criteria

Quality assurance was obtained by the daily instrumental setup and by statistical analysis of multiple replicates for each sample. Due to the nature of the instrument being sequential it is not possible to use an internal standard as the internal standard would not be analysed with each sample. In lieu of the presence of an internal standard the certified four element LC-MS polystyrene bead standard were routinely compared to the limits of size as stated in the certification.

Statistical analysis

The statistical analysis that was performed upon the results gathered within this chapter are R^2 correlation analysis of the standard ionic and particle calibration. A R^2 value of less than 0.996 was not utilised and the calibration was repeated either by reruns or remakes of the standards. Samples were all analysed at least three times in replicate and the average was calculated using the mean. From the mean the standard deviation was used to identify outliers that would be investigated on a sample by sample basis.

Results and Discussion

Before we look at the results of the daphnia in depth we had to analyse the gold nanoparticles to determine the standard response from the nanoparticles, this worked as both a calibration, i.e. we expect a mass of 10,105 ag to be a single 100 nm gold nanoparticle, and secondly as a basis for comparison for the real-time results, i.e. does the amount of peaks and responses suggest nanoparticles, or daphnia containing Au NPs. As can be seen in figure 7.2 there is almost continuous peaks from gold nanoparticles, while there is little to no background.

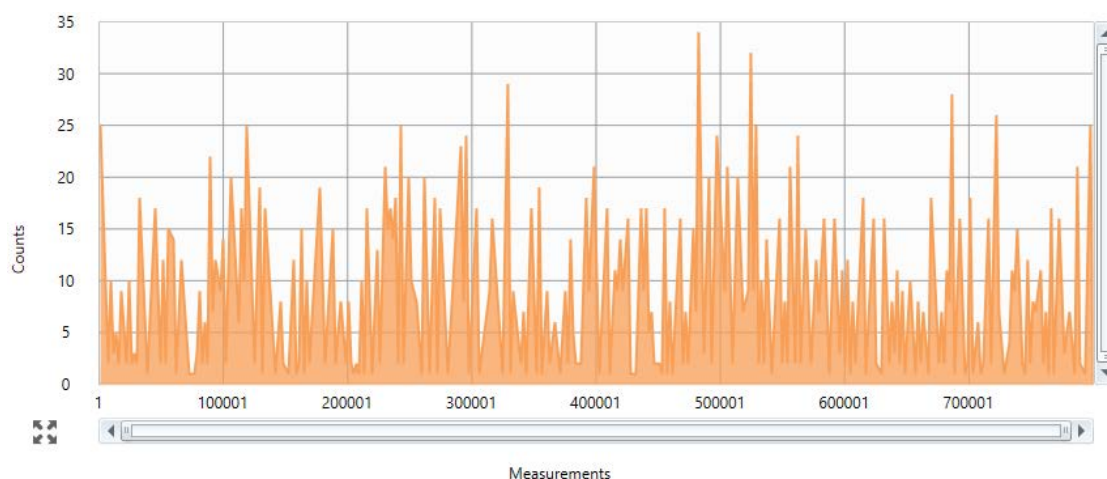


Figure 7.2: Real-time data from the gold nanoparticle calibration standard when run in the single cell ICP-MS.

The amount of responses that are present over 40 seconds sets a clear picture of the expected response for purely nanoparticles. Taking a closer look at the peaks, as seen in Figure 7.3 it can be seen that there are very little background gold ions present.

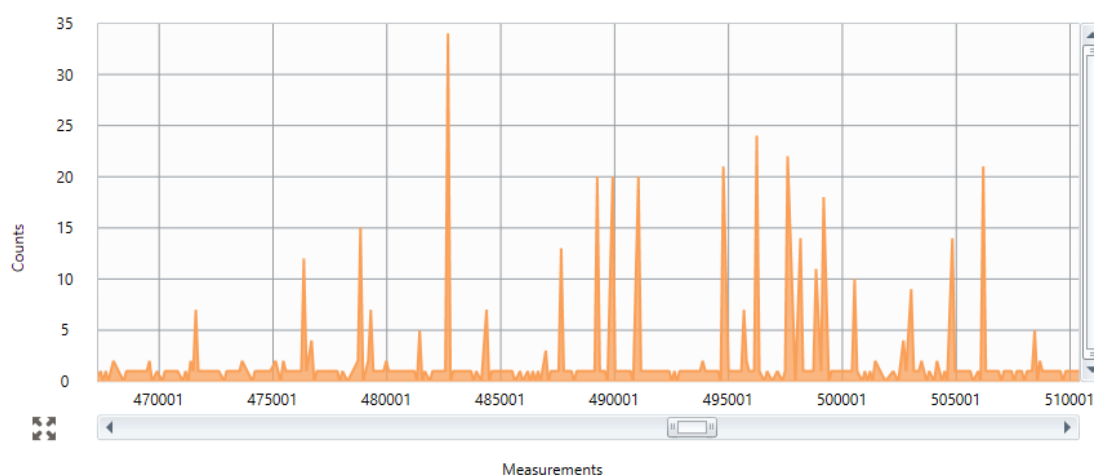


Figure 7.3: A zoom-in of a small section of the real-time results shown in figure 7.2, to demonstrate that there are large gaps between peaks that are not implicitly clear when viewing figure 7.2. Each peak corresponds to a gold nanoparticle.

During uptake of the sample, the autosampler creates a plug of 100 μL of sample that is dispensed into the instrument at a rate of 20 μL a minute to give a total time of sample exposure to the detector of five minutes. By expanding the length of analysis at the detector from 40 seconds to 360 seconds, and by shortening the delay before analysis to 100 seconds the instrument starts to analyse samples before the sample enters the plasma. With this expanded time range the entirety of the sample plug is recorded and no daphnia signals are missed. By ensuring that the instrument is not missing any of the daphnia, the very low concentration of individual daphnids per plug (around 10 – 50 individuals) is no longer a limiting factor to the analysis of daphnia.

Figure 7.4 presents the first 40 seconds of a sample of *daphnia pulex* and the introduction and arrival of daphids can be seen. For the first 120,000 readings each lasting 50 μs there are no daphnia hitting the detector and as such there are no detected peaks only the background signal which arises from the water. After

120,000 readings we begin to see the emergence of peaks that relate to gold particles, with a flurry of peaks at around 300,000 readings. At this time there are a number of peaks (indicative of multiple gold-nanoparticle containing daphnids), followed by a period of no daphnia and then some of the largest peaks from daphnia.

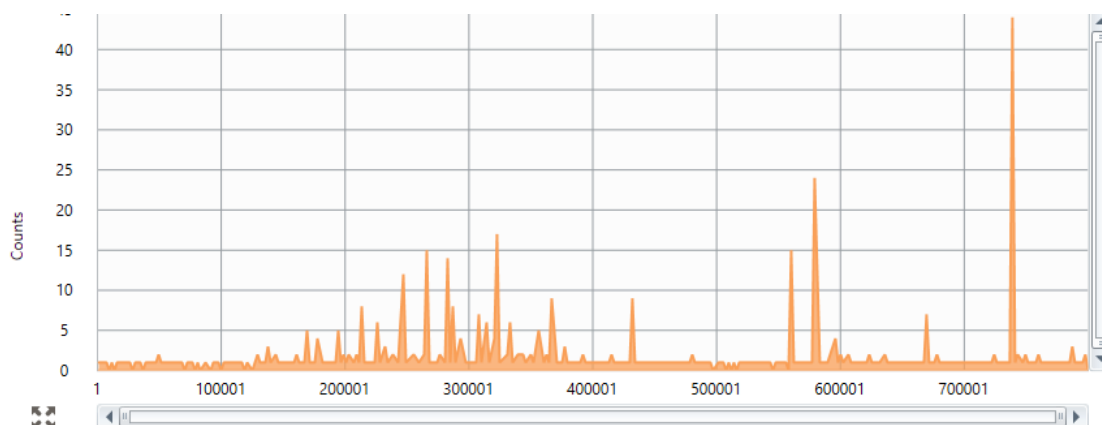


Figure 7.4: The first 40 seconds of a *daphnia pulex* analysis, with the daphnia arriving at the detector after 10,000 readings equivalent to 5 seconds.

It is most likely that the smaller neonate *Daphnia pulex* individuals were measured in the first set of peaks and then the larger neonate *Daphnia pulex* were detected at a later reading as they took longer to traverse the tubing from the sample tube, although this is not conclusively proven and is a subject of future study with the aim of conclusively determining if there is a size separation based on the association of gold or daphnid size. In figure 7.5 this can be seen more clearly with a flurry of peaks early that then settle to larger peaks with some smaller peaks that follow over the next 100 seconds.

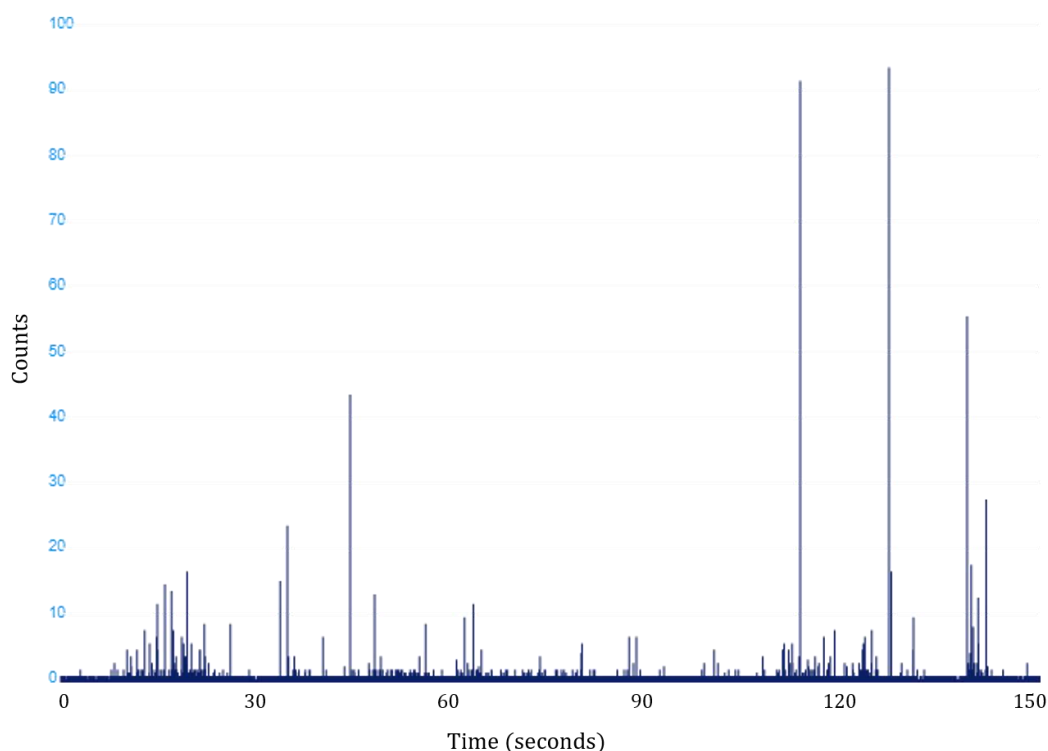


Figure 7.5: Zoom in of the first 150 seconds of the *Daphnia pulex* scan shown in figure 7.4. This scan continues for 360 seconds. Along the X axis is the length of time that the scan has been progressing, take note the increasing peak sizes as time increases.

The rate at which daphnia are up taken by the autosampler is dependent on two main parameters, namely, the number concentration of daphnia in the sample tube and the volume of solution in which the daphnia can reside comfortably ^{100,102,150}. Both of these parameters needed optimising as part of the development of the method. In the case of the concentration of daphnids within the sample tube during the introduction to the sClCP-MS instrument, if the concentration is too low (less than 30 organisms) it is unlikely that the probe will collect any more than 10 individuals per sampling due to the activity of the daphnia in that they will disperse away from the auto sampling probe and the fact that not all the individuals are within the pull/suction range for the probe. On the other end of the

scale if the concentration of daphnids is too high (estimated to be 100 individuals, but this limit has not yet been tested) in the sample tube it is very likely that the probe will become clogged with daphnids, which can also affect the tubing and nebuliser. By extension, this will also result in too low a dispersity of the daphnids leading to indistinguishable detector responses where there appears to be a constant high background. With regards to the volume of solution that the sample tube contains, if the volume of the solution is too large then there is more space in which the daphnids are able to swim within the sample tube, which causes the decreased uptake of daphnids by the autosampler probe, however this did lead to more active daphnia prior to analysis. On the other hand, if the volume was too low the daphnids bunched up in the remaining solution leading to the previously stated problem of clogging the autosampler tube during sample uptake, resulting in only the background being detected, additionally the resulting loss in volume also led to many of the daphnia dying prior to analysis, i.e. during the time that the samples were queued up for analysis, the effect on the integrity of the daphnia after death as it is possible that they were bursting is a subject of future study.

Looking at some partial scans that only depict 40 seconds of a 360 second scan of the daphnids there is a trend that most of the peaks have heights (y-axis) of about 15 – 25 counts (see figure 7.6), with some peaks having counts of above 50. This correlates well with the heights of the peaks that were observed for the 100 nm gold nanoparticles, suggesting that there is an average association of one 100 nm gold nanoparticle per daphnia peak (i.e. per spike of 25 counts). Where there are larger peaks this corresponds closely to the occurrence of multiple 100 nm gold nanoparticles per daphnia reading, suggesting that these organisms have internalised or adhered 2 or more 100 nm Au NPs.

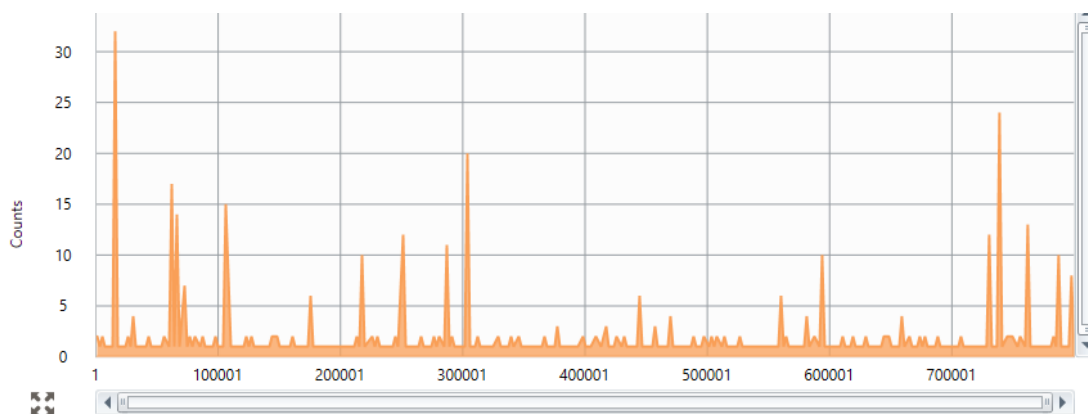


Figure 7.6: Average section of a scan, where most peaks are around 15 to 30 counts in height, corresponding to one 100 nm Au NP per daphnid event. There was a trend that the peak size increased over time but the majority of peaks were within the range of 15 to 30 counts, corresponding to 1 and 2 Au NPs, respectively.

The averaged results, gathered over multiple runs of daphnia replicates (three replicates per sample listed) showed that there is a wide and varied association of gold NPs by the daphnids. While on average the association of gold within the daphnia was close to that of the gold nanoparticle mass, at 4,057 ag in daphnids compared to the gold nanoparticle mass of 4,628 ag, there was a significant standard deviation from the mean of $\pm 2,473$ ag of gold. This large variance indicates the extent to which the association of gold nanoparticles with the daphnids (attachment, internalisation in gut, uptake into organisms) is dependent on the individual and suggests that there has been some dissolution of the gold nanoparticles¹⁰⁰ likely in the acidic environment of the daphnid guts. There was also a large variance in the concentration of peaks that were analysed with the highest concentration being 15,583 parts/mL and the lowest being 714 parts/mL, these concentrations are much larger than the concentration of daphnia that were analysed, suggesting that there was multiple cells or components being detected

for each daphnia that was analysed. The variance in gold response (counts, converted to mass of Au) and concentration can be seen in Table 7.2 and Figure 7.7.

Table 7.2: Averaged mass and cell concentration for multiple *Daphnia pulex* samples - in all cases the number of organisms and sample volume was constant, indicating that there is a wide variation in the mass of gold and concentration of the daphnia that were analysed.

Sample	Mean Mass (ag)	Peaks Conc. (parts/mL)
<i>Daphnia Pulex</i> 12/4/19	1,220	15,583
<i>Daphnia Pulex</i> 12/4/19	3,549	1,650
<i>Daphnia Pulex</i> 12/4/19	4,378	2,017
<i>Daphnia Pulex</i> 12/4/19	7,442	714
<i>Daphnia Pulex</i> 12/4/19	6,183	852
<i>Daphnia Pulex</i> 12/4/19	1,570	1,110
Average	4,057	3,654
Standard Deviation	2,473	5,865
Gold	4,628	36,211
Size of Nanoparticle (nm)	70	

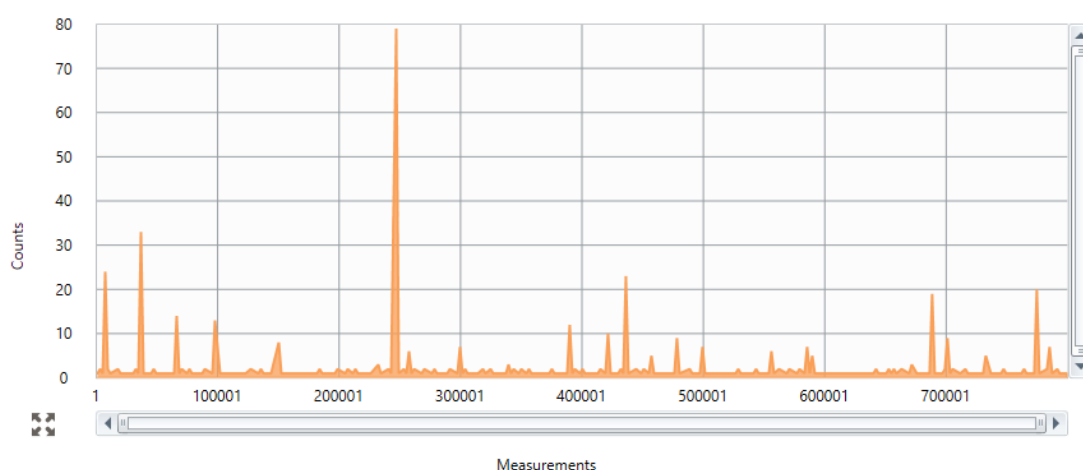


Figure 7.7: A representative scan indicating the large variance in size that can occur within a single the *daphia pulex* sample. The between sample variance further exaggerates these differences.

One consistent pattern that emerged during the analysis was the repeated pairing of two peaks; this was often hidden in the complete Realtime results but upon closer inspection it seems that when daphnids are analysed, they present a doublet peak. In most cases this peak arrangement is a larger peak followed by a smaller peak almost like an echo peak but there were enough instances of there being a smaller peak followed by a larger secondary peak. Typically, the difference in timing between the two peaks is less than 1,000 measurements (less than 0.05 seconds). I believe that this second peak (irrespective of whether it is bigger or smaller than the first peak) is the result of the size of the daphnia, as the daphnia have multiple sections and are significantly larger than a single cell for which the method was developed, and thus in theory the daphnia has an elongated ion cloud as the various parts of the daphnia get ionised at slightly different but detectably different times. Figure 7.8 shows some examples of these doublet peaks, showing also the variability in the size of the peaks, from the largest with a peak size of 75 counts to the smallest at 12 counts, although most peaks are around 15 – 20 counts which maps closely to the size of a single 100 nm gold nanoparticle within the daphnia.

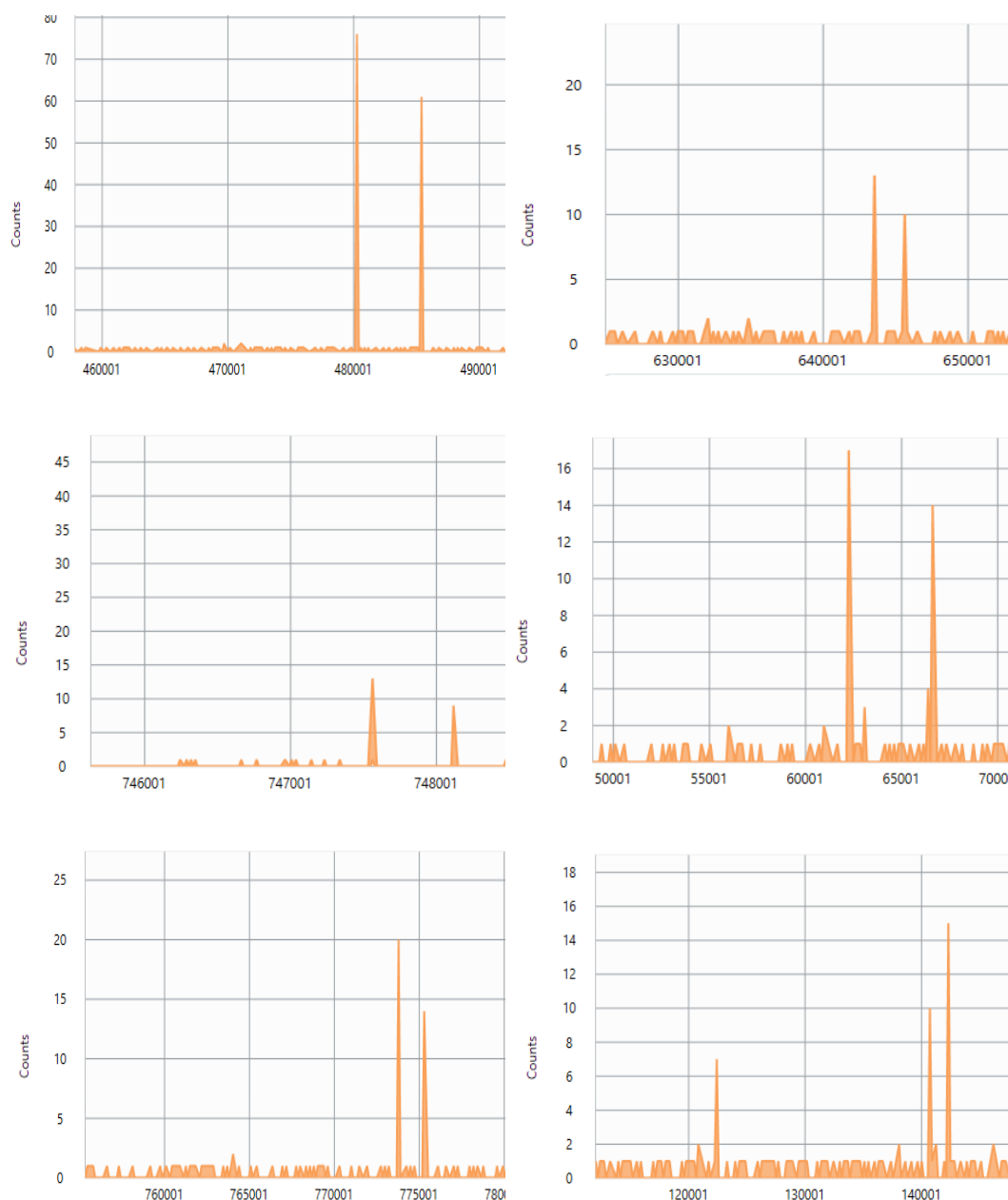


Figure 7.8: Examples of the doublet peaks that are consistently present within the *Daphnia pulex* analysis, most likely a result of the expanded ion cloud leading to two detection events for many of the individual daphnids.

Some of the analysis of the daphnids showed large peaks of above 100 counts, with a maximum over 600 counts as seen in Figure 7.9. These readings were again found to have the characteristic doublet peaks described in Figure 7.8 and were consistently present later in the scan times, reinforcing the idea that the

larger/older daphnia take longer to be transported to the detector and are detected during two consecutive detection events.

The masses that were derived from the larger peaks correspond to a mass of gold averaged to be 38,125 ag (shown as the large peaks in figure 7.10), over eight times larger than the individual gold nanoparticles that the daphnids were exposed to. The larger peaks also have a lower standard deviation of gold at 8,717 ag and a relatively consistent peaks concentration of 3,046. This concentration is close to that of the average from Table 7.3, higher than the concentration of the daphnids in solution, which could be symptomatic of the idea that each peak is not a single daphnia but part of a series of peaks each daphnia form after being ionised in the detector.

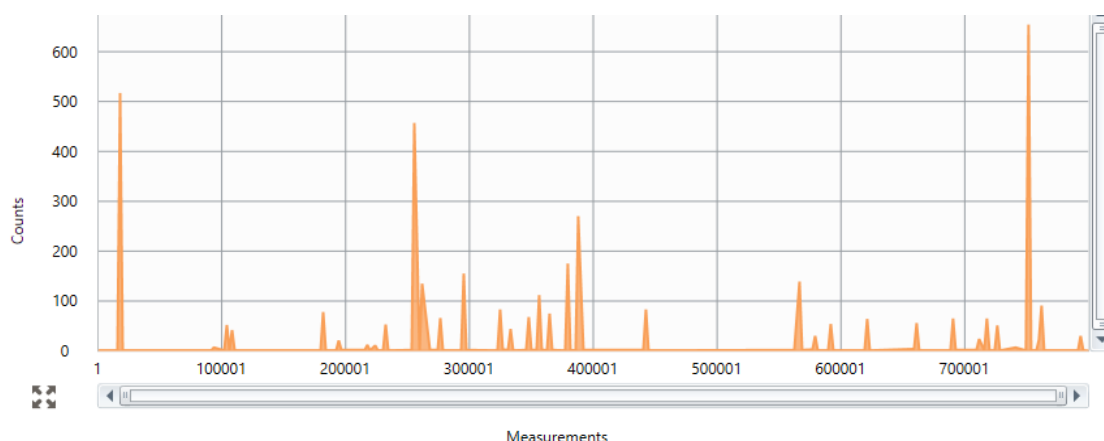


Figure 7.9: Examples of the larger peaks that were detected in the various *Daphnia pulex* samples. This particular sample's real-time data showed multiple very large peaks above 100 counts, many times larger than the average peak size of 15 – 30 counts, potentially indicative of ingestion of agglomerates of Au NPs.

Table 7.3: shows the averaged mass of gold and cell concentrations of daphnia of the samples that had above average peaks where above average was larger than 100 counts.

Sample	Mean Mass (ag)	Peaks Conc. (parts/mL)
<i>Daphnia Pulex</i> 12/4/19 Larger Peak	33,125	2,735
<i>Daphnia Pulex</i> 12/4/19 Larger Peak	33,060	2,735
<i>Daphnia Pulex</i> 12/4/19 Larger Peak	48,190	3,667
Average	38,125	3,046
StDev	8,717	538
Size of Nanoparticle (nm)	659	

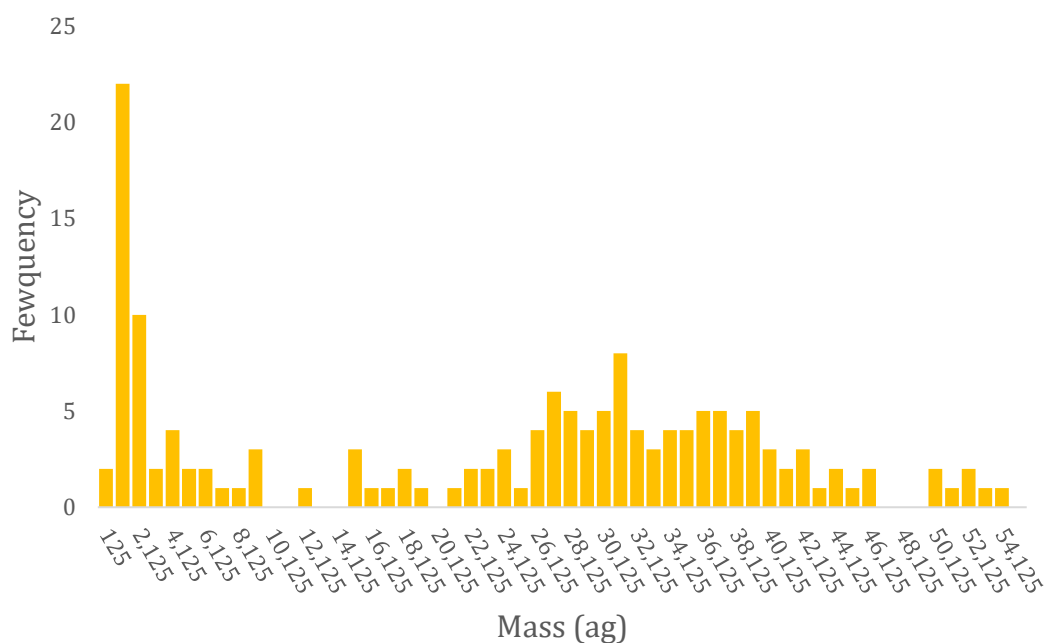


Figure 7.10: The frequency against mass in ag for the large peaks show in figure 7.9s real time, the mass of the peaks was regularly around 33,000 ag.

Conclusion

In conclusion the work that has been performed upon *Daphnia pulex* provides a proof of principle that it is possible to analyse entire organisms using single cell ICP-MS. The difficulties in size of the organism and the small concentration of daphnia individuals have been addressed by choosing a model organism that was on the limit of analysis, and by extending the length of analysis that the instrument recorded of the detection of daphnia it has been possible to repeatably and effectively analyse daphnia. Further optimisation would include better synchronisation of the organism sizes (all juveniles of the same age).

From the analysis of the daphnids there has been a variance in the association of gold nanoparticles and some dissolution of the particles as there is presence of gold in the daphnia at masses lower than the starting particle size. There also seems to be the analysis of multiple peaks per daphnid as there was consistent doublet peaks for each daphnia analysed, this could be evidence of the gold being associated or located throughout the body of the daphnia which is ionised at ever so slightly different times.

Chapter Eight

Recommendations for Future Study

With frequent set-backs in the form of temperamental instrumentation and prolonged technical issues, whether it was glassware within the ICP-MS melting to cell lines dying it has resulted in my studies only scratching the surface of what I intended to achieve. Therefore, this section will address the wide variety of different approaches and desires for future work, that given additional time to develop these burgeoning new techniques further I would pursue.

Complex nanoparticle size and density studies

Additional work proposed based on the use of this method is to measure the chemical changes of the hafnium doped titanium dioxide nanoparticles after three years post synthesis as well as other nanoparticles synthesised and well characterised by the research group, to again measure the chemical changes over time, and stability of the multi-component particles relative to simpler mono-component particles, both during storage, but also in various environmental compartments such as freshwater, seawater, sediment and soil. When applied to measuring the density of nanoparticles the exposure to more complex matrices would demonstrate the applicability of technique as a comparative method to DCS.

After developing the method for determination of size and density of complex, multi-component nanoparticles, it was used in a subsequent study on using Core-Shell $\text{NaHoF}_4@\text{TiO}_2$ ³⁸ to measure the size of the synthesised nanoparticles, and to determine and quantify their presence in real river systems against a high background of naturally occurring TiO_2 nanoparticles.

Another route of analysis of multielement nanoparticle analysis I would like to explore is comparisons between quadrupole ICP-MS and other forms for ICP-MS such as TOF-ICP-MS. As TOF-ICP-MS analyses all the elements it is possible to analyse multiple elements simultaneously which currently quadrupole ICP-MS struggles to achieve, the main concern here is the capabilities of TOF-ICP-MS in separating and discerning individual nanoparticles due to the spreading of ions in the instrument and the large dwell times.

Uptake and transformation of nanoparticles by Isopods

The results that have been discussed here within the analysis of gold uptake within isopods strongly suggests that there has been metallo-sequestration within the isopods. Thus, future work could explore the exact method of metallo-sequestration of the gold, which has not been fully analysed. Multiple questions remain as to the fate of the gold that has been sequestered, with what biological mechanism/pathways is gold being sequestered and the fate of gold within the isopods left unknown. It is predicated that the isopods are expelling the gold from their bodies but without further study this cannot be definitively said, to test this a time resolved study which analyses the uptake of gold nanoparticles and ions over time within isopods as compared to the changes in gold nanoparticles and ions available for uptake (i.e. analysing the feed stock over time). Another point of further study is which of the hepatopancreas cells are interacting with the gold. This can be determined by analysis of phosphorus and sulphur concentration within the isopods, possibly by the removal of hepatopancreas for analysis with single cell ICP-MS; this would allow accurate concentrations for phosphorus and sulphur as an indicator for metallo-sequestration within the isopods.

Intrinsic metal measurements (cells and potentially organisms)

The development of single cell analysis of intrinsic metal content of cells showed that it was possible to measure elevated concentrations of metals that are essential to cell function within cell lines by scICP-MS. Further work in this direction that is proposed is as follows:

Measurement of contaminant metal uptake within cells or algae (which have a size relative to the cell lines analysed) when exposed to environmentally relevant levels, with cell counting via the intrinsic levels of essential metals. This could take the form of analysis of algae or other microorganisms gathered from a water system with significantly high (above environmental background levels) metal levels to determine the cell by cell bioaccumulation of metals as opposed to the background found in the water system. I believe it is possible to determine the exact uptake of metals and the influence that this could have on a food chain (bioaccumulation and biomagnification potential).

Secondly, further work into the detection of intrinsic metals within cell lines by measuring an increased suite of elements to determine the feasibility to fingerprint cells is proposed. There were some indications of collections of elements within cell lines being specific to a cell line (for instance Mn and Co in HeLa cells), by increasing the suite of elements analysed it may be possible to build a clearer picture to determine if cell lines can be fingerprinted based off their intrinsic metal content and elemental concentration groupings. Similarly, co-variance of groups of intrinsic metals in response to different environmental challenges (e.g. elevated temperatures, pollution events, etc.) could potentially be

linked to established signalling pathways and eventually to adverse outcome pathways.

I think that it would be interesting to repeat this work on a TOF-ICP-MS instrument, the capabilities to measure the entire suite of elements simultaneously would provide a much higher degree of information on an individual cell, however the large dwell times of the technique potentially missing cells and decreasing the sensitivity/resolution may make this approach undesirable.

Single Organism ICP-MS

The study of organisms using single cell ICP-MS holds a wide array of possibilities for future work. As we were only in the preliminary stages of development of the method during the work outlined in this thesis there are many directions for continued work.

Firstly, would be to determine the state in which the daphnia are arriving to the plasma - while it is believed that they are arriving intact there is the possibility that they are being destroyed within the tubing and nebuliser. There are many factors that could account for this possibility including the nebuliser gas pressure being too high and bursting the daphnia (as is commonly a problem with plant cells which require a lower gas flow to mitigate) or simply the nebuliser or tubing bursting the daphnia during transport. This study is important for future work as it will demonstrate the survivability of multicellular organisms when analysed using SC-ICP-MS. To achieve this the spray chamber would be detached from the ICP-MS and placed within a holder with a net (for instance filter paper or a particle sieve) attached at the end of the chamber. The daphnia would be up taken by the

autosampler are normal but instead of being ionised in the plasma the state of the individual can be determined.

After determining the state of entry of multicellular organisms, studies into the uptake of nanoparticles by daphnia can commence with a higher degree of accuracy and care. From synchronising the life cycles of daphnia to introduction of environmentally relevant water systems and the use of combination of analytical methods there is large scope for detailed studies. Among the most pressing questions are whether metal/metal oxide particles can translocate from the gut into the tissue, and in what form. Similarly to the isopods mentioned above, Daphnia also shed their carapases which is a known mechanism for removal of toxicants, so single cell ICP-MS analysis of daphnids from the same exposure pre- and post-carapace shedding could shed important light here, coupled with analysis of the carapace themselves.

Thirdly I would propose to study the doublet peak that has been common in the current single cell ICP-MS scans for daphnia. Two aims would be proposed for this study, firstly to confirm with further studies the doublet peak being characteristic of daphnia (and possibly other similarly sized multicellular organisms) and secondly the origin of the doublet peak. Currently my hypothesis is that the peaks are related to the multiple sections of the daphnia body (perhaps the carapace being the large peak and the antenna being the small peak).

In further work the expansion of the tubing size and nebuliser diameter may potentially allow for the analysis of ever larger organisms and singular objects, since the current limits of the capabilities are tied explicitly to the size of the tubing and instrumentation. This could potentially allow or tracking of Daphnids over

their life cycle from neonates through juveniles to adults and how they process metals and metal-based nanoparticles at the different stages of their development. Further optimisation may also be sought by utilising fixed daphnids to reduce depuration, and the potential for organism-directed movement away from the detector.

Summary of the key findings

This thesis describes the development of single particle and single cell ICP-MS analytical techniques for environmental and ecotoxicological analysis. Three studies into instrumental set-up provided the basis for establishment of a standard operating procedure that includes determination of the limits of particle concentration, the standard transport efficiency set-up, and the dwell time for the detector. Aspects of sample handling and its effect on particle size were also explored: for example the method of storage of the particles was investigated (e.g. fridge, freezer) to see if storage method had a visible quantifiable difference on particle size and ionic concentration, which would then feed into subsequent experimental design steps for environmental samples. A single cell ICP-MS method was also later developed building on the work within this thesis.

Analysis of complex multi-element nanoparticles was performed to determine the distribution of the different elements within nanoparticles, i.e. to investigate whether the particle had a core shell structure or whether the second element was distributed throughout the particles, known as doping. Quadrupole based Single particle ICP-MS was able to determine the size and density of multiple, multielement nanoparticles and these results were comparable to other analytical

techniques (DLS, DCS and TEM) that were used as reference methods for size analysis.

Using single particle ICP-MS, gold nanoparticles or ions that had been ingested by organisms, specifically isopods, was analysed. While the working hypothesis was that the isopods would not take up the gold, the data demonstrated uptake of gold nanoparticles and ions, and transformation of both into a consistent nanoparticle size around 60 nm that was present in both ionic and gold fed isopod samples, and was emphasized in the hepatopancreas of the isopods.

Adapting the standard operating procedure for single particle ICP-MS to analyse metals and nanoparticles within individual cells, an SOP for single cell ICP-MS was developed. The goal of this study was to utilise measurement of the intrinsic metal within multiple cell lines as a means to count the cells as an internal standard essentially against which uptake of nanoparticles could subsequently be quantified. However, it was found that the amount of the intrinsic metals in cells were not consistent between biological replicates and were. However, it was still possible to measure the concentration reliably within cells that had been spiked with an intrinsic metal, opening up the avenue of analysis using internal standards to count cells, and environmental analysis of areas with high background levels of specific metals.

Finally, furthering single cell ICP-MS into single organism ICP-MS, with the analysis of entire daphnids (*Daphnia Magna* and *Daphnia Pulex*) that had been fed gold nanoparticles, it was possible to measure individual multicellular organisms, demonstrating proof of principle, which had not yet been shown.

Challenges faced during the research

During the research undertaken within this thesis there were many challenges faced from the instrument breaking down frequently to delays or problems with instruments and materials. Due to the prototype nature of the single cell ICP-MS set-up there were often times where I encountered problems with the instrument that were new to the engineers; of these, two of the most memorable were frequent melting of the torch and nebulizer breakages.

The single cell set-up necessitated a lower gas flow rate due to the desire not to burst the cells, this however meant that if there was a drop in gas flow (either from the instrument, a broken nebuliser or the gas company refilling the argon gas tank mid analysis) the plasma would melt the torch. The torch melting led to a completely new start-up procedure for the instrument, instead of just igniting the plasma it was now a requirement to check that the gas flow was correct first, as documented in the detailed SOP developed from this thesis.

The nebulisers have a very fragile tip that can be broken by the slightest touch. The original method for priming the instrument was to remove the nebuliser from the gas chamber; this proved to be a terrible method of priming the instrument due to the frequency of the nebuliser tip breaking during removal. In response, we changed the method to remove the tubing at the other end of the line avoiding the chance of damage altogether. This is now part of the SOP utilised by Perkin Elmer, developed as part of my thesis.

One of the major challenges that was faced was the instrument computer becoming corrupted in the early part of my second year. At the time there were multiple backups of the data stored upon the instrument computer and not upon

a dedicated external hard drive. During the early part of my second year the instrument computer became corrupted and suffered severe memory leaks resulting in the loss of about five years' worth of data, including most of the original tests and experiments that I ran to develop the SOP. Luckily, I had copies of some key data. After a new computer was installed it is now common practice to store the data in multiple places including on a dedicated external hard drive.

At the start of my PhD I had never cultured cells, so learning to culture multiple cells lines was somewhat of a challenge, while in principal fairly simple there was multiple times where my cultures died due to my inexperience before I was able to analyse the samples, other times the instrument had a fault on the day of analysis that meant that the cells could not be analysed. In all this resulted in a prolonged time to perform the numerous cell-based experiments in chapter 6. I did however turn this to advantage as it allowed me to see the variability of the intrinsic cell metal concentrations which might not have been apparent in biological replicates performed in very quick succession.

Perspectives on the future role spICP-MS and SC-ICP-MS have on the Nano-Science field

spICP-MS is a growing part of the nano science field with the number of laboratories that are using the method increasing every year, I can see it quickly becoming a key part of nanoscience analysis fitting into the suite of particle characterisation instruments like DLS and TEM. The elemental composition and distribution, size and concentration analysis coupled with the speed to receive results makes it a very desirable option for any new analytical laboratory and I am of the opinion that it would be a must have for a new nanometals synthesis or

nanomedicine / nanosafety laboratory due to the numerous outputs that can be achieved with a single instrument making it a catch-all instrument. In the future I can see that the number of publications per year is only going to increase and its inclusion in analytical presentations become commonplace. With numerous companies now producing spICP-MS instruments the capabilities of the technique will only improve whether it is to have higher sensitivity to smaller particles or to measure multielement nanoparticles with multiple detection techniques.

Single Cell ICP-MS is still a newly emerging technique that is already gaining traction within the community, it is quite foreseeable that as more manufacturers produce instrumentation that it also becomes part of the suite of analytical capabilities in nano laboratories. Key features are the developments towards integration with flow cytometry for example, enabling mass cytometry, which is likely to become a cornerstone of drug delivery approaches and chemical safety assessment as well as for nanomaterials. With the capabilities of the instrument only just being discovered, I can see the instrument expanding its reach to beyond just biological analysis and into geology and environmental analysis, this is due to the instruments ability to measure metals on any small particulate and I see no reason that this could not include microplastics or geologically relevant samples.

References

1. Daniel, M. C. & Astruc, D. Gold Nanoparticles: Assembly, Supramolecular Chemistry, Quantum-Size-Related Properties, and Applications Toward Biology, Catalysis, and Nanotechnology. *Chemical Reviews* **104**, 293–346 (2004).
2. Kamat, P. V. Photophysical, photochemical and photocatalytic aspects of metal nanoparticles. *J. Phys. Chem. B* **106**, 7729–7744 (2002).
3. Montano, M. D. *et al. Detection and Characterization of Engineered Nanomaterials in the Environment: Current State-of-the-Art and Future Directions.* (2014).
4. Panyam, J. & Labhasetwar, V. Biodegradable nanoparticles for drug and gene delivery to cells and tissue. *Adv. Drug Deliv. Rev.* **55**, 329–347 (2003).
5. The European Commission & The Joint Commission. COMMISSION RECOMMENDATION of 18 October 2011 on the definition of nanomaterial (Text with EEA relevance). *Off. J. Eur. Union* 2010–2012 (2011).
6. Beer, C., Foldbjerg, R., Hayashi, Y., Sutherland, D. S. & Autrup, H. Toxicity of silver nanoparticles-Nanoparticle or silver ion? *Toxicol. Lett.* **208**, 286–292 (2012).
7. Tuoriniemi, J., Cornelis, G. & Hassellöv, M. Size discrimination and detection capabilities of single-particle ICPMS for environmental analysis of silver nanoparticles. *Anal. Chem.* **84**, 3965–3972 (2012).
8. Zhang, Z., Yang, X., Shen, M., Yin, Y. & Liu, J. Sunlight-driven reduction of

- silver ion to silver nanoparticle by organic matter mitigates the acute toxicity of silver to *Daphnia magna*. *J. Environ. Sci. (China)* **35**, 62–68 (2015).
9. Jing, M. *et al.* Silver nanoparticles induce oxidative cell damage in human liver cells through inhibition of reduced glutathione and induction of mitochondria-involved apoptosis. *Toxicol. Lett.* **201**, 92–100 (2011).
 10. Ahamed, M., Alsalhi, M. S. & Siddiqui, M. K. J. Silver nanoparticle applications and human health. *Clin. Chim. Acta* **411**, 1841–1848 (2010).
 11. Foldbjerg, R. *et al.* PVP-coated silver nanoparticles and silver ions induce reactive oxygen species, apoptosis and necrosis in THP-1 monocytes. *Toxicol. Lett.* **190**, 156–162 (2009).
 12. Gunsolus, I. L. & Haynes, C. L. Analytical Aspects of Nanotoxicology. *Anal. Chem.* **88**, 451–479 (2016).
 13. Su, C.-K. & Sun, Y.-C. Considerations of inductively coupled plasma mass spectrometry techniques for characterizing the dissolution of metal-based nanomaterials in biological tissues. *J. Anal. At. Spectrom.* **30**, 1689–1705 (2015).
 14. Bednar, A. J. *et al.* Comparison of on-line detectors for field flow fractionation analysis of nanomaterials. *Talanta* **104**, 140–148 (2013).
 15. Mourdikoudis, S. & Pallares, R. M. Characterization techniques for nanoparticles : comparison and complementarity upon studying. *Nanoscale* **10**, 12871–12934 (2018).
 16. Cho, E. J. *et al.* Nanoparticle Characterization : State of the Art , Challenges , and Emerging Technologies. *Mol. Pharm.* 2093–2110 (2013).

17. Amable, L., Stephan, C., Smith, S. & Merrifield, R. An Introduction to Single Cell ICP-MS Analysis. 1–5 (2017).
18. Kodiha, M., Wang, Y. M., Hutter, E., Maysinger, D. & Stochaj, U. Off to the Organelles - Killing Cancer Cells with Targeted Gold Nanoparticles. *Theranostics* **5**, (2015).
19. Gray, E., Higgins, C. P. & Ranville, J. F. *Analysis of Nanoparticles in Biological Tissues using SP-ICP-MS*.
20. Arora, S., Jain, J., Rajwade, J. M. & Paknikar, K. M. Cellular responses induced by silver nanoparticles: In vitro studies. *Toxicol. Lett.* **179**, 93–100 (2008).
21. Dan, Y. *et al.* Characterization of gold nanoparticle uptake by tomato plants using enzymatic extraction followed by single-particle inductively coupled plasma-mass spectrometry analysis. *Environ. Sci. Technol.* **49**, 3007–3014 (2015).
22. Hansen, U. & Thünemann, A. F. Characterization of Silver Nanoparticles in Cell Culture Medium Containing Fetal Bovine Serum. *Langmuir* **31**, 6842–6852 (2015).
23. Asharani, P. V., Low, G., Mun, K., Hande, M. P. & Valiyaveetil, S. Cytotoxicity and Genotoxicity of Silver. **3**, 279–290 (2009).
24. Kokalj, A. J. Integration of behavioral tests and biochemical biomarkers of terrestrial isopod *Porcellio scaber* (Isopoda , Crustacea) is a promising methodology for testing environmental safety of chars * zari. **234**, 804–811 (2018).

25. Kubota, T., Yamanaka, M. & Agilent Technologies International Japan. Multi-element determination in populations of single cells by quadrupole ICP-MS. (2019). Available at: https://www.agilent.com/cs/library/posters/public/AWCPS_2017-J05_Kubota.pdf.
26. Panyam, J., Zhou, W.-Z., Prabha, S., Sahoo, S. K. & Labhasetwar, V. Rapid endo-lysosomal escape of poly(DL-lactide-co-glycolide) nanoparticles: implications for drug and gene delivery. *FASEB J.* **16**, 1217–26 (2002).
27. Tuoriniemi, J., Cornelis, G. & Hassellöv, M. Improving the accuracy of single particle ICPMS for measurement of size distributions and number concentrations of nanoparticles by determining analyte partitioning during nebulisation. *J. Anal. At. Spectrom.* **29**, 743 (2014).
28. Peters, R. *et al.* Single particle ICP-MS combined with a data evaluation tool as a routine technique for the analysis of nanoparticles in complex matrices. *J. Anal. At. Spectrom.* **30**, 1274–1285 (2015).
29. Peters, R., Wijma, E., Weigel, S. & Bouwmeester, H. Single Particle ICPMS : A screening method for inorganic nanoparticles.
30. Mitrano, D., Ranville, J. F. & Neubauer, K. Coupling Flow Field Flow Fractionation to ICP-MS for the Detection and Characterization of Silver Nanoparticles.
31. Degueldre, C. & Favarger, P. Y. Colloid analysis by single particle inductively coupled plasma-mass spectroscopy: A feasibility study. *Colloids Surfaces A Physicochem. Eng. Asp.* **217**, 137–142 (2003).

32. Degueldre, C., Favarger, P. Y. & Bitea, C. Zirconia colloid analysis by single particle inductively coupled plasma-mass spectrometry. *Anal. Chim. Acta* **518**, 137–142 (2004).
33. Plowman, B. J., Tschulik, K., Walport, E., Young, N. P. & Compton, R. G. The fate of nano-silver in aqueous media. *Nanoscale* **7**, 12361–12364 (2015).
34. PerkinElmer. Colorado School of Mines Uses a NexION 300Q ICP-MS to Obtain a Better Understanding of the Environmental Impact of Engineered Nanomaterials. *Perkin Elmer* (2012).
35. Mitrano, D. M. *et al.* Silver nanoparticle characterization using single particle ICP-MS. *J. Anal. At. Spectrom.* (2012). doi:10.1039/c2ja30021d
36. Mitrano, D. M. *et al.* Environmental Science Nano Tracking dissolution of silver nanoparticles at. *Environ. Sci. Nano* 248–259 (2014). doi:10.1039/c3en00108c
37. Misra, S. K., Dybowska, A., Berhanu, D., Luoma, S. N. & Valsami-Jones, E. The complexity of nanoparticle dissolution and its importance in nanotoxicological studies. *Sci. Total Environ.* **438**, 225–232 (2012).
38. Cui, X. *et al.* Core–Shell NaHoF₄@TiO₂ NPs: A Labeling Method to Trace Engineered Nanomaterials of Ubiquitous Elements in the Environment. *ACS Appl. Mater. Interfaces* **11**, 19452–19461 (2019).
39. Antony, J. J., Sivalingam, P. & Chen, B. Toxicological effects of silver nanoparticles. *Environ. Toxicol. Pharmacol.* **40**, 729–732 (2015).
40. Ellis, L.-J., Papadimitrakopoulos, A., Weigel, S. & Valsami-Jones, E. Synthesis and characterization of Zr- and Hf-doped nano-TiO₂ as internal standards for

- analytical quantification of nanomaterials in complex matrices. *R.Soc.open sci* **5**, (2019).
41. Donovan, A. R. *et al.* Single particle ICP-MS characterization of titanium dioxide, silver, and gold nanoparticles during drinking water treatment. *Chemosphere* **144**, 148–153 (2016).
 42. Dan, Y., Shi, H., Stephan, C. & Liang, X. Rapid analysis of titanium dioxide nanoparticles in sunscreens using single particle inductively coupled plasma-mass spectrometry. *Microchem. J.* **122**, 119–126 (2015).
 43. Merrifield, R., Amable, L. & Stephan, C. Single-Cell ICP-MS Analysis : Quantifying the Metal Concentration of Unicellular Organisms at the Cellular Level. **33**, 33–40 (2018).
 44. Institute of Medicine (US) Roundtable on Environmental Health Sciences, Research, and M., Goldman L, C, C. & Editors. *Implications of Nanotechnology for Environmental Health Research.* (2005).
 45. Madl, A. K., Pinkerton, K. E., Madl, A. K. & Pinkerton, K. E. Health effects of inhaled engineered and incidental nanoparticles Health effects of inhaled engineered and incidental nanoparticles. *Crit. Rev. Toxicol.* **8444**, (2009).
 46. Baddock, M., Boskovic, L., Strong, C., Mctainsh, G. & Bullard, J. Iron-rich nanoparticles formed by aeolian abrasion of desert dune sand. *G3* **14**, 3720–3729 (2013).
 47. Ermolin, M. S., Fedotov, P. S., Malik, N. A. & Karandashev, V. K. Chemosphere Nanoparticles of volcanic ash as a carrier for toxic elements on the global scale. *Chemosphere* **200**, 16–22 (2018).

48. Gislason, S. R. *et al.* Characterization of Eyjafjallajökull volcanic ash particles and a protocol for rapid risk assessment. *PNAS* **108**, (2011).
49. Gardea-torresdey, J. L. Interactions between CeO₂ Nanoparticles and the Desert Plant Mesquite: A Spectroscopy Approach. *ACS Sustain. Chem. Eng.* **4**, 1187–1192 (2016).
50. (ECHA), E. C. A. Note on substance identification and the potential scope of a restriction on uses of ‘ microplastics ’. (2019).
51. (ECHA), E. C. A. *ANNEX XV RESTRICTION REPORT P ROPOSAL FOR A RESTRICTION SUBSTANCE NAME (S): intentionally added microplastics IUPAC NAME (S): n / a EC NUMBER (S): n / a CAS NUMBER (S): n / a CONTACT DETAILS OF THE DOSSIER SUBMITTER: European Chemicals Agency (E.* (2019).
52. The European Commission. Restriction proposal for intentionally added microplastics in the EU – update. (2019). Available at: <https://echa.europa.eu/-/restriction-proposal-for-intentionally-added-microplastics-in-the-eu-update>.
53. The European Commission. Microplastics. (2019). Available at: <https://echa.europa.eu/hot-topics/microplastics>.
54. Stephan, C. & Neubauer, K. Single Particle Inductively Coupled Plasma Mass Spectrometry : Understanding How and Why Authors. *Perkin Elmer* 1–5 (2014).
55. Laborda, F., Bolea, E. & Jiménez-Lamana, J. Single particle inductively coupled plasma mass spectrometry: A powerful tool for nanoanalysis. *Anal.*

- Chem.* **86**, 2270–2278 (2014).
56. Stephan, C. & Hineman, A. ICP - Mass Spectrometry Iron Nanoparticles by SP-ICP-MS: Overcoming Spectral Interferences Using Universal Cell Technology. *Perkin Elmer* (2014).
 57. Degueldre, C. & Favarger, P. Thorium colloid analysis by single particle inductively coupled plasma-mass spectrometry. *Talanta* **62**, 1051–1054 (2004).
 58. Mitrano, D., Ranville, J., Neubauer, K. & Thomas, R. Field-Flow Fractionation Coupled with ICP-MS for the Analysis of Engineered Nanoparticles in Environmental Samples. **27**, (2012).
 59. Mitrano, D. M. *et al.* Silver nanoparticle characterization using single particle ICP-MS (SP-ICP-MS) and asymmetrical flow field flow fractionation ICP-MS (AF4-ICP-MS). *J. Anal. At. Spectrom.* **27**, 1131 (2012).
 60. Mitrano, D., Ranville, J. F. & Stephan, C. Quantitative Evaluation of Nanoparticle Dissolution Kinetics using Single Particle ICP-MS: A Case Study with Silver Nanoparticles.
 61. Peretyazhko, T. S., Zhang, Q. & Colvin, V. L. Size-controlled dissolution of silver nanoparticles at neutral and acidic pH conditions: Kinetics and size changes. *Environ. Sci. Technol.* **48**, 11954–11961 (2014).
 62. Mast, J. TEM and SP-ICP-MS Analysis of the Release of Silver Nanoparticles from Decoration of Pastry. (2015). doi:10.1021/acs.jafc.5b00578
 63. Liu, J. & Jiang, G. Silver nanoparticles in the environment. *Environ. Sci. Process. Impacts* **15**, (2013).

64. Gray, E. P. *et al.* Extraction and Analysis of Silver and Gold Nanoparticles from Biological Tissues Using Single Particle Inductively Coupled Plasma Mass Spectrometry. (2013). doi:10.1021/es403558c
65. Hadioui, M., Wilkinson, K. & Stephan, C. Assessing the Fate of Silver Nanoparticles in Surface Water using Single Particle ICP-MS. *ICP-MS Appl. note* 3–8 (2014).
66. Verleysen, E. *et al.* TEM and SP-ICP-MS Analysis of the Release of Silver Nanoparticles from Decoration of Pastry. *J. Agric. Food Chem.* **63**, 3570–3578 (2015).
67. Poda, A. R. *et al.* Characterization of silver nanoparticles using flow-field flow fractionation interfaced to inductively coupled plasma mass spectrometry. *J. Chromatogr. A* **1218**, 4219–4225 (2011).
68. Pinto, V. V *et al.* Colloids and Surfaces A : Physicochemical and Engineering Aspects Long time effect on the stability of silver nanoparticles in aqueous medium : Effect of the synthesis and storage conditions. *Colloids Surfaces A Physicochem. Eng. Asp.* **364**, 19–25 (2010).
69. Vance, M. E. *et al.* Nanotechnology in the real world: Redeveloping the nanomaterial consumer products inventory. *Beilstein J. Nanotechnol.* **6**, 1769–1780 (2015).
70. Elechiguerra, J. L. *et al.* Interaction of silver nanoparticles with HIV-1. *J. Nanobiotechnology* **3**, (2005).
71. Chen, L. Q. *et al.* Nanotoxicity of Silver Nanoparticles to Red Blood Cells : Size Dependent Adsorption , Uptake , and Hemolytic Activity. (2015).

72. Arora, S., Jain, J., Rajwade, J. M. & Paknikar, K. M. Interactions of silver nanoparticles with primary mouse fibroblasts and liver cells. *Toxicol. Appl. Pharmacol.* **236**, 310–318 (2009).
73. Chairuangkitti, P. *et al.* Silver nanoparticles induce toxicity in A549 cells via ROS-dependent and ROS-independent pathways. *Toxicol. Vitr.* **27**, 330–338 (2012).
74. Alammar, T., Chow, Y.-K. & Mudring, A.-V. Energy efficient microwave synthesis of mesoporous Ce_{0.5} M_{0.5} O₂ (Ti, Zr, Hf) nanoparticles for low temperature CO oxidation in an ionic liquid – a comparative study. *New J. Chem.* **39**, 1339–1347 (2015).
75. Merrifield, R. C., Stephan, C. & Lead, J. R. Single-particle inductively coupled plasma mass spectroscopy analysis of size and number concentration in mixtures of monometallic and bimetallic (core-shell) nanoparticles. *Talanta* **162**, 130–134 (2017).
76. Naasz, S., Weigel, S., Borovinskaya, O., Serva, A. & Peters, R. J. B. ICP-MS using quadrupole and time-of-flight. 835–845 (2018). doi:10.1039/c7ja00399d
77. Merrifield, R. C., Stephan, C. & Lead, J. R. Quantification of Au Nanoparticle Biouptake and Distribution to Freshwater Algae Using Single Cell - ICP-MS. *Environ. Sci. Technol.* **52**, 2271–2277 (2018).
78. Miyashita, S. *et al.* Time-resolved ICP-MS Measurement: a New Method for Elemental and Multiparametric Analysis of Single Cells. *Anal. Sci.* **30**, 219–224 (2014).

79. Ho, K.-S. & Chan, W.-T. Time-resolved ICP-MS measurement for single-cell analysis and on-line cytometry. *J. Anal. At. Spectrom.* **25**, 1114 (2010).
80. PerkinElmer. Single Cell Analysis. (2019). Available at: <https://www.perkinelmer.com/uk/category/single-cell-analysis>.
81. Kestens, V. *et al.* Supporting Information Improved Metrological Traceability of Particle Size Values Measured with Line-Start Incremental Centrifugal Liquid Sedimentation. *Langmuir* **33**, 1–10 (2017).
82. CPS Instruments Europe. *Introduction to Differential Sedimentation. CPS Instruments Europe*
83. Vegad, H. An introduction to particle size characterisation by DCS: Do you know the real size of your particles. *Anal. Ltd* 1–7
84. Stetefeld, J., Mckenna, S. A. & Patel, T. R. Dynamic light scattering : a practical guide and applications in biomedical sciences. *Biophys. Rev.* 409–427 (2016). doi:10.1007/s12551-016-0218-6
85. Malvern Instruments. Dynamic Light Scattering: An Introduction in 30 Minutes. *DLS Tech. note* 1–8
86. Winey, M., Meehl, J. B., Toole, E. T. O., Giddings, T. H. & Drubin, D. G. Conventional transmission electron microscopy. **25**, (2014).
87. Giard, D. J. *et al.* In Vitro Cultivation of Human Tumors : Establishment of Cell Lines Derived From. **51**, 1417–1423 (1973).
88. Deville, S. *et al.* Intracellular dynamics and fate of polystyrene nanoparticles in A549 Lung epithelial cells monitored by image (cross-) correlation

- spectroscopy and single particle tracking. *Biochim. Biophys. Acta - Mol. Cell Res.* **1853**, 2411–2419 (2015).
89. Wang, T. *et al.* Ultra-sensitive assay for paclitaxel in intracellular compartments of A549 cells using liquid chromatography-tandem mass spectrometry. *J. Chromatogr. B Anal. Technol. Biomed. Life Sci.* **912**, 93–97 (2013).
 90. Hirsch, C. Culturing A549 cells. 1–9 (2014).
 91. Lucey, B. P., Nelson-rees, W. A. & Hutchins, G. M. Henrietta Lacks , HeLa Cells , and Cell Culture Contamination. *Arch Pathol Lab Med* **133**, 1463–1467 (2009).
 92. Turner, T. Development of the Polio Vaccine: A Historical Perspective of Tuskegee University's Role in Mass Production and Distribution of HeLa Cells. *J Heal. Care Poor Underserved* **23**, 5–10 (2015).
 93. Goodwin, E. C. & Dimaio, D. Repression of human papillomavirus oncogenes in HeLa cervical carcinoma cells causes the orderly reactivation of dormant tumor suppressor pathways. *PNAS* **97**, 12513–12518 (2000).
 94. Landry, J. J. M. *et al.* The Genomic and Transcriptomic Landscape of a HeLa Cell Line. *Genetics* **3**, 1213–1224 (2013).
 95. Mittelman, D. & Wilson, J. H. The fractured genome of HeLa cells. *Genome Biol.* **14**, 111–114 (2013).
 96. Chavez, K. J., Garimella, S. V. & Lipkowitz, S. Triple Negative Breast Cancer Cell Lines: One Tool in the Searchfor Better Treatment of Triple Negative Breast Cancer. *Breast Dis.* **32**, 35–48 (2012).

97. Office of Ocean Exploration and Research. What is an isopod? *Office of Ocean Exploration and Research* (2019). Available at: <https://oceanexplorer.noaa.gov/facts/isopod.html>.
98. van Gestel, C. A. M., Loureiro, S. & Zidar, P. Terrestrial isopods as model organisms in soil ecotoxicology: a review. *Zookeys* **801**, 127–162 (3AD).
99. Bernardi, D. Chapter 2 . Introduction to Daphnia Biology Physiology , Metabolism , and Immunity. in *Ecology, Epidemiology, and Evolution of Parasitism in Daphnia [Internet]*. 1–21 (Bethesda (MD): National Center for Biotechnology Information (US, 2005).
100. Briffa, S. M., Nasser, F., Valsami-Jones, E. & Lynch, I. Uptake and impacts of polyvinylpyrrolidone (PVP) capped metal oxide nanoparticles on Daphnia magna Environmental Science Nano Uptake and impacts of polyvinylpyrrolidone (PVP) magna : role of core composition and acquired. *Environ. Sci. Nano* **5**, 1745–1756 (2018).
101. Shaw, J. R. *et al.* Daphnia as an emerging model for toxicological genomics. *Adv. Exp. Biol.* **02**, 5–7 (2008).
102. Nasser, F., Davis, A., Valsami-jones, E. & Lynch, I. Shape and charge of gold nanomaterials influence survivorship , oxidative stress and moulting of Daphnia magna Shape and Charge of Gold Nanomaterials Influence Survivorship , Oxidative Stress and Moulting of Daphnia magna. *Nanomaterials* **6**, (2019).
103. Pollution, C., Board, C. & Bhawan, P. Evaluation of Daphnia magna as an indicator of Toxicity and Treatment efficacy of Municipal Sewage Treatment

- Plant. *J. Appl. Sci. Environ. Mgt.* **11**, 61–67 (2007).
104. Nasser, F, Constantinou, J & Lynch, I. Nanomaterials in the environment acquire an “eco corona” impacting their toxicity to *Daphnia magna* — a call for updating toxicity testing policies Nanomaterials in the Environment Acquire an “Eco-Corona” Impacting their Toxicity to *Daphnia Magna* — a *C. Proteomics*. (2019). doi:10.1002/pmic.201800412
 105. Ellis, Laura-Jayne A.; Valsami-Jones, Eugenia; Lynch, I. Exposure medium and particle ageing moderate the toxicological effects of nanomaterials to *Daphnia magna* over multiple generations Environmental Science Nano the toxicological effects of nanomaterials to for standard test review? †. *Environ. Sci. Nano*. (2020). doi:10.1039/D0EN00049C
 106. Briffa, Sophie Marie; Nasser, Fatima; Valsami-Jones, Eugenia; Lynch, I. Uptake and impacts of polyvinylpyrrolidone (PVP) capped metal oxide nanoparticles on *Daphnia magna* Environmental Science Nano Uptake and impacts of polyvinylpyrrolidone (PVP) magna : role of core composition and acquired. *Environ. Sci. Nano* **5**, 1745–1756 (2018).
 107. Fryer, B. NexION 300 spICP-MS Analysis: Metal nanoparticle size and concentration. (2017). Available at: https://www.researchgate.net/publication/317935984_NexION_300_spICP-MS_Analysis_Metal_nanoparticle_size_and_concentration.
 108. Velgosova, O., Elena, Č., Málek, J. & Kavuli, J. Effect of storage conditions on long-term stability of Ag nanoparticles formed via green synthesis. *Int. J. Miner. Metall. Mater.* **24**, 1177–1182 (2017).

109. Huk, A. *et al.* RSC Advances. *RSC Adv.* 84172–84185 (2015).
doi:10.1039/c5ra10187e
110. Widdrat, M. *et al.* Keeping Nanoparticles Fully Functional: Long-Term Storage and Alteration of Magnetite. *Chempluschem* **79**, 1225–1233 (2014).
111. SONG, W., ZHANG, X., YIN, H., SA, P. & LIU, X. Preparation and Storage of Silver Nanoparticles in Aqueous. *Chinese J. Chem.* 717–721 (2009).
112. nanoComposix. *Nanoparticle Storage and Handling Procedures*. **1**, (2018).
113. Lee, S. *et al.* Nanoparticle size detection limits by single particle ICP-MS for 40 elements. *Environ. Sci. Technol.* **48**, 10291–10300 (2014).
114. Croteau, M.-N., Dybowska, A. D., Luoma, S. N. & Valsami-Jones, E. A novel approach reveals that zinc oxide nanoparticles are bioavailable and toxic after dietary exposures. *Nanotoxicology* **5**, 79–90 (2011).
115. Benn, T. M. & Westerhoff, P. Nanoparticle Silver Released into Water from Commercially Available Sock Fabrics. in *Ecology, Epidemiology, and Evolution of Parasitism in Daphnia [Internet]*. **42**, 4133–4139 (2008).
116. Cornelis, G. & Hassellöv, M. A signal deconvolution method to discriminate smaller nanoparticles in single particle ICP-MS. *J. Anal. At. Spectrom.* **29**, 134–144 (2014).
117. Merrifield, R. & Stephan, C. Transformations of Nanoparticles in Exposure Media Measured by SP-ICP-MS. *Appl. Note* (2016).
118. Liu, J., Murphy, K. E., MacCuspie, R. I. & Winchester, M. R. Capabilities of Single Particle Inductively Coupled Plasma Mass Spectrometry for the Size

- Measurement of Nanoparticles: A Case Study on Gold Nanoparticles. *Anal. Chem.* **86**, 3405–3414 (2014).
119. Laborda, F., Jiménez-Lamana, J., Bolea, E. & Castillo, J. R. Selective identification, characterization and determination of dissolved silver(i) and silver nanoparticles based on single particle detection by inductively coupled plasma mass spectrometry. *J. Anal. At. Spectrom.* **26**, 1362 (2011).
120. Lee, W.-W. & Chan, W.-T. Calibration of single-particle inductively coupled plasma-mass spectrometry (SP-ICP-MS). *J. Anal. At. Spectrom.* **30**, 1245–1254 (2015).
121. Böhme, S. *et al.* Multi-Element Single Particle ICP-MS Detection of Nanoparticles Using Quadrupole and Time of Flight Instruments. *Not yet Submitt.* 1–22
122. Va, M. & Sanz-medel, A. Critical comparison between quadrupole and time-of-flight inductively coupled plasma mass spectrometers for isotope ratio measurements in elemental speciation. *J. Anal. At. Spectrom.* **17**, 950–957 (2002).
123. Thomas, R. *Practical Guide to ICP-MS*. (2004).
124. Pace, H. E. *et al.* Determining Transport Efficiency for the Purpose of Counting and Sizing Nanoparticles via Single Particle Inductively Coupled Plasma Mass Spectrometry (vol 83, pg 9361, 2011). *Anal. Chem.* **84**, 4633 (2012).
125. Ellis, L.-J. A., Papadiamantis, A. G., Weigel, S. & Valsami-Jones, E. Synthesis and Characterisation of Zr and Hf doped nano-TiO₂ as reference materials

for nanosafety studies. *RSC Adv.*

126. Hindborg, L., Rønn, R. & Vestergård, M. Ecotoxicology and Environmental Safety Bioaccumulation of cadmium in soil organisms – With focus on wood ash application. *Ecotoxicol. Environ. Saf.* **156**, 452–462 (2018).
127. Romih, T. *et al.* Gold nanoparticles do not induce adverse effects on terrestrial isopods *Porcellio scaber* after 14-day exposure. *ACTA Biol. Slov.* **59**, 33–44 (2016).
128. Tarnawska, M. Nickel toxicity in the hepatopancreas of an isopod *Porcellio scaber* (Oniscidea). *Nucl. Instruments Methods Phys. Res. B* **260**, 213–217 (2007).
129. Ardestani, M. M., Straalen, N. M. Van & Gestel, C. A. M. Van. Uptake and elimination kinetics of metals in soil invertebrates : A review. *Environ. Pollut.* **193**, 277–295 (2014).
130. Hames, C. A. C. & Hopkin, S. P. A daily cycle of apocrine secretion by the B cells in the hepatopancreas of terrestrial isopods. *Can. J. Zool.* **69**, 1931–1937 (1991).
131. Ferreira, N. G. C. *et al.* Unravelling the molecular mechanisms of nickel in woodlice . *Environ. Res.* **176**, 108507 (2019).
132. Emsley, J. *Nature's Building Blocks: An A-Z Guide to the Elements.* (OUP Oxford., 2011).
133. Nielsen, F. H. & US Department of Agriculture. 16. Ultratrace Minerals. in *Modern nutrition of health and disease* 283–303 (1999).

134. Jong, W. H. De. Drug delivery and nanoparticles : Applications and hazards. **3**, 133–149 (2008).
135. Mesko, M. F., Mello, P. A. & Bizzi, C. A. Iodine determination in food by inductively coupled plasma mass spectrometry after digestion by microwave-induced combustion. *Anal Bioanal Chem* **398**, 1125–1131 (2010).
136. Lin, C., Yang, C., Ger, J., Deng, J. & Hung, D. Tetramethylammonium hydroxide poisoning Case reports. *Clin. Toxicol.* **48**, 213–217 (2010).
137. Park, S., Park, J., You, K., Shin, H. & Kim, H. Tetramethylammonium Hydroxide Poisoning during a Pallet Cleaning Demonstration. *J. Occup. Health* **55**, 120–124 (2013).
138. Romih, T., Kos, M. & Novak, S. Gold nanoparticles do not induce adverse effects on terrestrial isopods *Porcellio scaber* after 14-day exposure. (2016).
139. Tenuta, T. *et al.* Elution of Labile Fluorescent Dye from Nanoparticles during Biological Use. *PLoS One* **6**, (2011).
140. Wolfbeis, O. S. An overview of nanoparticles commonly used in fluorescent bioimaging. *Chem Soc Rev* **44**, 4743–4768 (2015).
141. Awasthi, M. & Chand, L. Interactions between zinc and cadmium uptake by free and immobilized cells of *Scenedesmus quadricauda* (Turp.) Breb . *Acta Hydrochim. hydrobiol.* **34**, 20–26 (2006).
142. Shahid, M., Dumat, C., Khalid, S., Schreck, E. & Xiong, T. Foliar heavy metal uptake , toxicity and detoxification in plants : A comparison of foliar and

- root metal uptake. *J. Hazard. Mater.* **325**, 36–58 (2017).
143. Jan, A. T., Azam, M., Siddiqui, K., Ali, A. & Choi, I. Heavy Metals and Human Health : Mechanistic Insight into Toxicity and Counter Defense System of Antioxidants. *Int. J. Mol. Sci.* **16**, 29592–29630 (2015).
144. Allowances, R. D. *et al. Recommended Dietary Allowances.* (1989).
145. Regulations, E. C. of F. Title 21: Food and Drugs. (2019). Available at: https://www.ecfr.gov/cgi-bin/text-idx?SID=10896471be7fb6ff7aae0acf00081a82&mc=true&node=pt21.2.101&rgn=div5#se21.2.101_19.
146. Monopoli, M. P. *et al. Physical - Chemical Aspects of Protein Corona : Relevance to in Vitro and in Vivo Biological Impacts of Nanoparticles.* 2525–2534 (2011).
147. Commonwealth of Australia. *UPDATE 1 . 1 : REVISION OF FLUORIDE (2017)*. (2017).
148. Misra, S. K. *et al. Isotopically Modified Nanoparticles for Enhanced Detection in Bioaccumulation Studies.* (2012).
149. May, T. W., Wiedmeyer, R. H., Survey, U. S. G. & Division, B. R. A Table of Polyatomic Interferences in ICP-MS. *At. Spectrosc.* **19**, 150–155 (1998).
150. Viant, M. R. Miniaturising acute toxicity and feeding rate measurements in *Daphnia magna*. *Ecotoxicol. Environ. Saf.* **139**, 352–357 (2017).

Appendices

Appendix 1: Worked example of nanoparticle calculations from chapter two.

Using results from a calibration that has already been performed the size of an unknown gold nanoparticle is calculated.

Transport efficiency

Gold nanoparticle and dissolved standards were run using the single particle ICP-MS and the following counts were reported.

Diameter of nanoparticle standard	Counts
0 nm	0.12
20 nm	6.55
40 nm	39.54
80 nm	500.01

Concentration of dissolved standard	Counts
0 µg / L	0.20
1 µg / L	1.99
2 µg / L	3.78
3 µg / L	7.02

The calibration graphs needed for the transport efficiency use mass so the diameter and concentration need to be converted into masses using equations A1.1 and A1.2 respectively.

Equation A1.1: Nanoparticle standard mass

$$M_p = \frac{\left(\frac{\pi \cdot d^3}{6} \cdot \rho\right)}{\omega_i}$$

Equation A1.2: Sample flow rate equation

$$S_f = \frac{m}{t \times \rho}$$

For nanoparticle standard the calculations are shown below.

Diameter of nanoparticle standard (nm)	Diameter of nanoparticle standard (cm)
0	0
20	0.000002
40	0.000004
80	0.000008

The density of gold is 19.3 g cm⁻³ so when the diameter and density of gold are imputed into equation 2.1 the following masses are calculated.

Equation 2.2: Nanoparticle standard mass calculation.

$$M_p = \frac{\pi \cdot d^3}{6} \cdot \rho$$

Mass of nanoparticle standard		Counts
grams	femtograms	
0	0	0.12
8.08×10^{-17}	0.081	6.55
6.47×10^{-16}	0.647	39.54
5.17×10^{-15}	5.174	500.01

The masses were then plotted against the counts for the masses to form a calibration graph (figure A1.1).

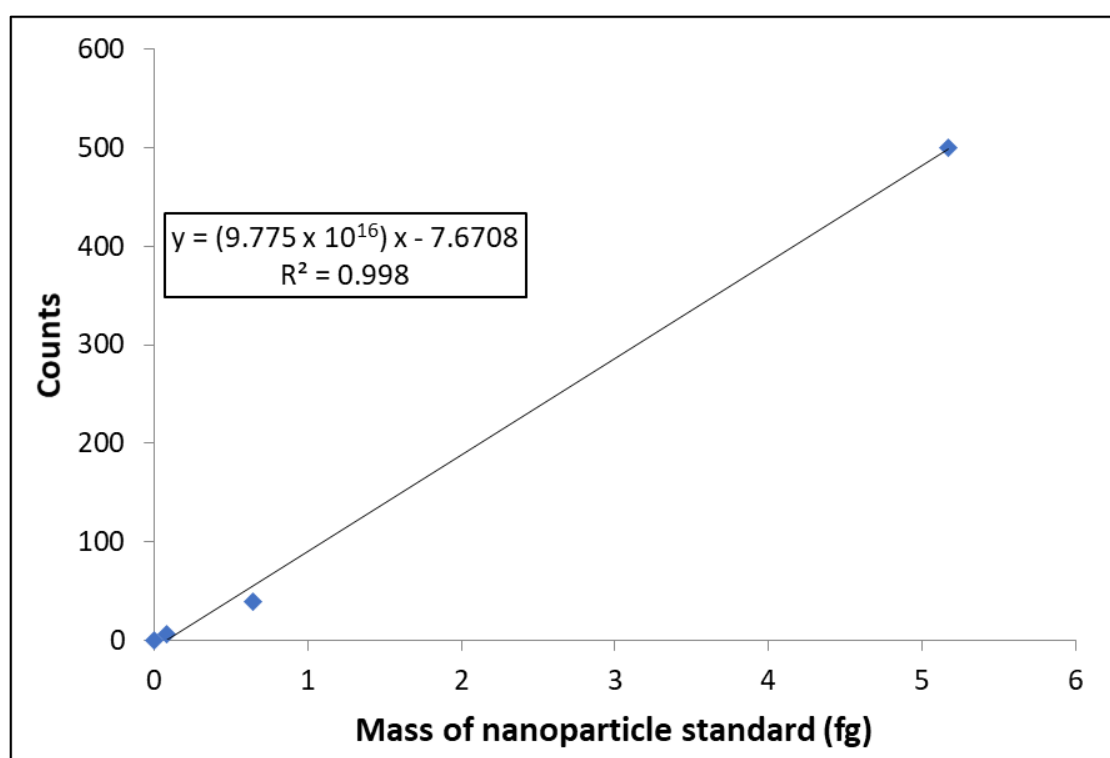


Figure A1.1: Calibration graph for nanoparticle standards against counts.

The linear slope of the line was found to be 9.775×10^{16} ; this is used later to determine the transport efficiency.

To calculate the dissolved standard the calculations are shown below.

Concentration of dissolved standard ($\mu\text{g dm}^{-3}$)	Concentration of dissolved standard ($\mu\text{g cm}^{-3}$)
0	0
1	0.001
2	0.002
3	0.003

The dwell time was 0.1 ms and the flow rate was $0.216 \text{ cm}^3 \text{ min}^{-1}$ which, when divided by 60,000, became $0.0000036 \text{ ms cm}^{-3}$. When all these variables are imputed into equation 2.3 the following masses are calculated.

Equation 2.3: Dissolved standard mass of a particle.

$$M_D = q_{liq} \cdot t_{dt} \cdot C$$

Mass of dissolved standard		Counts
grams	femtograms	
0	0	0.20
7.776×10^{-17}	0.078	1.99
1.5552×10^{-16}	0.156	3.78
2.3328×10^{-16}	0.233	7.02

The masses were then plotted against the counts for the masses to form a calibration graph (figure A1.2).

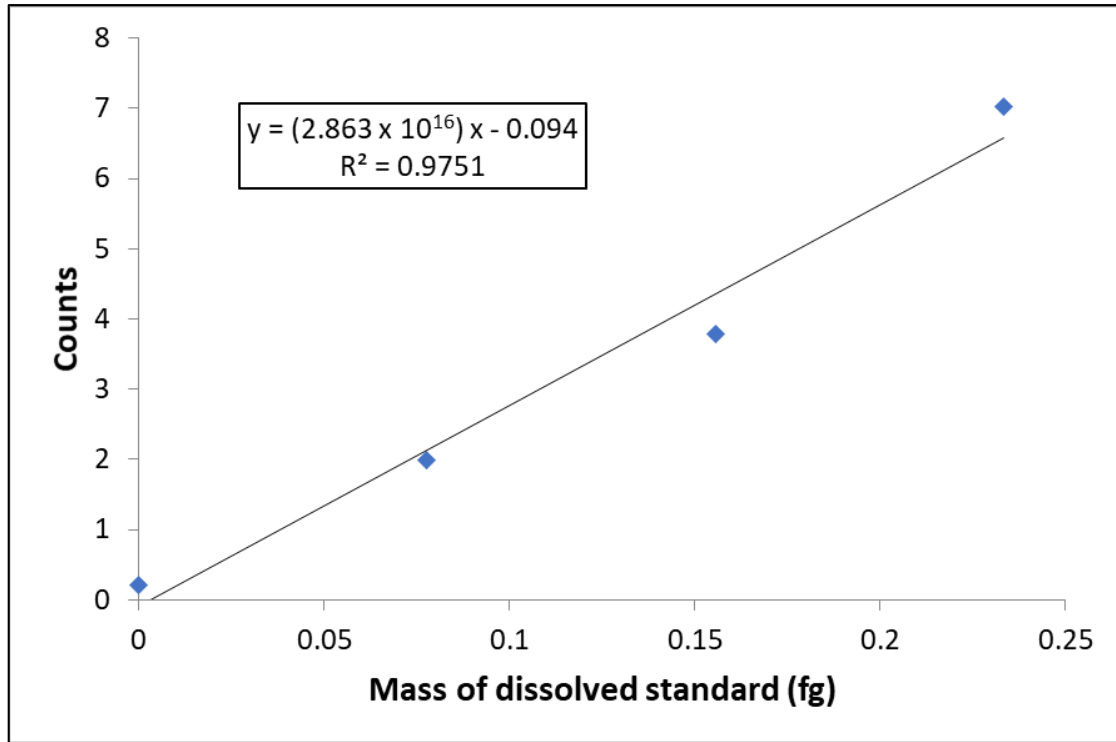


Figure A1.2: Calibration graph of ions as a measure of mass against counts.

The linear slope of the line was found to be 2.863×10^{16} ; this is used to determine the transport efficiency using equation 2.10.

Equation 2.10: Final transport efficiency calculation.

$$\eta_n = \frac{m_{diss}}{m_{rp}}$$

Which when the two linear slopes of the calibration curves are imputed into equation 2.10 provides a transport efficiency of 29 %.

$$29 \% = \frac{2.863 \times 10^{16}}{9.775 \times 10^{16}}$$

Dissolved standard calibration

Now that the transport efficiency has been calculated the dissolved standard calibration needs to be corrected using equation 2.11.

Equation 2.11: Corrected mass of dissolved standard.

$$M_D = q_{liq} \cdot t_{dt} \cdot \eta_n \cdot C$$

Mass of dissolved standard		Counts
grams	femtograms	
0	0	0.20
4.39×10^{-17}	0.044	1.99
8.79×10^{-17}	0.088	3.78
1.32×10^{-16}	0.132	7.02

The new masses are then plotted against the counts and the linear slope of the line will change (see figure A1.3).

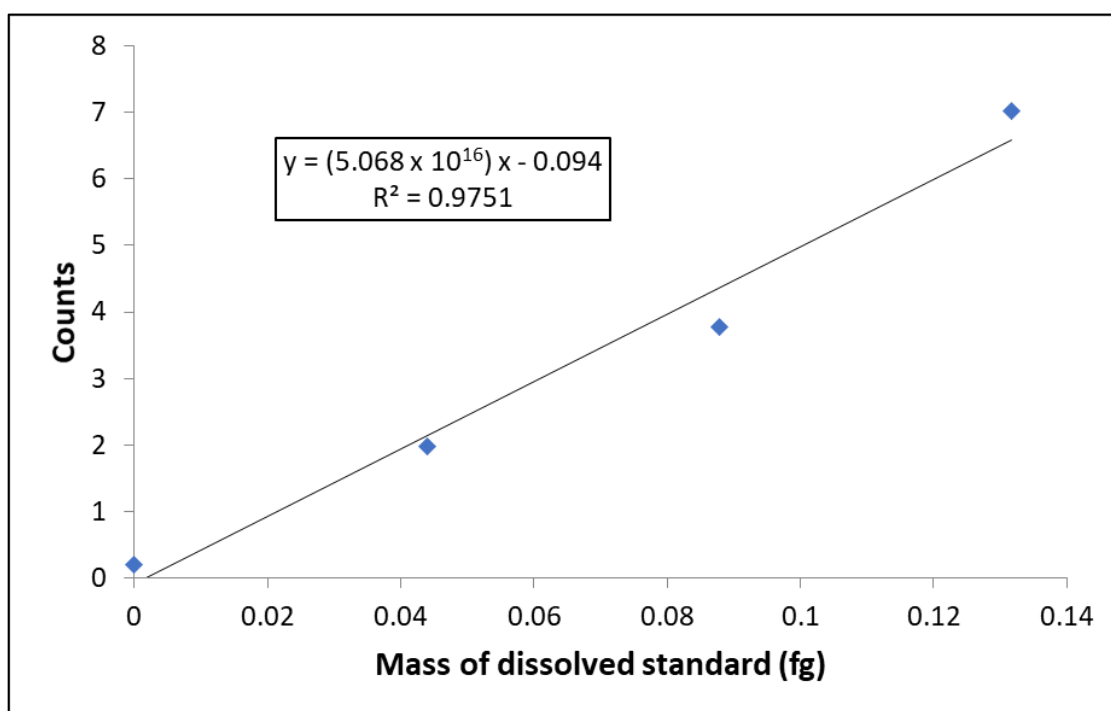


Figure A1.3: Ionic calibration of an element for analysis in spICP-MS.

The linear slope of the line was found to be 5.068×10^{16} ; this is used to determine the mass of the unknown gold nanoparticle sample.

Mass of unknown gold nanoparticles

For simplicity in demonstrating how the calculations work for the counts of the unknown gold nanoparticles they will be set to 1, 10 and 100, and the background counts will be 0.

Using equation 2.12 the mass of the nanoparticles can be calculated by imputing the previously calculated linear slope of the calibration curve, assuming 100% ionisation efficiency and mass fraction of pure gold nanoparticles being equal to 1 with the particle and background counts.

Equation 2.12: Nanoparticle mass calculation.

$$M_p = f_a^{-1} \cdot \left[\frac{\left(\frac{(I_p - I_{Bg d})}{\eta_i} \right)}{m} \right]$$

The nanoparticle with a count of 10 will demonstrated in the equation.

$$1.973 \times 10^{-16} g = 1^{-1} \cdot \left[\frac{\left(\frac{(10 - 0)}{1} \right)}{5.068 \times 10^{16}} \right]$$

The calculated masses of the three unknown gold nanoparticles are shown below.

Counts	Mass of unknown gold nanoparticle (fg)
1	0.0197
10	0.1973
100	1.9733

Spherical diameter of unknown gold nanoparticles

The mass of the nanoparticles is now known and the diameters can be determined using equation 2.14.

Equation 2.14: Diameter of spherical nanoparticle.

$$d = \sqrt[3]{\frac{6 \cdot M_p}{\pi \cdot \rho}}$$

The nanoparticle with a count of 10 that was used in the previous calculations for unknown nanoparticle mass will again be used to demonstrate the equations for calculation the spherical diameter of the unknown nanoparticle.

$$2.693 \times 10^{-6} cm = \sqrt[3]{\frac{6 \cdot 1.973 \times 10^{-16} g}{\pi \cdot 19.3 g cm^{-3}}}$$

The calculated spherical diameters of the three unknown gold nanoparticles are shown below.

Diameter (nm)	Mass of unknown gold nanoparticle (fg)
12.499	0.0197
26.929	0.1973
58.016	1.9733

Appendix 2: SOP for NexION 300 spICP-MS Analysis: Metal nanoparticle size and concentration.

Introduction

The preparation and method of analysis for metal nanoparticles using Single Particle ICP-MS is described in detail. A calibration is performed on a Perkin Elmer NexION 300D system using metal ions and a series of nanoparticle standards of the same metal as the nanoparticles analysed are used to create a calibration data which is later used to calculate the size of the sample nanoparticles analysed. The method of analysis and calibration is based on documentation provided by Perkin Elmer.


Instrument Setup and Calibration

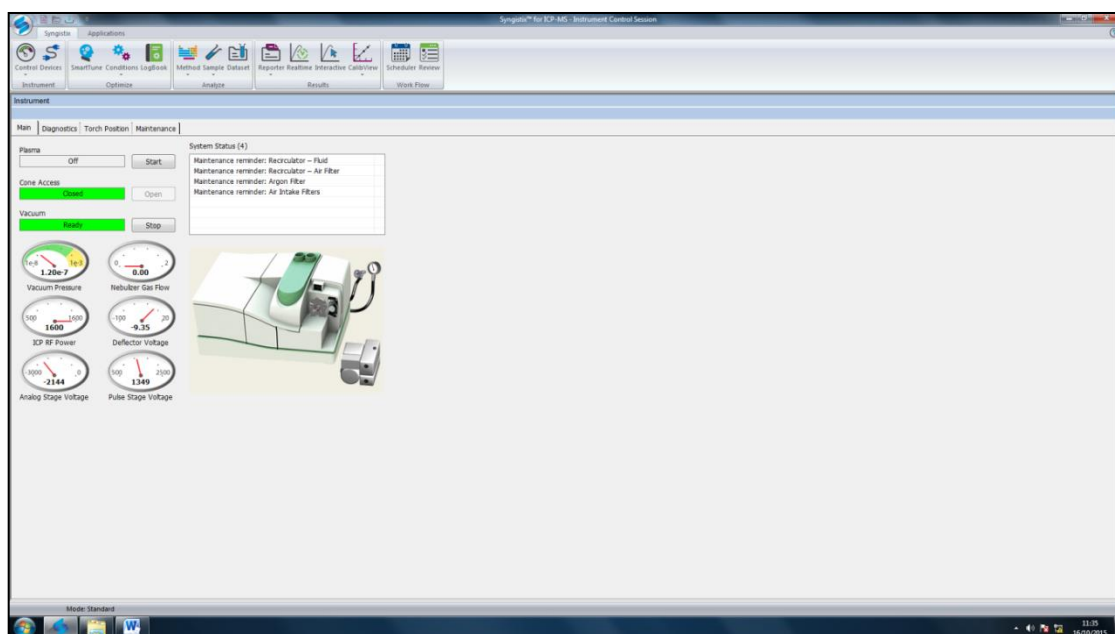
Instrument setup


1. First of all, check mechanical variables that are on the outside of the instrument, these mainly include:
 - a. Checking that the auto sampler probe is not damaged and is not blocked
 - b. That there is no leakage from any connections and components
 - c. Reviewing the state of **ALL** tubing and replacing any that are damaged, splits cause leaks and tubing that is old can block or form pulsing actions.

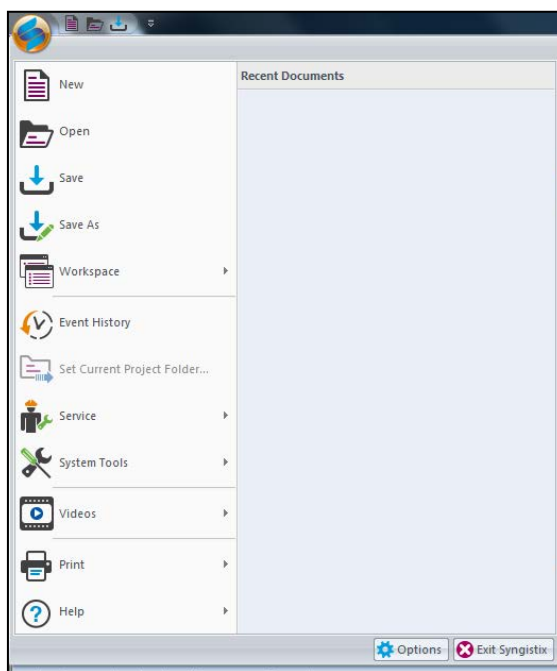
2. Turn on the Plasma by pressing  button on the NexION 300 instrument.

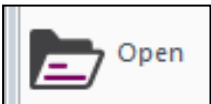
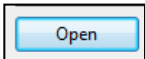
Step-by-step guide to system calibration

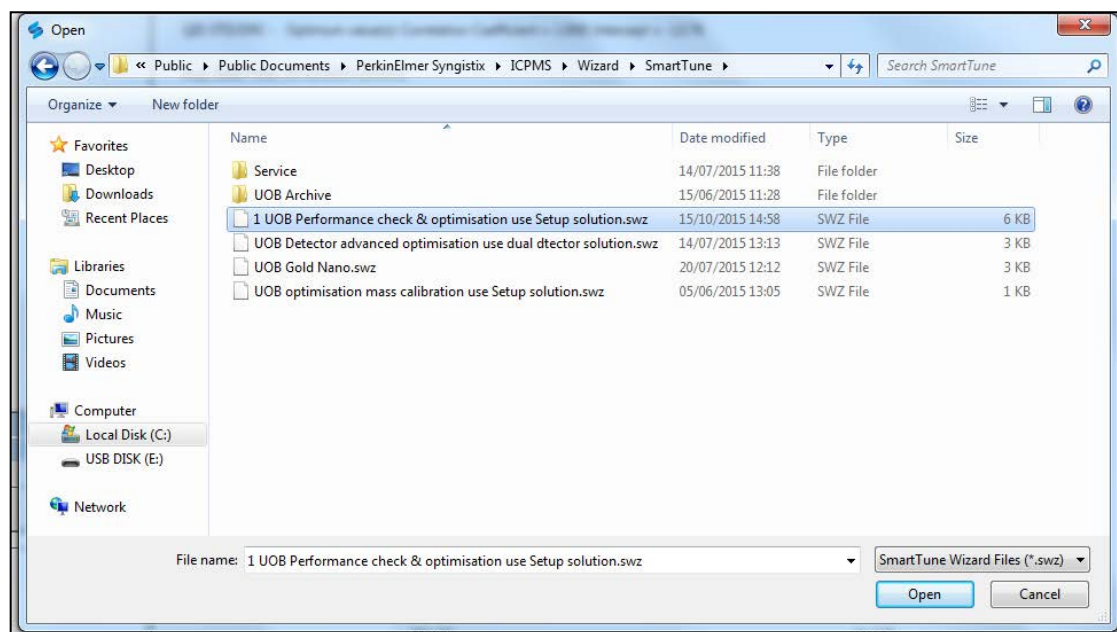
- 1) Load up Syngistix programme. Once the programme is opened click on  to bring up the smart tune wizard a set of operations should preload.

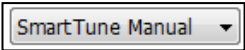


2) Click on  to bring a drop-down menu.

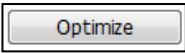


3) Click on  and select the appropriate file and press .

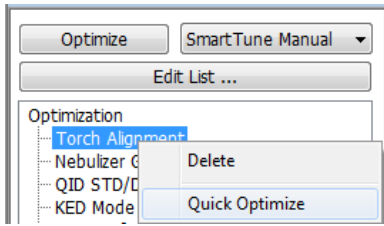
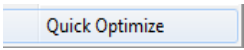


- 4) Select 'SmartTune Manual' from the drop down menu .
- 5) Place Auto sampler probe into solution named '**Perkin Elmer set up solution**', leave in this solution during system calibration.
- 6)

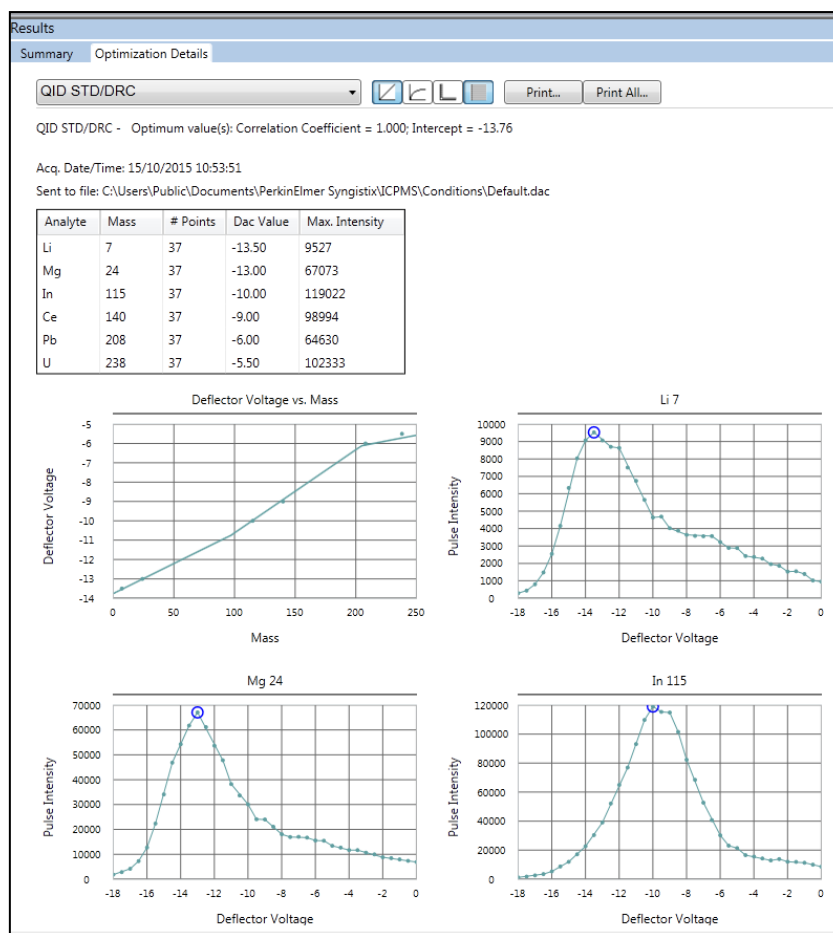
a) *Automatic Optimisation*

- i) Click and press , each of the operations will now be automatically optimised (proceeding down the line by automatically selecting the operation).

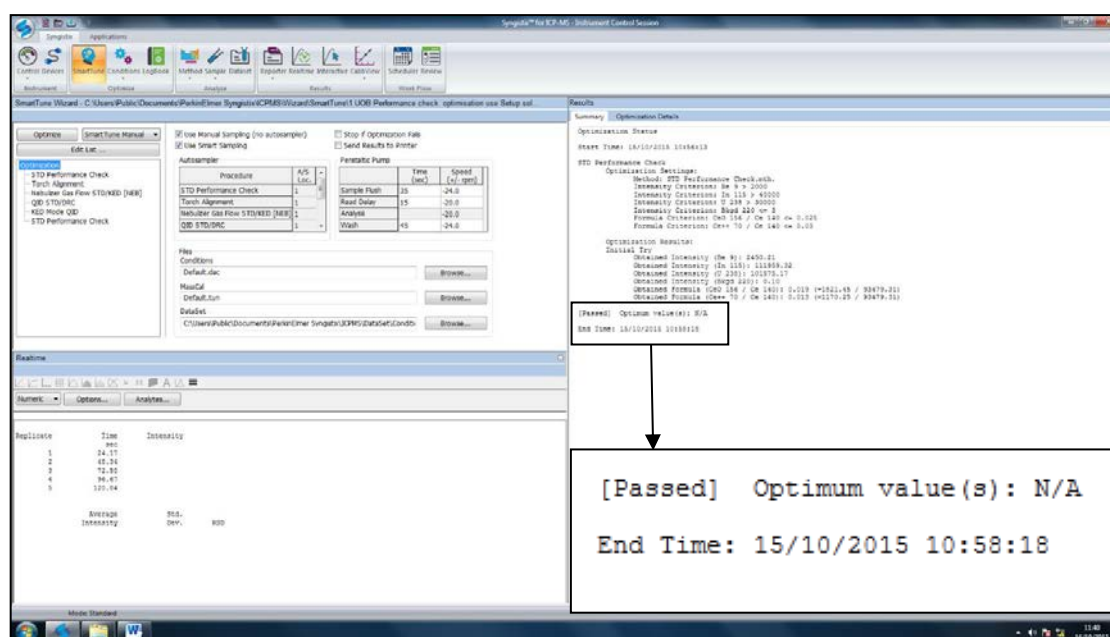
b) *Manual Optimisation*

- i) Right click on an optimisation  and in drop down box press  this will optimise only that optimisation.
- ii) Repeat step i) for the other optimisations (proceeding down the line by selecting the operation).

a report should be produced for each optimisation performed as seen in the diagram below for the QID STD/DRC optimisation performed.



7) After all the optimisations, have been performed press on the summary tab and read whether the optimisation has passed.

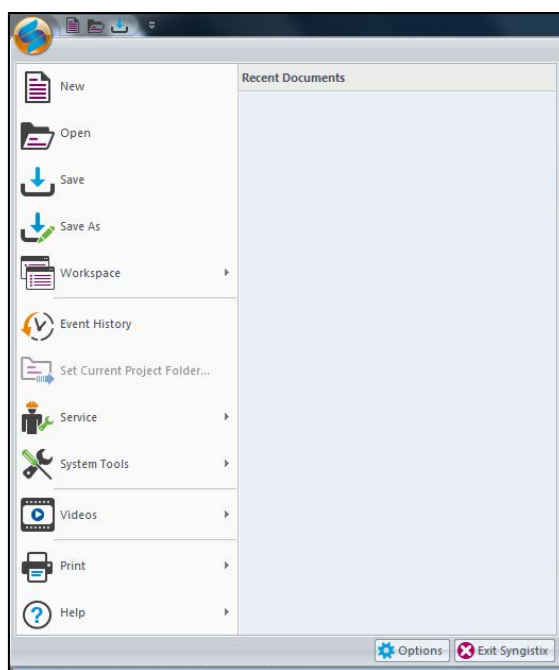


- 8) If the optimisation has failed then check the mechanical parts (the tubing, auto sampler probe and for leakages in the instrument) and then that the auto sampler probe is in the correct solution (Perkin Elmer Set-up solution).


SmartTune optimisation method creation



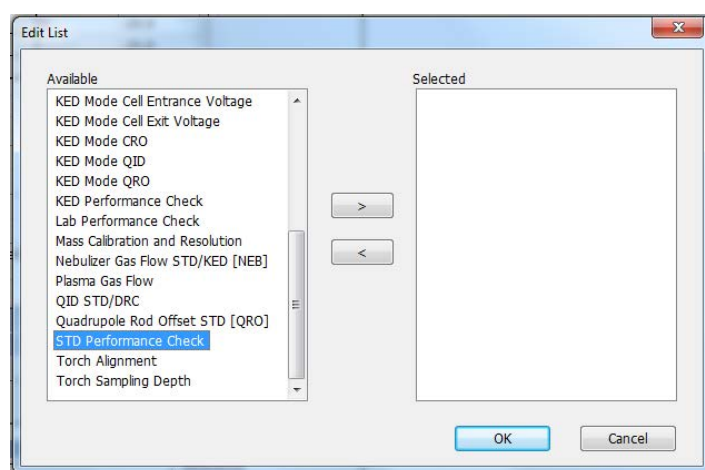
- 1) Click on the icon to bring a drop down menu.




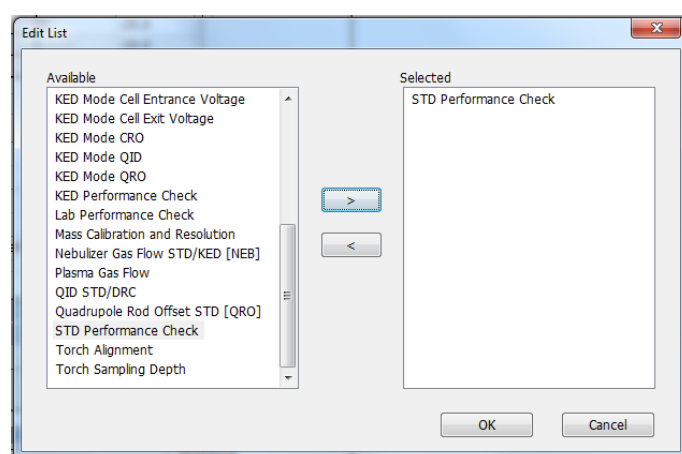
- 2) Select and click  from the drop down menu.

- 3) Click .

4) Select STD Performance Check.

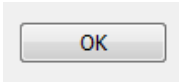


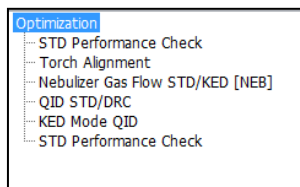
5) Click on  this will add STD Performance Check to the selected optimisation steps.



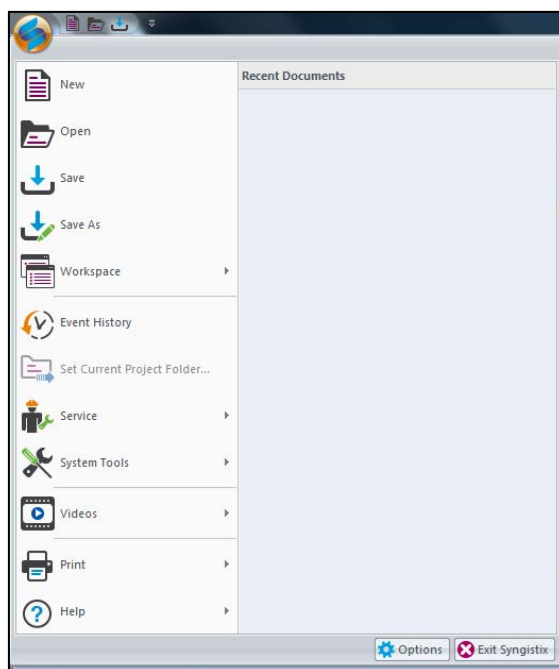
6) Repeat steps 4 and 5 by selecting optimisations in the following order.

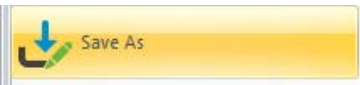
- a) Torch Alignment
- b) Nebulizer Gas Flow STD/KED [NEB]
- c) QID STD/DRC
- d) KED Mode QID
- e) STD Performance Check

- 7) Press  to complete the selection of optimisation. Presenting you with a list of optimisations.



- 8) Click on  to bring a drop down menu.

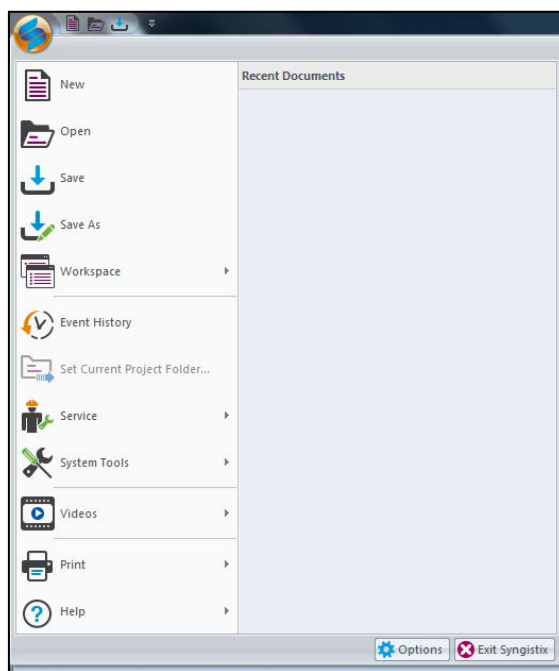


- 9) Click  and save to memorable place as the daily SmartTune method.

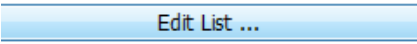
Elemental optimisation method creation

EXTRA STEP (not necessary but will give greater sensitivity that will help analysis of some elements)

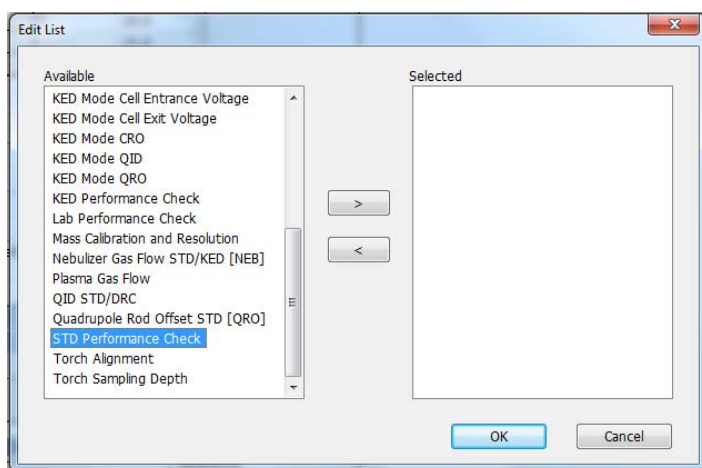
- 1) Click on  to bring a drop-down menu.




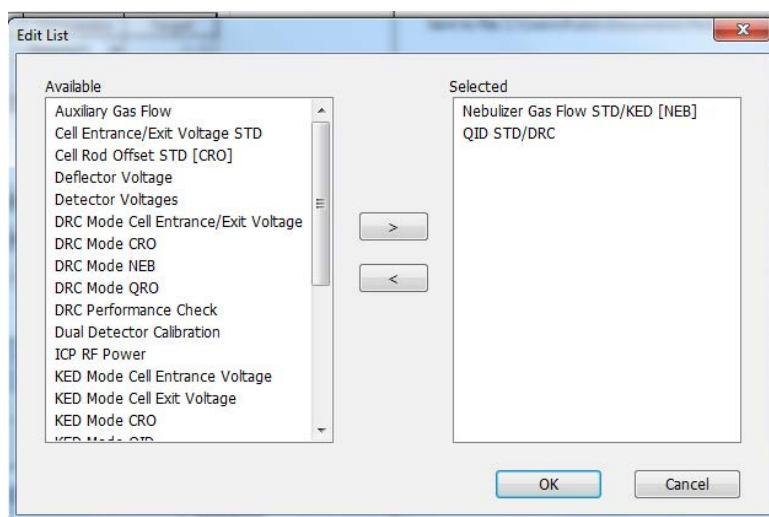
- 2) Select and click  from the drop down menu.

- 3) Click .

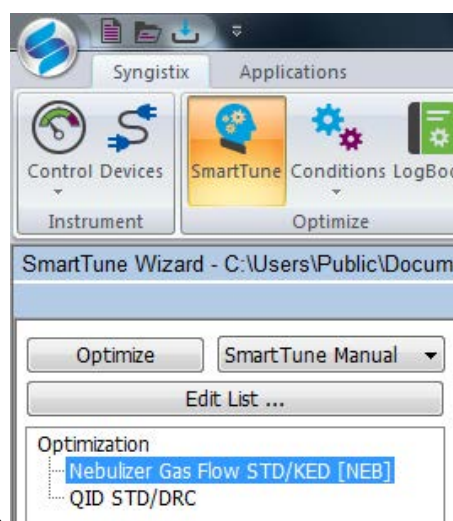
- 4) Select Nebulizer Gas Flow STD/KED [NEB].



- 5) Click on  this will add Nebulizer Gas Flow STD/KED [NEB] to the selected optimisation steps.

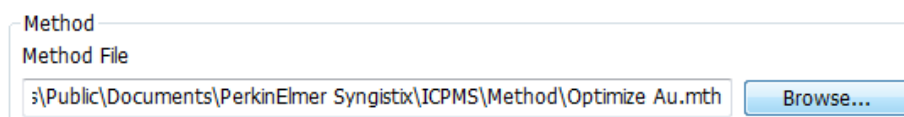


- 6) After adding Nebulizer Gas Flow STD/KED [NEB] to the selected optimisation steps add QID STD/DRC to the method by repeating steps 4 and 5 for QID STD/DRC.

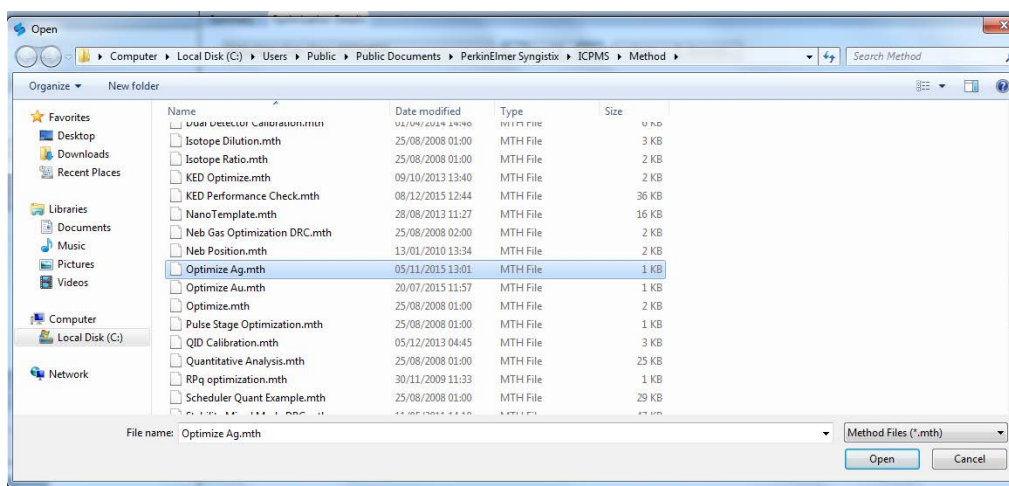


- 7) You will see Nebulizer Gas Flow STD/KED [NEB] click nebulizer gas

- 8) Press Browse... on the method file box.



- 9) Select the method for your metal that was prepared by the section on making a method and click open.



10) Click off the tick box for formula

Criteria

		Analyte	Operator	Analyte	Comparator	Target
Intensity	<input checked="" type="checkbox"/>				Maximum	0.00
Background	<input type="checkbox"/>				<=	0
Formula	<input checked="" type="checkbox"/>		/		<=	0.025

☐ Ramp ☒ Apply results to DRC Mode NEB

Criteria

		Analyte	Operator	Analyte	Comparator	Target
Intensity	<input checked="" type="checkbox"/>				Maximum	0.00
Background	<input type="checkbox"/>				<=	0
Formula	<input type="checkbox"/>		/		<=	0.025

☐ Ramp ☒ Apply results to DRC Mode NEB

11) Click on the tick box for ramp

Criteria

		Analyte	Operator	Analyte	Comparator	Target
Intensity	<input checked="" type="checkbox"/>				Maximum	0.00
Background	<input type="checkbox"/>				<=	0
Formula	<input type="checkbox"/>		/		<=	0.025


☒ Ramp ☒ Apply results to DRC Mode NEB

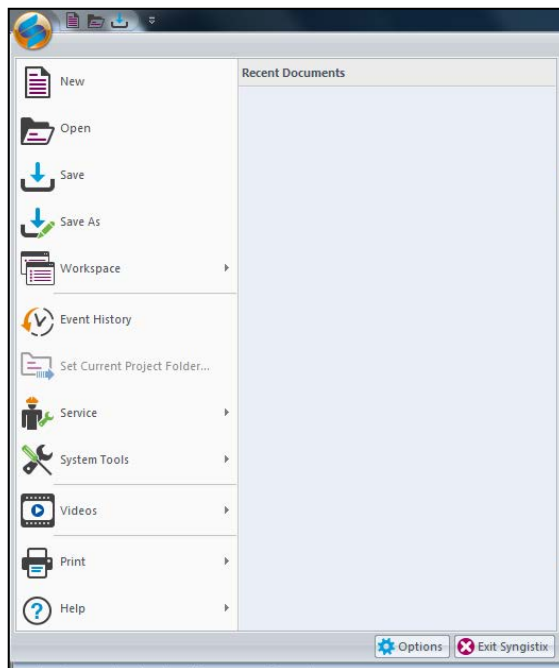
12) Click on the analyte box and choose your element for analysis


Criteria


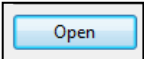
		Analyte	Operator	Analyte	Comparator	Target
Intensity	<input checked="" type="checkbox"/>	Au 196.967			Maximum	0.00
Background	<input type="checkbox"/>	Au 196.967			<=	0
Formula	<input type="checkbox"/>		/		<=	0.024

☒ Ramp ☒ Apply results to DRC Mode NEB


13) Click on  to bring a drop down menu.



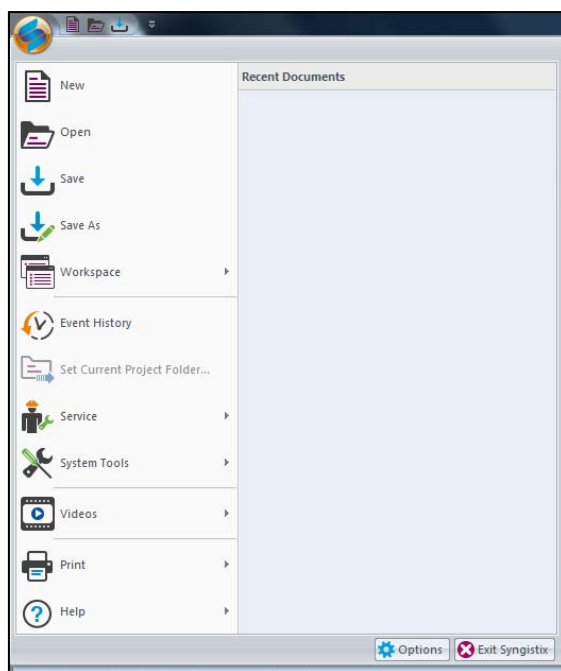
14) Click  and save to memorable place as the Element optimisation method.

15) Click on  and select the method just saved and press . Repeat optimisation using this method.

Elemental method creation

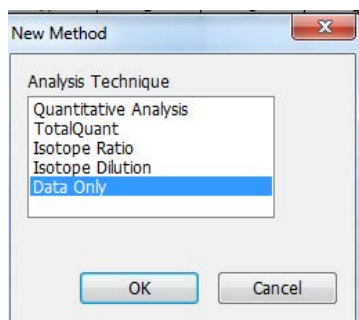
1. Click on the  tab of Syngistix.

2. Click on  to bring a drop down menu.



3. Select and click  from the drop down menu.

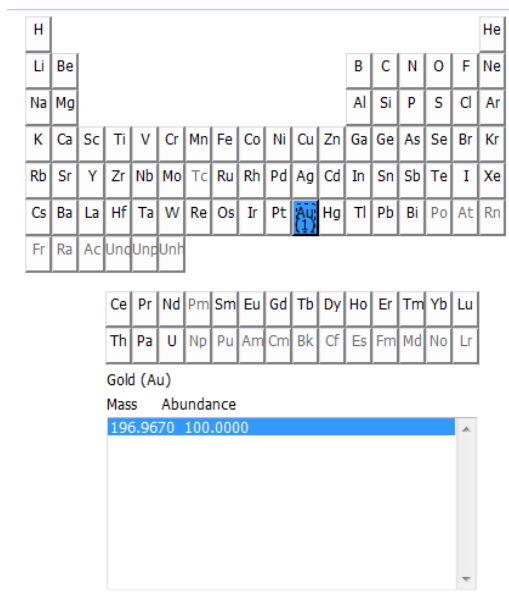
4. Select data only and press okay.



5. Select element on periodic table by left clicking on the element.

H																	He
Li	Be											B	C	N	O	F	Ne
Na	Mg											Al	Si	P	S	Cl	Ar
K	Ca	Sc	Ti	V	Cr	Mn	Fe	Co	Ni	Cu	Zn	Ga	Ge	As	Se	Br	Kr
Rb	Sr	Y	Zr	Nb	Mo	Tc	Ru	Rh	Pd	Ag	Cd	In	Sn	Sb	Te	I	Xe
Cs	Ba	La	Hf	Ta	W	Re	Os	Ir	Pt	Au	Hg	Tl	Pb	Bi	Po	At	Rn
Fr	Ra	Ac	Unq	Unp	Unh												
Ce	Pr	Nd	Pm	Sm	Eu	Gd	Tb	Dy	Ho	Er	Tm	Yb	Lu				
Th	Pa	U	Np	Pu	Am	Cm	Bk	Cf	Es	Fm	Md	No	Lr				

6. Select the specific isotope which is to be analysed (for gold there is only one so it is automatically selected, if more than one isotope is present then the most abundant will be automatically selected)



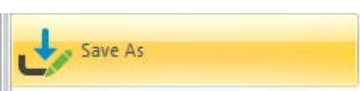
Mass	Abundance
196.9670	100.0000

7. The table will now automatically fill itself out presenting these values

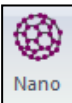
	Analyte	Begin Mass (amu)	End Mass (amu)	Scan Mode (*)	MCA Channels	Dwell Time per AMU (ms)	Integration Time (ms)	Corrections	Mode (*)	Cell Gas A	Cell Gas B	RP a	RP q
1	Au	196.967		Peak Hopping	1	50	2500		Standard	0	0	0	0.25

8. Set Sweeps/Reading to 50 and leave the other two set to one


Sweeps / Reading	Est. Reading Time
50	0:00:02.510
Readings / Replicate	Est. Replicate Time
1	0:00:02.510
Replicates	Est. Sample Time
1	0:00:02.510

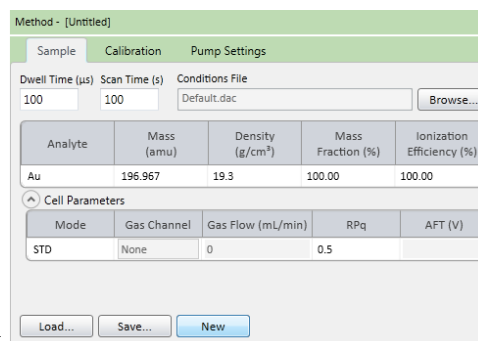
9. Click  and save to memorable place as the Element optimisation method.

Single particle ICP-MS method development

1. Click on the applications tab and then click on  to bring up the nano window.



2. In the nano applications window select the analysis tab .

A screenshot of the Nano Analysis window, titled 'Method - [Untitled]'. It has three tabs: 'Sample', 'Calibration', and 'Pump Settings'. The 'Sample' tab is active. It contains fields for 'Dwell Time (μs)' (100), 'Scan Time (s)' (100), and 'Conditions File' (Default.dac) with a 'Browse...' button. Below these is a table with columns: 'Analyte', 'Mass (amu)', 'Density (g/cm³)', 'Mass Fraction (%)', and 'Ionization Efficiency (%)'. The table has one row for 'Au' with values: 196.967, 19.3, 100.00, and 100.00. Below the table is a section for 'Cell Parameters' with a table with columns: 'Mode', 'Gas Channel', 'Gas Flow (mL/min)', 'RPq', and 'AFT (V)'. The table has one row for 'STD' with values: None, 0, 0.5, and empty. At the bottom are 'Load...', 'Save...', and 'New' buttons.

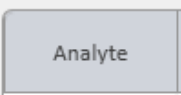
Analyte	Mass (amu)	Density (g/cm³)	Mass Fraction (%)	Ionization Efficiency (%)
Au	196.967	19.3	100.00	100.00

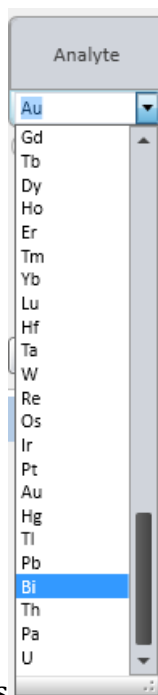
Mode	Gas Channel	Gas Flow (mL/min)	RPq	AFT (V)
STD	None	0	0.5	

3. In the  tab and the sample box

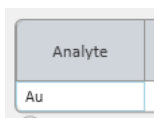
press



4. In the Method box press on the white box under  this will



bring up a drop down menu with elements . Select the element of interest for analysis (in this example gold). The analyte box will now have



the element chosen in the box.

5. Set the dwell and scan times to that which is appropriate for the experiment and change the mass fraction if working with complex nanoparticles to the mass fraction which the element analysed has in the compound (i.e in titanium dioxide, titanium accounts for 60% of the mass fraction so the mass fraction box has a value of 60.00)

Method - [Untitled] [Modified]

Sample Calibration Pump Settings

Dwell Time (μs) Scan Time (s) Conditions File

100 100 Default.dac Browse...

Analyte	Mass (amu)	Density (g/cm ³)	Mass Fraction (%)	Ionization Efficiency (%)
Au	196.967	19.3	100.00	100.00

Cell Parameters

Mode	Gas Channel	Gas Flow (mL/min)	RPq	AFT (V)
STD	None	0	0.5	

Load... Save... New

6. If using DRC for the element to be analyse click on the box below

Mode

STD

STD

DRC

and select

7. The Gas Flow (mL/min) will need to be set to that which is appropriate for the experiment, the RPq AFT (V) will also need to be set to that which is appropriate for the experiment.

8. Click on Calibration within the Analysis tab and the

Method - [Untitled]

Sample Calibration Pump Settings

Dwell Time (μs) Scan Time (s) Conditions File

100 100 Default.dac Browse...

Analyte	Mass (amu)	Density (g/cm ³)	Mass Fraction (%)	Ionization Efficiency (%)
Au	196.967	19.3	100.00	100.00

Cell Parameters

Mode	Gas Channel	Gas Flow (mL/min)	RPq	AFT (V)
STD	None	0	0.5	

Load... Save... New

box.

9. Input values for the ion standards into the right-hand part of the

	Dissolved Std	Au 196.967 (µg/L)
--	---------------	-------------------

 table giving

	Dissolved Std	Au 196.967 (µg/L)
1	STD1	1
2	STD2	2
3	STD3	3
4	STD4	
5	STD5	
6	STD6	
7	STD7	

10. Input values for the particle standards into the right-hand part of the

	Particle Std	Au 196.967 (nm)
1	STD1	10
2	STD2	30
3	STD3	50
4	STD4	
5	STD5	
6	STD6	
7	STD7	

	Particle Std	Au 196.967 (nm)
--	--------------	-----------------

 table (Step 10 is not necessary for the sample element but is for the transport efficiency element)

11. Click on Pump Settings within the



tab and the

Method - [Untitled]

Sample Calibration Pump Settings

Dwell Time (µs) Scan Time (s) Conditions File

100 100 Default.dac Browse...

Analyte	Mass (amu)	Density (g/cm³)	Mass Fraction (%)	Ionization Efficiency (%)
Au	196.967	19.3	100.00	100.00

Cell Parameters

Mode	Gas Channel	Gas Flow (mL/min)	RPq	AFT (V)
STD	None	0	0.5	

Load... Save... New

box

12. Set the Pump settings set to that which is appropriate for the experiment.

Peristaltic Pump


	Time (sec)	Speed (+/- rpm)
Sample Flush	35	-24.0
Read Delay	15	-20.0
Wash	45	-24.0

☒ Peristaltic Pump Under Computer Control


13. Press  and save to memorable place.

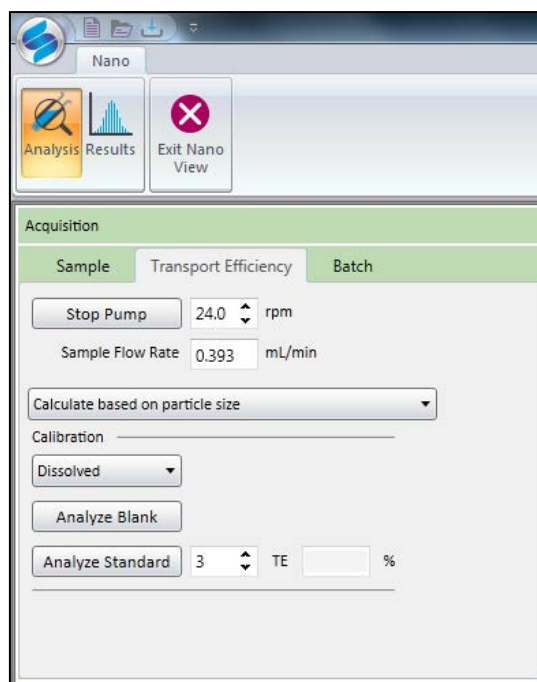
14. Repeat this entire process for each element that is to be analysed with the nano application.

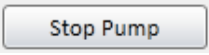
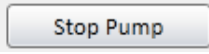
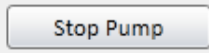
Step-by-step guide to Flow rate calculation

1. Click on the applications tab and then click on  to bring up the nano window.



2. In the nano applications widow select the analysis tab .
3. Within the acquisition tab select the transport efficiency tab.



4. Carefully weigh out 15g of MilliQ water into a flask. The mass needs to be accurately measured (to 2 decimal places) and recorded.
5. Stop the pump by pressing  .
6. Place sample introduction probe into the centrifuge flask containing 15 g of MilliQ water.
7. Set up a stopwatch.
8. Start the stopwatch and press  at exactly the same time.
9. Leave the pump running for three minutes.
10. After three minutes press  and reweigh the flask accurately to determine loss of mass during the three minute run.

11. Taking the calculated loss of mass the sample flow rate is calculated using equation A2.1.

Equation A2.1: Sample Flow rate equation

$$\text{Sample flow rate (ml min}^{-1}\text{)} = \frac{\text{mass loss (g)}}{\text{time (min)} \times \text{density of fluid (g ml}^{-1}\text{)}}$$

For simplicity it is assumed that the density of the water used is 1.0 g ml⁻¹, so the following values for the parameters are used.

Time = 3 minutes

Density of fluid = 1.0 g ml⁻¹

12. Once the flow rate is calculated input the value into

Sample Flow Rate	0.393	mL/min
------------------	-------	--------

Found within the transport efficiency tab in the acquisition box.

Step-by-step guide to transport efficiency calculation

1. In the nano applications widow select the analysis tab



2. Prepare dissolved gold standards with the following concentrations 1 ppb, 2 ppb, and 3 ppb.

3. Prepare particle gold standards with the following nanoparticle sizes 20 nm, 40 nm and 80 nm.


4. Within the method tab click on calibration tab.

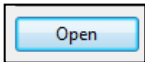
Method - C:\Users\Public\Documents\PerkinElmer Syngistix\IC...\Gold np 1st run.nmth [Modified]

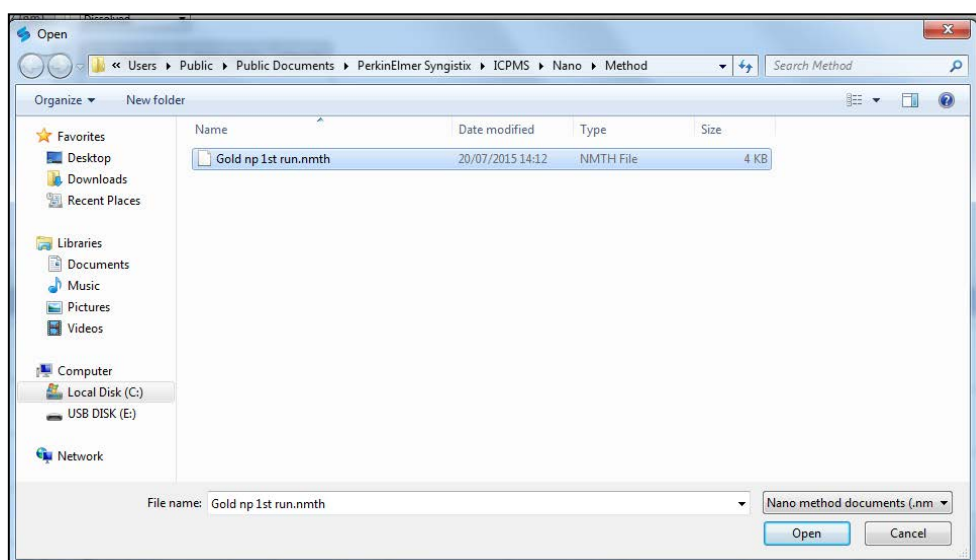
Transport Efficiency Calibration Pump Settings

	Dissolved Std	Au 196.967 (µg/L)		Particle Std	Au 196.967 (nm)
1	STD1	0	1	STD1	20.4
2	STD2	1	2	STD2	39.7
3	STD3	2	3	STD3	78.8
4	STD4	3	4	STD4	
5	STD5		5	STD5	
6	STD6		6	STD6	
7	STD7		7	STD7	

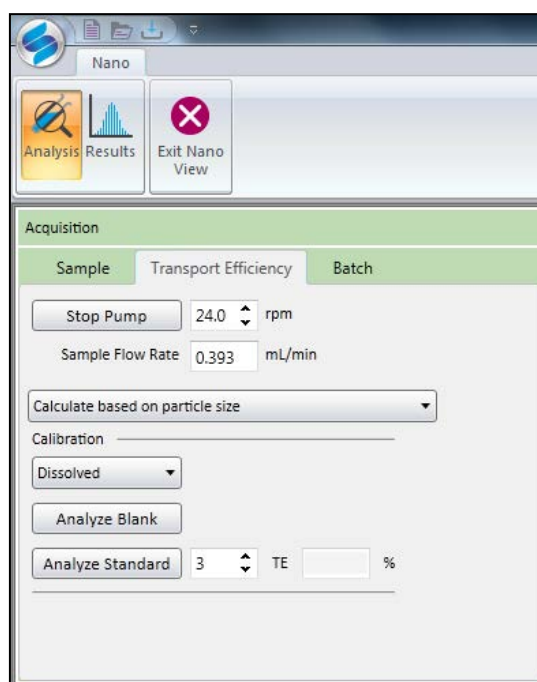
Load... Save... New

5. Select  within method tab and select a gold nano method that was previously made (see section single particle ICP-MS method creation), press

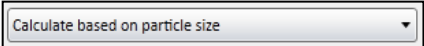
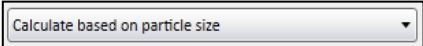
 to load the method.



6. Within the acquisition tab select the transport efficiency tab.

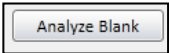


7. Click on drop down box either labelled  or

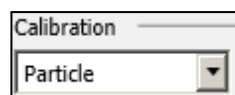
 and select 

8. Place the centrifuge tubes of standards (both particle and dissolved) and a procedural blank into the auto sampler rack.

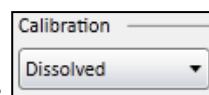
9. Place the sample introduction probe into the procedural blank.

10. Click the  button and wait for the NexION 350 to analyse the blank. If there are peaks with counts larger than 3, repeat the blank analysis; if problem persists a new procedural blank will need to be produced.

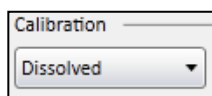
11. On the drop down tab either labelled



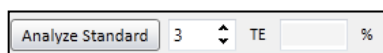
or



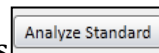
select



12. Place the sample introduction probe into the 1 ppb standard. Change

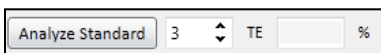


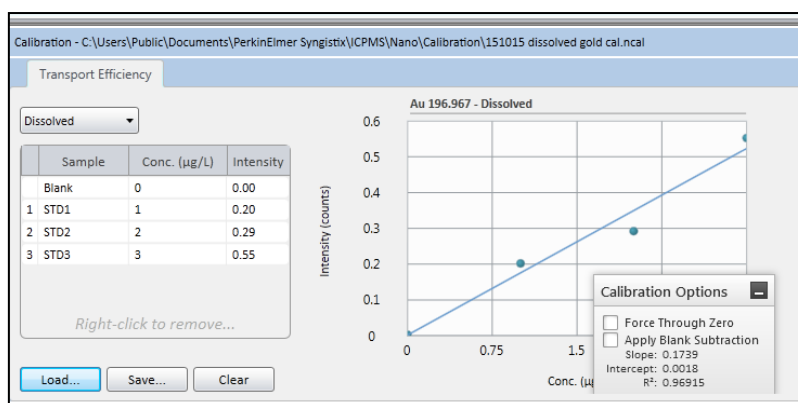
to have a value of 1 and press



the NexION 350 to analyse the standard.

13. Repeat step 15 with the 2 ppb and 3 ppb standards, with the only difference

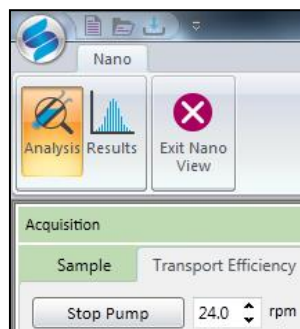
being changing  from 1 to 2 and 3. A calibration graph will be produced from the standards.



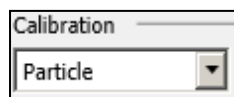
A r^2 value of over 0.996 is desired from the calibration, if the r^2 value is below this repeat the standards analysis; if problem persists, a new standard will need to be produced.

14. After all standards are calculated for transport efficiency place the sample introduction probe into 1% HCl for 1 minute to allow a wash of the system before

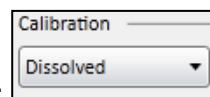
placing the sample introduction probe into MilliQ water. During the 1% HCl wash the pump speed can be turned up to 40 rpm.



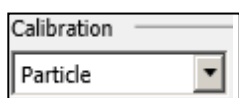
15. On the drop-down tab either labelled



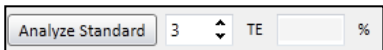
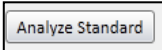
or

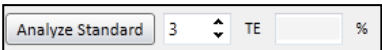


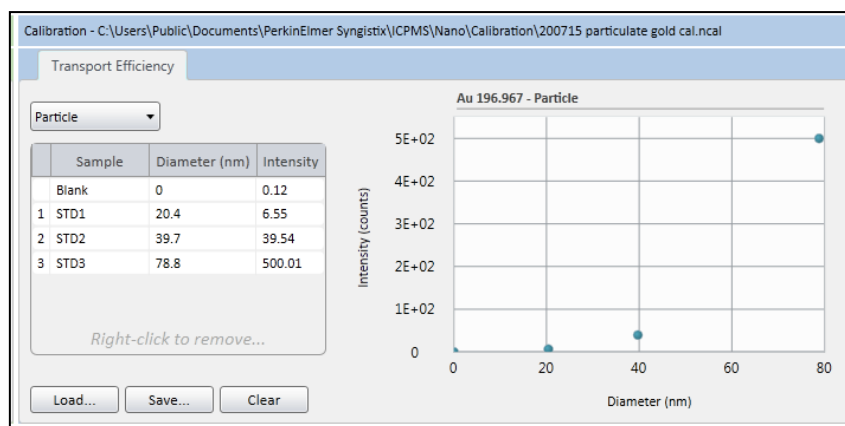
select



16. Place the sample introduction probe into the 20 nm nanoparticle standard.

Change  to have a value of 1 and press ; wait for the NexION 350 to analyse the standard.

17. Repeat step 12 with the 40 nm and 80 nm standards, with the only difference being changing  from 1 to 2 and 3. A calibration graph will be produced from the standards.




The results from the particle calibration do not necessarily need to be a linear progression.

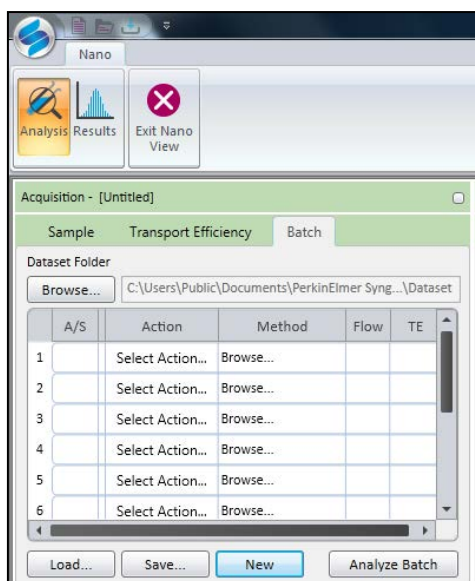
18. Within the acquisition tab and the transport efficiency tab there should

now be a % for the transport efficiency shown in TE %.

Sample analysis

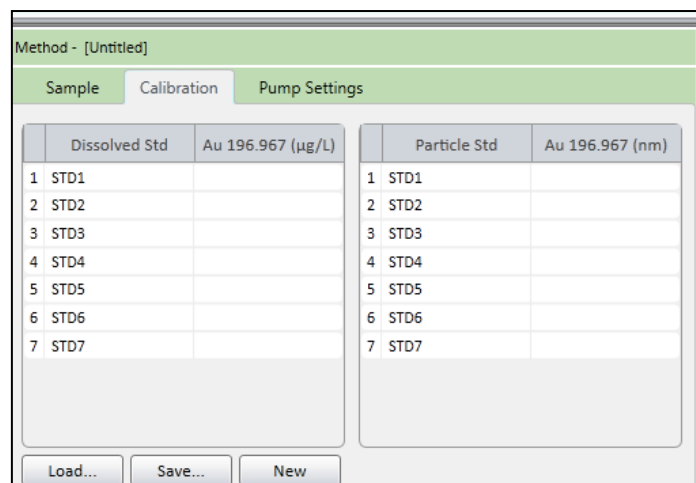
Step-by-step guide to sample analysis

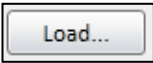
1. In the nano applications widow select the analysis tab .
2. Within the acquisition box select the batch tab.



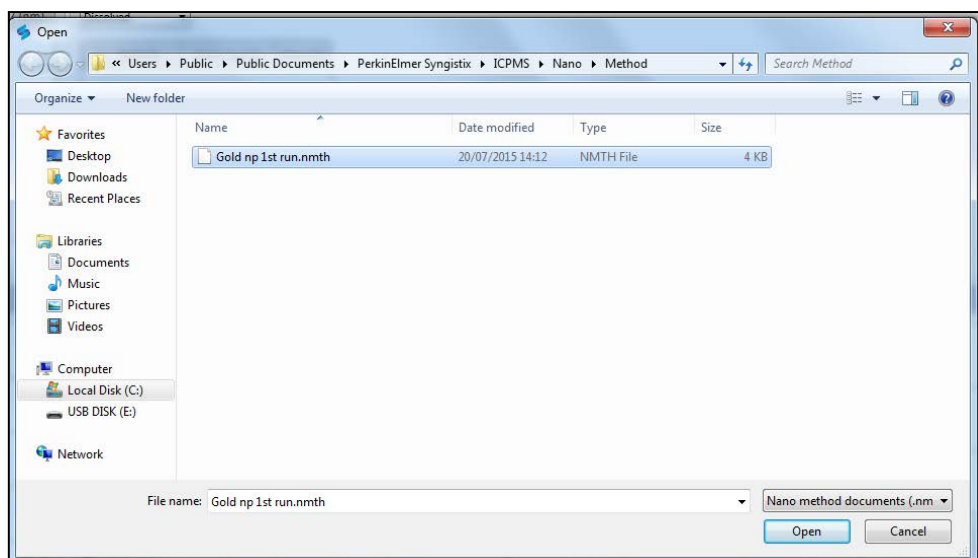
In the batch tab you are presented with a table which allows for a batch of samples, calibrations and blanks to be analysed.

1. Within the method box click on calibration tab.

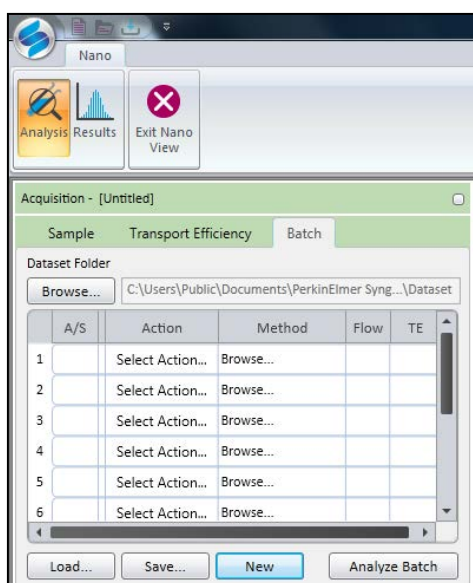


2. Select  within method tab and select previously made elemental nano method (see section single particle ICP-MS method creation),

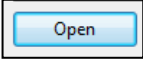
press  to load the method.

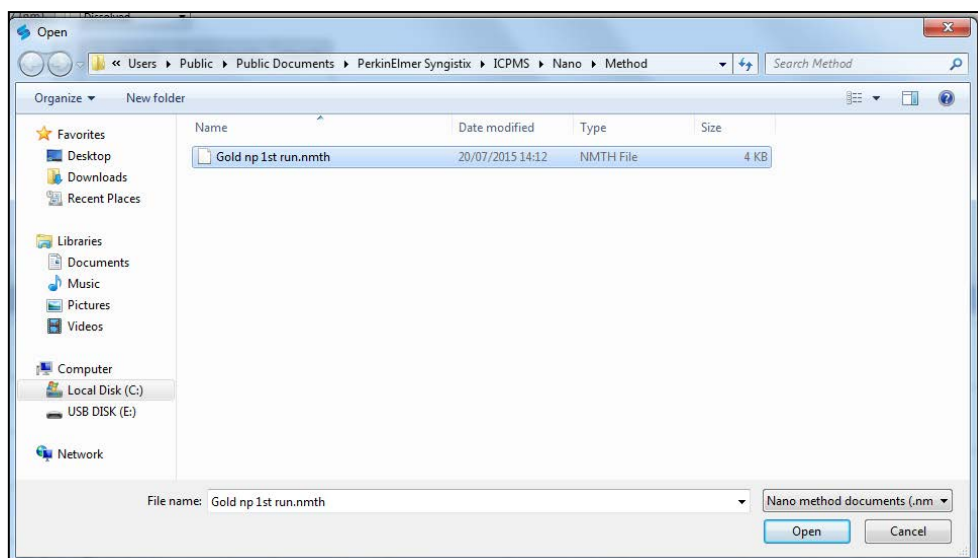


3. Within the acquisition box and batch table, click on a sample **Method** box.



A load screen is presented select the previously made elemental nano method

(see section single particle ICP-MS method creation), press  to load the method.



The method box will change from

Method
Browse...

 to

Method
Gold np 1st run.nmth

 (silver will have a different method file).

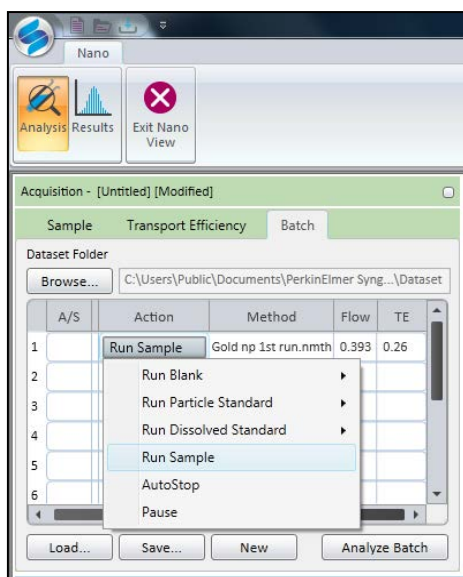
4. Prepare dissolved silver standards with the following concentrations 1 ppb, 2 ppb, and 3 ppb.

5. Within the acquisition tab and sample table, click on a sample **Action** box;

a drop down box will appear. Select and press

Run Dissolved Standard

.



The action box will change from to

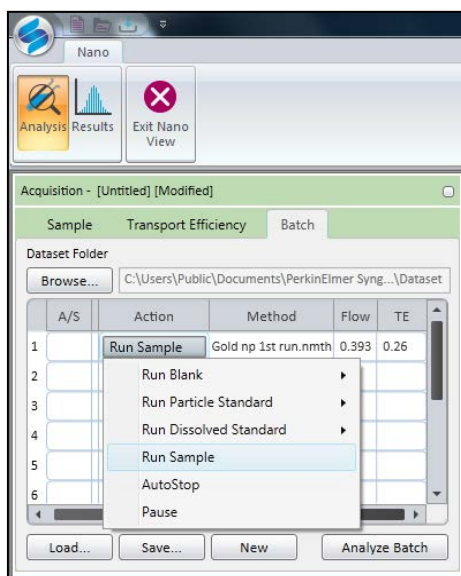
6. There are two more boxes to fill **A/S** and **Sample ID**, fill these two out with the name of the nanoparticle being analysed multiple times for the **Sample ID of the Dissolved Standard** (i.e. “1ppb metal run 1” for a 1 ppb metal standard) and the correct position in the auto sampler for **A/S**.

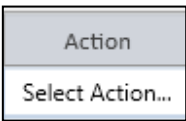
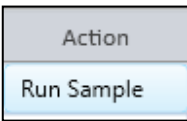
	A/S	Sample ID
1	1	Mix

7. Repeat steps 2, 3, 5, and 6; until all the Ionic standards have been added to the batch list making sure that the **A/S**, **Flow**, **TE**, **Action**, and **Method** are the same for each row; the **Sample ID** should be changed to show the run number of the standard (i.e. “1ppb metal run 1” followed by “1ppb metal run 2”... “3ppb metal run 1”).

8. Within the acquisition tab and sample table, click on a sample **Action** box;

a drop down box will appear. Select and press .



The action box will change from  to .

9. For the **Flow** and **TE** boxes input the calculated values determined in the two previous sections.

10. There are two more boxes to fill **A/S** and **Sample ID**, fill these two out with the name of the nanoparticle being analysed multiple times for the **Sample ID** (i.e. “metal nanoparticles sample 1” for the first metal sample to be analysed) and the correct position in the auto sampler for **A/S**.

	A/S	Sample ID
1	1	Mix

11. Repeat steps 2, 3, 6, 7, and 8; until the desired amount of sample replicates has been added to the batch list making sure that the **A/S, Flow, TE, Action,** and **Method** are the same for each row; the **Sample ID** should be change to show the run number of the sample (i.e. “metal nanoparticles sample 1” followed by “metal nanoparticles sample 2” ... “metal nanoparticles sample 1”)

12. The samples are now ready to be measured. In the batch tab of the

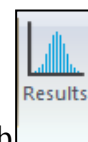
acquisition tab press the .

The NexION 350 will start to perform single particle analysis of the samples.

13. Repeat this process three times making sure that the **A/S, Flow, TE, Action,** and **Method** are the same for each row; the **Sample ID** should change to show the run number of the sample (i.e. “metal nanoparticles sample 1” followed by “metal nanoparticles sample 2” ... “metal nanoparticles sample 1”)

14. **If you run out of lines to put in samples right click on a line and you can insert a new line.**

Exporting results from Syngistix to excel for later interpretation



1. In the nano applications widow select the results tab
2. In the results tab there is a results table scroll down the table until you reach your set of results.

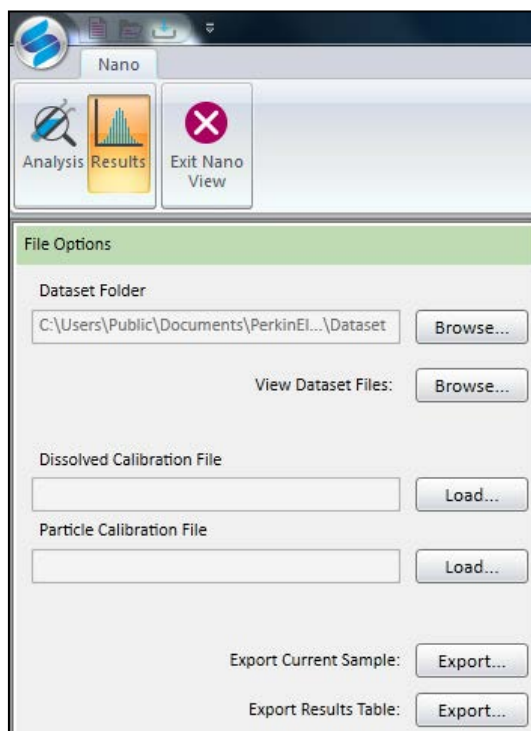
Sample	Analyte	Most Freq. Size (nm)	Mean Size (nm)	No. of Peaks	Mean Inten. (counts)	Part. Conc. (parts/mL)	Diss. Inten. (counts)	Diss. Conc. (ppb)
STD3	Au 196.967						0.55	
STD1	Au 196.967						0.2	
STD2	Au 196.967						0.29	
Blank	Au 196.967						0.01	
STD1	Au 196.967						0	
Blank	Au 196.967						0	
STD2	Au 196.967						0.05	
STD3	Au 196.967						0.11	
STD4	Au 196.967						0.11	
Blank	Au 196.967						0	0
Blank	Au 196.967						0	-0.001
STD1	Au 196.967			2095	1.17	238028	0	0.008
STD2	Au 196.967			199	32.16	178148	0.01	0.115
STD3	Au 196.967			1808	15.21		0	0.005
Blank	Au 196.967						0	-0.01
STD1	Au 196.967			1567	1.17	195959	0	-0.003
STD2	Au 196.967			167	34.22	138953	0.01	0.097
STD3	Au 196.967			1571	19.63		0	0
Mix	Au 196.967	15	17	5603	3.03	3290076	0.01	-0.098

3. Once the set of results that are desired to be exported are selected, press

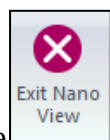
either Export Results Table: or Export Current Sample: depending on whether you want to export all the samples that have been analysed or just the current selected sample.

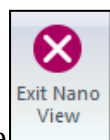
The option of exporting current selected sample provides detailed results for the sample, whilst the export results table option provides the results found within the results table but not any further detail.

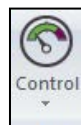
These options are found with the file options tab.

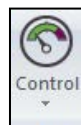


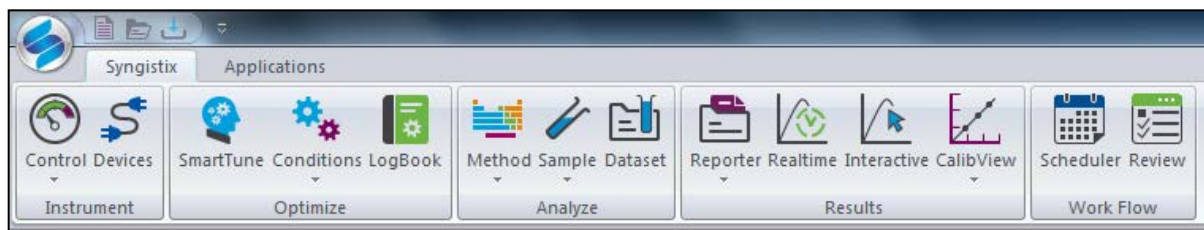
Step-by-step guide to shut down



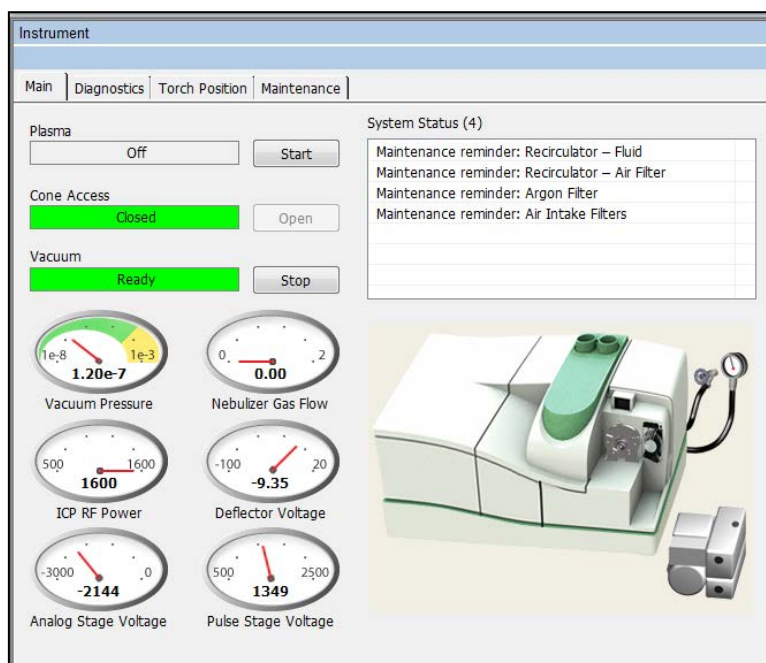
1. In the nano applications widow select the  tab. This will bring the program back to the main Syngistix pages.



2. Click on the Syngistix tab and then click on  to bring up the control tab.



3. In the control window press the plasma start/stop button to stop the plasma. Don't turn off Cone Access or the Vacuum.



Preparing reagents, standards and samples

Equipment needed

- 50 mL plastic (Polypropylene) centrifuge tubes
- 10 - 100 μL adjustable pipette
- 100 - 1000 μL adjustable pipette
- 50 - 5000 μL adjustable pipette
- Pipette tips
- Waste bottle
- MilliQ water flask
- NexION 300/350 ICP-MS

Chemicals

- 1000ppm metal plasma emission standard
- 1000ppm gold plasma emission standard
- BBI nanoparticle gold Solution 20 nm
- BBI nanoparticle gold Solution 40 nm
- BBI nanoparticle gold Solution 80 nm

Preparing Samples

Samples should be prepared in anticipation of analysis beforehand; each sample's preparation will be dependent on the sample and as such a method of sample preparation is not listed here.

Preparing Standards

Two sets of standards were prepared for use in calibration; a set of three ionic standards and three nanoparticle standards.

Ionic standard preparation

The ionic standards were prepared from a stock solution of ICP-MS metal standard, with a starting concentration of 1001 mg dm⁻³ (5.082 mM or 1001 ppm) and all were diluted with MilliQ water.

Using the calculation found in equation 3.1 the following dilutions were performed to provide the ionic standards for calibration.

Equation 3.1: Standard dilution equation using concentration and volumes.

$$Concentration_1 \times Volume_1 = Concentration_2 \times Volume_2$$

Where the units are the same for both concentration terms and also the volume terms are of the same units.

Concentration ₁ (mg dm ⁻³)	Volume ₁ (μL)	Concentration ₂ (mg dm ⁻³)	Volume ₂ (μL)	Concentration ₂ in ppb
1,001	500	10.01	50,000	10,000
10.01	500	0.1001	50,000	100
0.1001	500	0.001001	50,000	1
0.1001	1,000	0.002002	50,000	2
0.1001	1,500	0.003003	50,000	3

Using this method on calibrated pipettes provides an estimated maximum error of 2.3% from the desired concentrations.

Nanoparticle standard preparation

Nanoparticle standards are prepared in the following method using BBI Solutions gold standards.

Each nanoparticle solution starts with a differing number of nanoparticles per dm⁻³, it is recommended that standards need to have around 50 nanoparticles per dm⁻³; as such each of the BBI solutions will need to be diluted in a different way. Pipette inaccuracy is of less importance here as the particle concentrations need to be just around 50,000.

The method of dilution is the same using the calculation found in equation 3.1 the following dilutions were preformed to provide then nanoparticle standards for calibration using **MilliQ water** for dilutions.

Equation 3.1: Standard dilution equation using concentration and volumes.

$$\text{Concentration}_1 \times \text{Volume}_1 = \text{Concentration}_2 \times \text{Volume}_2$$

Where the units are the same for both concentration terms and also the volume terms are of the same units.

Gold Nanoparticle Standards

20 nm

Concentration ₁ (nanoparticles per dm ⁻³)	Volume ₁ (dm ⁻³)	Concentration ₂ (nanoparticles per dm ⁻³)	Volume ₂ (dm ⁻³)
700,000,000	0.00005	700,000	0.05
700,000	0.00005	700	0.05
700	0.0035	49	0.05

40 nm

Concentration ₁ (nanoparticles per dm ⁻³)	Volume ₁ (dm ⁻³)	Concentration ₂ (nanoparticles per dm ⁻³)	Volume ₂ (dm ⁻³)
90,000,000	0.0005	900,000	0.05
900,000	0.0005	9,000	0.05
9,000	0.0003	54	0.05

80 nm

Concentration ₁ (nanoparticles per dm ⁻³)	Volume ₁ (dm ⁻³)	Concentration ₂ (nanoparticles per dm ⁻³)	Volume ₂ (dm ⁻³)

11,000,000	0.0001	110,000	0.05
22,000	0.0001	44	0.05

Appendix 3: SOP for NexION 300 single cell ICP-MS Analysis

Contents

Introduction	273
Pre-starting the plasma checks	273
Starting the Plasma	298
Daily calibration of the instrument	299
Setting up the instrument for single cell analysis	301
Creating a new method for analysis.....	307
Setting up the batch analysis	310
Analysing/interpreting samples	314
Exporting samples.....	319
Appendix 1: SmartTune optimisation method creation.....	319

Preface

This Quick Start SOP describes the operation of the Syngistix Single Cell-Application module for the PerkinElmer NexION 300 Series Inductively Coupled Plasma Mass Spectrometer.

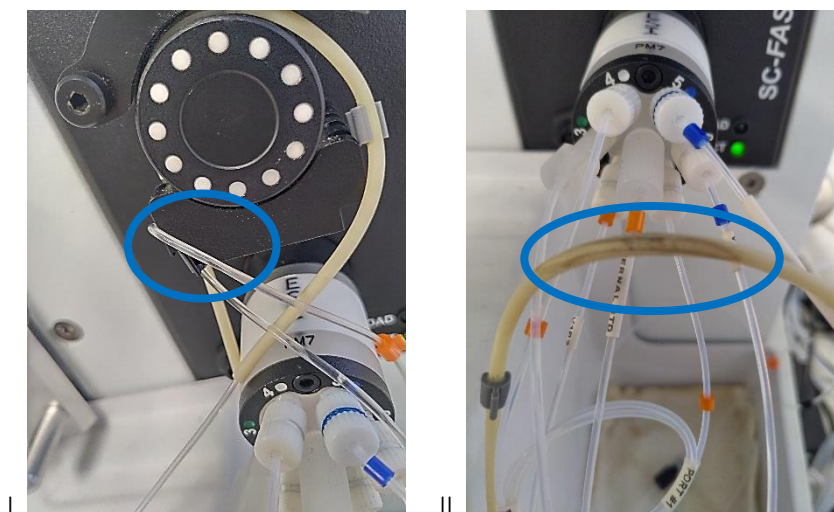
Suggested methods for sample preparation serve only as reference. Analytical conditions should always be optimized for the sample(s) of interest to attain the most accurate and precise results possible.

Introduction

The preparation and method of analysis for metal using Single Cell ICP-MS is described in detail. The method is described from start to finish from preliminary checks to turning of the instrument and exportation of data. Some interpretation of the data is also provided to aid in analysis.

Pre-starting the plasma checks

1. Check tubing for splits and pinches.



When checking the tubing it may not be clear that the tubing is damaged. In image I the clear tubing makes it hard to see that there is a pinch within the blue circle. While in image II it is much clearer that the waste tubing is damaged and needs to be replaced. The waste tubing is heavily worn and if allowed to run for any significant time will split along the black lines.

- a. Replace if needed.
2. Check that tubing is connected to the correct places.



First check that the peristaltic pump tubing connectors are tight (in blue circles) so that there is no leakage from the tubes. When the sample or waste is traveling through these tubes if there are any blockages (either from the sample or a pinching of the tubes) the connectors can build up pressure and pop off the connectors leaking sample and waste on the instrument. This should be avoided but if the tubing does pop off the connector first replace the tubing, if that does not fix the problem then reverse the tubing on the peristaltic pump; this will reverse the flow of the sample through the tubing and could possibly dislodge the blockage back out of the tubes. Then put all the tubing back the correct way on the pump.



Next check that the correct tubing is connected to the correct ports. These should already have been set up correctly when the autosampler was set up but it is always good to check that the tubes connect to where you expect them to connect to. Do this briefly by following the flow of each tube. The tubing should also have little tags that say which port they connect too (see blue circles).

After ensuring the tubes are connected to correct ports next test that the tubing connectors are finger tight by feel. If they are loose then tighten them with your fingers.



Do the same as you did for the tubes above with these connections. Testing that the tubes are finger tight and connected to the correct place.

3. Check water containers.
 - a. Refill if empty or close to empty



These are the water containers for the rinse/wash of the autosampler. Ensure that the container is mostly full with ultrapure water before proceeding. The autosampler will use most a container (3/4) in about 6 hours of use.



These two containers are the blank solution and carrier solutions they take longer to empty but need to be freshly refilled as to limit the effects of the environment and avoid contamination of the blank solution. Again as before these should be filled with ultrapure water for almost all situations.

4. Check that the single cell Gas chamber is in the instrument.



- a. If not carefully remove the cyclonic gas chamber from the instrument
 - b. Place carefully the Asperon gas chamber into the instrument and connect the gas tubes to the correct outlets.
5. Check that the neb gas and aux gas tubes are (finger) tight on gas outlets.



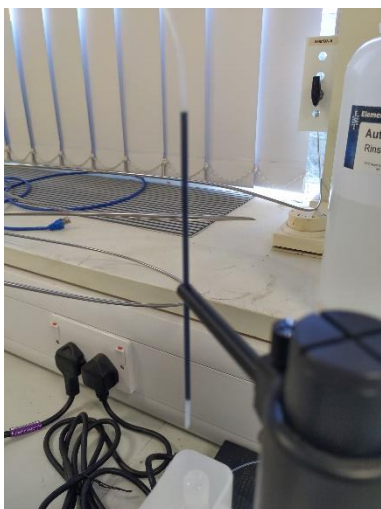
6. Check that the Autosampler is turned on.



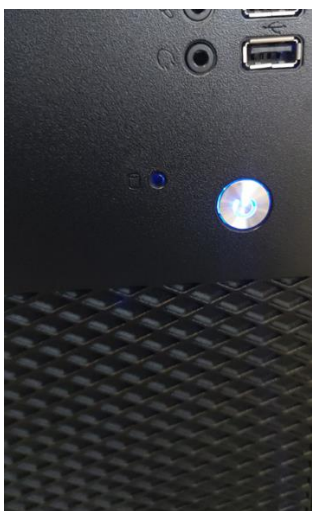
- a. If turned off by the plug turn it back on
- b. If turned off at the autosampler turn back on via switch at the back



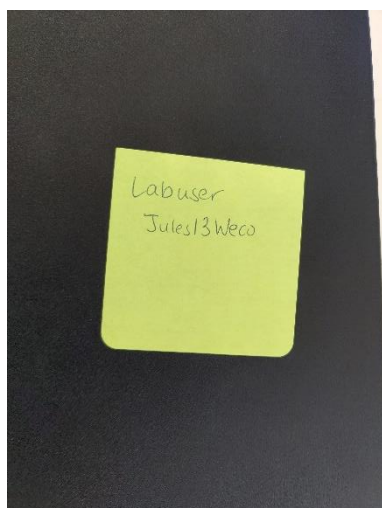
7. Check the state of the autosampler trays, probe, and syringes.
 - a. This is a cursory search looking for any broken parts and significant air bubbles.



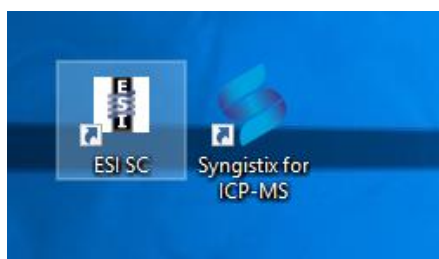
8. Check if the instrument computer is turned on.



- a. If not turn on and log on, the password is on the top of the PC.

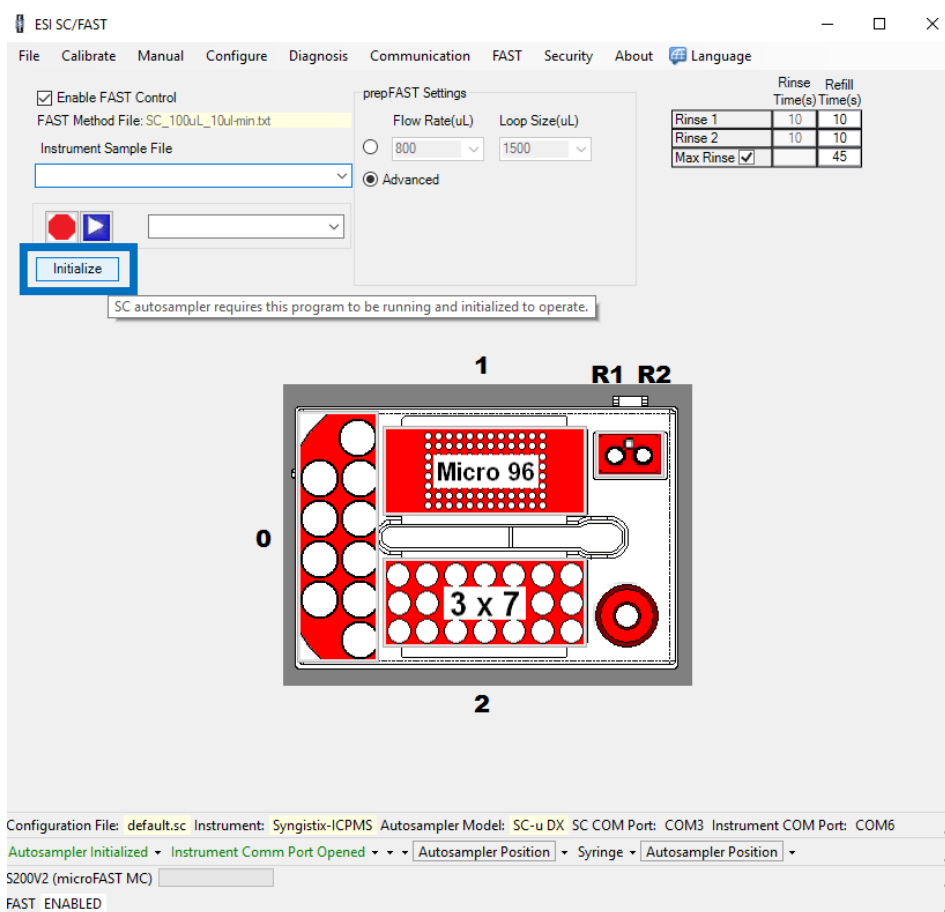


9. Load up ESI SC.
 - a. You MUST do this before opening Syngistix

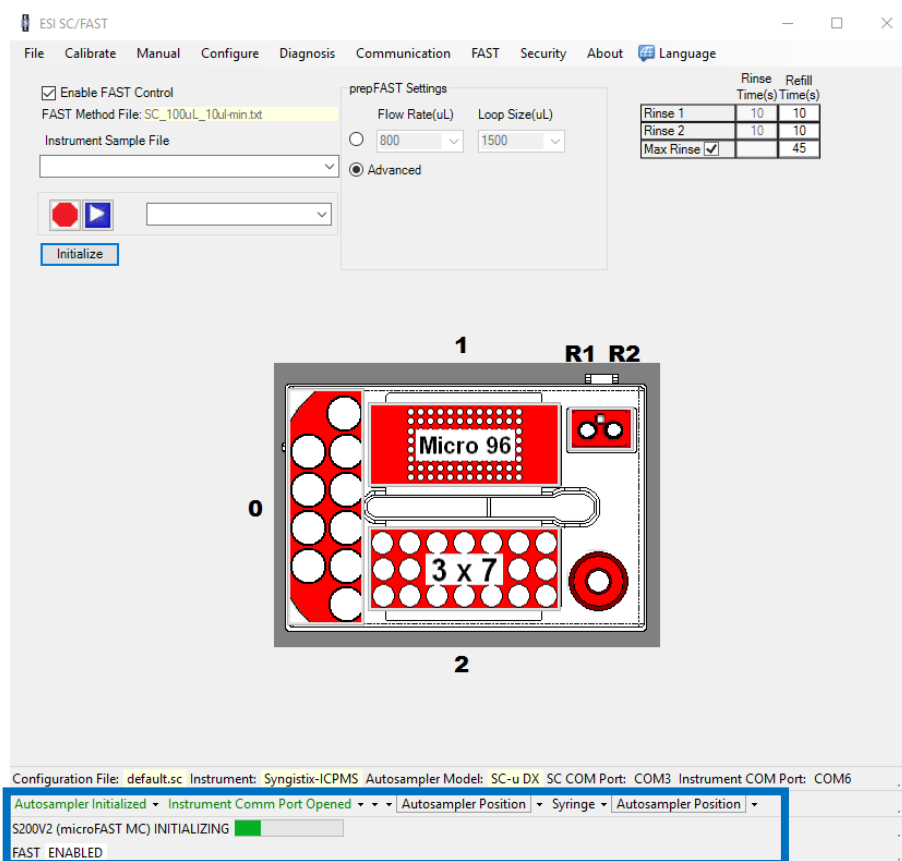


First start up ESI SC. This is important as if it is not launched first the autosampler will not speak to Syngistix

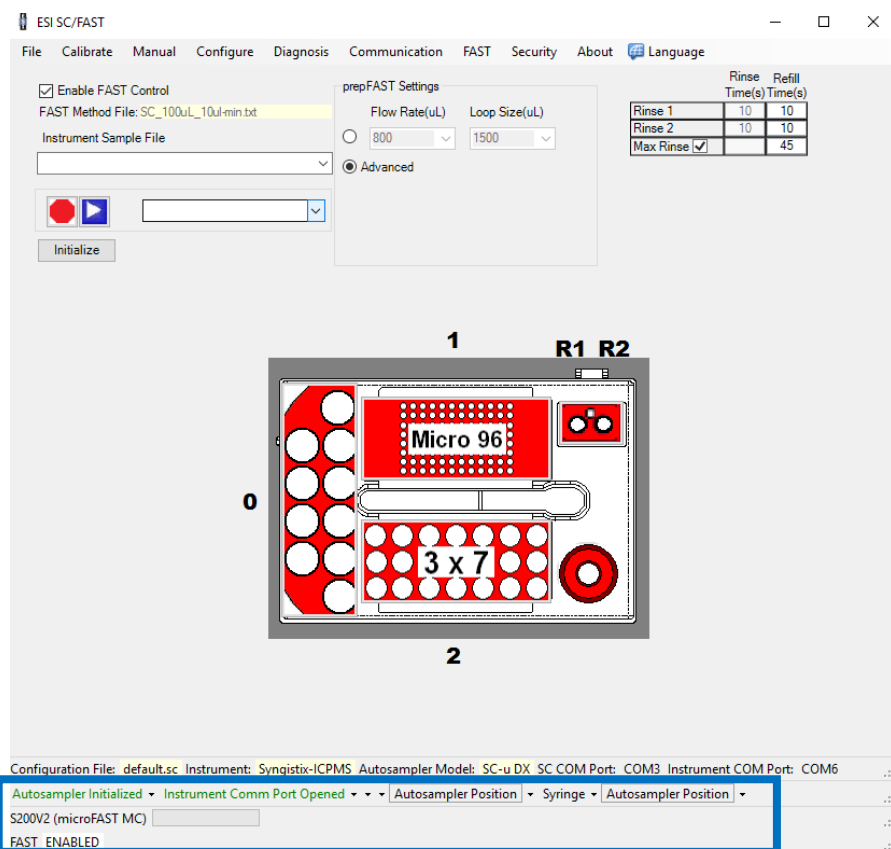
10. Initialise the autosampler
 - a. Check that the autosampler is talking to the computer



Next click Initialize in ESI SC program (See blue square).

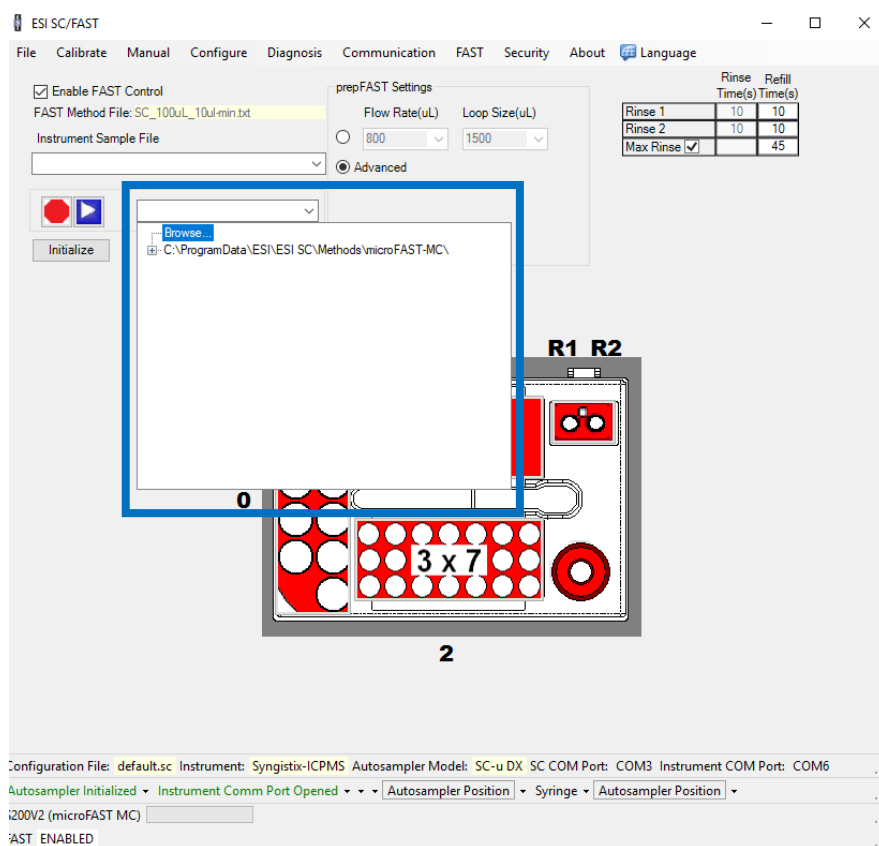


The autosampler will initialize. (See blue square)

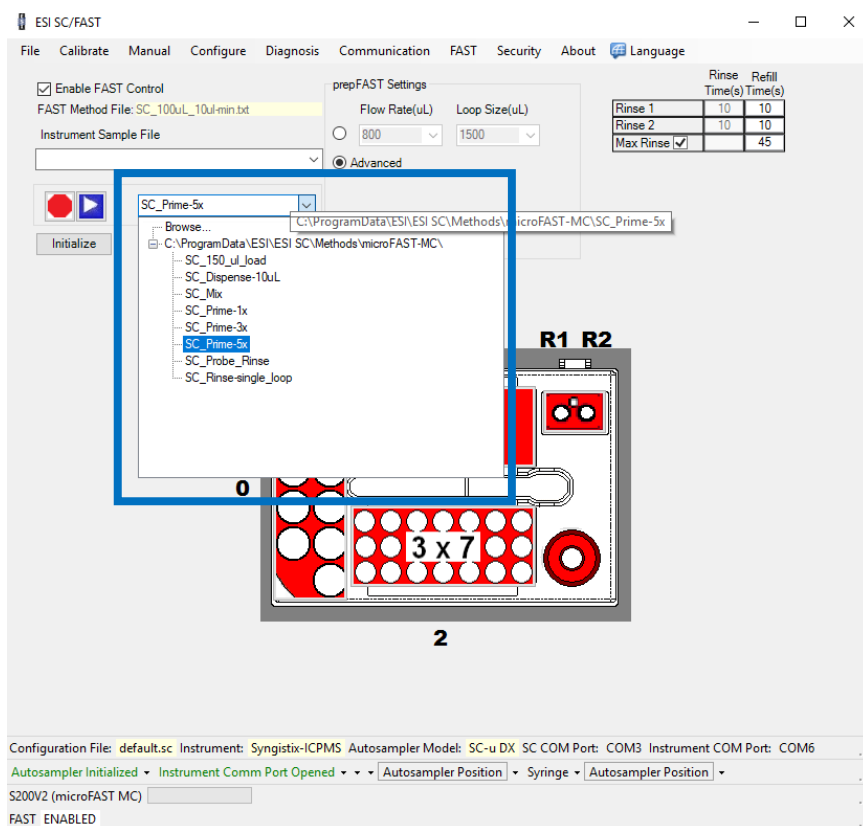


After Initialization, there will be no process ongoing (See blue square).

11. Load up 5x prime

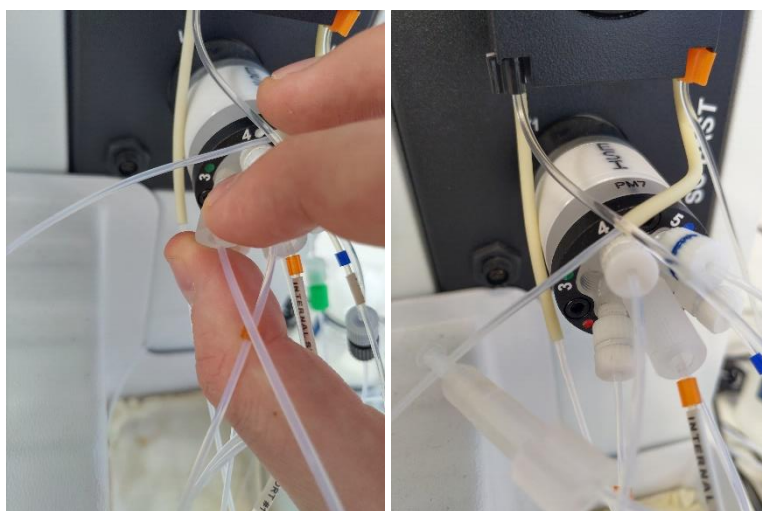


Click the drop down box and the + box to reveal options for manual setup.

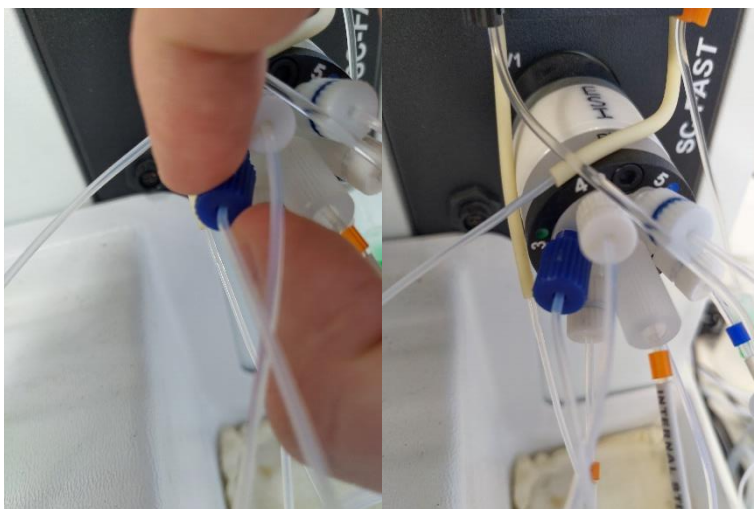


Select SC_Prime-5x. This will prime the tubing by washing and clearing the tubes of any leftover sample and fill the tubes with MQ water.

12. Replace sample inlet tubing from the Asperon inlet with the spare sample tubing.
 - a. The end that needs to be replaced is connected to slot 3 on the ESI front below the peristaltic pump.

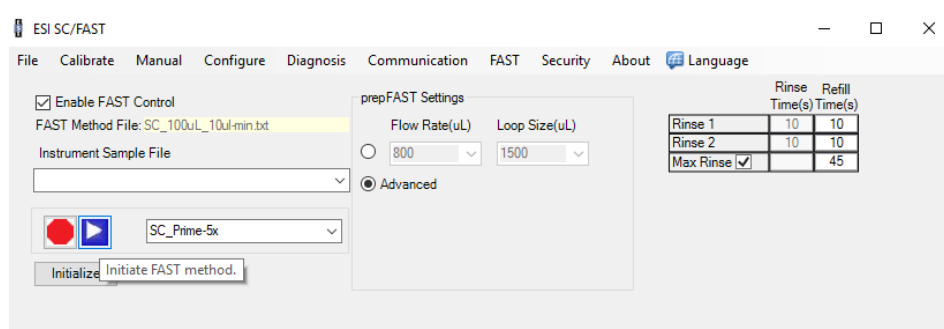


Remove the original sample tube from port 3.



Place into port 3 the spare sample tubing, making sure it is finger tight. This tubing is not attached to any other parts and can be allowed to rest on a paper towel, while the autosampler primes fluid will be pushed out of the tubing.

13. Run 5x Prime



Press the  button to start the prime.

S200V2 (microFAST MC)
FAST ENABLED FAST Sub-Method: C:\ProgramData\ESI\ESI SC\Methods\microFAST-MC\SC_Prime-5x

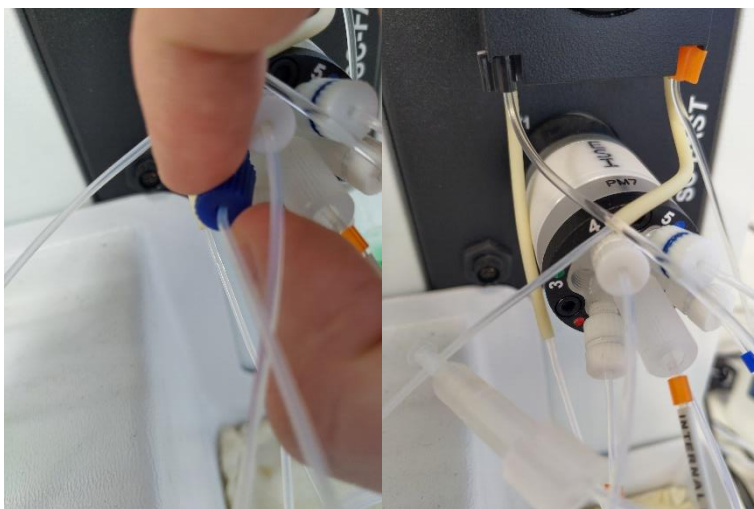
You will see this message as the prime runs.

S200V2 (microFAST MC)
FAST STOPPED

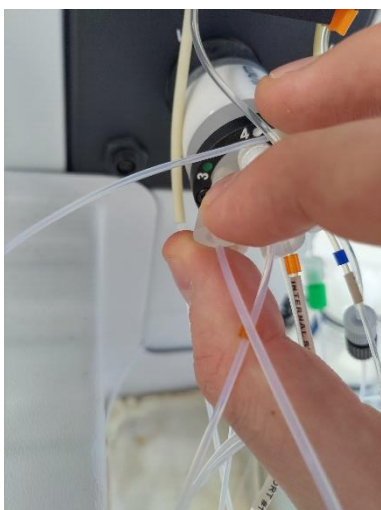
The prime will end when this message is present. Do not start any other samples or autosampler actions until you see this message, doing so can crash the autosampler system requiring a manual reboot.

14. Replace spare sample tubing with the Asperon sample tubing.

- a. The end that needs to be replaced is connected to slot 3 on the ESI front below the peristaltic pump



Remove the spare sample tube from port 3.

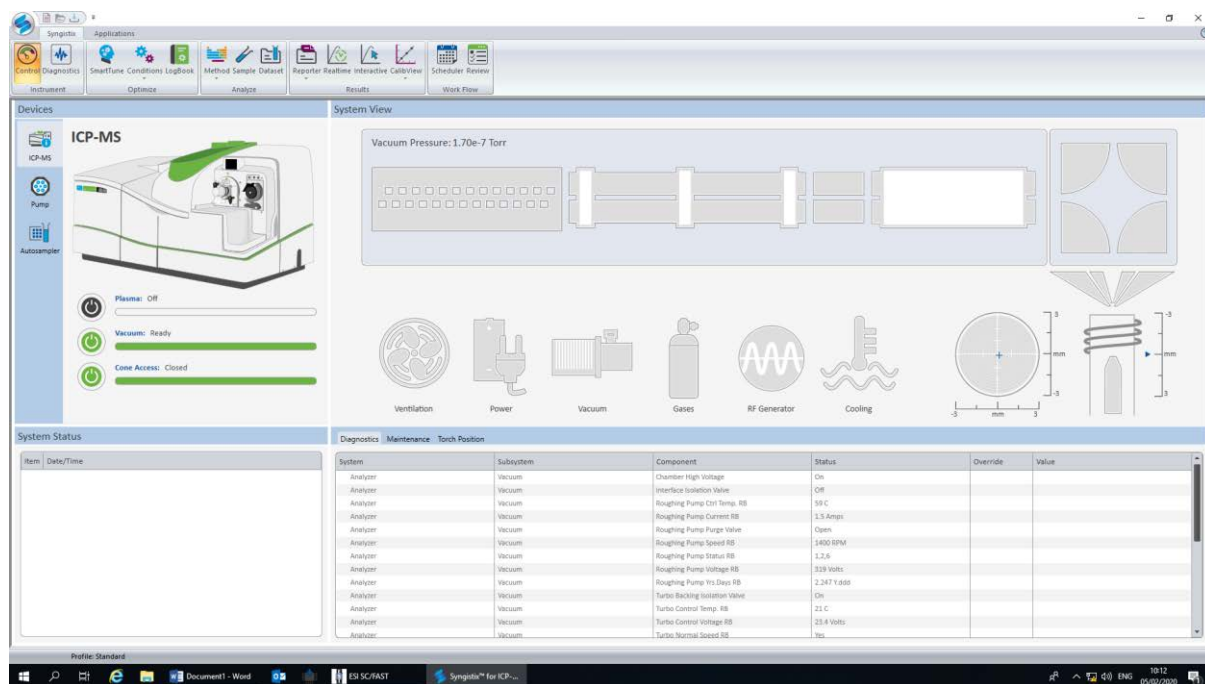


Place into port 3 the original sample tubing, making sure it is finger tight.

15. Open Syngistix

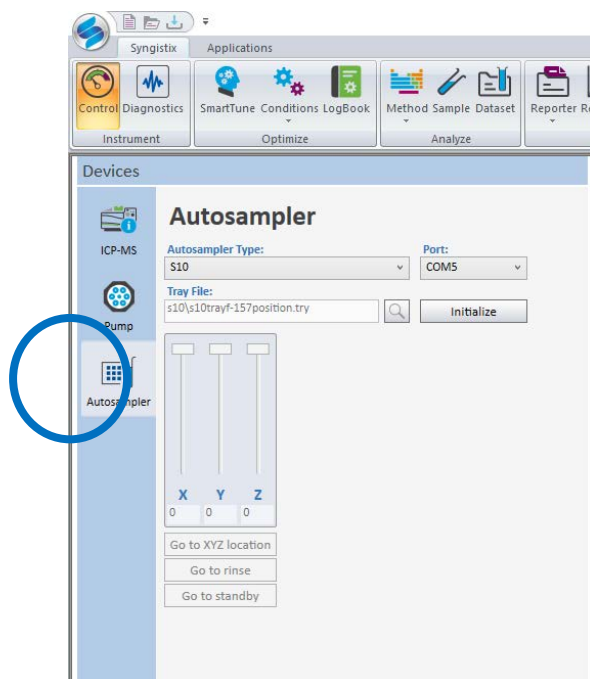


Next we start up Syngistix, by double clicking on this icon.

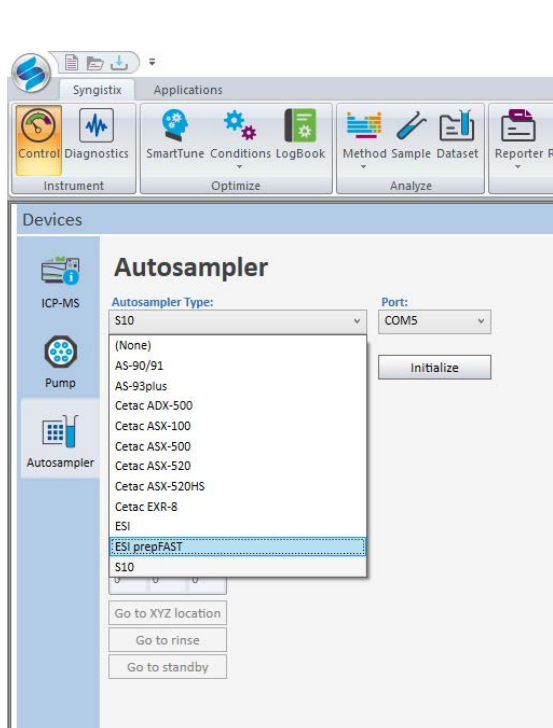


When Syngistix opens you will be presented with this screen.

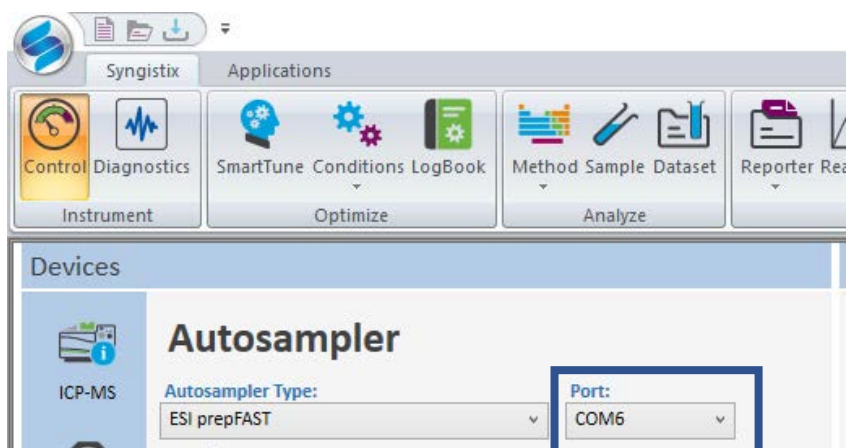
16. Go to autosampler tab on front page



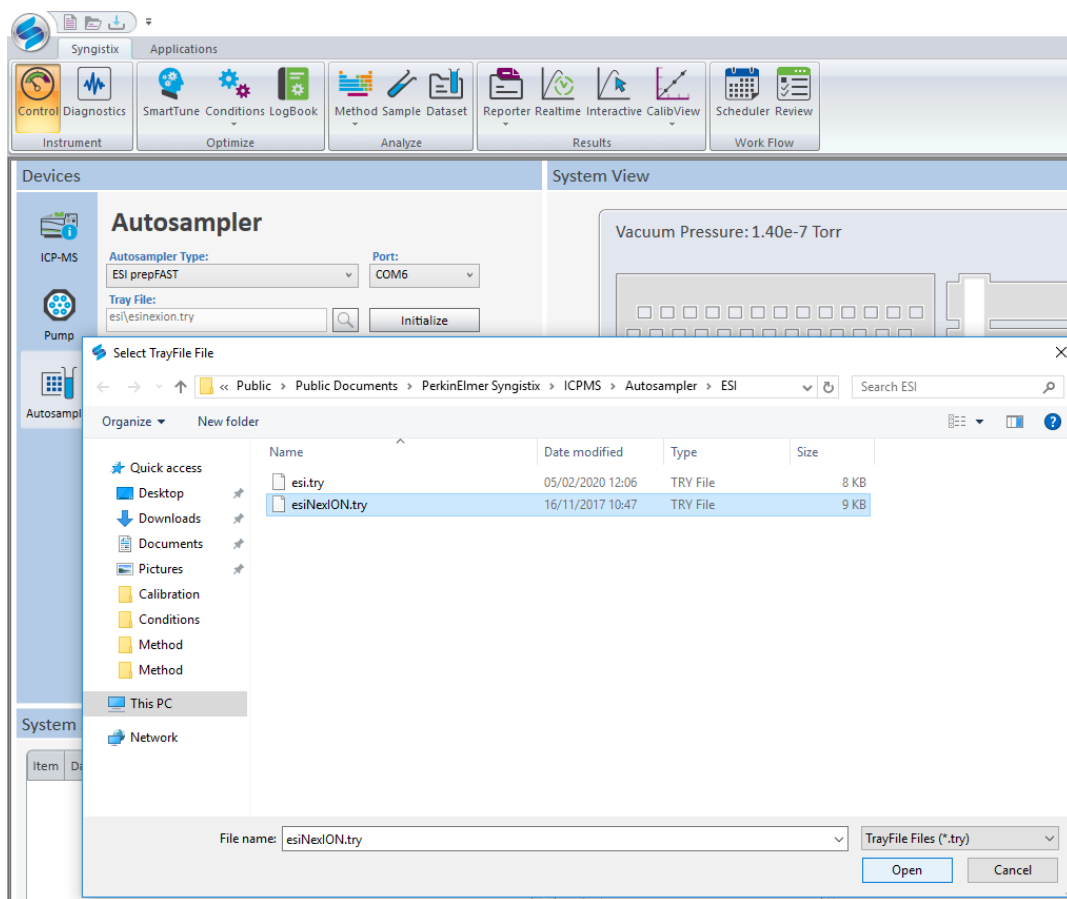
17. Set the autosampler type to ESI SC



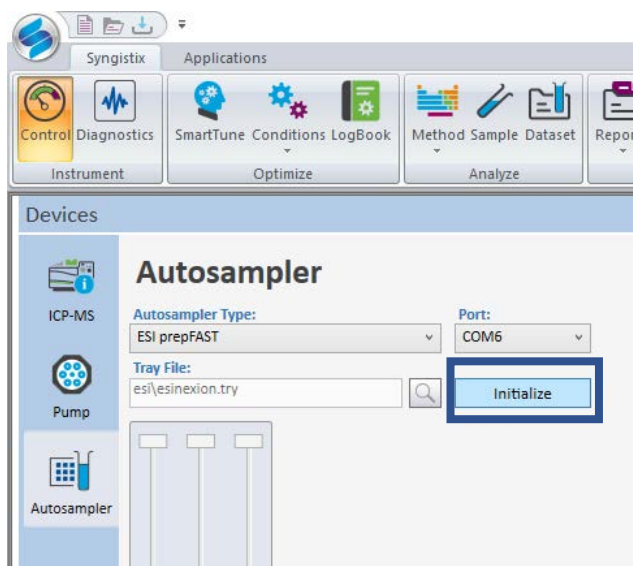
18. Set communication port to 6



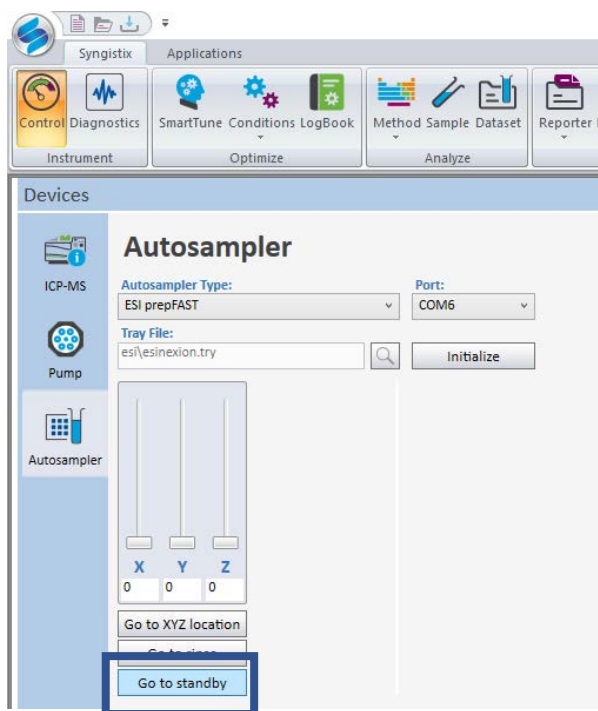
19. Set tray type to NexlON



20. Initialise the autosampler

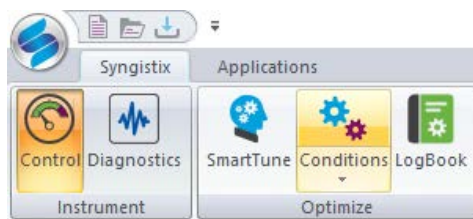


21. Click **Go to standby**.



a. This will test that the autosampler is talking to Syngistix

22. Go to conditions



Click on conditions.

Conditions - C:\Users\Public\Documents\PerkinElmer Syngistix\ICPMS\Conditions\default cyclonic.dac

QID | Dual Detector | Manual Adjust | **Advanced Optimize** | Cell Parameters

Profile: Standard
View DAC Values: ☐ Active ☒ All


DAC: 1.06 Nebulizer Gas Flow [NEB]

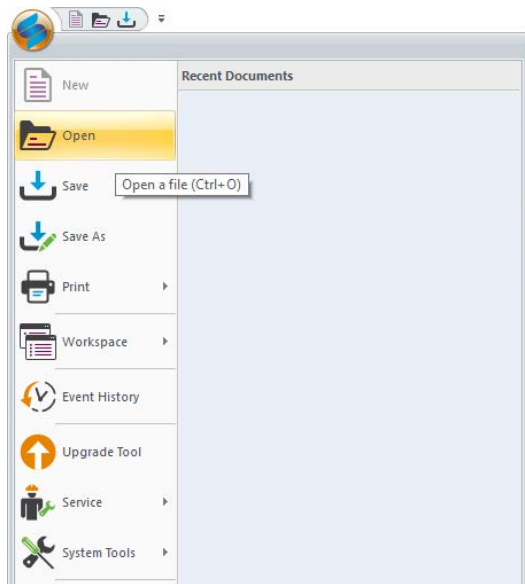
	Standard	Helium KED	Ammonia DRC	Description	Step Value	Settling Time (sec.)	Minimum Value	Maximum Value
1	1.06	1.06	1.06	Nebulizer Gas Flow [NEB]	0.01	10	0	1.5
2	1.2	1.2	1.2	Auxiliary Gas Flow	0.025	10	0.6	2
3	18	18	18	Plasma Gas Flow	0.5	10	10	20
4	1600	1600	1600	ICP RF Power	50	15	400	1600
5	-2150	-2150	-2150	Analog Stage Voltage	-100	2	-3000	0
6	1350	1350	1350	Pulse Stage Voltage	50	2	0	2500
7	12	12	12	Discriminator Threshold	5	0	0	1000
8	-9.25	-9.25	-9.25	Deflector Voltage	0.25	0	-100	20
9	0	-12	-9	Quadrupole Rod Offset [QRO]	0.5	1	-26	26
10	-5	-8	-7	Cell Entrance Voltage	1	1	-60	20
11	-5	-27	-7	Cell Exit Voltage	1	1	-60	20
12	-13	-15	-2	Cell Rod Offset [CRO]	1	1	-40	10
13		475	200	Axial Field Voltage [AFT]				
14		0	0	RPa				
15		0.25	0.45	RPq				
16		5	0.6	Gas Flow				

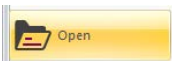
Take note the name of the file (on our system it is labelled as “Default Cyclonic.dac” as to refer to the cyclonic chamber) on your system this filename may be different or even just default.dac. Also take note of the gas flow rates for the Nebuliser gas flow and Axillary gas flow. Our system is set to 1.2 for axillary gas flow and this is what it should be for both set up, note that if this decreases then there will be similar problems to a lack of gas flow from the Nebuliser. The nebuliser gas flow for cyclonic system is currently set to 1.06 (yours may be lower or higher than this) which is far too high for the HEN set up. So we need to change the conditions of the set up.

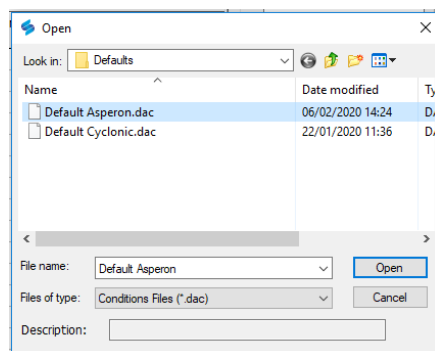
We have separate condition files for the Cyclonic and Asperon gas chambers but you may not. As such I would suggest that you change ONLY the nebuliser gas flow to 0.5.

23. Set the correct conditions.

To change a condition file you need to click the  icon. Which brings down a drop down menu.




Click on . This will bring up the condition files.

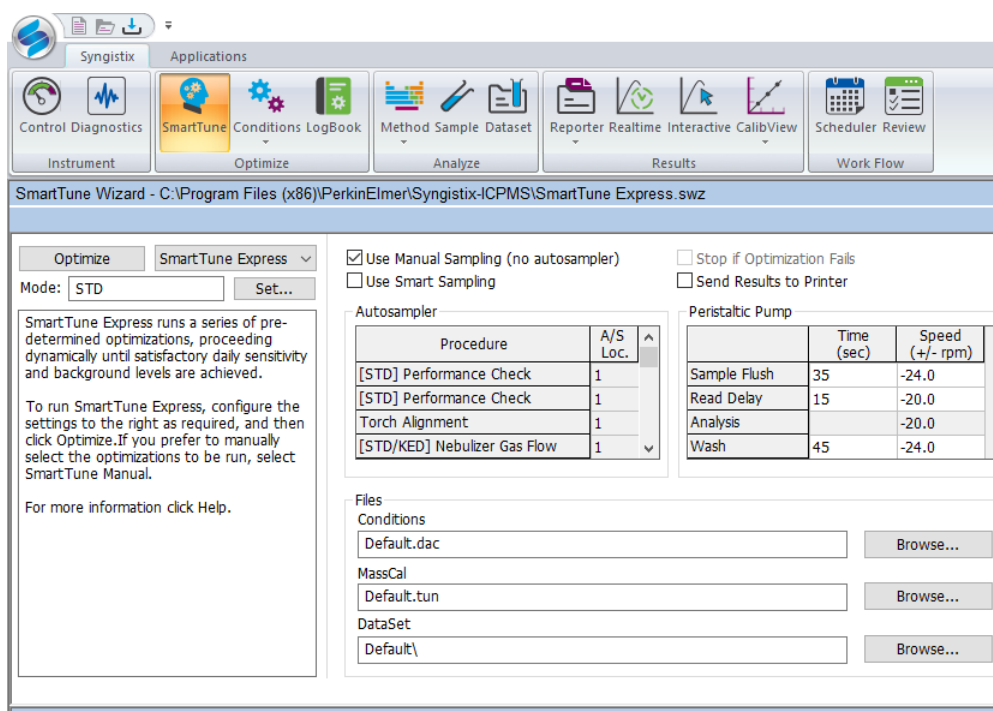


Select the condition file related to single cell setup file (on our system it is labelled as “Default Asperon.dac” as to refer to the Asperon chamber) and click open.

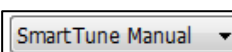
24. Go to Smarttune




Click on  to bring up the smart tune wizard a set of operations should preload.

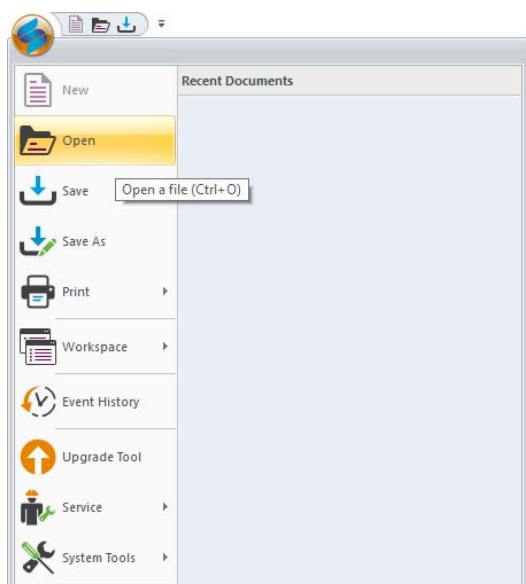


25. Select 'SmartTune Manual' from the drop down menu

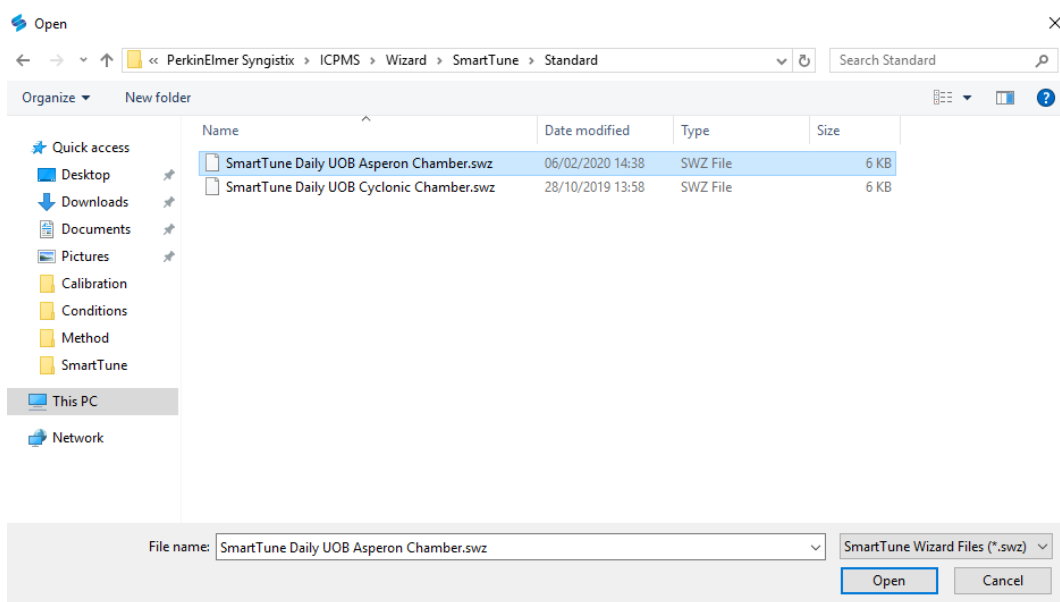


26. Set to the correct smarttune

To change a condition file you need to click the  icon. Which brings down a drop down menu.




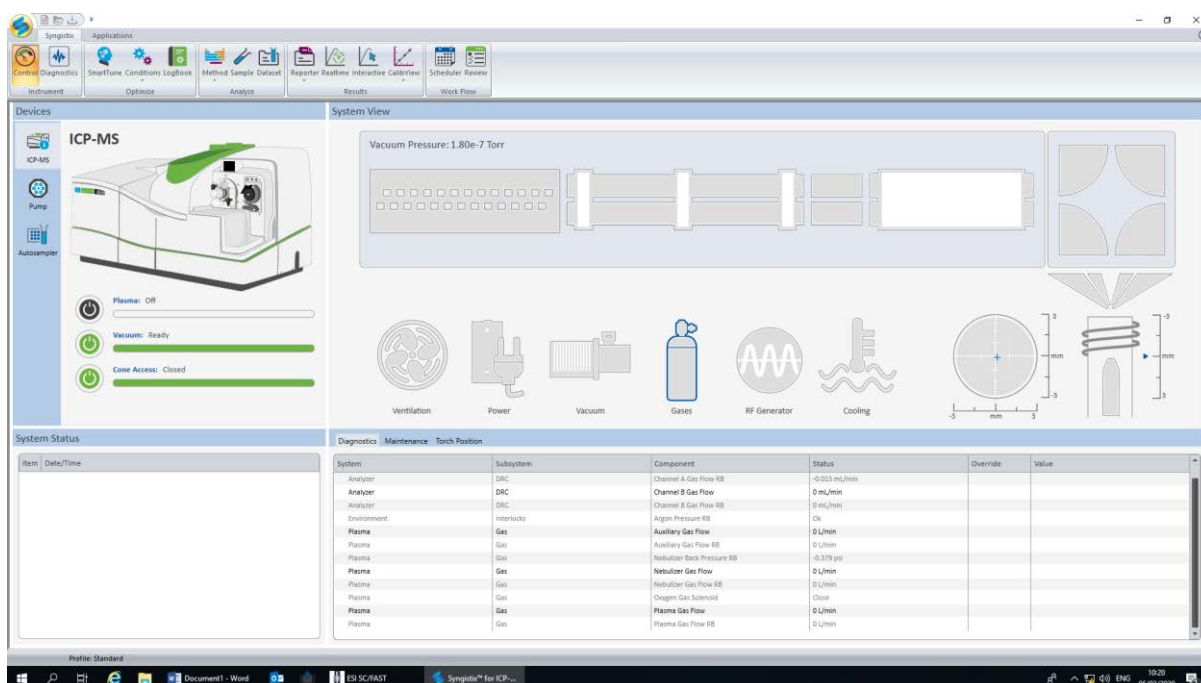
Click on . This will bring up the condition files.



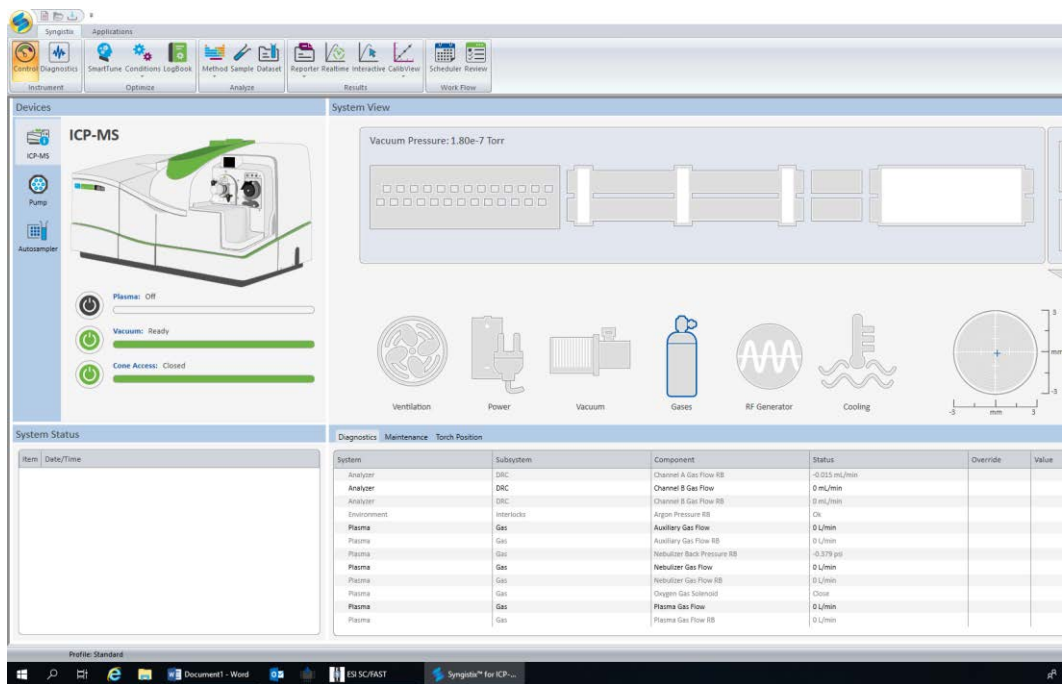
Select the condition file related to single cell setup file (on our system it is labelled as “SmartTune Daily UOB Asperon Chamber.swz” as to refer to the Asperon chamber) and click open.



27. Return to the  page




28. Test the gas flow and back pressure



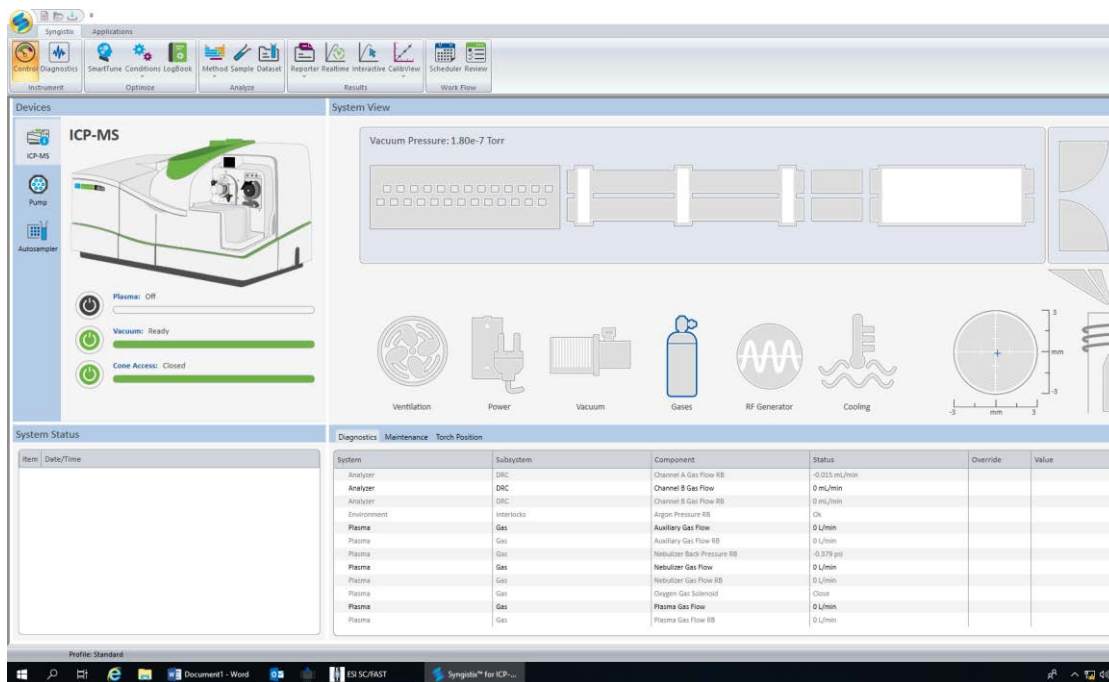
Notice the plasma is off, this is important as we first need to test the gas backpressure.




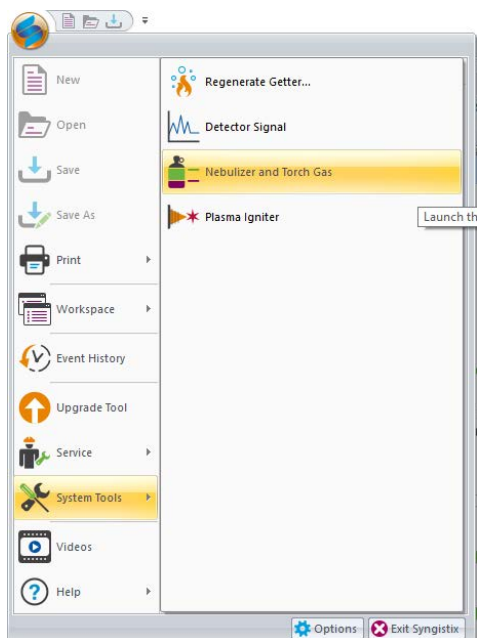
Click on the  icon. This will bring up the gas systems checks.

System	Subsystem	Component	Status
Analyzer	DRC	Channel A Gas Flow RB	-0.009 mL/min
Analyzer	DRC	Channel B Gas Flow	0 mL/min
Analyzer	DRC	Channel B Gas Flow RB	0.003 mL/min
Environment	Interlocks	Argon Pressure RB	Ok
Plasma	Gas	Auxiliary Gas Flow	0 L/min
Plasma	Gas	Auxiliary Gas Flow RB	0 L/min
Plasma	Gas	Nebulizer Back Pressure RB	-0.573 psi
Plasma	Gas	Nebulizer Gas Flow	0 L/min
Plasma	Gas	Nebulizer Gas Flow RB	0 L/min
Plasma	Gas	Oxygen Gas Solenoid	Close
Plasma	Gas	Plasma Gas Flow	0 L/min
Plasma	Gas	Plasma Gas Flow RB	0 L/min

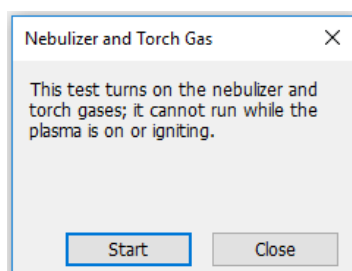
We are looking for the Plasma systems. Specifically the Nebulizer back pressure RB.



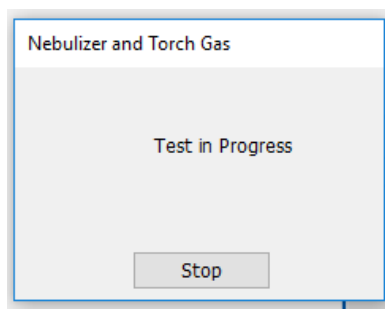
To test the status of the Nebulizer back pressure RB, we need to pump gas through the nebulizer. To do this we click on the  icon. Which brings down a drop down menu.



Go to  System Tools and then to  Nebulizer and Torch Gas. Click  Nebulizer and Torch Gas.



Click  on the pop up.



The test will then start.

Let the test run for about a minute, this will allow the nebuliser backpressure to stabilise.

Diagnostics Maintenance Torch Position			
System	Subsystem	Component	Status
Analyzer	DRC	Channel A Gas Flow RB	-0.007 mL/min
Analyzer	DRC	Channel B Gas Flow	0 mL/min
Analyzer	DRC	Channel B Gas Flow RB	0.001 mL/min
Environment	Interlocks	Argon Pressure RB	Ok
Plasma	Gas	Auxiliary Gas Flow	1.2 L/min
Plasma	Gas	Auxiliary Gas Flow RB	1.199 L/min
Plasma	Gas	Nebulizer Back Pressure RB	23.508 psi
Plasma	Gas	Nebulizer Gas Flow	0.5 L/min
Plasma	Gas	Nebulizer Gas Flow RB	0.496 L/min
Plasma	Gas	Oxygen Gas Solenoid	Close
Plasma	Gas	Plasma Gas Flow	15 L/min
Plasma	Gas	Plasma Gas Flow RB	15.011 L/min

Our nebuliser backpressure RB is 23.508 psi, this is much lower than that you would find with a cyclonic chamber (normally around 40+ psi) but is fine for single cell analysis. Based upon the cells that you are testing it is possible that the back pressure will be lower due to a lower gas flow rate. It is only a concern when the gas pressure is too high or more importantly when the gas pressure is too low. Too low is usually below 10 psi but certain cells may require this low a gas pressure.

29. Check that the gas backpressure is above 10 psi, preferably above 15 psi, but below 50 psi

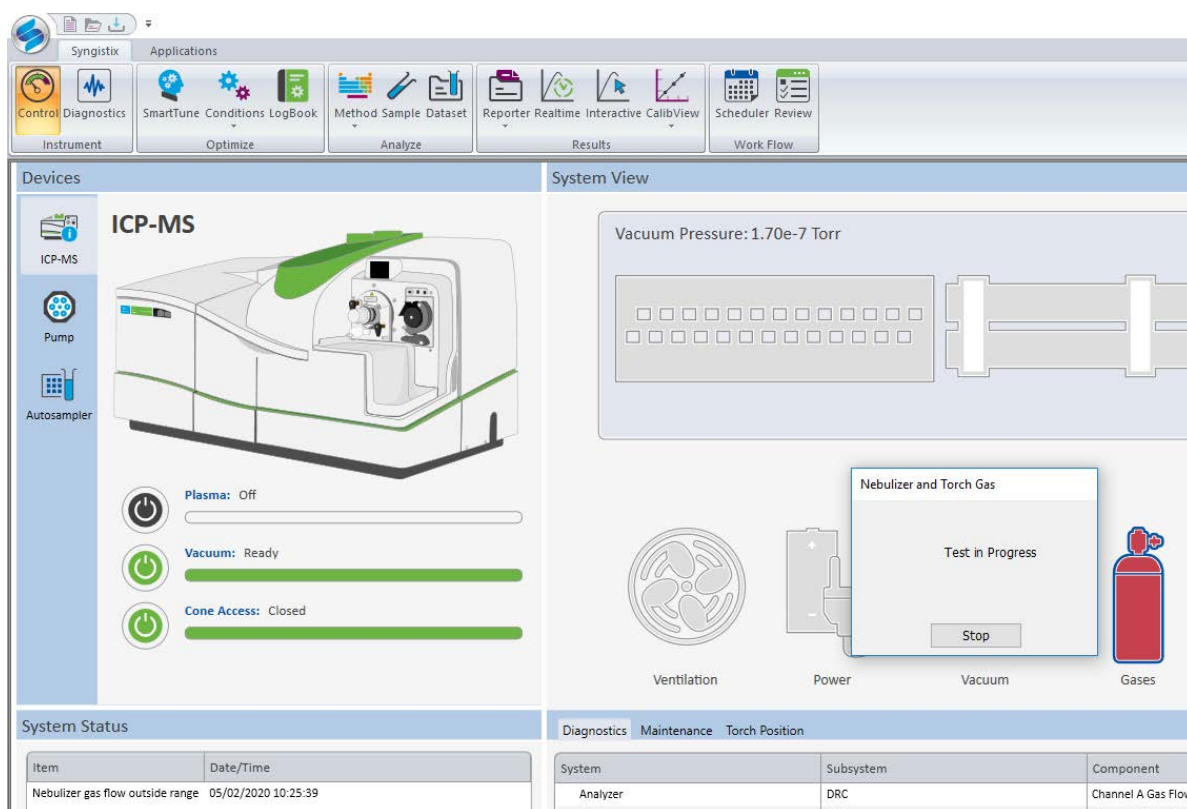
- a. If below check that the gas flow.
 - i. If the gas flow is low the backpressure could be too low
 - ii. Check the gas flow pressure into the instrument, it is possible that the tank is low and/or they are currently changing/refilling it.



- iii. Check the nebuliser, as it may have cracked. The nebuliser below has a cracked tip and is broken, you may also see the inner tubing has cracked and this will have the same effect.



- 1. Replace the nebuliser.
- b. If above 50 psi
 - i. Check that the conditions are not set up for cyclonic systems
 - 1. If it is set up for a cyclonic system change accordingly
 - ii. Check for blockages in the tubing and glassware that could be causing backpressure to build.



If you get this error message where the gas flow is outside of the range it is likely because the system is currently set up for a cyclonic chamber and not a HEN chamber that is needed for Single Cell.

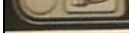
30. End the gas flow test
 - a. Wait for the gas flow to stop. The instrument will not start until this is achieved

Starting the Plasma

Now that you have concluded the pre-plasma ignition checks you can start the plasma. It is important to have done these checks as they will decrease the amount of issues that the instrument will encounter.

31. Start the plasma.



Turn on the Plasma by pressing  button on the NexION 300 instrument.

32. Watch the plasma as it ignites and for about 10 minutes after through the viewing port.




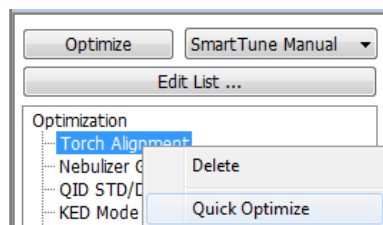
This is the view through the viewing port, there is a clean plasma without any melting or glowing from the touch.

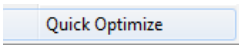
- a. You are watching for any glowing in the torch. If the torch is glowing then watch to see if it progresses/enlarges
 - i. If it enlarges IMMEDIATELY turn off the plasma, the torch is melting
 - ii. If it begins to decrease in size, keep watching to see if there are any more changes. If the glowing stops then the plasma has likely settled and stabilised.
 - b. Keep a watch on the plasma to check if a glowing develops in the torch while analysing.
33. If the plasma has stabilised then you may proceed to the daily instrumental set up.

Daily calibration of the instrument

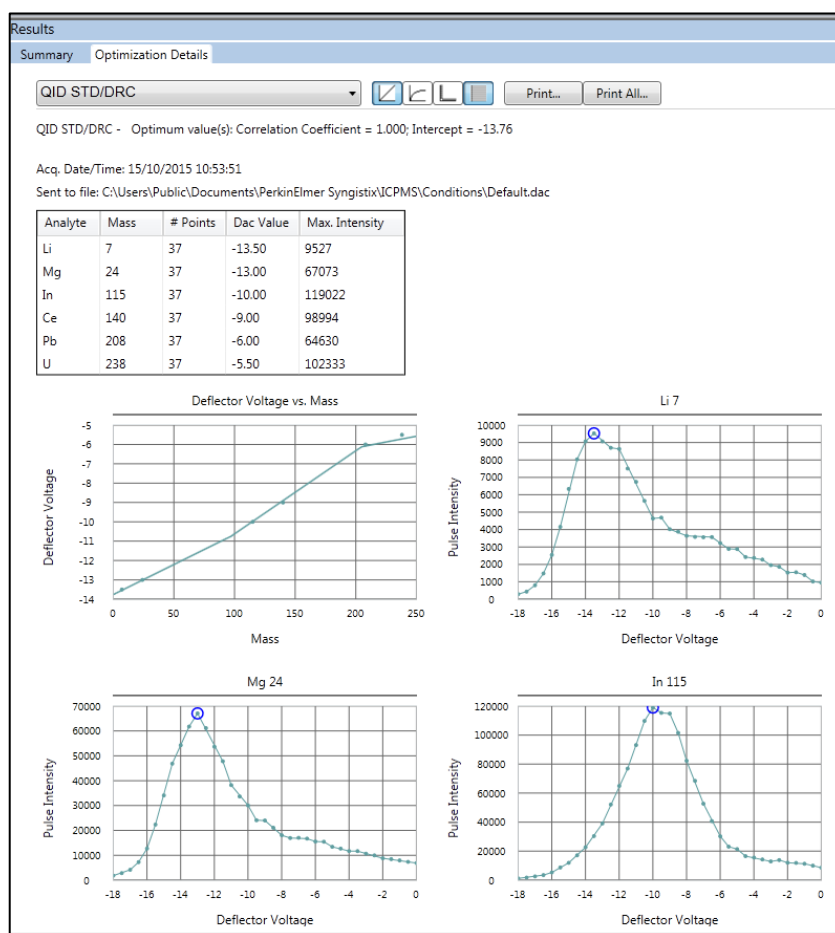


34. Go to  .
35. Go Optimization by Optimization to manually optimize the instrument.

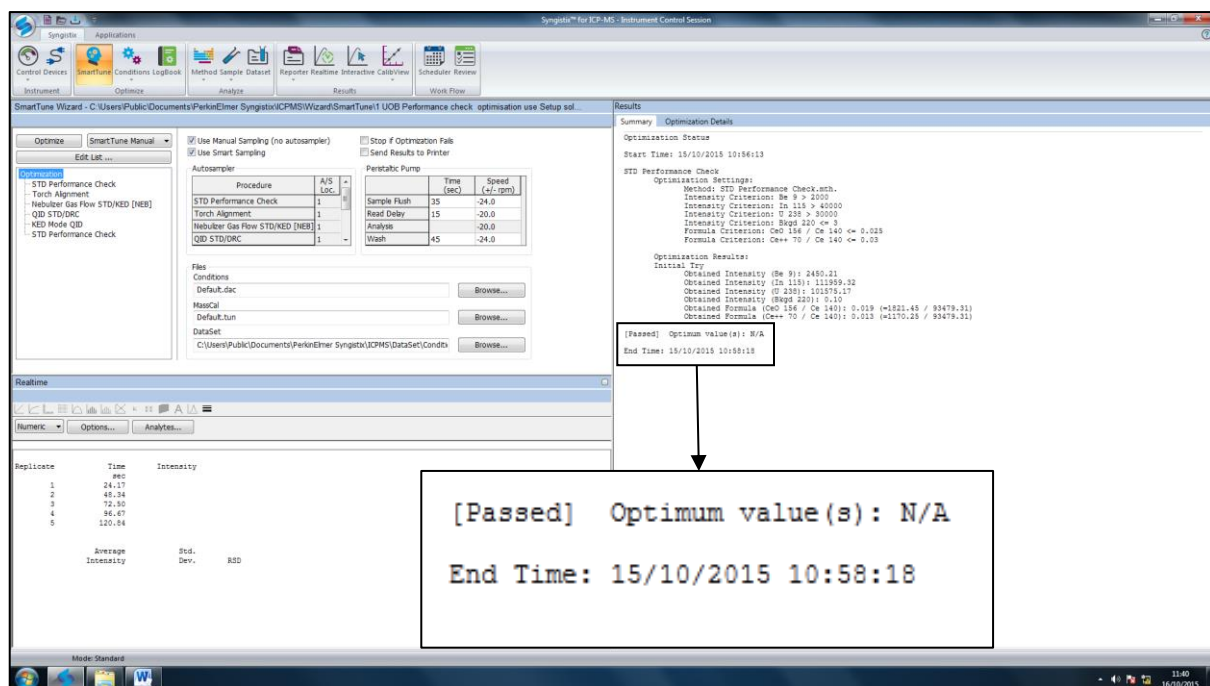


- a. Right click on an optimisation and in drop down box press  this will optimise only that optimisation.
- b. Repeat step i) for the other optimisations (proceeding down the line by selecting the operation).

A report should be produced for each optimisation performed as seen in the diagram below for the QID STD/DRC optimisation performed.



36. After all the optimisations, have been performed press on the summery tab and read whether the optimisation has passed.

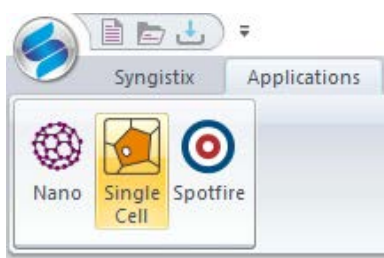



37. If the optimisation has failed then check the mechanical parts (the tubing, auto sampler probe and for leakages in the instrument) and then that the auto sampler probe is uptaking the correct solution (Perkin Elmer Set-up solution).

Setting up the instrument for single cell analysis




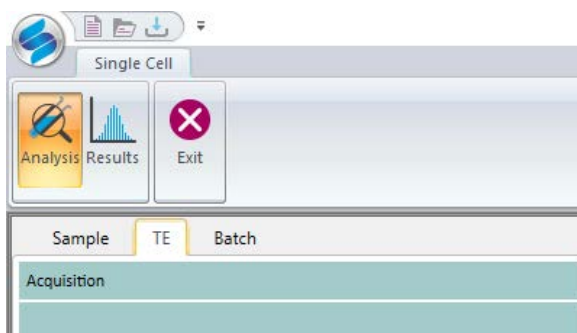
38. Click on the applications tab and then click on  to bring up the single cell window.



39. In the single cell applications widow select the analysis tab .



40. In the  tab go to the TE tab

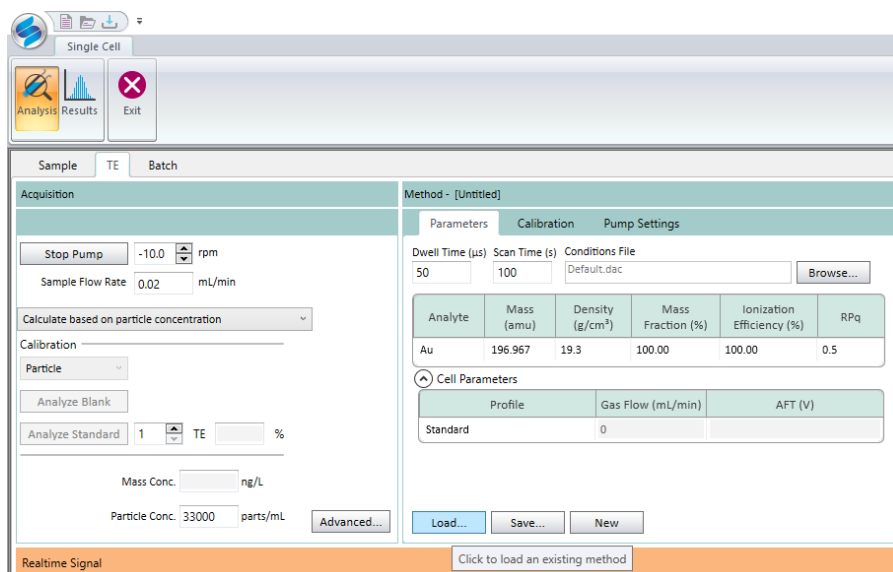


41. Put in the flow rate (which is 0.02).

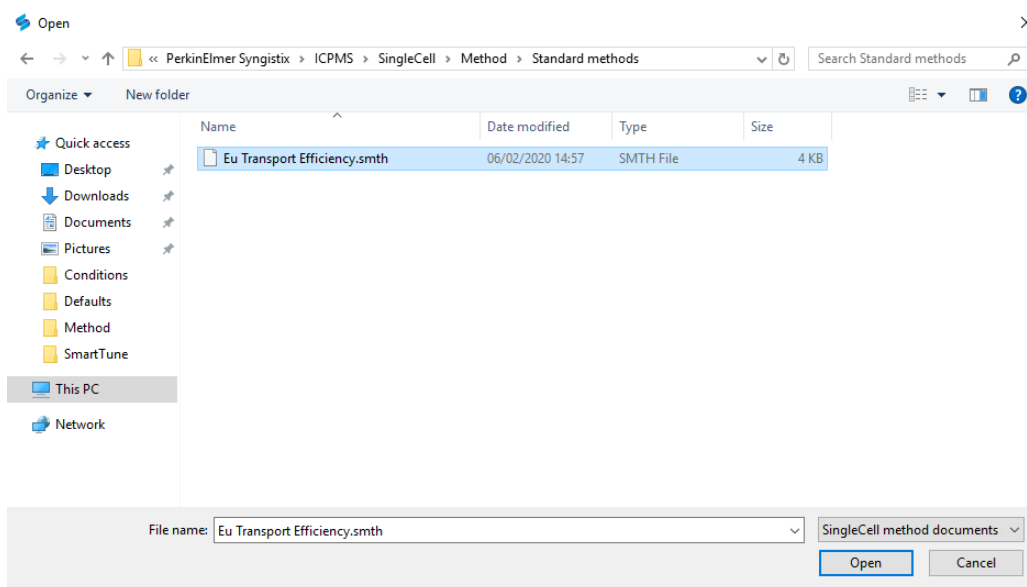
42. Put in the particle concentration of your single cell standard. This should be on the certificate for the particle standard. We use a four element polystyrene bead with a concentration of 33,000 beads per mL.

43. On the Methods tab click

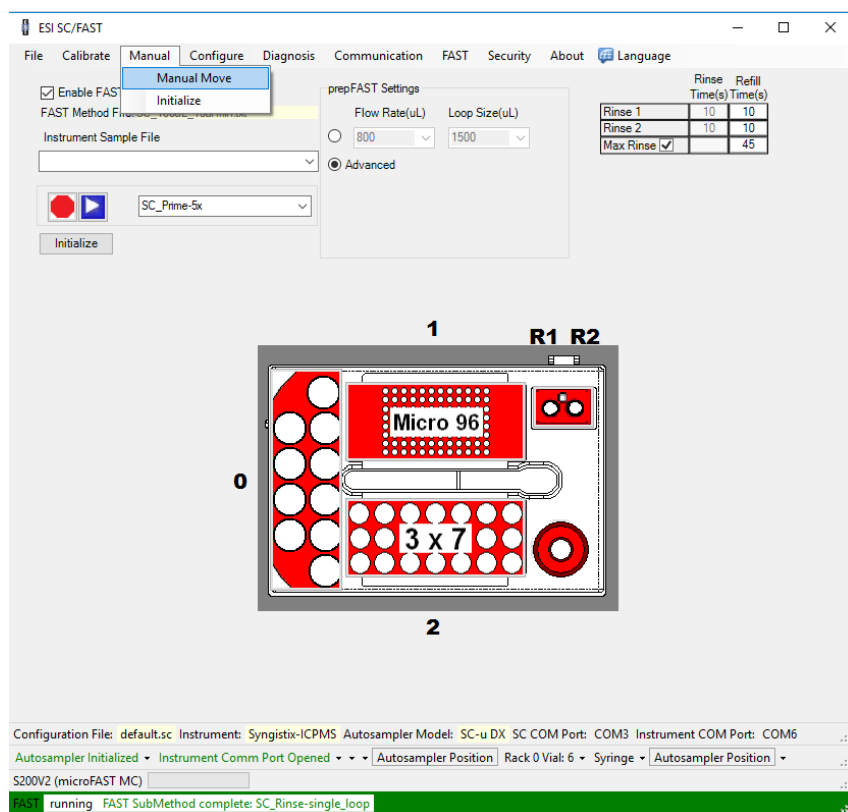
Load...



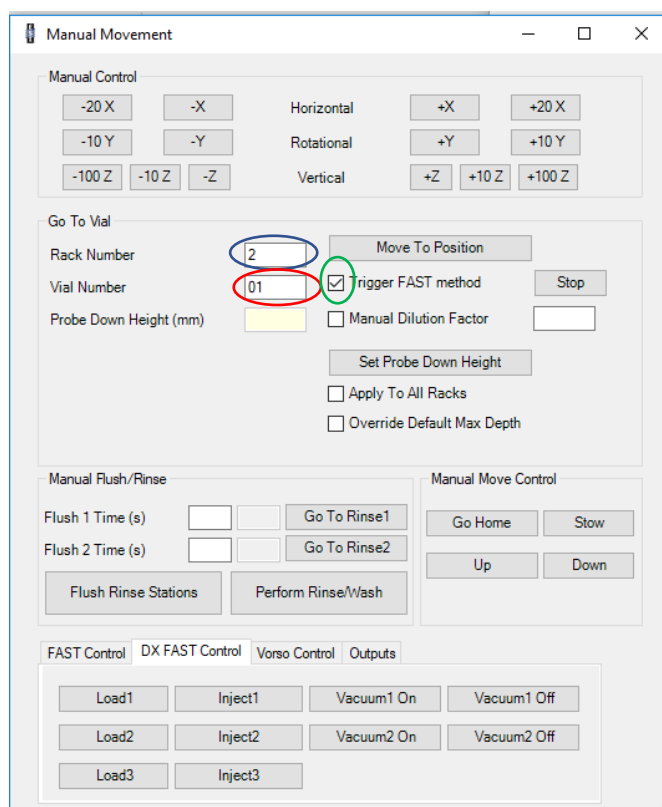
44. Open up the correct transport efficiency method file found at C:\Users\Public\Documents\PerkinElmer Syngistix\ICPMS\SingleCell\Method\Standard methods. (Note yours may be different but for the four element standard we use at UOB this is the correct method file)



45. On the ESI SC program go to Manual and open up the **Manual Move** screen.



46. Put in the rack number (Blue circle), vial number (Red circle) and click trigger FAST method (Green circle).



47. Click **Move To Position**, this will start the manual sampling.

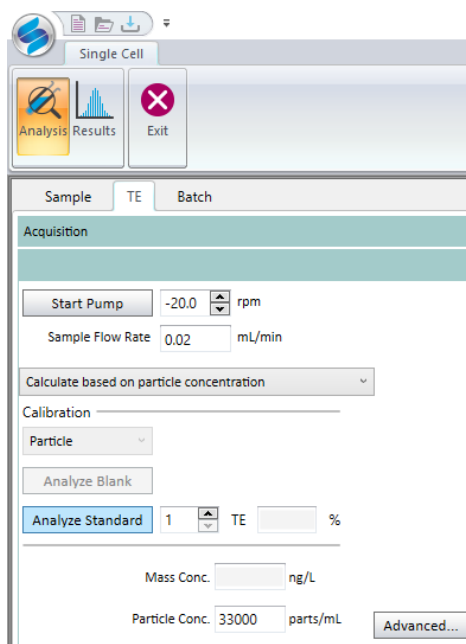
The screenshot shows the 'Manual Movement' window. In the 'Go To Vial' section, 'Rack Number' is 2 and 'Vial Number' is 01. The 'Move To Position' button is highlighted. Below it are checkboxes for 'Trigger FAST method' (checked), 'Manual Dilution Factor', 'Set Probe Down Height', 'Apply To All Racks', and 'Override Default Max Depth'. Other sections include 'Manual Control' with buttons for -20 X, -X, -10 Y, -Y, -100 Z, -10 Z, -Z, Horizontal, Rotational, Vertical, +X, +20 X, +Y, +10 Y, +Z, +10 Z, +100 Z. The 'Manual Flush/Rinse' section has buttons for 'Go To Rinse1', 'Go To Rinse2', 'Flush Rinse Stations', and 'Perform Rinse/Wash'. The 'Manual Move Control' section has 'Go Home', 'Stow', 'Up', and 'Down' buttons. At the bottom, there are tabs for 'FAST Control', 'DX FAST Control', 'Vorsor Control', and 'Outputs', with buttons for 'Load1', 'Inject1', 'Vacuum1 On', 'Vacuum1 Off', 'Load2', 'Inject2', 'Vacuum2 On', 'Vacuum2 Off', 'Load3', and 'Inject3'.

48. The autosampler will now move to position and start to uptake the calibration beads.

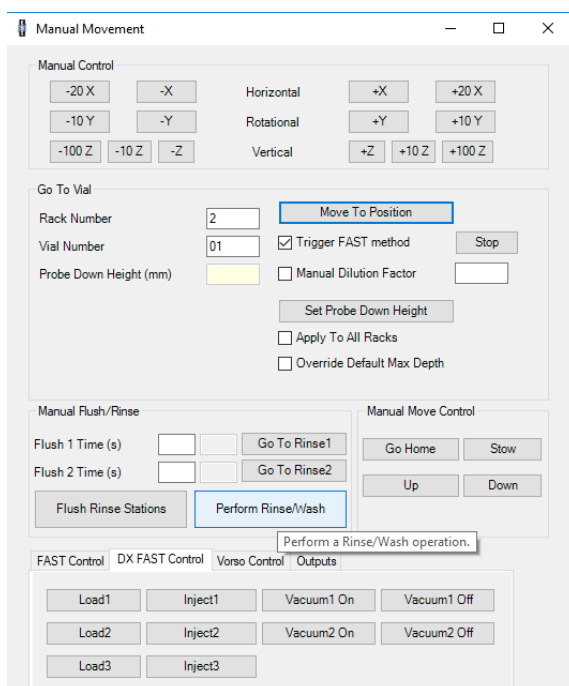
The screenshot shows the software status bar. It displays configuration details: Configuration File: default.sc, Instrument: Syngistix-ICPMS, Autosampler Model: SC-u DX, SC COM Port: COM3, Instrument: S200V2 (microFAST MC). The status bar indicates 'Autosampler Initialized', 'Instrument Comm Port Opened', 'Autosampler Position', 'MoveInto Rack 2 Vial: 1', and 'Syringe'. A green bar at the bottom shows 'FAST running' and 'FAST Sub-Method: SC_Mix'.

49. When the autosampler has begun to uptake sample on syngisitix press **Analyze Standard**.

This is when you can see the sample being moved along the sample tubing. This will look like a plug of sample with a bubble of gas on either side that travels away from the probe.



50. At the end of the analysis the autosampler will not automatically wash the tubing and probe. This is done by clicking **Perform Rinse/Wash**. The end of analysis is when the transport efficiency sample run is finished on syngistix.



51. Exit the manual movement pop up.
52. You will now have a transport efficiency

Creating a new method for analysis

53. In the sample box and parameters tab press

New

Method - [Untitled]

Parameters Calibration Pump Settings

Dwell Time (μs) Scan Time (s) Conditions File

50 100 Default.dac Browse...

Analyte	Mass (amu)	Density (g/cm ³)	Mass Fraction (%)	Ionization Efficiency (%)	RPq
Au	196.967	19.3	100.00	100.00	0.5

Cell Parameters

Profile	Gas Flow (mL/min)	AFT (V)
Standard	0	

Load... Save... New

54. In the Method box press on the white box under

Analyte

this will bring up a

Analyte

Au

Gd
Tb
Dy
Ho
Er
Tm
Yb
Lu
Hf
Ta
W
Re
Os
Ir
Pt
Au
Hg
Tl
Pb
Bi
Th
Pa
U

drop down menu with elements. Select the element of interest for

analysis (in this example gold). The analyte box will now have
chosen in the box.

Analyte

Au

the element

55. The mass and the density will change accordingly to the analyte of interest. Typically, the most abundant isotope is used, although another isotope may be selected. **The**

density and mass fraction have to be changed based on the particle nature/composition and should be kept to defaulted values when analysing the ionic standards. Update the density value according to the particle material. This information may be found in the material documentation or from a scientific website.

56. Set the dwell and scan times. We use a standard dwell time of 50 μ s and scan time of 40s. This is to provide a fast analysis time with a good level of resolution. It is also our laboratory standard settings. If your samples need a different dwell or scan time feel free to change them, just note it in your experimental report that you are deviating from the laboratory standard.

Method - [Untitled] [Modified]

Parameters Calibration Pump Settings

Dwell Time (μ s) Scan Time (s) Conditions File

50 40 Default.dac Browse...

Analyte	Mass (amu)	Density (g/cm ³)	Mass Fraction (%)	Ionization Efficiency (%)	RPq
Au	196.967	19.3	100.00	100.00	0.5

Cell Parameters

Profile	Gas Flow (mL/min)	AFT (V)
Standard	0	

Load... Save... New

57. Set the correct conditions file,

Method - [Untitled] [Modified]

Parameters Calibration Pump Settings

Dwell Time (μ s) Scan Time (s) Conditions File

50 40 Default.dac Browse...

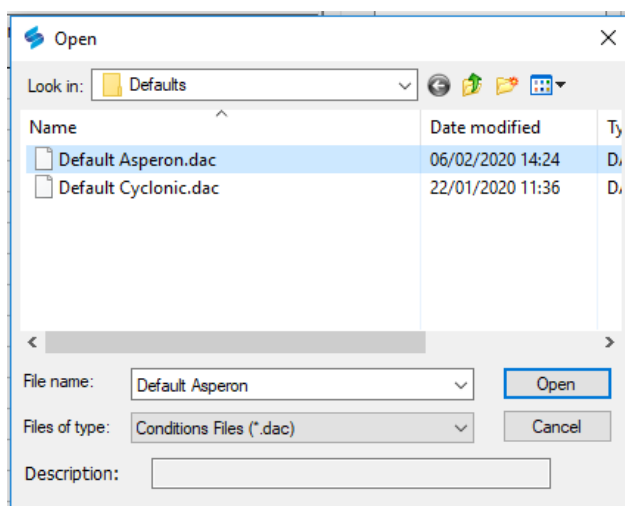
Analyte	Mass (amu)	Density (g/cm ³)	Mass Fraction (%)	Ionization Efficiency (%)	RPq
Au	196.967	19.3	100.00	100.00	0.5

Cell Parameters

Profile	Gas Flow (mL/min)	AFT (V)
Standard	0	

Load... Save... New

58. Select the condition file related to single cell setup a file (on our system it is labelled as "Default Asperon.dac" as to refer to the Asperon chamber) and click open.



59. On the calibration tab, input the size/mass of any particle standards and ionic standard concentrations that you are using.

Method - [Untitled] [Modified]

Parameters Calibration Pump Settings

	Dissolved Std	Au 196.967 (µg/L)		Particle Std	Au (ag)	Au (nm)
1	STD1	1	1	STD1	10.105	10
2	STD2	2	2	STD2	80.844	20
3	STD3	3	3	STD3	272.847	30
4	STD4		4	STD4		
5	STD5		5	STD5		
6	STD6		6	STD6		
7	STD7		7	STD7		

Load... Save... New

60. In pump settings tab change the settings for both the timing to at least 180s (this is the minimum amount of time it takes for the sample to get to the detector from uptake), I recommend to use from 210s as this allows for sample to arrive in plenty of time for analysis. Set the speed to -2.0, this is the slowest the peristaltic pump can be set, we want to minimise the effect of the variable flow rate of the peristaltic pump has on the flow rate.

Method - [Untitled] [Modified]

Parameters Calibration **Pump Settings**

Peristaltic Pump

	Time (sec)	Speed (+/- rpm)
Sample Flush	210	-2.0
Read Delay	0	-2.0
Wash	120	-2.0

☒ Peristaltic Pump Under Computer Control

Load... Save... New

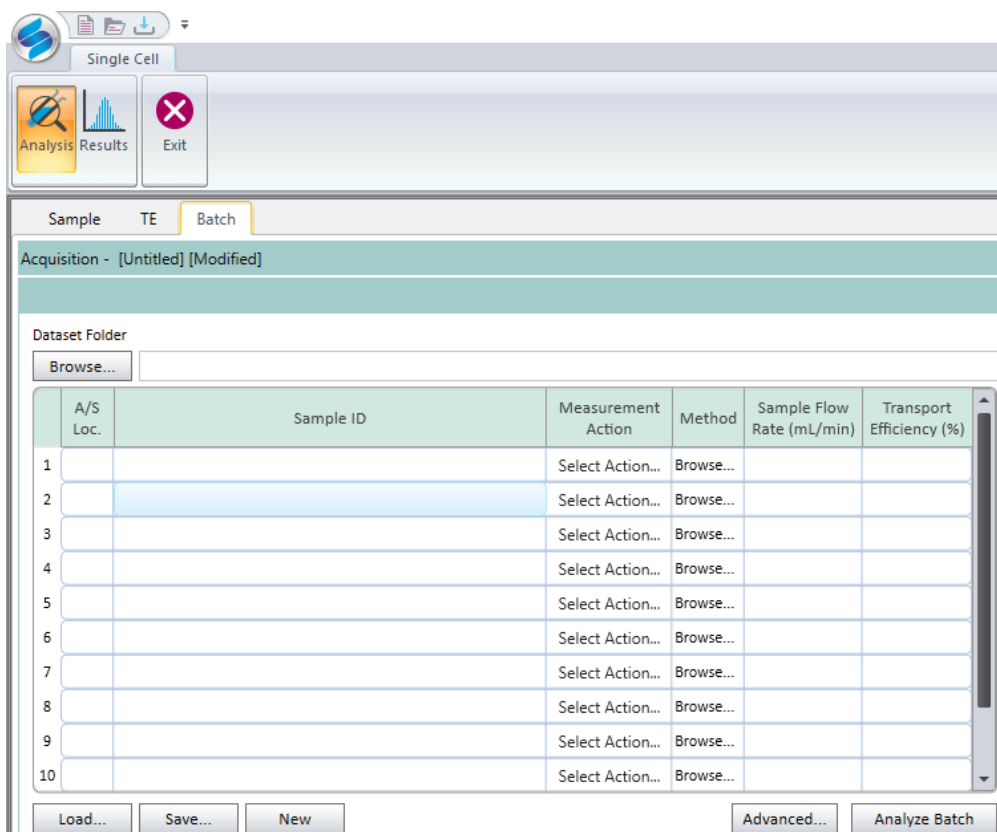
Setting up the batch analysis

To run samples I would highly recommended that you use Batch analysis. This is because it is significantly easier and more reliable to run a batch than to manually test your samples and/or calibrations. The ESI autosampler does not automatically perform the wash step after running the sample analysis, in addition it is not always clear when the manual sample wash and analysis are complete; prematurely stopping either the wash or analysis can cause the autosampler to crash or act unexpectedly.

61. Place your samples into the sample racks.



62. In the  tab go to the Batch tab.



63. Firstly, fill the Autosampler Location, this is where the sample is on the ESI autosampler. The position is slightly different to the ESI manual move position. All the samples are have a three digit code, YXX where Y is the Rack number and XX is the Vial number. For example sample number 1 on rack 0 would be 001 while sample number 1 on rack 1 would be 101.

64. Next is the Sample ID, input whatever your sample is called in here.

65. The Measurement Action is how the sample is measured (in this case sample may refer to calibration standard). It is a drop-down list with six options, most times you will be using Run sample.

Run Blank – You will have the choice between the particle and dissolved blanks. This is for calibrations of the analytes of interest.

Run Particle Standard – Will allow you to set up a calibration of the particle standards within the batch. Hovering over the option will show a list of the particle calibrations that are within your currently loaded method.

Run Dissolved Standard - Will allow you to set up a calibration of the dissolved standards within the batch. Hovering over the option will show a list of the dissolved calibrations that are within your currently loaded method.

Run Sample – This will run your samples using the method selected in the next box. Select this for your samples.

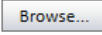
Autostop – Autostop is very useful to add to the end of runs, whenever the instrument gets to this measurement action it will turn off the plasma and end the run. This measurement option is useful for longer runs that will end at an inconvenient time, such as a sample run that would end late at night. With this measurement action you can set up the instrument, allow it run overnight and know that the instrument will turn off when the sample run has ended. Place this at the end of your sample batch file.

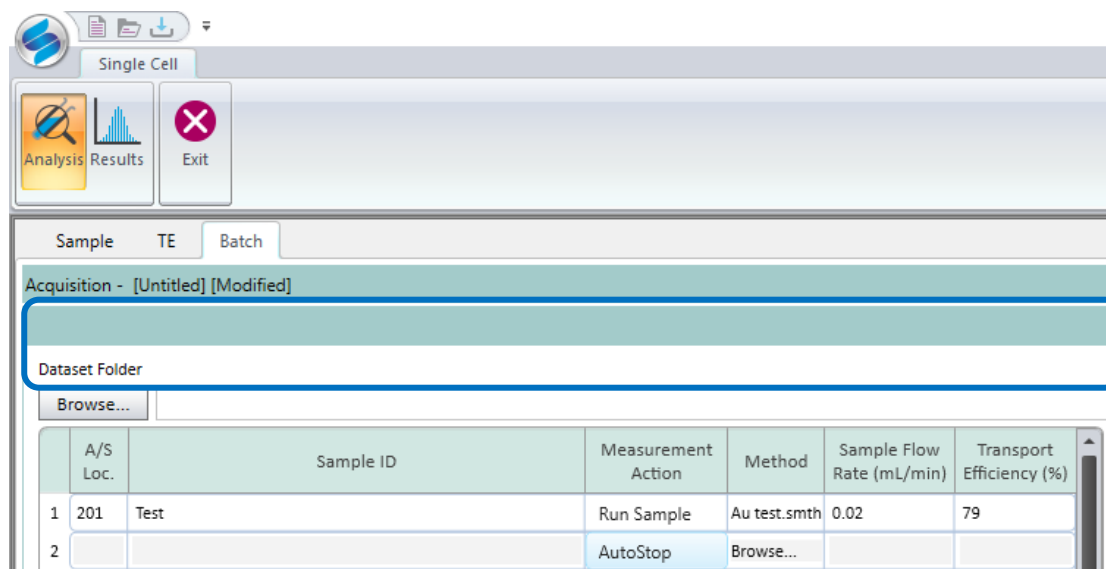
Pause – The pause measurement option will pause the run at that point until you tell the run to continue. It is best used for two main uses, firstly after calibrations so that you can review the calibration and decide if to continue to the sample analysis. Secondly it is useful for when the run is larger than what can fit on the sample rack as it will allow you to ensure that the sample rack has been switched for the new samples before continuing.

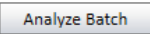
	A/S Loc.	Sample ID	Measurement Action	Method	Sample Flow Rate (mL/min)	Transport Efficiency (%)
1	201	Test	Select Action...	Browse...		
2						
3						
4						
5						
6						
7			Select Action...	Browse...		
8			Select Action...	Browse...		
9			Select Action...	Browse...		
10			Select Action...	Browse...		

66. Enter the method of analysis. This can be inputted by either pasting the method file location on the computer or by clicking on the method box and selecting the method.
67. Enter the Sample Flow Rate which is always 0.02 mL/min.
68. Next enter the Transport Efficiency this is whatever your calculated transport efficiency from earlier was.
69. Continue to enter sample lines until the batch is complete. If you reach a point where you need a new sample batch line, right click and you will be given the option to add a new line.

- a. The easiest method that I have found for filling out the batch table is to construct the table within Excel (or similar program) as this will allow you to construct the entire table and to drag down sample lines to auto fill. It is then as simple as copy and pasting the Excel table into the batch table. This also allows for an extra backup of the sample table that can be used if the instrument crashes or for reporting purposes.
70. The final step is to load the dataset folder. If the dataset folder is not loaded before a sample is run the program does not know where to save the sample data and WILL crash, losing all sample data.

To load the dataset folder, click . This will bring up a window, from here you will need go to C:\Users\Public\Documents\PerkinElmer Syngistix\ICPMS\SingleCell\Dataset (Note yours may be at a different location). You may want to create a new dataset folder for your samples so that they are not in general dataset folder, but this is not necessary to run samples.



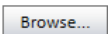
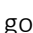

71. Now that the batch has been set up and the dataset folder loaded save the batch so that if there are any crashes you can quickly reload your run.
72. Lastly to start the analysis, click .
73. The samples will now be analysed, you should not need to do anything but leave the instrument to run the batch. Do maintain a watch on the instrument checking the water levels in the wash containers (if nearing empty refill with ultrapure water), a cursory watch on the tubing (checking for splits and pinches) and keep an eye on the torch for glowing on the glass (representative of the gas pressure dropping or the nebuliser is blocked/cracked).

Analysing/interpreting samples

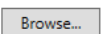
While you can check the results of the samples during the analysis and it is usually not a problem, I would advise to let your samples run and then check the results at a later date. This is because when a new sample is added to the dataset after analysis if you are on an unsaved edited sample file then the run will pause until you either save the changes or decline to save the file. Additionally, if the sample file that you are loading/viewing is significantly large (and they are sometimes prone to being over 100mb [Average size of a file is 10mb]) and the program tries to proceed to new part of the analysis Syngistix will likely crash, as it fails to load so much data.



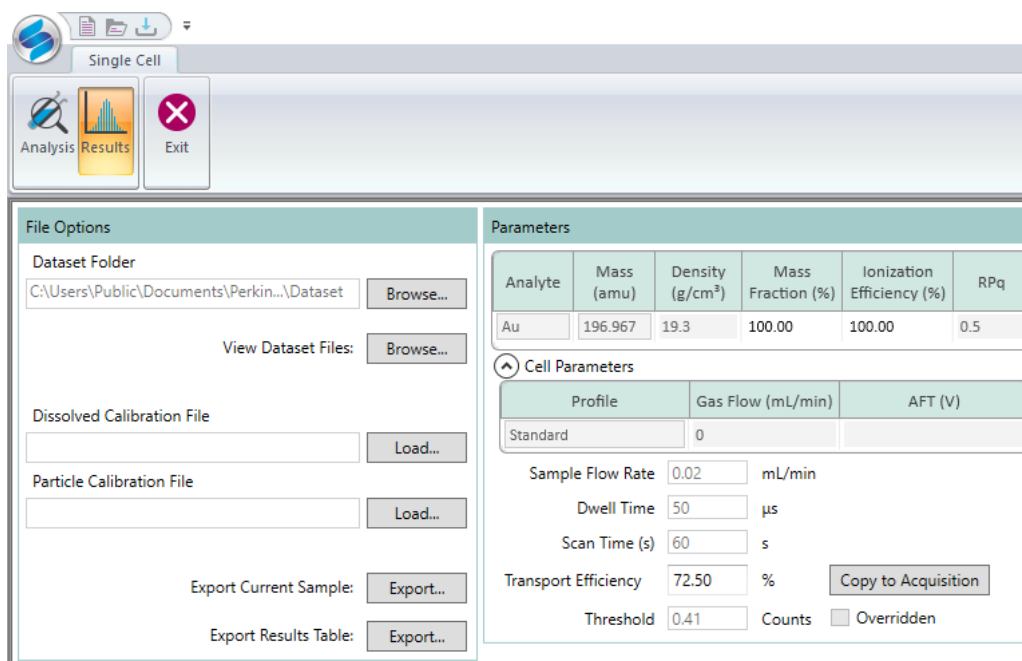
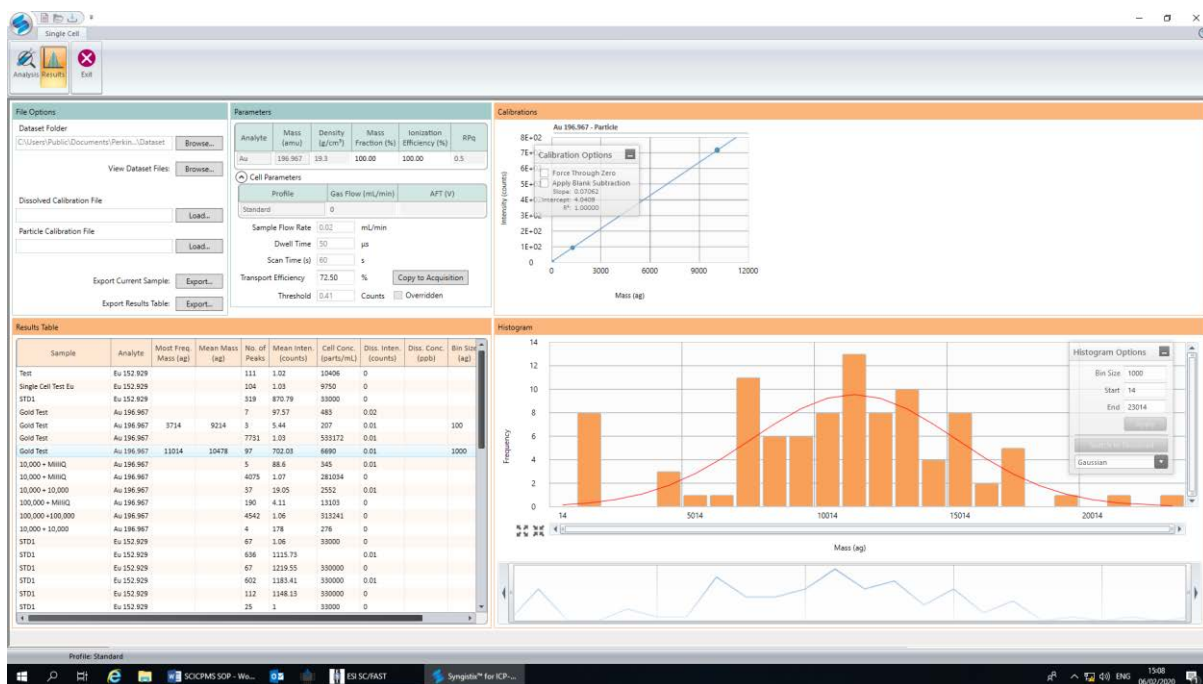
74. Go to the  tab.

75. Load the dataset folder, click . This will bring up a window, from here you will need  to  (Note yours may be at a different location).

Loading the dataset folder will load all the samples that have been analysed and saved in that dataset. If you want to look at a specific sample you can use


View Dataset Files:  instead.

76. You will be presented with four panels; we will look at them in detail now going clockwise from top left.



In the top left we have the file options and parameters panels.

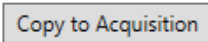
In the file options panel, you have the current loaded dataset folder, currently loaded dissolved and particle calibration files and the buttons for exporting the current sample and results table.

The dissolved and particle calibration files will be empty if your sample had been analysed with a set of loaded calibrations, however you can load any calibrations for your samples by clicking .

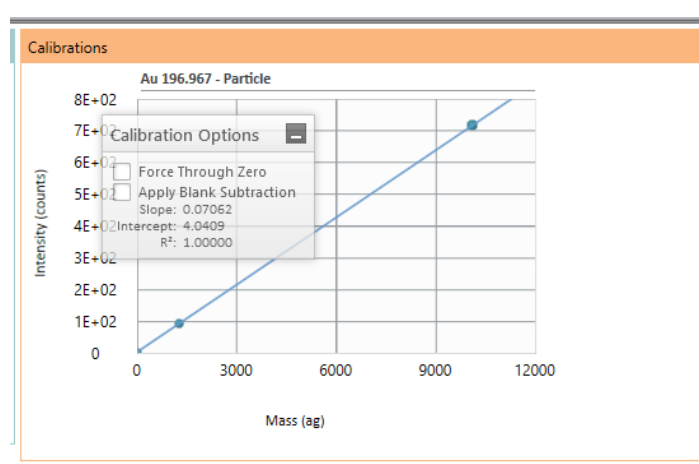
Export current sample will create a CSV file that relates to the currently loaded sample. This will only have data for the currently highlighted sample in the results table. This will provide the binned frequencies of the sample as well as the distribution curve and line of fitting chosen as data and in a graph. Useful for individual sample representation.

Export results table will create a CSV file of the entire results table, this will have all the data that is present within the results table but not individual distribution curves. Useful for overall results, mass sample reporting and for seeing the trends in samples.

In the parameters panel there are all the parameters that relate to the individual sample. The top set of parameters are related to the method, you can change the ionisation efficiency and the mass fraction. The mass fraction is the ratio of element analysed within the compound. For example TiO_2 has a 60% mass fraction of Ti. You may need to change the mass fraction if the sample you are analysed is not 100%. Changing the mass fraction of the sample to lower than 100% will increase the mass calculated by Syngisitix for the sample.

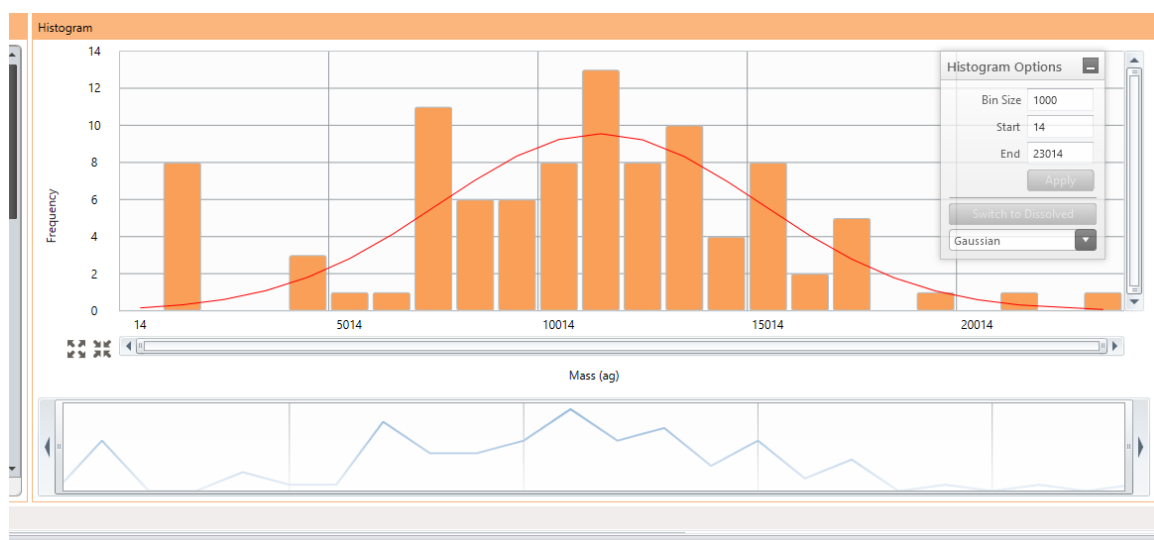
Next is a set of parameters that cannot be changed; the flow rate, dwell time, and scan time. Below them is the transport efficiency which can be changed. It may be found that the transport efficiency was incorrect and you have rerun the calculation resulting in a different efficiency, in which case you can change to the new value. Otherwise you shouldn't really need to change the transport efficiency, but if you do bear in mind that a change in the transport efficiency will result in a change in the cell concentration. Next to the transport efficiency is , if you press this button then whatever the transport efficiency for this sample will be transferred to the manual sample transport efficiency (note this will not import the transport efficiency to the batch table).

Finally is the Threshold, the threshold is the level of counts that this sample sees as background counts. Syngisitix will automatically calculate this number based of the peaks and counts observed during analysis, however you can set the threashold before analysis to be whatever you want. You should set the treashold with caution as it will directly impact what Syngisitix sees as being peaks and what it sees as dissolved. In my experience I only set the threashold after running a matrix matched blank, for example a tap water blank has a background of 3 counts I may set the entire batches threashold to 3 as I know that is what the blank correction will be.



To the left of the file options and parameters panels is the Calibrations panel, here the dissolved and particle calibrations for the currently selected sample will be shown. If there are no calibration graphs present then the sample has no calibration assigned to it currently, this can be due to the method changing during the batch such as if you were measuring multiple elements within each sample. To fix this just load a calibration file using the load button in the file options panel.

On each of the calibration graphs you can also force the line of best fit though zero, and apply a blank subtraction which subtracts the blank from the data points. Both of these options will change the results of the currently selected sample so bear that in mind.



Results Table

Sample	Analyte	Most Freq. Mass (ag)	Mean Mass (ag)	No. of Peaks	Mean Inten. (counts)	Cell Conc. (parts/mL)	Diss. Inten. (counts)	Diss. Conc. (ppb)	Bin Size (ag)
Test	Eu 152.929			111	1.02	10406	0		
Single Cell Test Eu	Eu 152.929			104	1.03	9750	0		
STD1	Eu 152.929			319	870.79	33000	0		
Gold Test	Au 196.967			7	97.57	483	0.02		
Gold Test	Au 196.967	3714	9214	3	5.44	207	0.01		100
Gold Test	Au 196.967			7731	1.03	533172	0.01		
Gold Test	Au 196.967	11014	10478	97	702.03	6690	0.01		1000
10,000 + MilliQ	Au 196.967			5	88.6	345	0.01		
10,000 + MilliQ	Au 196.967			4075	1.07	281034	0		
10,000 + 10,000	Au 196.967			37	19.05	2552	0.01		
100,000 + MilliQ	Au 196.967			190	4.11	13103	0		
100,000 + 100,000	Au 196.967			4542	1.06	313241	0		
10,000 + 10,000	Au 196.967			4	178	276	0		
STD1	Eu 152.929			67	1.06	33000	0		
STD1	Eu 152.929			636	1115.73		0.01		
STD1	Eu 152.929			67	1219.55	330000	0		
STD1	Eu 152.929			602	1183.41	330000	0.01		
STD1	Eu 152.929			112	1148.13	330000	0		
STD1	Eu 152.929			25	1	33000	0		

Single Cell

Analysis Results Exit

File Options:

- Dataset Folder: Browse...
- View Dataset Files: Browse...
- Dissolved Calibration File: Load...
- Particle Calibration File: Load...
- Export Current Sample:
- Export Results Table:

Parameters:

Analyte	Mass (amu)	Density (g/cm ³)	Mass Fraction (%)	Ionization Efficiency (%)	RPQ
---------	------------	------------------------------	-------------------	---------------------------	-----

Cell Parameters:

- Profile: Gas Flow (mL/min): AFT (V):
- Sample Flow Rate: mL/min
- Dwell Time: μ s
- Scan Time (s): s
- Transport Efficiency: %
- Threshold: Counts ☐ Overridden

Calibrations:

Results Table:

Sample	Analyte	Most Freq. Mass (ag)	Mean Mass (ag)	No. of Peaks	Mean Inten. (counts)	Cell Conc. (parts/mL)	Diss. Inten. (counts)	Diss. Conc. (ppb)	Bin Size (ag)	Std
--------	---------	----------------------	----------------	--------------	----------------------	-----------------------	-----------------------	-------------------	---------------	-----

Histogram:

Profile: Standard


Windows: SOPMS SOP - W... | IS SCRAST | Symyx™ for ICP...

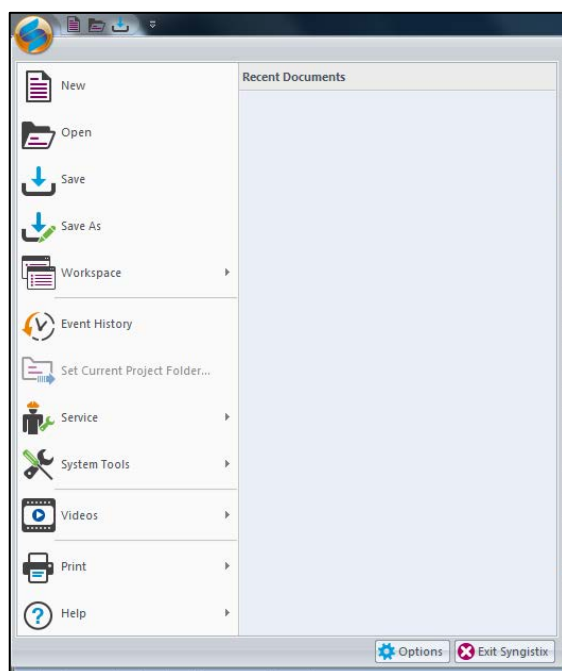
15:06 06/02/2020

Exporting samples

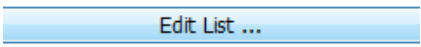
Appendix 1: SmartTune optimisation method creation



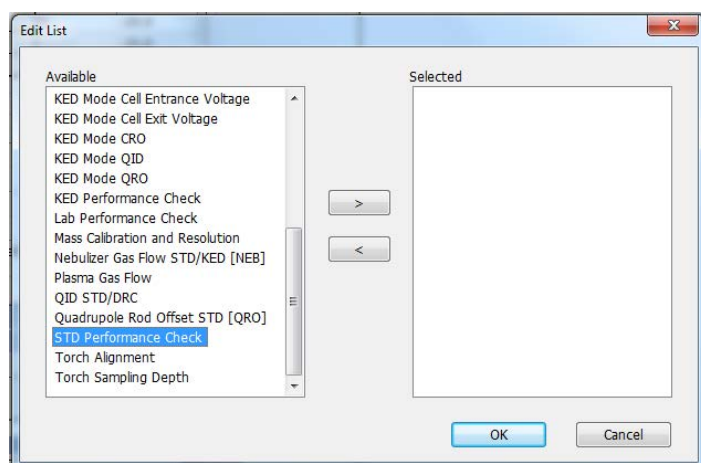
10) Click on  to bring a drop down menu.



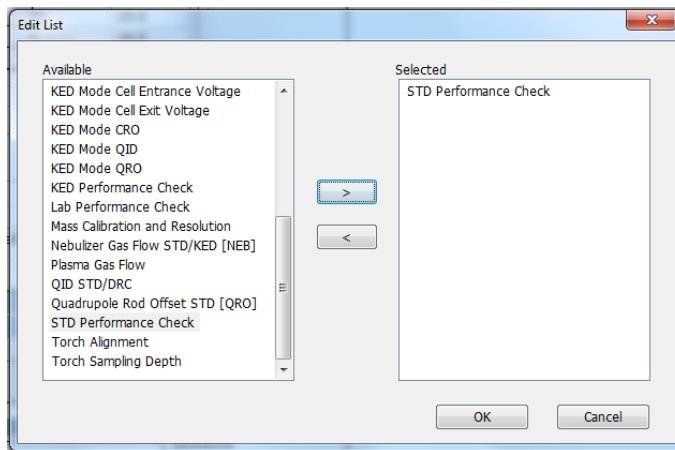
11) Select and click  from the drop down menu.

12) Click .

13) Select STD Performance Check.



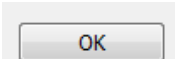
14) Click on  this will add STD Performance Check to the selected optimisation

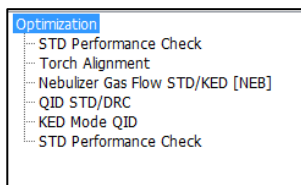



steps.

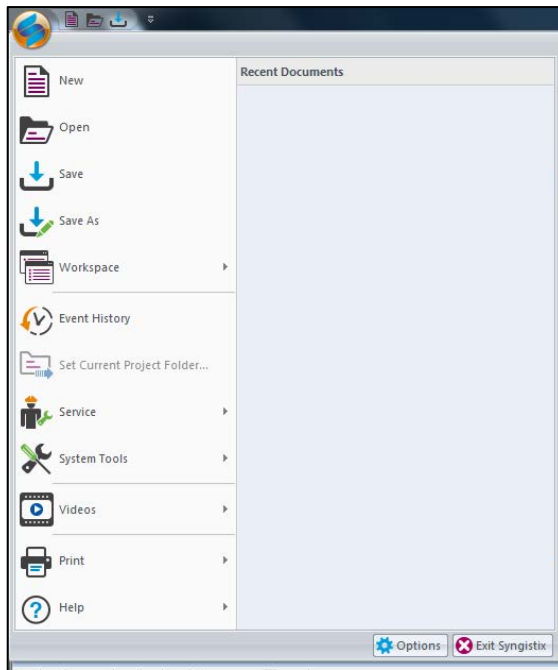
15) Repeat steps 4 and 5 by selecting optimisations in the following order.

- a) Torch Alignment
- b) Nebulizer Gas Flow STD/KED [NEB]
- c) QID STD/DRC
- d) KED Mode QID
- e) STD Performance Check

f) Press  to complete the selection of optimisation. Presenting you with a list of optimisations.



1. Click on  to bring a drop down menu.



2. Click  and save to memorable place as the daily SmartTune method.